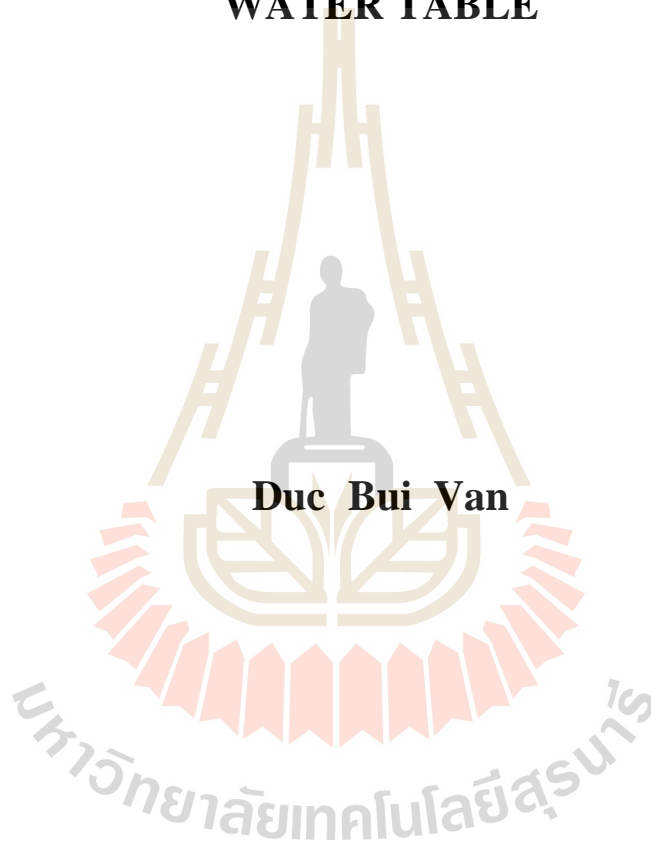


**SEEPAGE RESPONSES OF MECHANICAL
STABILIZED EARTH WALL STRUCTURES
INDUCED BY RISING OF UPSTREAM
WATER TABLE**

Duc Bui Van



**A Thesis Submitted in Partial Fulfillment of the Requirements for the
Degree of Doctor of Philosophy in Civil Engineering**

Suranaree University of Technology

Academic Year 2016

การตอบสนองจากการไหลในดินเนื่องจากการยกตัวของระดับน้ำใต้ดิน
ในกำแพงกันดินเสริมกำลัง



วิทยานิพนธ์นี้เป็นส่วนหนึ่งของการศึกษาตามหลักสูตรปริญญาวิศวกรรมศาสตรดุษฎีบัณฑิต
สาขาวิชาวิศวกรรมโยธา
มหาวิทยาลัยเทคโนโลยีสุรนารี
ปีการศึกษา 2559

**SEEPAGE RESPONSES OF MECHANICAL STABILIZED
EARTH WALL STRUCTURES INDUCED BY RISING OF
UPSTREAM WATER TABLE**

Suranaree University of Technology has approved this thesis submitted in partial fulfillment of the requirements for the Degree of Doctor of Philosophy.

Thesis Examining Committee


(Prof. Dr. Suksun Hopibulsuk)

Chairperson


(Assoc. Prof. Dr. Avirut Chinkulkijniwat)

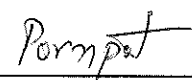
Member (Thesis Advisor)


(Prof. Dr. Panich Voottipruex)

Member


(Assoc. Prof. Dr. Chatchai Jothityangkoon)


Member


(Asst. Prof. Dr. Pornpot Tanseng)

Member


(Prof. Dr. Sukit Limpijumnong)

Vice Rector for Academic Affairs
and Innovation


(Assoc. Prof. Flt. Lt. Dr. Kontorn Chamniprasart)

Dean of Institute of Engineering

ดึก บุษวัน : การตอบสนองจากการไหลในดินเนื่องจากการยกตัวของระดับน้ำใต้ดินใน
กำแพงกันดินเสริมกำลัง (SEEPAGE RESPONSES OF MECHANICAL STABILIZED
EARTH WALL STRUCTURES INDUCED BY RISING OF UPSTREAM WATER
TABLE) อาจารย์ที่ปรึกษา: รองศาสตราจารย์ ดร.อวิรุทธิ์ ชินกุลกิจนิวัฒน์, 241 หน้า

วิทยานิพนธ์นี้ประกอบด้วยสองส่วน ในส่วนแรกนำเสนอผลการตรวจวัดการตอบสนอง
จากการไหลในดินเนื่องจากการยกตัวของระดับน้ำใต้ดิน ด้วยแบบจำลองกายภาพร่วมกับการ
วิเคราะห์เชิงตัวเลขด้วยวิธีทางไฟไนต์อีลิเมนต์ เพื่อศึกษาปัจจัยที่ส่งกระทบต่อการตอบสนอง
ดังกล่าวภายในกำแพงกันดินเสริมกำลังทั่วไปที่นิยมใช้ดินเม็ดหยาบเป็นวัสดุถม การศึกษาเริ่มจาก
การทดสอบในแบบจำลองกายภาพเพื่อจำลองการระบายน้ำภายในกำแพงโดยแบ่งออกเป็นสอง
เงื่อนไข ได้แก่ กำแพงกันดินเสริมกำลังที่ไม่มีระบบระบายน้ำ และมีระบบระบายน้ำเพื่อป้องกันน้ำ
ไหลเข้าพื้นที่เสริมกำลังโดยใช้วัสดุประกอบทางธรณีเทคนิค(geocomposite) ซึ่งเป็นวัสดุที่
ประกอบด้วยตาข่ายสังเคราะห์ทางธรณีเทคนิค(geonet) เป็นแกนกลางและประกบด้วยวัสดุเส้นใย
สังเคราะห์ทางธรณีเทคนิค(geotextile) ผลการทดสอบที่ได้จะนำไปสอบเทียบกับผลการจำลองเชิง
ตัวเลขด้วยวิธีไฟไนต์อีลิเมนต์ เพื่อให้ได้แบบจำลองที่ถูกต้องในการนำไปศึกษาปัจจัยที่มีอิทธิพลต่อ
การระบายน้ำภายในกำแพงกันดิน ผลการศึกษาจากแบบจำลองเชิงกายภาพ พบว่า การติดตั้งระบบ
ระบายน้ำด้วยวัสดุประกอบทางธรณีเทคนิค สามารถช่วยลดปริมาณความชื้นรวมทั้งแรงดันน้ำที่
เกิดขึ้นภายในพื้นที่เสริมกำลังได้เป็นอย่างดี นอกจากนี้ การศึกษาปัจจัยที่มีอิทธิพลต่อการตอบสนอง
การไหลของน้ำในกำแพงกันดินจากแบบจำลองเชิงตัวเลข ซึ่งแสดงในรูปของการกระจายระดับ
ความอิ่มตัวด้วยน้ำประสิทธิผล(effective saturation, S_e) และระดับเส้นผิวน้ำดิน(phreatic surface)
พบว่า การตอบสนองการไหลดังกล่าวขึ้นอยู่กับคุณลักษณะการอุ้มน้ำ(Water Retention Character,
WRC) ของดินถมและของวัสดุเส้นใยสังเคราะห์ทางธรณีเทคนิค รวมทั้งอัตราส่วนระหว่างค่า
สัมประสิทธิ์การซึมผ่านได้ของวัสดุประกอบทางธรณีเทคนิคต่อค่าสัมประสิทธิ์การซึมผ่านได้ของ
ดินถมหรือที่เรียกว่าอัตราส่วนสัมประสิทธิ์การซึมผ่านได้(permeability ratio, $K_{r,net}$) คุณลักษณะ
การอุ้มน้ำของดินถมจะส่งผลต่อการกระจายระดับความอิ่มตัวด้วยน้ำประสิทธิผลภายในกำแพงกัน
ดินทั้งในและนอกพื้นที่เสริมกำลัง ในขณะที่การเพิ่มขึ้นของ $K_{r,net}$ ทำให้เกิดการเพิ่มของระดับเส้น
ผิวน้ำภายในพื้นที่เสริมกำลัง

ส่วนที่สองของวิทยานิพนธ์นำเสนอผลการจำลองเชิงตัวเลขด้วยวิธีทางไฟไนต์อีลิเมนต์
เพื่อศึกษาความเป็นไปได้ของการใช้ดินที่ไม่ผ่านข้อกำหนดสำหรับการใช้เป็นดินถมในกำแพงกัน
ดินเสริมกำลัง(marginal soil) มาใช้เป็นวัสดุถมในกำแพงกันดินที่มีการติดตั้งวัสดุประกอบทางธรณี

เทคนิคเป็นระบบระบายน้ำ ในการจำลองจะแบ่งออกเป็นสองรูปแบบจำลอง ได้แก่ 1) รูปแบบการใช้ดินเดิมตามธรรมชาติด้านนอกพื้นที่เสริมกำลังและใช้ดินทรายเป็นวัสดุถมภายในพื้นที่เสริมกำลัง (L-S scenario) และ 2) รูปแบบการใช้ดินเดิมด้านนอกกำแพงกันดินเสริมกำลังและดินที่ไม่ผ่านข้อกำหนดเป็นดินถมในพื้นที่เสริมกำลัง (L-L scenario) ผลการจำลองในรูปแบบที่ 1 พบว่า การเปลี่ยนแปลงคุณสมบัติเชิงกลศาสตร์ของดินภายนอกพื้นที่เสริมกำลังส่งผลกระทบต่อผลกระทบเพียงเล็กน้อยต่อการกระจายระดับความอิ่มตัวด้วยน้ำประสิทธิผลภายในพื้นที่เสริมกำลัง แต่จะส่งผลกระทบอย่างมากภายนอกพื้นที่ดังกล่าว โดยเมื่อดินมีคุณลักษณะการอุ้มน้ำสูง การกระจายระดับความอิ่มตัวด้วยน้ำประสิทธิผลและแรงดันน้ำภายนอกพื้นที่เสริมกำลังจะสูงตามไปด้วย สำหรับผลการจำลองในรูปแบบที่ 2 พบว่า การใช้ดินที่ไม่ผ่านข้อกำหนดเป็นวัสดุถมภายในพื้นที่เสริมกำลัง ทำให้เกิดการกระจายระดับความอิ่มตัวด้วยน้ำประสิทธิผลภายในพื้นที่ดังกล่าวสูงตามไปด้วย และเปลี่ยนแปลงตามคุณลักษณะการอุ้มน้ำของดิน นอกจากนี้ ผลการจำลองยังแสดงให้เห็นถึง อิทธิพลของอัตราส่วนระหว่างค่าสัมประสิทธิ์การซึมผ่านได้ของตาข่ายสังเคราะห์ทางธรณีเทคนิคต่อค่าสัมประสิทธิ์การซึมผ่านได้ของของดินถมภายนอกพื้นที่เสริมกำลัง (K^{outer}) และอัตราส่วนระหว่างค่าสัมประสิทธิ์การซึมผ่านได้ของตาข่ายสังเคราะห์ทางธรณีเทคนิคต่อค่าสัมประสิทธิ์การซึมผ่านได้ของดินถมภายในพื้นที่เสริมกำลัง (K^{inner}) ต่อระดับของเส้นผิวน้ำภายในพื้นที่เสริมกำลัง โดยเมื่อ K^{outer} มีค่าต่ำลงจะทำให้ระดับของเส้นผิวน้ำภายในพื้นที่เสริมกำลังสูงขึ้น ในทางกลับกัน เมื่อ K^{inner} มีค่าต่ำกว่า 1765 ระดับของเส้นผิวน้ำภายในพื้นที่เสริมกำลังจะลดลงตามการลดลงของ K^{inner} แต่ระดับดังกล่าวจะไม่เปลี่ยนแปลงเมื่อ K^{inner} มีค่าสูงกว่า 1765

DUC BUI VAN : SEEPAGE RESPONSES OF MECHANICAL
STABILIZED EARTH WALL STRUCTURES INDUCED BY RISING OF
UPSTREAM WATER TABLE. THESIS ADVISOR: ASSOC. PROF.
AVIRUT CHINKULKIJNIWAT, Ph.D., 241 PP.

MECHANICAL STABILIZED EARTH WALL / WATER RETENTION
CHARACTER / GEOCOMPOSITE DRAIN / CAPILLARY BARRIER

This thesis comprises two main parts. The first part established to simulate a typical scenario of Mechanical Stabilized Earth (MSE) walls. The primary target of this part was to figure out the influential factors affecting drainage design considerations for MSE walls using granular soils. Initially, series of physical experiments were conducted under two conditions: with, and without geocomposite drain. The experimental results obtained from physical models of MSE walls were then utilized to perform a series of parametric study using Plaxis 2D. The parametric results indicate that the seepage responses were primarily governed by the Water Retention Character (WRC) of the backfill materials, as well as of geotextiles, and the ratio between the saturated hydraulic conductivity of geonet to that of the soil, $K_{r,net}$. Specifically, the WRC of the soil reflects the distribution of effective saturation in the backfills both inside and outside the protection zone. The lower magnitude of $K_{r,net}$ results in a higher level of the phreatic surface in the protected zone. Another finding from the first main part is the effect of “capillary break phenomenon”, the lower magnitude of suction at breakthrough point results in greater amount of water accumulation along the interface. The second part intended to simulate two practical scenarios of MSE walls, in which marginal soil was utilized. In the first scenario, namely L-S, the protected zone was fully filled with sandy soil and the soil outside the

protected zone was in place lateritic soil. The L-S scenario aimed to investigate the influence of hydraulic properties of the soil outside the protected zone on the seepage responses. In addition, the use of different types of soils inside and outside the protected zone was considered through this scenario. The second scenario, namely L-L, was set up to investigate the influence of the use of poorly drained materials on flow response in MSE walls. The computed results show that the hydraulic properties of the soil outside the protected zone play a little role in the moisture profiles in the protected zone, and vice versa. Instead, it significantly affects the moisture content in the unreinforced zone, the greater amount of fine particles (lower g_u and g_n values) of the soil outside the protected zone brings about the wider distribution of high moisture content in the unprotected zone. The ratio of the hydraulic conductivity of geonet to that of the soil outside the protected zone, K^{outer} , play a major role in the level of the phreatic surface in the protected zone. It was also found that the permeability ratio between geonet and the soil placed inside the protected zone, K^{inner} , affected the level of the phreatic surface inside the protected zone, if the magnitude K^{inner} of less than the critical value of 1765. The lower value of K^{inner} results in a lower phreatic surface in the protected zone found. In the case that the geocomposite has insufficient drainage capacity as well as the thickness of drainage system is not well-founded, the use of the backfill material having lower hydraulic conductivity might aggrade the phreatic surface in the unprotected zone. A greater fine particle content (lower g_u and g_n values) in the soil outside the protected zone, results in a wider distribution of the high-water-content area.

School of Civil Engineering

Academic Year 2016

Student's Signature

Advisor's Signature

ACKNOWLEDGEMENTS

It's been three years since the author obtained a great opportunity to pursue his Ph.D degree at School of Civil Engineering, Suranaree University of Technology (SUT), Thailand - the Land of Smiles, under the supervision of Associate Professor Dr. Avirut Chinkulkijniwat. The author would take this chance to express his deep gratitude to him, especially, thank for his time and unlimited patience in explaining all relevant background of the problem considered in this research work. This doctoral dissertation would not have been possible without his elaborate supervision. The author is greatly indebted to his supervisor for all lessons that the author has learned from the supervisor.

Above all, the author would like to acknowledge with profound gratitude to a key person who gave the author such a great opportunity to study and pursue his doctoral degree at School of Civil Engineering, Professor Dr. Suksun Horpibulsuk, who is always a special inspiration to all of us.

The author would like to sincerely thank Assistant Professor Dr. Ponport Tangseng for influential lectures, enlightening the numerical concepts and computations. My sincere thanks must go to the members of my examination committee, Professor Dr. Suksun Horpibulsuk – Chair of the Ph.D thesis examining committee., Associate Professor Dr. Chatchai Jothityangkoon., Assistant Professor Dr. Pornpot Tanseng., Professor Dr. Panich Voottipreux., and my thesis advisory Associate Professor Dr. Avirut Chinkulkijniwat. They generously gave their time to offer me valuable comments toward improving this research.

The administrative staffs at School of Civil Engineering are memorable not

only for their prompt support but also for kind care. I have especially benefited from the truly professional support from Mrs. Natthaya Kingkhokkrud. The momentous contribution of Dr. Somjai Yubonchit, who, most importantly, was a friend in time of need, a valuable source of fascinating discussions about unsaturated soil mechanics. Special thanks must go to my friend, Artit Udomchai, who initially performed the physical models and provided us very good experimental results that play a vital role in our research works. Also sincere thanks to my classmates and Thai friends: Mr. T. Yaowarat, Miss. I. Limrat, Mr. K. Pruempronchai, Miss. H. Maskong.

The author'd like to sincerely thank Professor Dr. H Tr VO., Professor Dr. Ph Q NGUYEN., Associate Professor Dr. C V DAO., Dr. Q V NGUYEN., Dr. H D NGO., D Th DO., Y Th PHAM., Nh V NGUYEN., Dr. A Ng DO., K V DANG., Dr. M V NGUYEN., Dr. M T TRAN for their great lectures since the author was a student at Department of Underground Construction and Mining. The sincerest thank also goes to my colleagues at Hanoi University of Mining and Geology, Viet Nam.

Finally, I would like to express my heartfelt thanks to my wife Hien, who providing moral support, well take care of my beloved kids, Long and Phuong. To my family, my brother's family Nghia, my sister's family Dung and most vitally my parents who always encourage me, instill me the appreciation for knowledge. Equally, I would express my gratefulness to my parent-in-law, Hanh-Luong, without their personal sacrifices I was not able to focus on studying. I cannot forget friends who went through hard times together, cheered me on, and inspired me over the many years H. Hiep, M. Hung, V. Hien, B. Yen, A T LE, Tr V NGUYEN, Th D PHAM. This research was financially sponsored by the Suranaree University of Technology through the SUT-Ph.D Scholarship Program in 2014 batch.

TABLE OF CONTENTS

| | Page |
|--|-----------|
| ABSTRACT (THAI)..... | I |
| ABSTRACT (ENGLISH)..... | III |
| ACKNOWLEDGEMENTS..... | V |
| TABLE OF CONTENTS..... | VII |
| LIST OF TABLES..... | XIV |
| LIST OF FIGURES..... | XVI |
| SYMBOLS AND ABBREVIATIONS..... | XXIIV |
| CHAPTER | |
| I INTRODUCTION..... | 1 |
| 1.1 Problem statement..... | 1 |
| 1.2 Research objectives..... | 5 |
| 1.3 Thesis rganization..... | 6 |
| 1.4 Scope and Limitation..... | 7 |
| 1.5 References..... | 7 |
| II THEORETICAL BACKGROUND AND LITERATURE | |
| REVIEW..... | 12 |
| 2.1 Historical advancement of reinforced earth techniques..... | 12 |
| 2.2 Behavior and performance of MSE walls..... | 15 |
| 2.2.1 Fundamental behaviors of reinforced earth structures | 15 |

TABLE OF CONTENTS (continued)

| | Page |
|---|------|
| 2.2.1.1 Mechanism of soil – reinforcement interaction..... | 15 |
| 2.2.1.2 Mechanism of stress transfer..... | 17 |
| 2.2.2 Performance of MSE walls..... | 18 |
| 2.3 Prime constituents of MSE walls | 20 |
| 2.3.1 Backfill materials..... | 20 |
| 2.3.2 Reinforcing materials | 23 |
| 2.3.2.1 Inextensible reinforcing elements..... | 23 |
| 2.3.2.2 Extensible reinforcing elements..... | 29 |
| 2.3.3 Facing elements..... | 26 |
| 2.4 Outlines of recent design criteria for MSE walls..... | 26 |
| 2.4.1 Design criteria for internal stability..... | 32 |
| 2.4.1.1 Rupture failure..... | 32 |
| 2.4.1.2 Pullout failure | 33 |
| 2.4.2 Design criteria for external stability..... | 39 |
| 2.4.2.1 Sliding over foundation..... | 40 |
| 2.4.2.2 Bearing capacity failure..... | 41 |
| 2.4.2.3 Overturning of MSE wall..... | 43 |
| 2.4.2.4 Global failure..... | 43 |
| 2.5 Case studies of MSE walls failures..... | 45 |

TABLE OF CONTENTS (continued)

| | Page |
|---|------|
| 2.6 Recent strategies to handle seepage flow of MSE walls..... | 52 |
| 2.6.1 Potential sources of water and drainage systems..... | 53 |
| 2.6.2 Methods to eliminate the effect of seepage flow..... | 54 |
| 2.6.2.1 Combined base drain and back drain..... | 57 |
| 2.6.2.2 Discontinuous back drain..... | 58 |
| 2.6.2.3 Drainage within the protected zone..... | 58 |
| 2.7 Conceptual elucidation of the principal properties of unsaturated soil..... | 59 |
| 2.7.1 Shear strength of unsaturated soil..... | 59 |
| 2.7.1.1 Shear strength of unsaturated soil based on independent stress variables approach..... | 61 |
| 2.7.1.2 Shear strength of unsaturated soil based on effective stress approach..... | 64 |
| 2.7.1.3 Shear strength of unsaturated soil based on suction stress approach..... | 67 |
| 2.7.2 Water flow through unsaturated geomaterials..... | 69 |
| 2.7.2.1 Movement of moisture through unsaturated soil, flow equation..... | 70 |
| 2.7.2.2 Soil suction..... | 73 |
| 2.7.2.3 Soil water retention characteristics..... | 78 |
| 2.7.2.4 Permeability function for unsaturated medium..... | 87 |

TABLE OF CONTENTS (continued)

| | Page |
|---|------------|
| 2.7.2.5 Capillary barrier..... | 93 |
| 2.8 In summary..... | 99 |
| 2.9 References..... | 101 |
| III INFLUENTIAL FACTORS AFFECTING DRAINAGE DESIGN | |
| CONSIDERATIONS FOR MECHANICAL STABILIZED | |
| EARTH WALLS USING GEOCOMPOSITES..... | 116 |
| 3.1 Statement of problem | 117 |
| 3.2 Materials used in this study | 120 |
| 3.3 Establishment for numerical and physical experiments..... | 124 |
| 3.3.1 Numerical background..... | 124 |
| 3.3.2 Physical Experiments | 126 |
| 3.3.3 Numerical modeling..... | 130 |
| 3.4 Results and Discussions..... | 140 |
| 3.4.1 Experimental results..... | 140 |
| 3.4.2 Model Calibration..... | 143 |
| 3.5 Parametric Study..... | 149 |
| 3.5.1 Effect of the van Genuchten parameters of the | |
| backfill..... | 149 |
| 3.5.1.1 The van Genuchten parameter g_a | 149 |
| 3.5.1.2 The van Genuchten parameters g_n | 152 |

TABLE OF CONTENTS (continued)

| | Page |
|---|------------|
| 3.5.1.3 The saturation parameters S_{res} and S_{sat} | 155 |
| 3.5.2 Effect of van Genuchten parameters of the geotextile | 157 |
| 3.5.2.1 The van Genuchten parameter g_a | 157 |
| 3.5.2.2 The van Genuchten parameters g_n | 160 |
| 3.5.2.3 The saturation parameters S_{res} and S_{sat} | 161 |
| 3.5.3 Effect of hydraulic conductivity ratio | 163 |
| 3.6 Conclusions..... | 165 |
| 3.7 References..... | 167 |
| IV SEEPAGE RESPONSES IN MSE WALLS UTILIZE IN- PLACED MARGINAL SOILS AS FILL MATERIALS WITH GEOCOMPOSITES FOR DRAINAGE..... | 171 |
| 4.1 Statement of problem | 172 |
| 4.2 A brief literature on geotechnical properties of in-placed marginal soils..... | 176 |
| 4.3 Materials | 178 |
| 4.4 Parametric study results..... | 184 |
| 4.4.1 Seepage responses in the L-S scenario..... | 184 |

TABLE OF CONTENTS (continued)

| | Page |
|---|------|
| 4.4.1.1 Effect of the g_a of in-placed marginal soil outside the protected zone..... | 185 |
| 4.4.1.2 Effect of the g_n of in-placed marginal soil outside the protected zone..... | 187 |
| 4.4.1.3 Effect of S_{res} and S_{sat} of in-placed marginal soil outside the protected zone..... | 190 |
| 4.4.1.4 Effect of the hydraulic conductivity ratio..... | 192 |
| 4.4.2 Seepage responses in the L-L scenario..... | 195 |
| 4.4.2.1 Effect of the g_a of the compacted in-placed marginal soil inside the protected zone | 195 |
| 4.4.2.2 Effect of the g_n of the compacted in-placed marginal soil inside the protected zone..... | 196 |
| 4.4.2.3 Effect of S_{res} and S_{sat} of the compacted in- placed marginal soil inside the protected zone | 198 |
| 4.5 Discussions..... | 198 |
| 4.5.1 Distribution of the water content..... | 198 |
| 4.5.2 Location of the outer phreatic surface..... | 200 |
| 4.5.3 Level of the inner phreatic surface..... | 202 |
| 4.6 Conclusions..... | 206 |

TABLE OF CONTENTS (continued)

| | Page |
|--|------------|
| 4.7 References..... | 207 |
| V CONCLUSIONS AND RECOMMENDATIONS | 212 |
| 5.1 Summary and Conclusions..... | 212 |
| 5.2 Recommendations for future works | 215 |
| 5.3 References..... | 217 |
| APPENDIX | |
| APPENDIX A. List of publications | 219 |
| BIOGRAPHY | 241 |

มหาวิทยาลัยเทคโนโลยีสุรนารี

LIST OF TABLES

| Table | Page |
|---|------|
| 2.1 A designated of tall MSE walls built worldwide (after Sankey, 2004) | 14 |
| 2.2 Backfill criteria of reinforced soil (Korner et al., 2005)..... | 21 |
| 2.3 Magnitude of constant factor nr (Chai, 1992)..... | 38 |
| 2.4 Recommended minimum factors of safety (AASHTO, 2002)..... | 44 |
| 2.5 Undesirable field performance cases (after Koerner et al., 2005)..... | 50 |
| 2.6 Undesirable field performance cases (after Koerner et al., 2005) | 51 |
| 2.7 Some recent approaches to minimize the effect of seepage flow..... | 56 |
| 2.8 Empirical mathematical equations for water retention characteristic curve (after Too et al., 2014)..... | 79 |
| 2.9 A summary of experiential permeability equations $k(E)$ (after Fredlund, 1993) | 89 |
| 2.10 The variation of magnitude of u | 91 |
| 3.1 VG and VGM model parameters and saturated hydraulic conductivity of the materials used in the physical test..... | 122 |
| 3.2 Properties of thirteen nonwoven geotextiles..... | 132 |
| 3.3 VG and VGM model parameters of the geotextiles assigned in the numerical experiment..... | 133 |
| 3.4 VG and VGM model parameters assigned to every case in the numerical experiment..... | 134 |

LIST OF TABLES (continued)

| Table | Page |
|--|------|
| 3.5 Input data for numerical simulation..... | 138 |
| 4.1 Soil characteristics for use within reinforced zone (Sandri, 2005)..... | 173 |
| 4.2 MSE walls utilized high fine-grained soils as backfill (after Mitchell, 1995) | 174 |
| 4.3 Summary of typical geotechnical engineering properties of marginal soils.. | 178 |
| 4.4 van Genuchten model parameters of the materials used in this study..... | 179 |
| 4.5 Model parameters for each case in the L-S scenario..... | 181 |
| 4.6 Model parameters for each case in the L-L scenario..... | 182 |

LIST OF FIGURES

| Figure | | Page |
|---------------|--|-------------|
| 2.1 | Typical components of an MSE wall (adopted from Long, 1995)..... | 12 |
| 2.2 | Mean construction costs for various retaining wall structures (adopted from Koerner, 1998) | 13 |
| 2.3 | Effect of reinforcement on a soil element (adopted from Nand, 2005) | 16 |
| 2.4a | Frictional stresses transfers between soil particles and reinforcement (adopted from Christopher et al., 1990) | 18 |
| 2.4b | Soil passive (bearing) resistance on reinforcement surface (adopted from Christopher et al., 1990) | 18 |
| 2.5 | Location of potential failure surface in MSE walls reinforced by metallic reinforcements (adopted from Schlosser and Long, 1974) | 20 |
| 2.6a | Soil bearing reinforcements (adopted from Suksiripattanapong et al., 2013)..... | 24 |
| 2.6b | Installation of bearing reinforcements in some highway projects in Thailand..... | 24 |
| 2.7 | Types of extensible reinforcing materials | 25 |
| 2.8 | Fasteners between the facing and reinforcing element used in highway projects in Bangkok, Thailand..... | 27 |
| 2.9 | A typical flow chart of process design of MSE walls using geosynthetic reinforcement (adopted Johnson, 2012)..... | 29 |
| 2.10 | Potential failure mechanism of MSE wall: (a) modes of external failure, (b) modes of internal failure failure (adopted from Nand, 2005)..... | 32 |

LIST OF FIGURES (continued)

| Figure | Page |
|--|------|
| 2.11 Location of potential failure envelopes for the internal stability analysis (adopted from Voottipruex, P., et al., 2001 and AASHTO, 2002)..... | 34 |
| 2.12 Variation of earth pressure coefficient with depths for different approaches (adopted from Voottipruex et al., 2001 and AASHTO, 2002..... | 35 |
| 2.13 Typical external forces acting on the MSE body (adopted from Voottipruex, P., et al., 2001)..... | 40 |
| 2.14 The location of the resultant force underneath foundation for various distribution of pressure beneath MSE wall (adopted from Voottipruex, P., et al., 2001)..... | 41 |
| 2.15 An actual failure of MSE wall (adopted from Scarborough et al., 2005) | 47 |
| 2.16 Loosing sand from MSE wall (adopted from Chen et al., 2007)..... | 48 |
| 2.17 Common potential sources of incident water permeate to an MSE wall..... | 53 |
| 2.18 Drainage systems recommended for MSE wall (adopted from Koerner, 2011): (a) internal drainage for surface water within reinforced soil mass, (b) external drainage for surface water placed behind reinforced zone (adopted from Koerner et al., 2011)..... | 55 |
| 2.19 Base drain and vertical back drain (adopted from Koerner, 2005) | 57 |
| 2.20 Use of continuous and intermittent geocomposite back drains (adopted from TenCate Geosynthetics, Inc) | 58 |
| 2.21 A stress state distributed on a soil element in an unsaturated soil..... | 60 |
| 2.22 Extended Mohr-Coulumb failure surface based on independent stress variables approach (adopted form Lu and Likos, 2004)..... | 61 |

LIST OF FIGURES (continued)

| Figure | Page |
|---|------|
| 2.23 Theoretical relationship between unsaturated shear strength envelope and soil water characteristic curve (adopted from Lu and Likos, 2004)..... | 64 |
| 2.24 Different configuration of effective stress factor $\bar{\sigma}$ (adopted from Lu and Likos, 2004)..... | 66 |
| 2.25 Shear strength of unsaturated soils in suction stress, net normal stress and shear stress surface (Lu and Likos, 2004)..... | 68 |
| 2.26 Shear strength of unsaturated soils in $\bar{\sigma} - (\bar{\sigma} - u_a)$ plane (Lu and Likos, 2004)..... | 69 |
| 2.27 Conceptual moisture movements through partially saturated with pore size soil.... | 73 |
| 2.28 A typical profile of matric suction in a homogeneous sedimentary layer under various surface flux boundary conditions (adopted from Lu and Likos, 2004)..... | 74 |
| 2.29 Osmotic pressure head through a semipermeable membrane (adopted from Lu and Likos, 2004)..... | 76 |
| 2.30 Forces equilibrium in a capillary tube (adopted from Fredlund and Rahardddjo, 1993)..... | 78 |
| 2.31a Typical soil characteristic curve of a soil..... | 80 |
| 2.31b Soil water characteristic curves for a sandy soil, a silty soil, and a clayey soil..... | 83 |
| 2.32 Water retention curves estimated using Brooks and Corey model for various values of the model parameters..... | 83 |
| 2.33 Water retention curves obtained from van Genuchten model for various values of the model parameters..... | 83 |

LIST OF FIGURES (continued)

| Figure | Page |
|--------|--|
| 2.34 | Relative moisture conductivity curves obtained from van Genuchten model.....93 |
| 2.35 | The response of flow due to capillary barrier at the interface between unsaturated fine and coarser soil layers (Shackelford et al., 1994; Mancarella, Doglioni et al., 2012).95 |
| 2.36 | Conceptual development of capillary barrier system formed at the boundary between small and large pore size soils: (a) low obstructed water level, (b) intermediate obstructed water level, and (c) obstructed water level at starting breakthrough point (adopted from Lu and Likos, 2004).....96 |
| 3.1 | Water retention characteristic curves and grain-size distribution of the soil used in this part.....121 |
| 3.2a | Wetting phase WRC curves of 13 geotextiles reported by Iryo, 2003 and of the geotextiles used in the physical test.....123 |
| 3.2b | WRC curves of all geotextiles assigned to the numerical experiment.....123 |
| 3.3 | Schematic diagram of water retention characteristic curve.....125 |
| 3.4 | Sketch of the physical test and its instrumentation.....127 |
| 3.5 | Phreatic surface, surface settlement, and lateral movement at each upstream water level.....142 |
| 3.6 | Measured moisture contents in reinforced zone (a), and (b) in unreinforced zone for case I (without geocomposite drain installed) and case II (with geocomposite drain installed)143 |
| 3.7 | Mesh discretization of the models.....145 |

LIST OF FIGURES (continued)

| Figure | Page |
|--|------|
| 3.8 Measured and calculated phreatic surfaces and water contents for MSE walls (a) case I (without geocomposite drain installed) and (b) case II (with geocomposite drain installed) | 146 |
| 3.9 Time series plot for water content for MSE wall case I (without geocomposite drain installed) (a), and (b) case II (with geocomposite drain installed)..... | 148 |
| 3.10 Effective saturation profile along vertical section located (a) 5 cm left, and (b) 5 cm right of the geocomposite for various magnitudes of g_a of soil..... | 150 |
| 3.11 Typical water retention characteristic curve with low and high g_a values..... | 151 |
| 3.12 Phreatic surface (bold lines) and effective saturation contour lines (dashed lines) in the MSE wall for various magnitudes of g_n of soil..... | 153 |
| 3.13 Typical water retention characteristics for low (a), and (b) high g_n values..... | 154 |
| 3.14 Phreatic surface (bold lines) and effective saturation contour lines (dashed lines) in the MSE wall for the lowest and highest values of S_{res} (a) and (b) S_{sat} of soils assigned in the numerical experiment..... | 156 |
| 3.15 Effective saturation profiles along the soil-geotextile interface for various magnitudes of g_a of geotextile..... | 157 |
| 3.16 Hydraulic conductivity functions of the soil and geotextile with various magnitudes of g_a of geotextile..... | 159 |
| 3.17 Effective saturation profiles along the soil-geotextile interface for various magnitudes of g_n of geotextile..... | 160 |

LIST OF FIGURES (continued)

| Figure | Page |
|--------|---|
| 3.18 | Phreatic surfaces (bold lines) and effective saturation contour lines (dashed lines) in the MSE model for the lowest and highest values of S_{res} (a) and (b) S_{sat} of soils assigned in the numerical experiment.....162 |
| 3.19 | Variation in phreatic surface in the protected zone for (a) various ratios between the hydraulic conductivity of the geotextile and that of soil and (b) various ratios between the hydraulic conductivity of the geonet and that of soil.....164 |
| 4.1 | Location of marginal lateritic soil in Casagrande's chart Biswal, (adopted from Sahoo et al., 2016)177 |
| 4.2 | (a) Grain size distribution of the studied soils and (b) WRC of the materials used in this study.....181 |
| 4.3 | (a) WRC curves of the considered marginal soils and (b) WRC curves for different types of marginal soils obtained from previous studies.....184 |
| 4.4 | (a) Effective saturation profiles along the vertical sections located at 5cm apart to either side of the soil-geocomposite interface, outside and inside the protected zone, for varying g_a values of the native in-placed marginal soil for L-S scenario and (b) varying g_a values of the compacted marginal soil for L-L scenario.....186 |
| 4.5 | Variation in the phreatic surface outside the protected zone for varying g_a values for marginal soil (solid line for the L-S scenario and dashed line for L-L scenario)...187 |
| 4.6 | Phreatic surface and effective saturation contour lines in the MSE wall for varying g_n values of the native in-placed marginal soil for the L-S scenario.....189 |

LIST OF FIGURES (continued)

| Figure | | Page |
|--------|--|------|
| 4.7 | Phreatic surfaces and effective saturation contour lines in the MSE wall for varying S_{res} (a) and (b) S_{sat} of the native in-placed marginal soil for the L-S scenario..... | 191 |
| 4.8 | Effect of the permeability ratio on the inner phreatic surface level..... | 193 |
| 4.9 | Phreatic surface and effective saturation contour lines in the MSE wall for varying g_n values of the compacted marginal soil for the L-L scenario..... | 197 |
| 4.10 | (a) Typical water retention characteristic curve, (b) typical k-function curve..... | 191 |
| 4.11 | Magnitude of suction at the water breakthrough point for varying values of g_a and g_n | 201 |
| 4.12 | (a) Incident and reflected angles and (b) flow vectors from calculation case A of the L-S scenario..... | 204 |

SYMBOLS AND ABBREVIATIONS

| | | |
|------------------|---|---|
| a | = | soil parameters which is related to Air Entry Value of the soil |
| u | = | skin friction angle between reinforcement and soil |
| S | = | incident angle which is an angle between an incident flow line and a line normal to the soil-geocomposite interfacial plane (deg) |
| ν' | = | effective Poisson's ratio |
| $\{\prime$ | = | internal soil friction angle |
| t | = | coefficient of effective stress |
| $\}$ | = | pore size distribution index |
| $\gamma_{d\max}$ | = | maximum dry unit weight (kN/m^3) |
| τ | = | shear strength of unsaturated soil |
| τ' | = | effective stress |
| τ^s | = | suction stress |
| τ_n | = | total normal stress |
| τ_a | = | average normal stress |
| w | = | volumetric water content |
| w_{sat} | = | saturated volumetric water content |
| w_r | = | residual volumetric water content |
| W^b | = | nonlinear of soil suction |

SYMBOLS AND ABBREVIATIONS (Continued)

| | | |
|----------------------------|---|---|
| \mathfrak{E} | = | matric suction |
| E' | = | effective modulus of elasticity |
| FS | = | factor of safety |
| g_a | = | fitting parameter (m^{-1}) |
| g_c | = | fitting parameter (-) |
| g_n | = | fitting parameter (-) |
| G_s | = | specific gravity |
| h | = | total head (m) |
| h_p | = | suction head (m) |
| h_c | = | height of capillary rise (m) |
| H_e | = | equivalent height of MSE wall |
| k | = | saturated hydraulic conductivity (m/day) |
| k_r | = | relative hydraulic conductivity (-) |
| k_x | = | hydraulic conductivity in the x direction (-) |
| k_y | = | hydraulic conductivity in the y direction (-) |
| k_ψ | = | unsaturated soil permeability (-) |
| $K_{r, \text{text}_{lat}}$ | = | ratio between the hydraulic conductivity of geotextile in lateral direction and to that of soil (-) |

SYMBOLS AND ABBREVIATIONS (Continued)

| | | |
|---------------------|---|--|
| K_{r,txt_long} | = | ratio between the hydraulic conductivity of geotextile in lateral direction and to that of soil (-) |
| $K_{r,net}$ | = | ratio between the hydraulic conductivity of geonet to that of soil (-) |
| K^{outer} | = | ratio between the hydraulic conductivity of geonet to that of soil placed outside the protected zone (-) |
| K^{inner} | = | ratio between the hydraulic conductivity of geonet to that of soil placed inside the protected zone (-) |
| L_r | = | length of soil reinforcement |
| L_e | = | effective length of soil reinforcement |
| $N_q, N_c, N\gamma$ | = | bearing factors |
| p_b | = | pullout bearing force of soil reinforcement |
| p_n | = | total pullout bearing force of soil reinforcement |
| R_s | = | radius of meniscus |
| S | = | degree of saturation (%) |
| S_e | = | effective degree of saturation (-) |
| S_{sat} | = | degree of saturation at suction of zero (-) |
| S_{res} | = | degree of saturation at residual water content (-) |
| T_s | = | surface tension |

SYMBOLS AND ABBREVIATIONS (Continued)

| | | |
|-------|---|------------------------------------|
| u_a | = | pore air pressure (kPa) |
| u_w | = | pore water pressure (kPa) |
| AEV | = | pore water pressure |
| CS | = | compacted sandy soil |
| MSE | = | mechanically stabilized earth |
| NL | = | native lateritic soil |
| DR | = | time-domain reflectometer |
| USCS | = | unified soil classification system |
| VG | = | van Genuchten |
| VGM | = | van Genuchten – Mualem |
| WRC | = | water retention characteristic |

CHAPTER I

INTRODUCTION

1.1 Problem statement

Initially introduced in 1969 by Vidal (1969), reinforced soil techniques, later known as Mechanically Stabilized Earth (MSE) walls, that are constructed by placing alternative reinforcement layers and compacted soil behind a facing element to form a composite structure have been widely employed for different site conditions for decades. The interaction of the backfill material and reinforcements form a relatively flexible, coherent block that is able to sustain significant loads and movements as well as tolerate much larger settlements compared to conventional cast-in-place concrete walls (known as concrete retaining structures), particularly differential settlements. It is also believed that MSE walls are gravity structures that usually made of unsaturated earthen soil (Saito et al., 2009). Recently, the use of MSE walls has become increasingly prevalent in the development of transportation and other projects primarily due to having numerous advantages over conventional retaining structures such as construction process is fast and easy, site preparation is less, construction work doesn't require experienced skilled craftsmen with special skills (Elias et al., 2001).

However, along with the attractiveness of the use of the reinforced earth techniques, there have been numerous failures cases of MSE walls occurred. Even with very few MSE walls fail completely, but there have many walls which have not

well performed as expected. Most investigations indicate that the performance of reinforced earth structures is a function of the properties of both the earth reinforcement and the geotechnical characteristics of the fill material.

The poor performance of MSE walls is associated with the quality of construction process, accuracy of design works, lessening of weak foundations where MSE walls are placed on Alzamora and Anderson (2009). It is also recognized that good structure performance is primarily governed by the amount of moisture content maintaining in the reinforced earth structures. The higher moisture content, the higher pore water pressure developed. The larger pore water pressure generated, the larger movements taken place in the reinforced part (later called the protected zone), hence the failures might be occurred. Previous researchers (Alzamora et al., 2009; Koerner & Soong, 2000; Leshchinsky & Han, 2004; Mahmood, 2009; Shibuya et al., 2007) stated that most of the failures of MSE walls were frequently attributed to inadequate drainage and the presence of water within or behind the reinforced zone (later termed as the protected zone) which related to the accumulation and rising of rainfall behind that structures (Shibuya et al., 2007). However, both the current design guidelines and construction manual of MSE do not consider any water inside and adjacent to the protected zone (AASHTO, 2002; BS, 1995; Christopher et al., 1998; Leshchinsky & Han, 2004; Mitchell, 1995). Similarly, most criteria have been established only based on grain size distribution.

To deal with the development of pore water pressure as well as to eliminate the effect of pore water pressure, some works have been reported that the alternative usage of prefabricated composite sheet drains can provide a solution enabling speedy drainage while lowering construction costs (Koerner & Soong, 2000; Koerner &

Koerner, 2011; McKean & Inouye, 2001; Mitchell, 1995). The prefabricated composite sheet drains is a type of a sandwich-structured composite formed by attaching two thin nonwoven geotextile layers to a core which made of geonet. Although there have been many reported case studies on the successful implementation of geocomposite in drainage systems, there have been limited numerical simulations of drainage for MSE walls using geocomposite (Koerner and Soong, 2005; Yoo and Jung, 2006). Previous studies indicate that geotextiles' water retention characteristics (WRC) are similar to those of coarse-grained soils such as gravels and sands (Bathurst, 2007; Bouazza et al., 2006; Iryo and Rowe, 2003; Knight and Kotha, 2001; Lafleur et al., 2000; Morris, 2000; Nahlawi et al., 2007; Stormont et al., 1997; Stormont and Morris, 2000). Therefore, the drainage capacity of geocomposite might be affected by WRC of nonwoven geotextiles, hence seepage responses. However, there is no known work that incorporates the WRC of geotextiles in those reported numerical simulations. Similarly, the influence of WRC of fill materials has not taken into consideration.

In Thailand and other tropical climate countries, the residual soils are often marginal soils which cover large areas; consequently, the well-graded gravel materials are not readily available in the vicinity of typical construction sites, especially constructing in mountainous areas where a larger amount of fill materials are often required due to long distance, high-rise wall. Marginal soils provide suitable engineering properties such as high shear strength, low compressibility but just fail to meet the fine particle and plasticity index requirements which are of particular interest to the construction industry as a potential replacement material for granular soils. A large number of reinforced soil structures have been designed and constructed using

marginal soils. The overall long-term performance of these earth structures has been reported to be remarkable. The system has not exhibited signs of distress. Nevertheless, numerous failures cases of MSE walls that utilized marginal soils as fill materials have also reported. Among several reasons for MSE failure, the common one found is caused by loss of backfill. The loss of fill material is usually associated with significant amounts of water that permeates through the embankment. Once this phenomenon begins, piping will take place, followed by carrying out the backfill with the water (Chen et al., 2007). The laboratory experiments and field performance of reinforced soil walls with marginal backfill materials was extensively reviewed by Zornberg and Mitchell (1994) and Mitchell (1995). Koerner and Soong (2001) documented 26 case histories of MSE wall failures in the United States, 17 cases of which were related to low permeability soil backfills. They concluded that if marginal soils were allowed in the protected zone, any water ponding that occurs behind or beneath the protected zone), must be properly collected and discharged. Although the moisture susceptibility is major concerned in MSE wall using marginal backfill material, no previous attempt has conducted a parametric study to gain insight knowledge on this critical point particularly when the protected zone is well encapsulated with a drainage system.

As a type of unsaturated materials, the behavior of reinforced earth structures is believed mainly governed by the moisture responses inside its body. Specify, the shear strength and stress state of unsaturated materials are normally changed with changing in moisture content or soil suction. Therefore, finding the factors that affect the moisture response is necessary to prevent and/or eliminate the influence of moisture responses on the performance of reinforced earth structures.

The first main part of this thesis is to figure out the most influential factors that affect drainage design considerations for MSE using geocomposite by performing a series of experiments, in which granular soils employed as backfill materials. Throughout this part, the influence of WRCs of nonwoven geotextile and backfill on the seepage responses was examined.

The second main part of this thesis is to assess two feasible scenarios that utilize in-placed soils as fill materials. The prime aim of these scenarios is to evaluate the use of high fine-grained soil for MSE walls in term of seepage responses. Similarly, effect of unsaturated flow parameters of fine-grained in-placed marginal soils on seepage responses was also examined by carrying out a series of parametric studies.

The outcomes of the thesis are first to contribute a better understanding of the influence of WRCs of backfill as well as of geocomposite, on the performance of MSE walls. Secondly, the finding from this thesis might also facilitate the selection of suitable geocomposite drains for better implementation of MSE walls. Lastly, the outcomes of this research may contribute a superior comprehension on the use of fine-grained soils as backfill for MSE walls.

1.2 Research Objectives

The depiction in the above section of problem statement implies that water combined with low permeability backfill may somewhat lead to poor performance such as excessive deformation or actual collapse of MSE walls. It also indicates that the use of low quality backfill is feasible if a properly designed drainage system is installed. It is thus the main objective of this research is to examine the seepage

responses of reinforced earth structures induced by leveling of the upstream water table that frequently takes place in the mountainous areas. The below are two specific goals:

1.2.1 To determine the most sensitive unsaturated flow parameters that affect drainage considerations for MSE walls using geocomposite.

1.2.2 To examine the use of fine-grained in-placed marginal soils as backfill materials for MSE walls on the seepage responses inside the MSE walls.

1.3 Thesis organization

This thesis is organized in five chapters, in addition to this Introduction. The corresponding references section and outlines of each chapter are presented as below:

The second chapter provides a comprehensive literature review of MSE walls relevant to this research is presented. The basic theories of MSE walls are introduced. They consist of a brief historical story of the development of reinforced soil techniques, mechanisms of strengthening soil as well as the performance of MSE walls, review of current design practice of MSE walls. Next, case studies related to the failure of MSE walls associated with inadequate drainage are summarized. This chapter ends with a background of flow through unsaturated soil and soil water characteristics literature.

The third chapter starts with outlines of materials properties, experiments including physical experiments, numerical simulations that employed throughout this thesis. After the successful calibration of the model, the parametric studies were done by using Plaxis. Next part discloses the influential factors affecting drainage design considerations for MSE walls using geocomposite.

The fourth chapter firstly presents geotechnical properties of in-placed soils. Subsequently, series of numerical sensitivity analysis to examine the use of in-placed marginal soils as backfill were performed.

The fifth chapter is a summation of the main conclusions withdrawn from this research. At the end of the chapter, future research directions that based on incompleteness of present work are also provided.

1.4 Scope and limitation

This research does not cover other factors which may negatively impact the performance of geocomposite, hence flow responses in MSE walls such as fine particle clogging in soil and geotextile, the effect of joint of geocomposite, and also the effect of compressive stress on the hydraulic conductivity of geocomposite.

The finding from this research was obtained from a mini physical scale of MSE wall, which may lead to the current finding of the influence of critical permeability ratio on the level of the phreatic surface inside the protected zone is seemingly valid only for this mini scale. Similarly, the geocomposite drain was assumed as a continuous section of geocomposite drain.

1.5 References

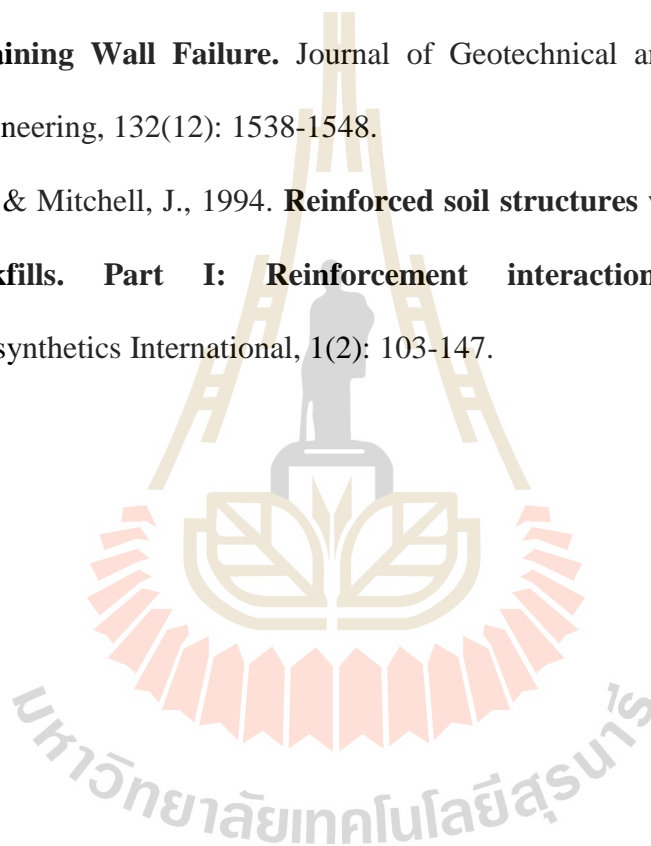
AASHTO., 2002. **Standard Specifications for Highway and Bridge**. American Association of State of Highway and Transportation Officials, Washington DC

- Alzamora, D. E., & Anderson, S., 2009. **Review of mechanically stabilized earth wall performance issues**. Paper presented at the Transportation Research Board (TRB), 2009 Annual Meeting CD-ROM.
- Bathurst, R. J., 2007. **Geosynthetics Classification**. IGS Leaflets on Geosynthetics Applications, IGS Education Committee, available at www.geosyntheticssociety.org.
- Bouazza, A., Freund, M., & Nahlawi, H., 2006. **Water Retention of Nonwoven Polyester Geotextiles**. *Polymer Testing*, 25(8), 1038-1043.
- BS, B. S., 1995. **Code of Practice for Strengthened/Reinforced Soils and Other Fills**. British Standard Institution, London, UK.
- Chen, D. H., Nazarian, S., & Bilyeu, J., 2007. **Failure analysis of a bridge embankment with cracked approach slabs and leaking sand**. *Journal of Performance of Constructed Facilities*, 21(5): 375-381.
- Christopher, B., Gill, S., Juran, I., Mitchell, J., Schlosser, F., & Dunnicliff, J., 1990. **Reinforced Soil Structures, volume 1. Design and Construction Guidelines**. U.S Department of Transportation Federation Highway Administration.
- Christopher, B., Zornberg, J., & Mitchell, J., 1998. **Design guidance for reinforced soil structures with marginal soil backfills**. Paper presented at the Sixth International Conference on Geosynthetics. Atlanta, Georgia, US, 2, 797-804.
- Elias, V., Christopher, B. R., Berg, R. R., 2001. **Mechanically Stabilized Earth Walls and Reinforced Soil Slopes Design and Construction Guidelines:**

- Federal Highway Administration, US Department of Transportation.,
Publication No.FHWA NHI-00-043., 394 pages.
- Iryo, T., & Rowe, R. K., 2003. **On the Hydraulic Behavior of Unsaturated Nonwoven Geotextiles**. *Geotextiles and Geomembranes*, 21(6): 381-404.
- Knight, M., & Kotha, S., 2001. **Measurement of Geotextile-Water Characteristic Curves Using a Controlled Outflow Capillary Pressure Cell**. *Geosynthetics International*, 8(3): 271-282.
- Koerner, R., & Soong, T.-Y., 2000. **Design of Drainage Systems for Segmental Retaining Walls**. *Proceedings of the 14th GRI Conference, Folsom,PA*, 323-351
- Koerner, R. M., & Koerner, G. R., 2011. **The Importance of Drainage Control for Geosynthetic Reinforced Mechanically Stabilized Earth Walls**. *Journal of GeoEngineering*, 6(1): 3-13.
- Koerner, R. M., & Soong, T.-Y., 2001. **Geosynthetic Reinforced Segmental Retaining Walls**. *Geotextiles and Geomembranes*, 19(6), 359-386.
- Koerner, R. M., & Soong, T.-Y., 2005. **Analysis and Design of Veneer cover Soils**. *Geosynthetics International*, 12(1): 28-49.
- Lafleur, J., Lebeau, M., Faure, Y. H., Savard, Y., Kehila, Y., 2000. **Influence of Matric Suction on the Drainage Performance of Polyester Geotextiles**. *Proceedings of 53rd Annual Conference of the Canadian Geotechnical Society*, 1115-1122.
- Leshchinsky, D., & Han, J., 2004. **Geosynthetic Reinforced Multitiered Walls**. *Journal of Geotechnical and Geoenvironmental Engineering*, 130(12): 1225-1235.

- McKean, J., & Inouye, K., 2001. **Field Evaluation of the long-term Performance of Geocomposite Sheet Drains**. *Geotextiles and Geomembranes*, 19(4): 213-234.
- Mitchell, J., 1995. **Reinforced Soil Structures with Poorly Draining Backfills Part II: Case Histories and Applications**. *Geosynthetics International*, 2(1): 265-307.
- Morris, C. E., 2000. **Unsaturated flow in nonwoven geotextiles**. Paper presented at the GeoEng 2000: International Conference on Geotechnical and Geological Engineering, Melbourne, Australia, 19-24 Nov, 2000
- Nahlawi, H., Bouazza, A., & Kodikara, J., 2007. **Characterisation of Geotextiles Water Retention using a Modified Capillary Pressure Cell**. *Geotextiles and Geomembranes*, 25(3): 186-193.
- Saito, M., Shibuya, S., Mitsui, J., Hara, K., 2009. **L-Shaped Geodrain in Embankment Model Test and Numerical Simulation**. *Geosynthetics in Civil and Environmental Engineering*, 428-433
- Shibuya, S., Kawaguchi, T., Chae, J., 2007. **Failure of Reinforced Earth as Attacked by Typhoon No. 23 in 2004**. *Soils and Foundations*, 47(1): 153-160.
- Stormont, J. C., Henry, K. S., Evans, T. M., 1997. **Water retention functions of four nonwoven polypropylene geotextiles**. *Geosynthetics International*, 4(6): 661-672.
- Stormont, J. C., & Morris, C. E., 2000. **Characterization of Unsaturated Nonwoven Geotextiles**. *Geotechnical Special Publication*, 153-164.

- Vidal, H., 1969. **The Principle of Reinforced Earth**. Highway Research Record No. 282, Transportation Research Board: Washington, D.C.
- Vulova, C., & Leshchinsky, D., 2003. **Effects of Geosynthetic Reinforcement Spacing on the Performance of Mechanically Stabilized Earth Walls**. Federal Highway Administration Report FHWA-RD-03-048
- Yoo, C., & Jung, H.-Y., 2006. **Case history of Geosynthetic Reinforced Segmental Retaining Wall Failure**. Journal of Geotechnical and Geoenvironmental Engineering, 132(12): 1538-1548.
- Zornberg, J., & Mitchell, J., 1994. **Reinforced soil structures with poorly draining backfills. Part I: Reinforcement interactions and functions**. Geosynthetics International, 1(2): 103-147.



CHAPTER II

THEORETICAL BACKGROUND AND LITERATURE REVIEW

An extensive literature review was carried out on a number of relevant topics. This review covers research in the following areas: 1) A brief history of advancement of reinforced earth techniques, 2) Mechanism and performance of MSE walls, 3) Typical characters of primary constituents of MSE walls, 4) Outlines of recent design criteria for MSE walls, 5) Case studies of MSE walls failure related to flow of water through reinforced soil masses and current techniques to deal with seepage water flow in MSE walls. The chapter ends with the conceptual elucidation of the principal properties of unsaturated soil.

2.1 Historical advancement of reinforced earth techniques

The concept of reinforced earth was firstly initiated for thousands of years since temples of the Babylonian and Sumerian constructed in the ancient Mesopotamian valley (Ingold, 1982). Later on, the reinforced earth techniques were also exploited to build the Great Wall of China in the early of the 7 century B.C. In the ancient time, the techniques of reinforced earth were included positioning of woods, reeds, hemp, or another form of tensile reinforcement to layers of compacted soil (Kerisel, 1993).

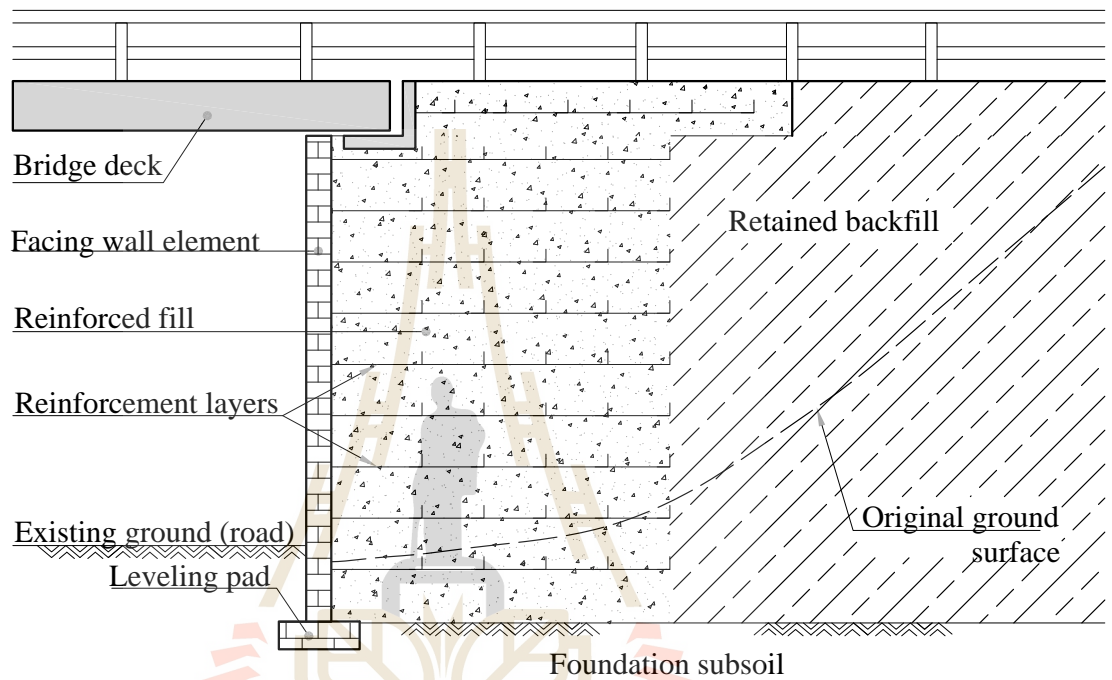
Recently, by virtue of the development of technology those early reinforcing materials have been mostly replaced by artificial materials which provide much higher strength, such as metal strips, geotextiles, geogrids, hence a better performance of reinforced earth structures (or termed as MSE walls).

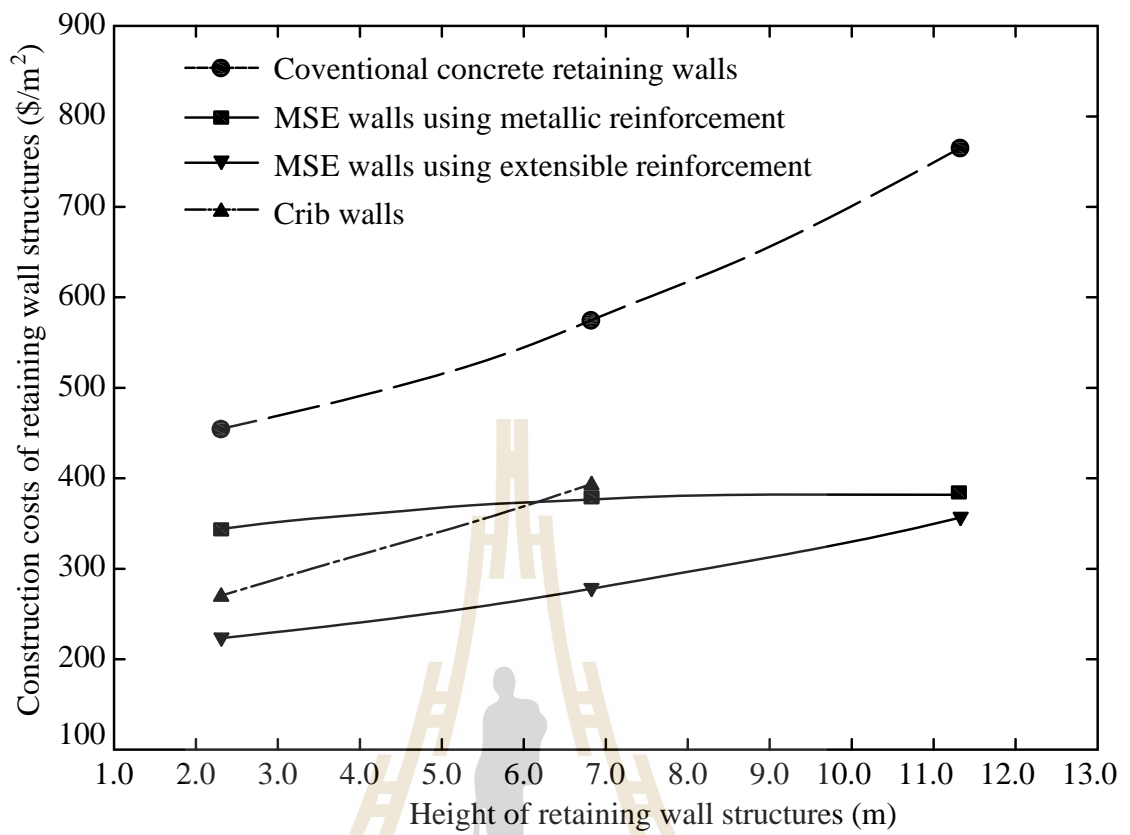
Modern reinforced soil techniques were initially invented in 1957 by a French engineer and architect, Henri Vidal. By 1967, several major MSE walls were built in Europe (Vidal, 1969). Thereafter, the use of reinforced soil techniques was first exploited during repairing a major landslide on Highway No. 39 in the Los Angeles National Forest, CA, the US in 1971. Recently, the MSE walls have been generally recognized as a standard wall type on America's Highways (Alzamora and Anderson, 2009)

Due to its advantages over the conventional retaining forms, the MSE walls have been broadly utilized as retaining wall structures in more than 30 countries throughout the world. The advantages of the MSE walls were illustrated in previous researches (Elias et al., 2001), such as the economic, ease of construction, moderate skilled labors requirement. The MSE walls could be able to tolerate much larger differential settlements than reinforced concrete retaining wall which is unable to accommodate significant differential settlements, it can also be built in poor soil foundation areas. Typical components of an MSE wall are shown in **Figure 2.1**. A summary of MSE walls with its height is larger than 10 meters is summarized in **Table 2.1**. The application of MSE walls may vary from one site to another, but it is possible to be applied in these following conditions:

☑ MSE walls can be used as temporary structures for highway projects.

☑ MSE walls can be exploited as soil retention structures or sea wall.





มหาวิทยาลัยเทคโนโลยีสุรนารี

Table 2.1 A designated of tall MSE walls built worldwide (after Sankey, 2004)

| Places of construction | | | Max. height (m) | Year Complete | Remarks |
|--------------------------------|---------------|--|--------------------|------------------|--|
| Highway 39, | Angeles | | 11 | 1971 | Landslide repair on highway 39 |
| National Forest, CA, USA | | | | | |
| Route I-80, | Glenns Ferry, | | 13.7 | 1977 | To support the Route I-80 |
| USA | | | | | |
| Tweepad Wingwalls, | South | | 41 | 1979 | Diamond mine crusher headwall |
| Africa | | | | | |
| Labadie Plant Slot, | Missouri, | | 20 | 1981 | Supports open coal slot |
| USA | | | | | |
| Calgary, Alberta, Canada | | | 9 | 1984 | Cohesive soil |
| Tsing Yi Island, Hong Kong | | | 40 | 1993 | n/a |
| Santa Barbara primary | | | 22 | 1994 | n/a |
| crushing retaining wall, Chile | | | | | |
| Unicoi County, | Tennessee, | | 28 | 1994 | |
| USA | | | | | |
| Pont de Normandy, France | | | 24 | 1995 | |
| Kennedy Interchange | Atlanta, | | 30 | 1996 | n/a |
| Georgia, USA | | | | | |
| Antelope Mine expansion | | | 22 | 1997 | Scoria rock backfill |
| campbell county, USA | | | | | |
| Crusher retaining wall smokey | | | 23 | 1997 | Designed for 0.25g seismic acceleration |
| valley mine, Nevada, USA | | | | | |
| Kemess Mines South project, | | | 32 | 1997 | Support 830,000 pound haul trucks |
| British Columbia, Canada | | | | | |
| Bingham county truck dump | | | 38 | 1999 | Wall instrumented by Utah state university |
| reloads copperton, Utah, USA | | | | | |
| Mine highway, Arizona, | USA | | 24 | 2000 | Hybrid RE wall |

Table 2.1 A designated of tall MSE walls built worldwide (continued)

| Places of construction | | | Max. height (m) | Year complete | Remarks |
|------------------------------------|--|--|--------------------|------------------|--|
| Crushing system expansion, | | | 32 | 2001 | Mine wall supporting bridge crane |
| Victor, Victor, Colorado, USA | | | | | |
| Route 288, Richmond, USA | | | 24 | 2002 | High friction backfill |
| Springfield interchange, | | | 20 | 2002 | High friction (gravel) backfill |
| Virginia, USA | | | | | |
| Hartsfield Airport runway, | | | 20 | 2003 | n/a |
| georgia, USA | | | | | |
| Port of Seattle, South of Seattle, | | | 46 | 2008 | Expansion of Seattle-Tacoma airport |
| USA | | | | | |
| Hebei, China | | | 40 | 2016 | Railroad truck along the mountain side |

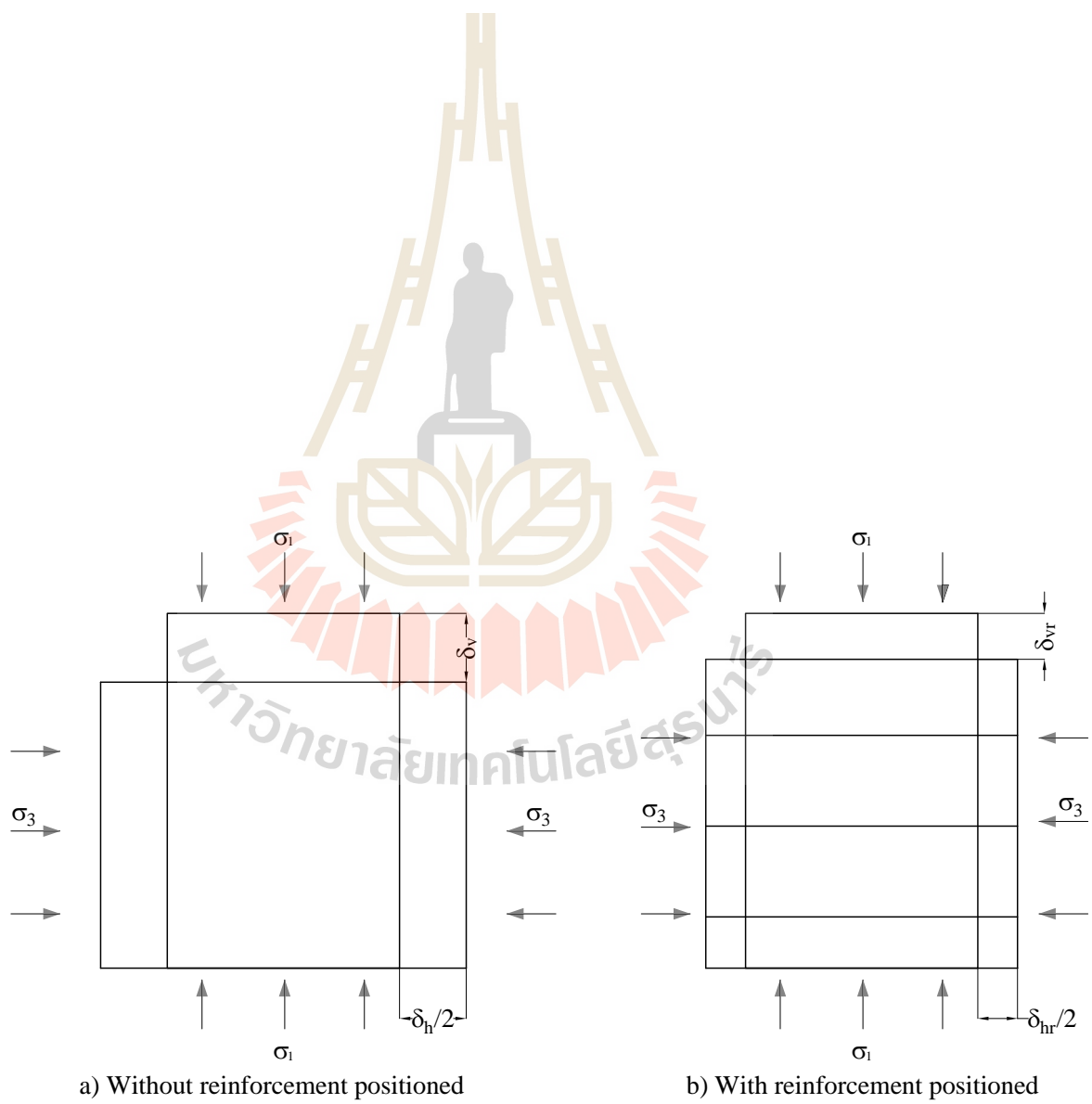
2.2 Behavior and performance of MSE walls

The fundamental behaviors and the performances of MSE walls are briefly described throughout this section. The behaviors of MSE walls are presented in terms of interaction and stresses transferred between main constituents of MSE walls. Lastly, several typical performances of MSE walls are shortly illustrated.

2.2.1 Fundamental behaviors of reinforced earth structures

2.2.1.1 Mechanism of soil – reinforcement interaction

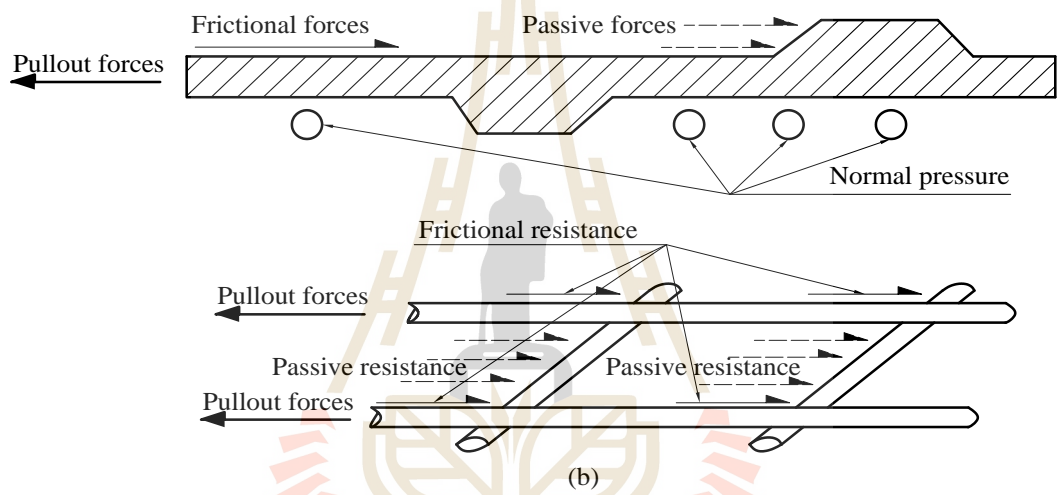
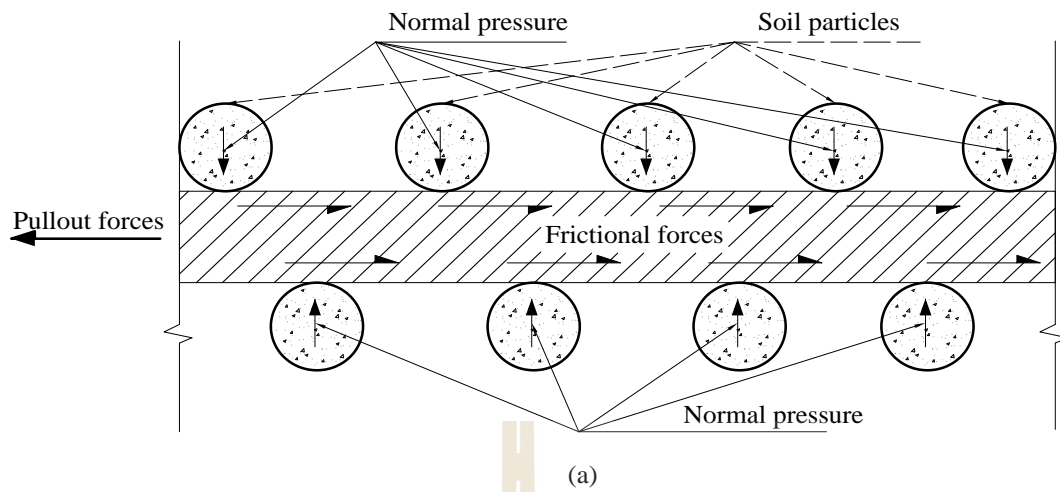
A typical MSE wall comprises four main constituents including alternative reinforcement layers, compacted soil, facing elements and leveling pads (**Figure 2.1**). These four prime constituents have different properties, but a flexible composite structure might be formed due to the simultaneous combination of these four main constituents. The tensile strength of soil is generally found to be lower than



The movements of soil particles are mainly attributed to the development of friction at the interface before sliding takes place. Because of the friction between soil particles and reinforcements, the bonding force is built up. Zornberg and Mitchell (1994) described that the bond strength between the permeable reinforcements and the soil might be higher than undrained soil strength if the transmissivity of geosynthetics is high enough to drain the accumulated water at the soil-reinforcement interface. If an MSE wall is fully filled with a type of cohesionless soil, the bond resistance might be friction that is dependent upon the roughness state of reinforcement and soil. If the backfill is a cohesive soil, the bond resistance is adhesive.

2.2.1.2 Mechanism of stress transfer

The prime function of reinforcements is to limit the movements of MSE walls. In order to fulfill this role, stresses must be transferred from soil elements to the reinforcements. As a reinforced soil mass is subjected to an external stress, the stresses will be generated and transferred within the reinforced soil body. These stresses are generally exhibited in two well-known transfer mechanisms including friction (**Figure 2.4 a**) and/or passive (bearing) resistance as illustrated in the **Figure 2.4 b**. The former one builds up if having a relative movement takes place. The second form defines as passive and/or bearing resistance with its direction is found to be perpendicular to the direction movement of the soil and reinforcement. The participation of each transfer mechanism is significantly affected by several aspects such as the roughness of the reinforcement surface (skin friction), normal pressures, geometry of reinforcement, soil characteristic (Elias et al., FHWA, 2001).



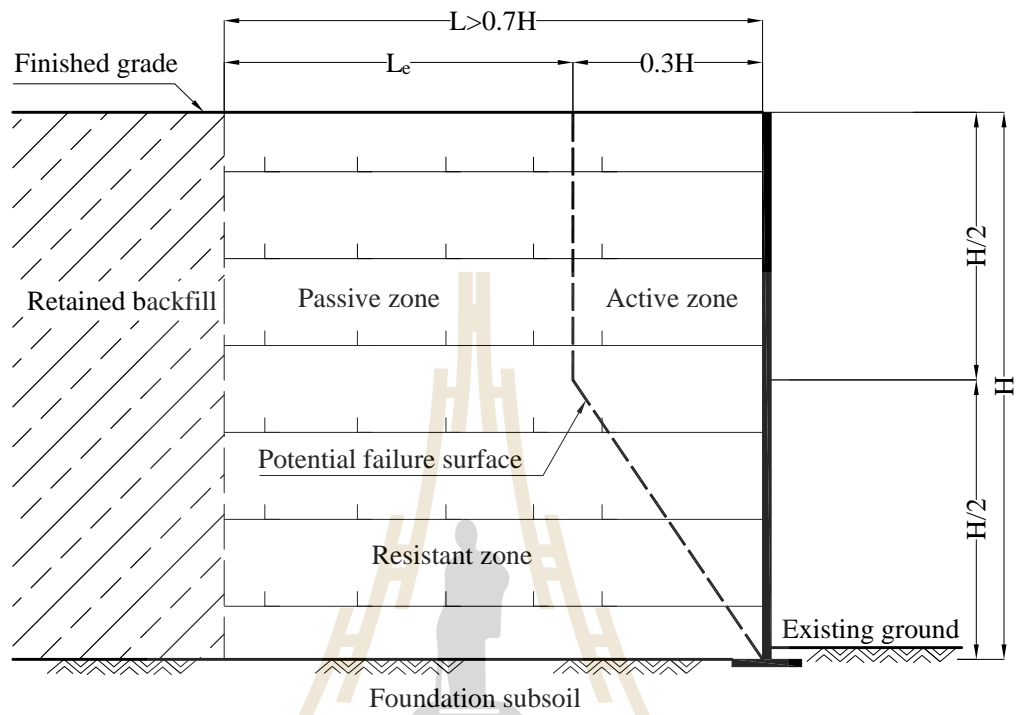
executed by the internal equilibrium of stresses in reinforced soil constituents as well as their strengths.

Schlosser and Long (1974) described that an MSE wall comprises two zones, an active and a passive (or resistant) zone (**Figure 2.5**). These zones are separated by a locus of maximum tension points, T_{\max} , defined as failure surface.

The active zone is laid between the failure surface and the facing wall, where shear stresses developed at the interface between soil and reinforcement is directed towards outside. The movement of reinforced soil that placed within the active zone is restrained by pullout resistance that developed along the soil reinforcements. The passive zone is defined as an area where the interface shear forces on reinforcements are oriented away from the facing elements. The location of the passive zone is behind the failure surface.

The performance of MSE walls was demonstrably described by Mitchell and Zornberg (1995), in which they stated that the performance of MSE walls was significantly affected by the excess pore water pressure, especially for the case that fine-grained marginal soils utilize as backfill.

Moreover, the performance of MSE walls is also significantly dominated by the types of embedded reinforcing materials as well as the forms of soil reinforcements. For examples, the failure of MSE wall with geosynthetics is not so fast and usually accompanied by a larger deformation due to its high extensibilities compared to metallic reinforcements. Another difference is observable in the long-term performance due to the creep phenomenon of geosynthetics. The deformation of geosynthetic reinforced structures generally builds up with time, while the classical



2.3.1 Backfill materials

Among four primary constituents, backfill plays a vital role in the overall performance as well as the construction cost of MSE walls. In term of performance of MSE walls, the selected fill materials should be preferably cohesionless and also have a large friction angle. The backfill should be predominantly coarse - grained soils due to their high strength, drainage and durability properties. Recently, several criteria for backfill have been introduced and applied as shown in **Table 2.2**.

Table 2.2 Backfill criteria of reinforced soil (Koerner et al., 2005)

| Sieve size | Particle size, mm | Requirement of grain size | | |
|---------------------------------|----------------------|---------------------------|-------------|-------------------|
| | | NCMA (1997) | FHWA (1998) | Koerner (1998) |
| Grain size distribution % finer | | | | |
| - | 100 | 75-100 | - | - |
| No.4 | 4.76 | 20-100 | 100 | 100 |
| No.10 | 2.0 | - | - | 90-100 |
| No.40 | 0.42 | 0-60 | 0-60 | 0-60 |
| No.100 | 0.15 | - | - | 0-5 |
| No.200 | 0.075 | 0-35 | 0-15 | 0 |
| Plasticity index | | <20 | <6 | <6 |
| PH range | | 5 – 10 | 5 – 10 | |
| Chlorides, ppm | | < 200 | < 200 | < 200 |
| Sulphates, ppm | | < 1000 | < 1000 | < 1000 |

It can be seen from those three popular criteria, the most rigorous one was recommended by Koerner (1998), in which the amount of particles pass the No. 200

sieve must be approaching to zero, this standard implies that the material is used for backfill should be optimum ones such as clean sand. According to the NCMA, the amount of particles pass sieve No. 200 and plasticity index can be equal to magnitudes of 35%, 20, respectively.

Another feasible type of materials that might be used for MSE walls is fine-grained marginal soils, a type of low permeability materials. Despite being failed to meet the fine particles and plasticity index requirements, the use of such low permeability materials become more popular due to their suitable engineering properties and the recommended backfill materials are scarce. In addition, Stulgis (2005) introduced that in tropical climate countries, granular materials are not readily available in the vicinity of typical construction sites. The residual soils are often marginal lateritic soils which cover large areas in most tropical climate countries. As a result of this natural condition, the consideration of the use of recommended materials as backfill for MSE walls becomes an unmanageable phase. Practically, when considering the need for reducing the construction cost, the use of in-placed marginal soils is a priority. Therefore, it might state that the use of high fine-grained soils for reinforced fill is a realistic demand (Stulgis, 2005). However, as in-placed marginal soils are utilized as backfill materials, care must be paid to the moisture response inside the reinforced soil mass. Previous researchers (Zornberg and Mitchell, 1994; Mitchell, 1995; Koerner and Soong, 2001) stated that both seepage water and accumulation of water appeared behind and under the reinforced system should be either prevented or properly collected and discharged

2.3.2 Reinforcing materials

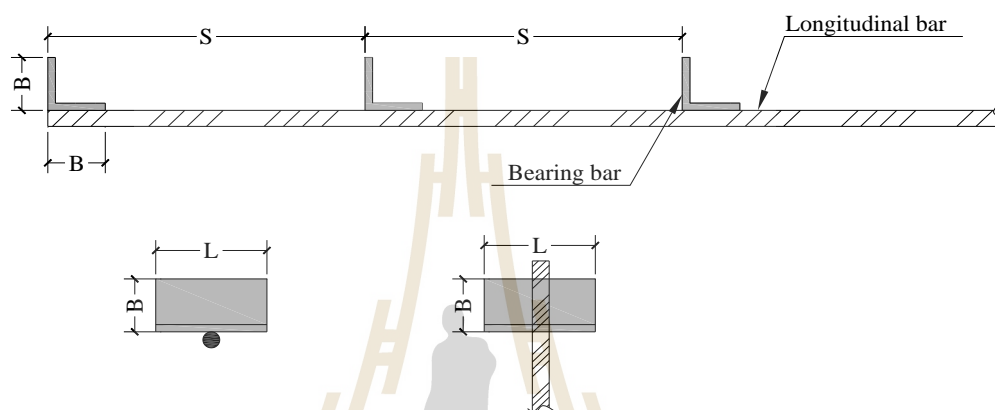
Along with the evolution of reinforced soil techniques, various types of materials have been introduced and developed to be used as reinforcing materials. The use of reinforcing materials in the interior of the soil mass may enhance the tensile strength for soil mass, hence a better stability of MSE walls. Reinforcing materials may have different characteristics, but in terms of extensibility the reinforcing materials could be categorized into two groups, they are inextensible (generally related to steel reinforcements) and extensible reinforcement (generally related to geosynthetic reinforcements).

2.3.2.1 Inextensible reinforcing elements

Recently, several types of inextensible reinforcing elements have been widely used for MSE walls, such as strips, grids, wire meshes. The typical characteristics of some popular inextensible reinforcements are described as:

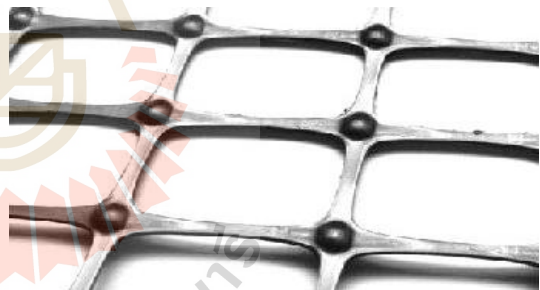
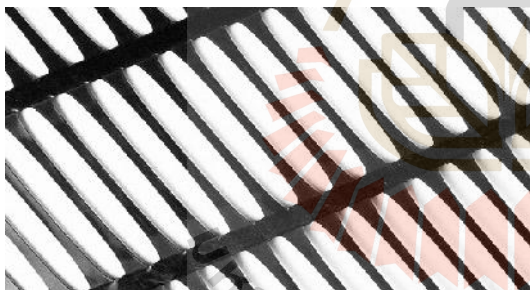
☑ **Continuity steel strips:** The concept of the use of continuity strips has been broadly used for decades. The main advantage of the continuity steel strips is to achieve a better quality of reinforcement connection. Depending upon the specific applications, the dimension of continuity strips could be varied with its breadth is normally laid in a range of (5-100) mm and thickness of (3-5) mm (Nand, 2005). In order to achieve a better performance by increasing the friction between the reinforcing materials and surrounding compacted soils, several protrusions, such as ribs or gloves, are normally attached to the steel strip elements.

☑ **Grids:** This is a type of an open structure which comprises two elements, transverse elements (or bearing elements) and longitudinal members (**Figure 2.6.**).





(a) <http://www.geotextile-fabric.com/products.html>



Uniaxial Geogrid

Biaxial Geogrid

(b) (<http://www.geoace.com/e/geogrid-geogrids.htm>)



(c)

☑ **Geotextiles:** Geotextile is a type of permeable geosynthetic, which is made of textile materials (Elias et al., FHWA, 1998). Two popular types of geotextile are widely used as reinforcement layers, woven geotextile and non woven geotextile (**Figure 2.7a**). Due to their specific hydraulic properties, geotextiles can also function as drainage, separator layers.

☑ **Geogrids:** Geogrids are opening structures formed by bonding polymer strips at their cross points. The primary function of geogrids is to resist the tensile force and add tensile strength to soil matrix. Geogrids are normally formed in two forms, namely uniaxial and biaxial as illustrated in **Figure 2.7 b**.

2.3.3 Facing elements

Positioning in front of the wall, the facing elements contribute to the aesthetics of MSE walls since they are only visible part of the completed MSE walls. The other functions of the facing elements are to prevent soil and reinforcing elements from weathering effect and to retain fill materials.

The facing elements and soil reinforcements need to be fastened using dowels, rods, hexagon headed screws, nuts and bolts (**Figure 2.8**). The considered material is used to make the fasteners should be well-matched with the design life of MSE walls. The designed magnitude of connection strength should be smaller than that of the service-state-connection strength (AASHTO, 2002; INDOT, 2013).

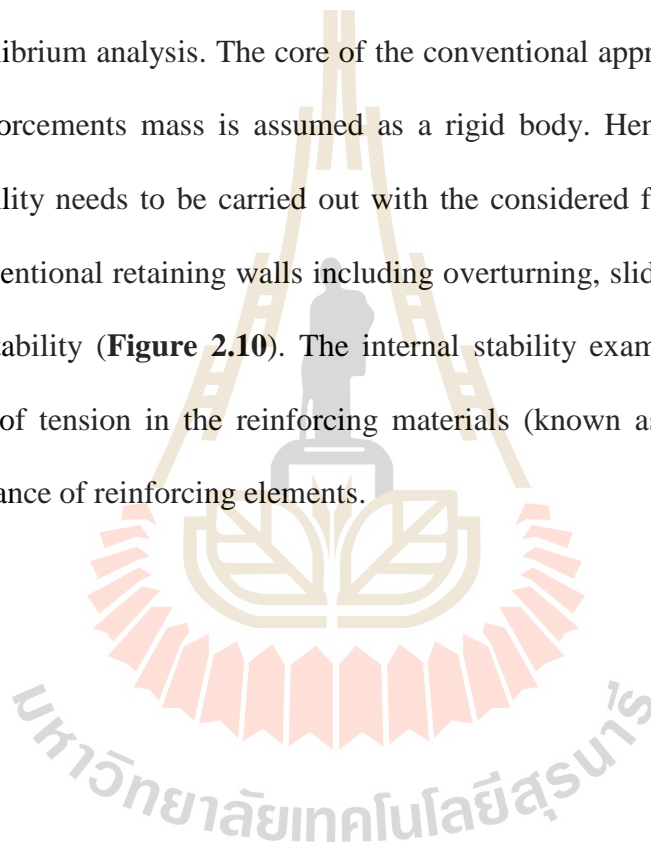


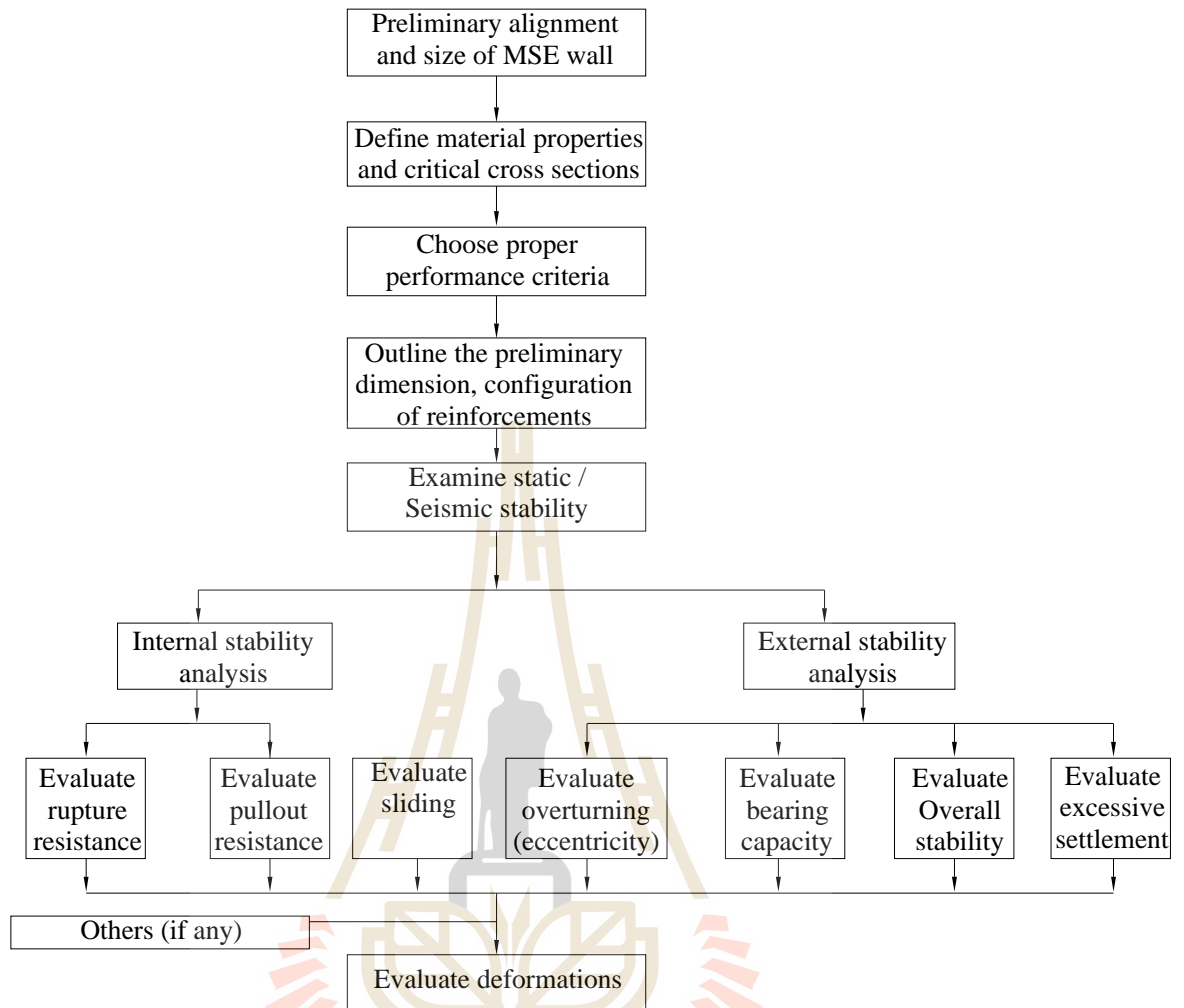
Figure 2.8 Fastener between the facing and reinforcing element used in highway projects in Bangkok, Thailand



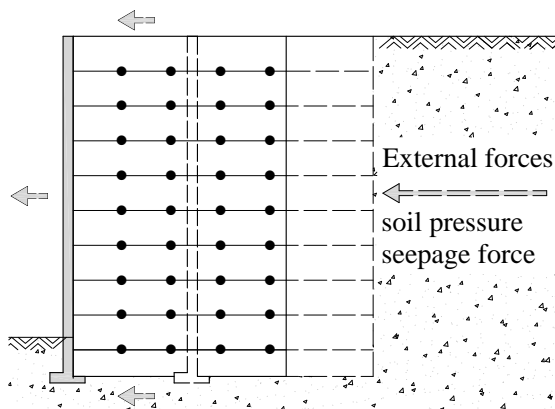
MSE walls comprises: internal and external stability assessment (Lee et al., 1973; Mitchell and Villet, 1987; Anderson et al., 1995; AASHTO, 2002).

Previous researchers (McGown et al., 1998; Horpibulsuk and Niramitkornburee, 2010; Suksiripattanapong et al., 2013) stated that the principal of evaluation of external stability was exactly the same as that for designing the conventional retaining walls, which based on the conventional approach, namely limiting equilibrium analysis. The core of the conventional approach is the composite backfill-reinforcements mass is assumed as a rigid body. Hence, the evaluation of external stability needs to be carried out with the considered failure modes same as those in conventional retaining walls including overturning, sliding, bearing capacity, and global stability (**Figure 2.10**). The internal stability examination comprises an examination of tension in the reinforcing materials (known as rupture failure) and pullout resistance of reinforcing elements.

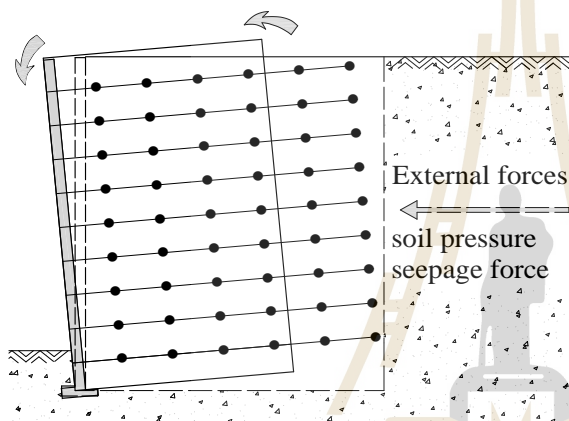




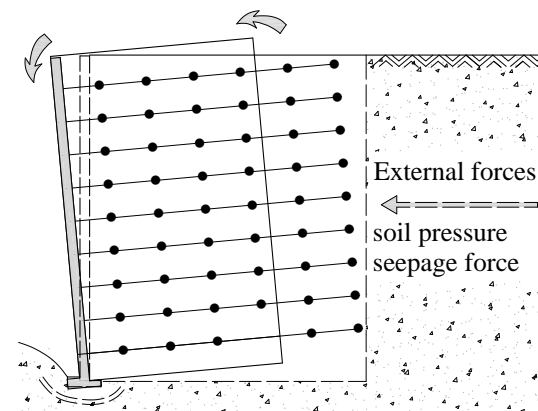
มหาวิทยาลัยเทคโนโลยีสุรนารี



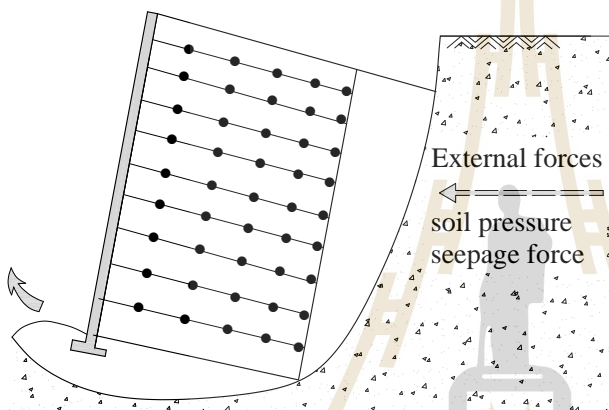
Sliding failure



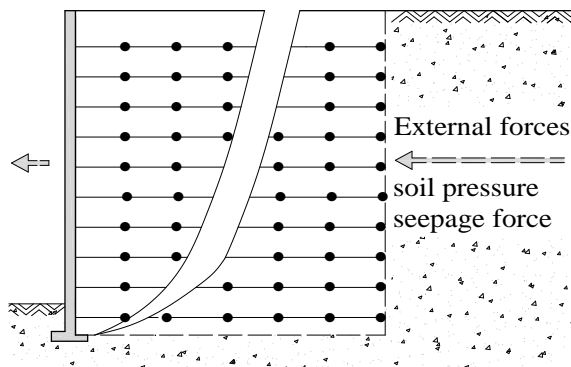
Overturning



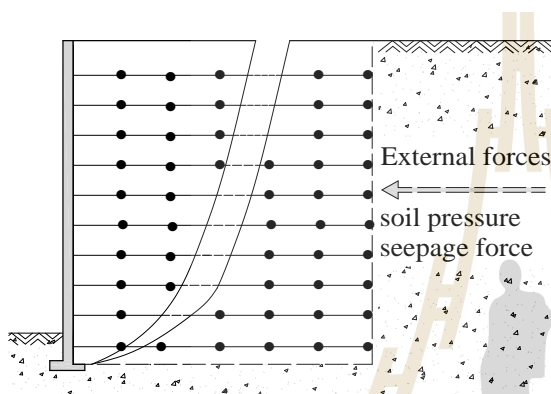
Bearing capacity failure



Global/slip failure



Tension failure



Pullout failure

forms including rupture of and pullout of reinforcements from the backfill soil. Thus, the safety against structural failure needs to be examined with respect to the rupture and the pullout of reinforcement and also reinforcing to facing connection failure.

2.4.1.1 Rupture failure

The first failure form is related to the rupture or breakage or elongation of the reinforcing materials. The rupture failure is mainly attributed to the development of the tensile forces of the soil reinforcements, consequently, the reinforcement is overly stretched following by large movements even the MSE wall could be collapsed. The factor of safety due to the rupture of reinforcement ($FS_{rupture}$) is computed as:

$$FS_{rupture} = \frac{T_{ult}}{T_{max}} \quad (2.1)$$

where $FS_{rupture}$ is the factor of safety due to the rupture of reinforcement, T_{ult} is the ultimate in-air tensile force of reinforcement, T_{max} is the maximum reinforcement loads that can be computed in the following manner:

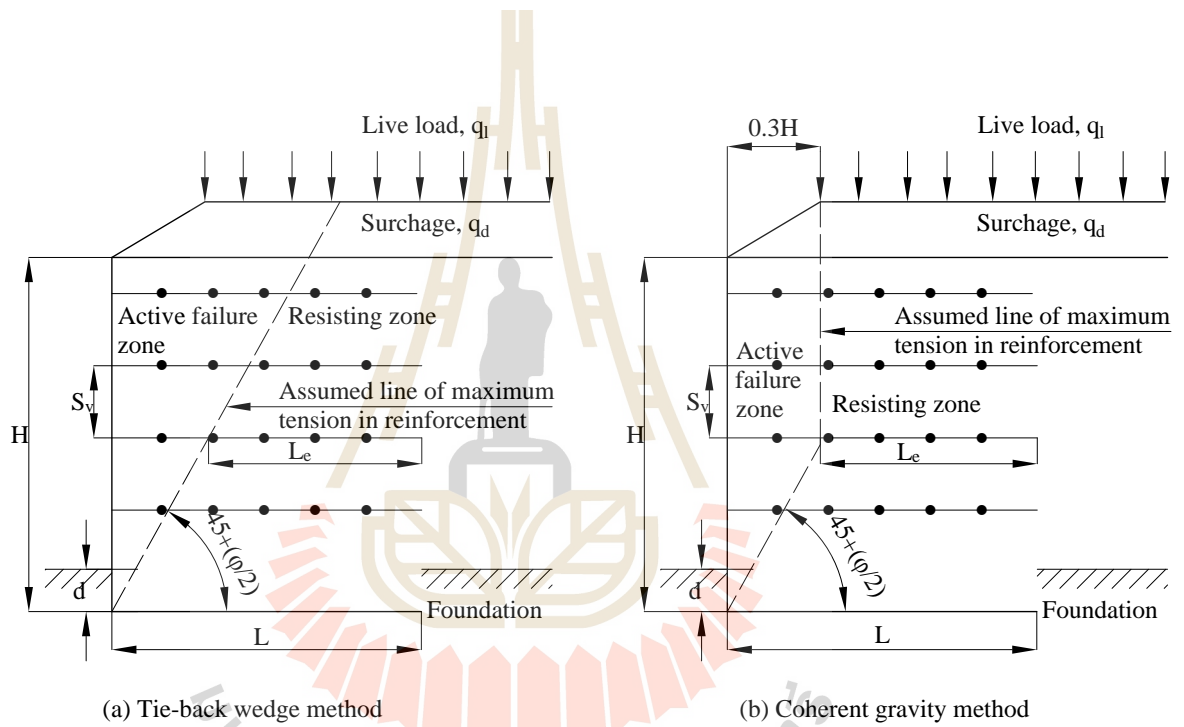
$$T_{max} = \dagger_H S_v = K_r \dagger_v S_v \quad (2.2)$$

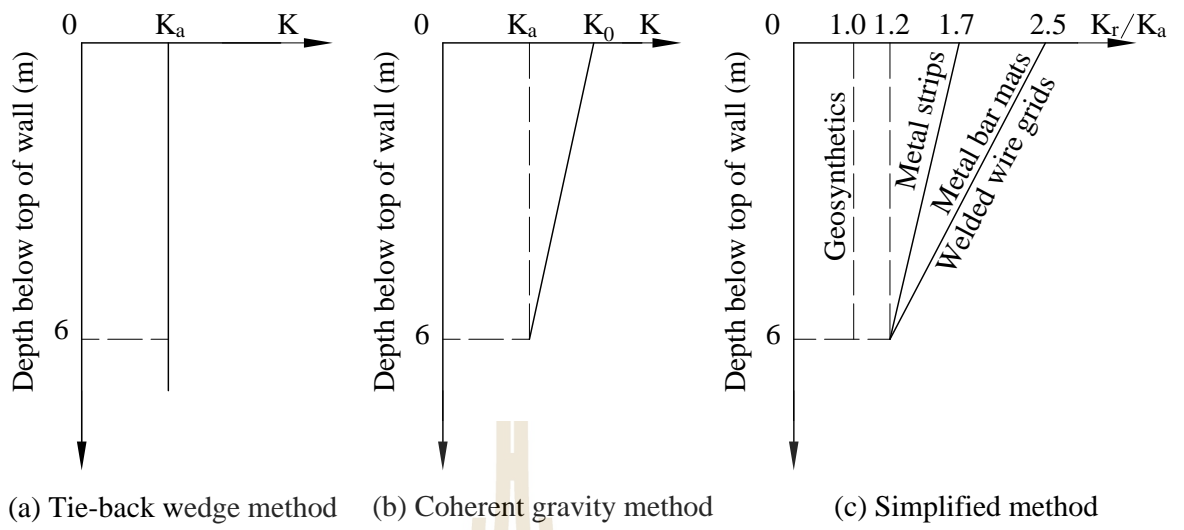
where \dagger_v is overburden pressures, S_v is the vertical spacing of the reinforcement, K_r is coefficient lateral earth pressure which computed based on the mode of failure envelopes considered as shown in **Figure 2.11** and **Figure 2.12**. In the case that the tie-back failure envelope which based on Coulomb/Rankine failure envelope is used for analysis (**Figure 2. 12a**), the lateral earth pressure coefficient K_r is defined as:

$$K_r = K_a = \tan^2 \left(45^\circ - \frac{\phi'}{2} \right)$$

$$K_0$$

$$K_0 = 1 - \sin \phi'$$





$$FS_{pullout} = \frac{P_{max} L_e}{T_{max}}$$

T_{max}

P_{max}

P_f

P_b

resistance is mobilized by soil bearing on the grid transverse members (Bergado et al., 1993; Horpibulsuk and Niramitkornburee, 2010). Therefore, the total pullout resistance, P_{\max} is expressed as:

$$P_{\max} = P_f + P_b \quad (2.6)$$

Bergado et al., (1993) stated that the proportion of friction to bearing resistance of steel grid was 10 percent and 90 percent, respectively. The value of friction resistance is computed as:

$$P_f = (c_a + \tau'_a \tan u) A_s \quad (2.7)$$

where c_a is adhesion of backfill, $c_a = \gamma \cdot c$, u is skin friction angle between reinforcement layer and soil, $u = 0.7w$, τ'_a is the average normal stress, $\tau'_a = 0.75\tau'_v$, (Nielsen and Anderson, 1984), A_s is the frictional area between soil and reinforcement, $A_s = (2b + 2t)L_e$

A similar equation might be used to compute the pullout resistance was proposed by (Jewell et al., 1984) illustrated as:

$$P_f = 2L_r W_r \tau'_n \gamma_{gs} \tan u \quad (2.8)$$

where L_r is designed length of reinforcement, W_r is designed width / diameter of reinforcement, τ'_n is normal stress, γ_{gs} is friction of grid surface area providing direct shear resistance.

Because the pullout resistance might be developed on the reinforcement beyond the failure envelope, hence the term of effective length, L_e , is generally used with its magnitude is computed as:

For the tieback wedge method

$$L_e = L - (H_e - z) \tan(45 - \frac{\phi}{2}) \quad (2.9)$$

For coherent gravity failure envelope

$$L_e = L - 0.3H \quad (2.10)$$

where L is total length of reinforcement in each layer, H is designed height of MSE walls, H_e is equivalent height of MSE wall.

$$H_e = H + \frac{q_d + q_l}{\gamma_f} \quad (2.11)$$

where q_d is the surcharged load, q_l is the live load.

Those above equations are normally employed to compute the pullout resistance of single bearing element (Bergado and Jin-chun, 1994). If having number of bearing elements, the largest magnitude of pullout bearing resistance described as (Horpibulsuk and Niramitkornburee, 2010; Chai, 1992):

$$R = \frac{P_n}{nP_b} \quad (2.12)$$

where P_b is the bearing resistance of single bearing element, P_n is the total bearing resistance with n bearing numbers, R bearing ratio.

The magnitude of pullout resistance was found to be dependent on the geometry of grid reinforcement, thus a dimensionless term of bearing member spacing ratio of S/D is taken into account, where S is defined as the distance between two

contiguous bearing numbers and D is the thickness or diameter of the bearing element. It is, then, the magnitude of the bearing ratio R can be described as:

$$R = a + b\left(\frac{S}{D}\right)^{nr} \quad (2.13)$$

where nr is a constant that depending on the friction angle of backfill shown in **Table 2.3** (Chai, 1992). a, b are constants computed based on two conditions as follows (Bergado et al., (1994, 2001)):

Condition 1: The maximum pullout force equals to friction resistance when S/D of 1.

$$P_n = 2LW (c' + \sigma'_v \tan \phi') \quad (2.14-1)$$

where LW is cross section of interface between soil/reinforcement.

Condition 2: The bearing ratio, R equals to 1.0, when the S/D of 45. Consequently,

$$p_n = nP_b \quad \text{when } S/D = 45 \quad (2.14-2)$$

where n bearing numbers

Table 2.3 Magnitudes of constant factor nr (Chai, 1992)

| No | Backfill soil friction angle (degree) | nr |
|----|---------------------------------------|------|
| 1 | <25 | 1 |
| 2 | 25 – 35 | 3/4 |
| 3 | 35 – 45 | 2/3 |
| 4 | > 45 | 0.5 |

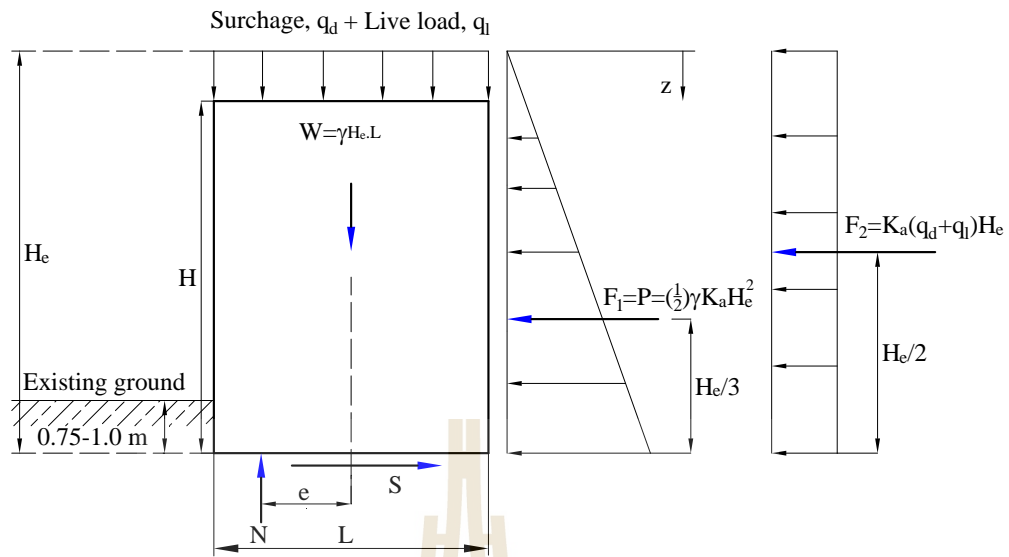
In short, under internal stability analysis, MSE walls may be failed due to pullout of the soil reinforcements or due to the breakage of soil reinforcements. The former failure form takes place when the maximum frictional resistance developed along the surface of the soil reinforcements is achieved. The factor of safety for internal stability analysis, $FS_{internal}$, is considered as the minimum value of safety factor obtained from rupture and that computed from pullout failure analysis:

$$FS_{internal} = \min (FS_{rupture} ; FS_{pullout}) \quad (2.15)$$

2.4.2 Design criteria for external stability

External stability analysis is predominately executed based on the conventional method, in which the external instability happens as arising a failure surface passes behind and underneath all prime constituents of the MSE walls. Thus, the criteria for external stability analysis for MSE walls must comply with that employed for conventional gravity retaining walls such as sliding of MSE over foundation soil, overturning of reinforced soil mass around its toe (limiting eccentricity), bearing capacity failure, overall stability (Tensar, 1986; FHWA, 1998; NCMA, 2009).

Depending on the specific conditions, an MSE wall might be subjected to various external loads. The common external forces that acting on an MSE wall comprises the reaction at the base, N , lateral earth pressure, P , water pressure, surcharge and live loads (**Figure 2. 13**).



F_d

$$FS_{sliding} = \frac{\sum \text{resisting forces, } F_r}{\sum \text{driving forces, } F_d}$$

$$F_r = S + cL = W \tan \phi + cL = \gamma H_e L \tan \phi + cL = L(\gamma H_e \tan \phi + c)$$

$$F_d = F_1 + F_2 = \frac{1}{2} \gamma H_e^2 K_a + (q_d + q_l K_a H_e) \quad (2.17)$$

2.4.2.2 Bearing capacity failure

The safety factor of an MSE wall against the bearing capacity failure of foundation, $FS_{bearing}$, is defined as:

$$FS_{bearing} = \frac{\text{Ultimate bearing capacity, } q_{ult}}{\text{Maximum pressure underneath foundation, } q_{max}} \quad (2.18)$$

$$q_{ult} = cN_c + \gamma d(N_q - 1) + \frac{1}{2} \gamma B' N_\gamma \quad (2.19)$$

where d is embedded depth of foundation, B' effective width or Meyerhof's reduced width of foundation which equals to $(B - 2e)$, B is the designed width, e is eccentricity of resultant force acting underneath of foundation. N_q, N_c, N_γ are defined as bearing factors (Meyerhof, 1963; Bergado and Jin-Chun, 1994; Horpibulsuk and Niramitkornburee, 2010)

$$N_q = e^{f \tan \phi} \tan^2 \left(45 + \frac{\phi}{2} \right) \quad (2.19 \text{ a})$$

$$N_c = (N_q - 1) \cot \phi \quad (2.19 \text{ b})$$

$$N_\gamma = 2(N_q + 1) \tan \phi \quad (2.19 \text{ c})$$

The distribution of pressure that developed underneath foundation might be formed in two forms depending on the position of the resultant forces as shown in **Figure 2.14**.

$$q_{\max} = \frac{N}{B} \left(1 + \frac{6e}{B}\right) \quad \text{when } e < B/6$$

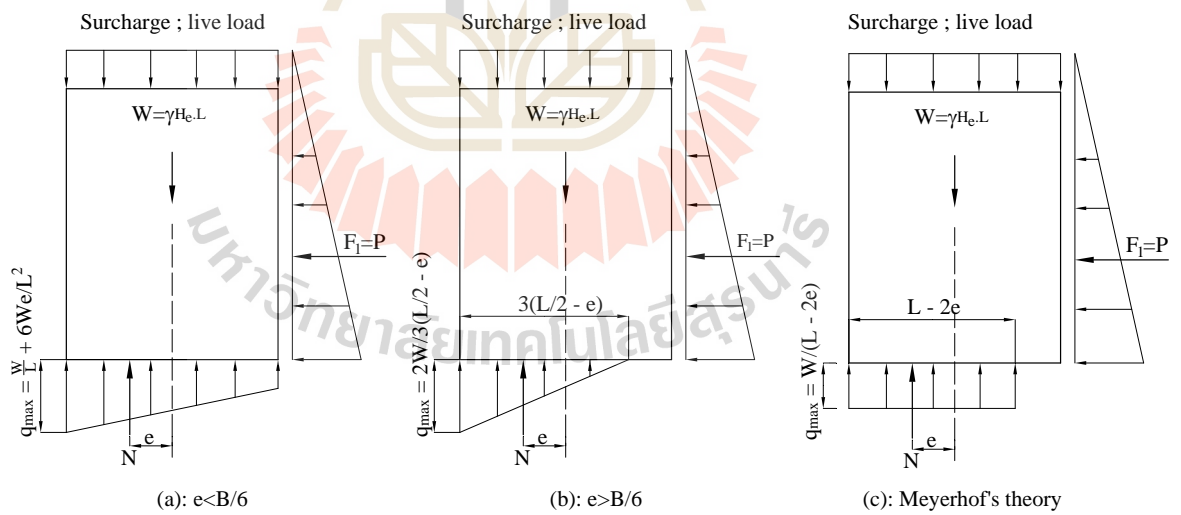
$$q_{\max} = \frac{N}{B'} = \frac{2N}{3\left(\frac{B}{2} - e\right)} \quad \text{when } e > B/6$$

$$q_{\max} = \frac{N}{B'} = \frac{2N}{(B - 2e)}$$

N

B

e



2.4.2.3 Overturning of MSE wall

Similar to conventional retaining walls, MSE walls tend to horizontally move outward from the face or overturn their own toes due to the thrust acting beside, which causes the driving moment developed. The factor of safety against overturning of MSE wall, FS_{overturn} , is defined as:

$$FS_{\text{overturn}} = \frac{\sum \text{Moments resisting}, M_r}{\sum \text{Moment overturning}, M_d} \quad (2.22)$$

$$M_r = W_{\text{net}} \frac{B}{2} \quad (2.23)$$

$$M_d = P \frac{H_e}{3} \quad (2.24)$$

where overturning moment, M_d , is developed due to driving forces, W_{net} is the weight of the equivalent height wall.

2.4.2.4 Global failure

The typical character of global failure is that the bi-linear slip failure surface completely passes through and under the protected zone. This type of failure is representative of the bearing capacity of the foundation materials. The global stability failure may be taken place under some complex conditions, such as high surcharge loads, weak soil foundation. The evaluation of global failure can be relied on the approach of limiting equilibrium analyses. The fundamental of these analyses are that the configuration of assumed potential failure plane needs to be evaluated until the lowest magnitude of safety factor found. The computed safety factor needs to be less than the allowable value (**Table 2.4**)

Table 2.4 Recommended minimum factors of safety (AASHTO, 2002)

| No | Modes of failure | Minimum of factor of safety |
|-------------------|--|-----------------------------|
| External failures | | |
| | <i>Sliding failure</i> | 1.5 |
| | <i>Overturning failure</i> | 2.0 |
| | <i>Bearing capacity & excessive settlement</i> | 2.0 – 2.5 |
| | <i>Global / Overall stability</i> | 1.3 – 1.5 |
| Internal failures | | |
| | <i>Pullout failure</i> | 1.5 |
| | <i>Tension failure (tensile overstress)</i> | 1.0 |
| | <i>Internal sliding</i> | 1.5 |
| Local stability | | |
| | <i>Facing connection</i> | 1.5 |
| | <i>Block connection</i> | 1.5 |
| | <i>Bulging</i> | 1.5 |

In summary, to achieve the required performance and service life of MSE wall, the behavior of reinforcement should be clearly understood, also the appropriate methods that mainly depend on the reinforcement types need to be precisely chosen. Among four popular methods including coherent gravity method, simplified method, tieback wedge method, and structure stiffness method, the coherent gravity was recommended to be appropriate for the case that MSE walls reinforced by metallic reinforcements, and the tieback wedge method was recommended for MSE wall using extensible reinforcements (Anderson et al., 2012). Similarly, to minimize the possibility of failure of MSE walls, three vital stability analyses such as external stability, internal stability, global stability should be thoroughly examined.

2.5 Case studies of MSE walls failures

Along with the growth of MSE walls, a numerous failures cases of MSE walls have been reported. Most observations and researches suggest that poor performance is linked to construction activities, some can be attributed to design, material selection and alleviation of weak foundation structures are also other causes of instability of MSE walls.

A failure case of MSE wall was investigated by Burwash and Frost (1991), the MSE wall was fully filled with low plastic clay. Prior to the first sign of settlement behind the wall was found, the MSE wall was satisfactorily performed for 16 months. The investigation found that the crucial cause induced the distress of the wall was related to the saturation of backfill. Particularly, the water content of backfill was exceedingly increased compared to that obtained during the construction process, as a result of this, the backfill was found to be saturated and got much softer than when filled. The reason for saturation occurred was related to ponding of surface water during a heavy rain of 40 mm in 24 hours.

Elias and Swanson (1983) performed a study on the termination of earthwork due to adverse weather condition when constructing an MSE wall that was built during the winter of 1978-1979 in Virginia – USA. The wall was found to be tilted of around 250 to 300 mm compared to designed location after a normal rainfall happened. After investigation on possible causes of the movements, they found that the exploit of high fine-grained backfill (the backfill contained up to 50% fines) with steel strips might bring about a considerable decrease in pullout capacity. Accordingly, the internal instability of MSE wall was observed.

26 poor performance cases of MSE walls in United State were examined by Koerner and Soong (2000). They found that 17 of 26 cases were related to the use of low permeability backfill, kind of poorly draining material, in the protected zone. In conclusion they suggested that if the MSE walls filled with this type of backfill, a proper drainage system needs to be positioned within the MSE walls.

In his research, Stulgis (2005) stated that the use of poorly draining backfill was a major cause of poor performance of the MSE wall that was undergone a significant movement. As the backfill gets moisture due to rainfall, groundwater infiltration, or other sources, the hydrostatic pressure can be built up, consequently, the stability of MSE walls can be significantly affected.

In conclusion of an investigation on an MSE wall's failure, Narejo and Ramsey (2001) stated that the primary cause of MSE wall failure was associated with hydrologic design issues. They suggested that the influence of seepage responses could be minimized by positioning a drainage system on top of, and at the front of MSE walls. Also, to prevent the backfill from "flowing", a filter geotextile should be positioned. Lastly, due to providing a high benefit/cost ratio, a geocomposite drainage system should be placed in MSE walls.

Hossain et al., (2011) conducted an assessment of an MSE failure that was constructed in May 2004, in Texas, USA. After 5 year-service, the movement of MSE wall was found with its magnitude of more than 150 mm wide. The MSE wall was then reinforced, but the rate of wall movement was considerably increased of around of (2.5-4 mm/month) since June 2010, even several facing panels were bulged. In conclusion, they reported that the reason for the significant movement of MSE wall

was because of the exploit of high fine-grained soils, with the magnitude of fine-grained particle found of around 15%.

There were two case histories of MSE walls failures described throughout a research conducted by Scarborough (2005). Clayey soil backfill and geosynthetic reinforcements were used to construct those MSE walls. One of the two walls failed, namely wall A, and the other undergone a large deformation, but still remained in service. After carrying out an investigation, they exploded that the reason for the failure of wall “A” was likely because of poor drainage system installed. Particularly, due to the use of inadequate drainage system, the water pressure behind the facing was built up leading to the failure of wall “A”, while only because of insufficient geogrid reinforcements, the serviceability of wall “B” was significantly affected. In conclusion, they suggested that the process design, as well as the geotechnical engineers, need to pay more attention to the importance of seepage responses within the MSE walls, type of drainage system placed within the compacted soil mass.



Figure 2.15 An actual failure of MSE wall (adopted from Scarborough, 2005)

In their research, Chen et al., (2007) found that the loosing sand from MSE wall was because of the seepage water that flows through the MSE wall via the juncture as well as the ruptured points of drainage system.

Shibuya et al., (2007) reported an investigation on a terrible failure of an MSE wall in Yabu City that took place in 2004 after typhoon attack. Specifically, the reduction in soil strength was associated with the insufficient capacity of the drainage system, even the MSE wall was designed and built under the design code. Lastly, they concluded that the conventional drainage system recommended in the current design manuals was not applicable for a large amount and/or high level of ground water that occurs in the mountainous area.

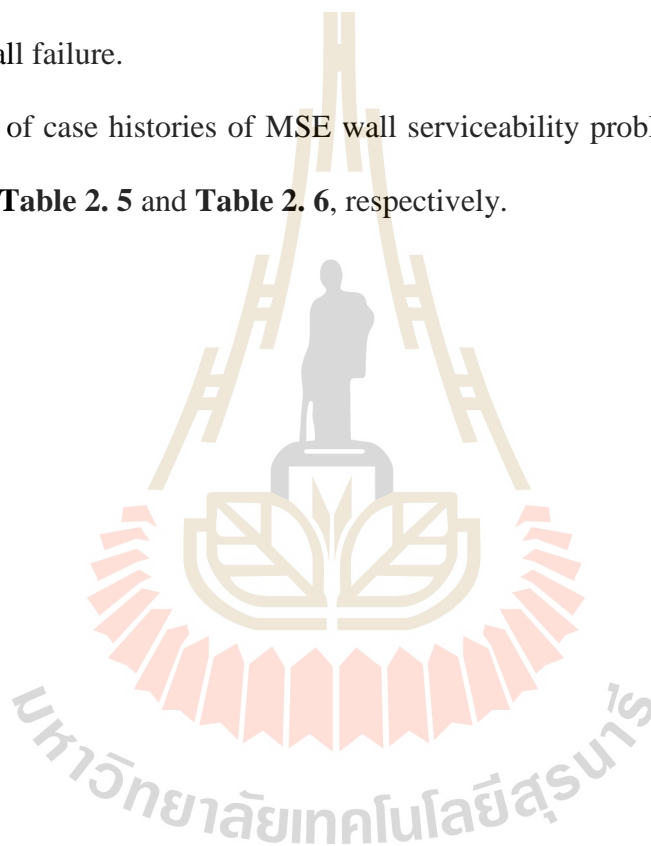


Figure 2.16 Loosing sand from MSE wall (adopted from Chen et al., 2007)

Mahmood (2009) conducted an examination on a failure of an MSE wall that was constructed in Maryland (USA). The MSE wall was observed a significant movement, especially at the top of the wall. The obtained results showed that the

movement of the top of wall was around of 12 inches to 18 inches. To predict the possible causes, the computer program Plaxis was utilized to perform a series of numerical analysis, mode of failure, as well. In conclusion, they reported that the combination of affecting aspects, such as inadequate installation geogrid, insufficient length of geogrid, was the main cause of the failure of the wall. Besides, the use of poorly draining backfill, and improper drainage system, was also another factor that caused the wall failure.

A list of case histories of MSE wall serviceability problem and actual failure are shown in **Table 2. 5** and **Table 2. 6**, respectively.



| No | Facing | GS-Type | Year | Service Time | Cause | Problem | Soil backfill | Weather condition | Literatures |
|----|--------|---------|------|--------------|------------|-------------------------|---------------|-------------------|------------------------|
| 1 | CAW | GG | 1984 | 3 years | Design | Wall rotated | Clay (ML-CL) | Cold climate | Burwash & Frost, 1991 |
| 2 | CAW | GG | 1990 | | Design | Bulged | Sandy soil | - | Christopher, 1993 |
| 3 | SRW | GG | 1990 | | Design | Bulged | Sandy soil | Unkown | Bathurst & Simac, 1994 |
| 4 | SRW | GG | 1994 | UCP | Design | Bulged | - | Rainy | Sandri, 1997 |
| 5 | SRW | GG | 1994 | UCP | Contractor | Bulged | - | - | Sandri, 1997 |
| 6 | SRW | GG | 1994 | UCP | Contractor | Low configuration | - | - | Sandri, 1997 |
| 7 | SRW | GG | 1994 | UCP | Contractor | Positioning of block | - | - | Sandri, 1997 |
| 8 | SRW | GG | 1994 | UCP | Contractor | Depth of footing | - | - | Sandri, 1997 |
| 9 | SRW | GG | 1995 | 6 months | Design | Deformed throughout | Clay | Rainy | Koerner, 1998 |
| 10 | PPW | GG | 1995 | 4 years | Design | Bulged | Clayey silt | - | Koerner, 1998 |
| 11 | SRW | GG | 1998 | 8 years | Design | Bulged | Silty clay | Rainy | Koerner, 1998 |
| 12 | CSL | n/a | 2005 | 10 years | Design | Loss of backfill | Sandy gravel | - | Chen et al., 2007 |
| 13 | PPW | SM | 2009 | 5 years | Design | Bulging of facing panel | Granular soil | - | Hossain et al., 2011 |

Table 2. 6 Case histories of walls actual failures (adopted from Koerner et al., 2005)

| No | Facing | GS-Type | Year | Life Time | Cause | Reason | Soil backfill | Weather condition | Literatures |
|----|--------|---------|------|-----------|-------------|-----------------------|-------------------|-------------------|------------------------|
| 1 | Timber | GT | 1987 | 3 months | Constructor | Connection overlooked | No compaction | - | Richardson, 1998 |
| 2 | SRW | GG | 1990 | 6 months | Constructor | GG-overlooked | Clay | - | Leonards, et al., 1997 |
| 3 | SRW | GG | 1992 | 2 months | Design | Global/compound | Sand | Dry | Berg, et al., 1997 |
| 4 | CAW | GG | 1992 | - | Design | | Silty clay | | Huang, 1994 |
| 5 | CAW | GG | 1992 | - | Design | Hydrostatic pressure | Silty clay | | Huang, 1994 |
| 6 | SCP | GG | 1992 | - | Design | | Silty clay | Heavy rain | Huang, 1994 |
| 7 | SRW | GT | 1993 | 3 years | Design | | Silty clay | | Gassner, et al., 1998 |
| 8 | SRW | GT | 1994 | 2 years | Constructor | GT overlooked | Clay | | Gassne, et al., 1998 |
| 9 | SRW | GG | 1994 | - | Design | | improper drainage | Rainy | Sandri, 1997 |
| 10 | SRW | GG | 1996 | 1 year | Design | | Clay | Heavy rain | Koerner, 1998 |
| 11 | SRW | GG | 1997 | 1 year | Design | Hydrostatic pressure | Clay | | Koerner, 1998 |
| 12 | SRW | GG | 1998 | 1.5 years | Design | | Clay (ML-SP) | Rainy | Koerner, 1998 |
| 13 | SRW | GG | 1998 | 8 months | Design | | Silty Clay | | Koerner, 1998 |
| 14 | SRW | GG | 1998 | 1 year | Design | | Clayey Silt | | Koerner, 1998 |

Notes:

CAW = covering around wall

SRW = segmental retaining wall

PPW = Precast panel wall

GG = Geogrid

GT = Geotextile

UCP = Under Construction Process

SM = Steel Wire Mesh

- not applicable to problem.

From the literature review of recent design criteria and histories failures cases of MSE walls, several conclusions can be withdrawn as follows:

☑ *As a kind of compacted soil, reinforced soils are generally stiff and strong since it is able to sustain soil suction. However, excessive deformation has been reported which found to be due to the decrease in soil suction, especially under wetting process, which leads to a poor performance of reinforced soils.*

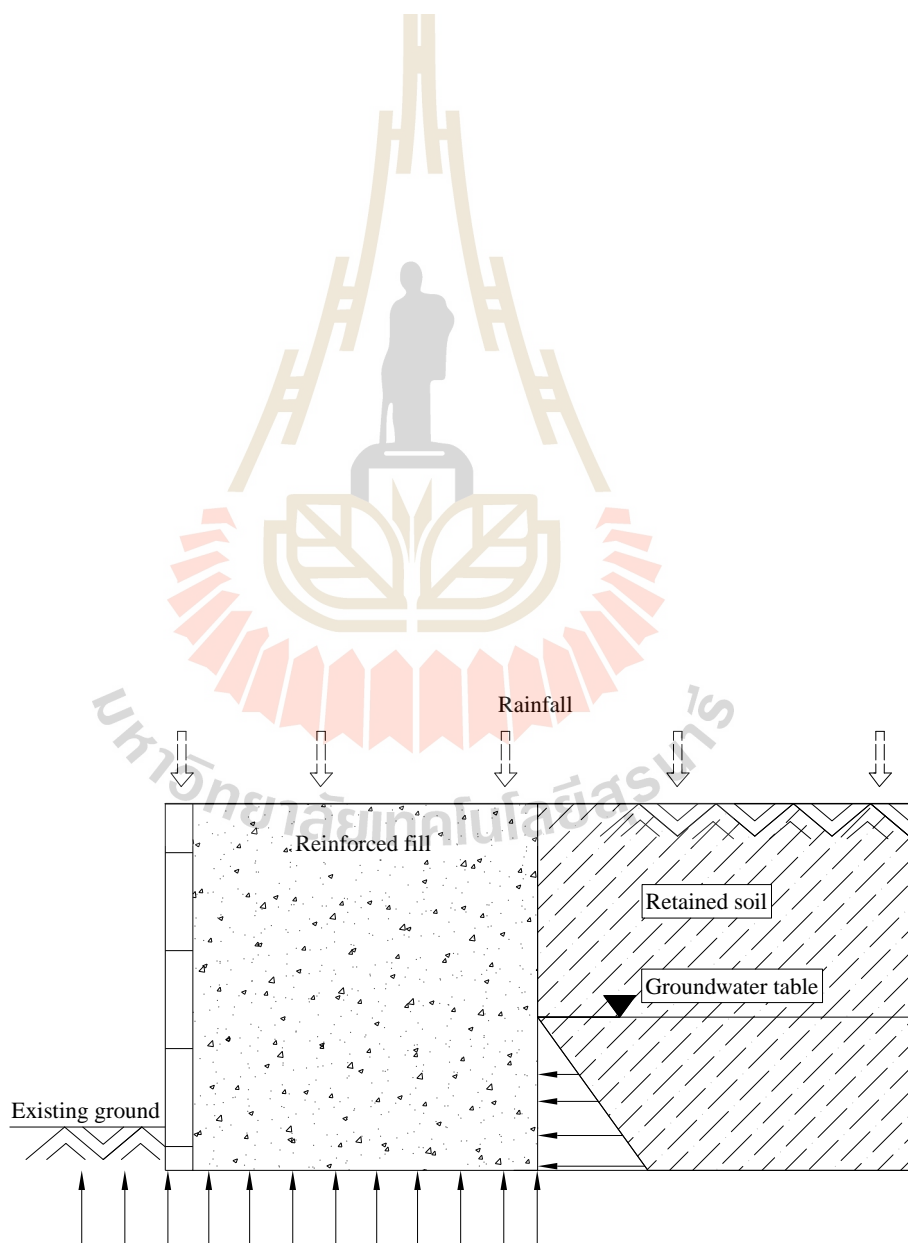
☑ *The existence of water within and nearby the MSE walls can cause the insecurity of MSE wall due to the development of pore water pressure, hydrostatic pressure.*

☑ *Obviously, there is a significant influence of seepage responses on the stability of MSE wall. However, the current design criteria and construction manual for MSE walls do not much consider effects of such vital aspects. Similarly, the regular design code of MSE walls is assumed to contain “free drainage” components such that all accumulated water could be speedily discharged around or/and through the protected zone mass. This must be an expected design, but it also implies that the MSE wall must be fully filled with gravel material or sands.*

☑ *The use of in-placed marginal soils as backfill becomes more frequent. This scenario is feasible if drainage behind the protected zone could be positioned.*

2.6 Recent strategies to handle seepage flow of MSE walls

As summarized from the case studies of MSE walls failures, it might be obviously found that most failures of MSE walls were predominantly related to the improper drainage system as well as the seepage water flow within or nearby the protected zone. The influence of water pressure on the performance of MSE walls is apparently found, it increases the driving forces significantly, whereas the soil



To minimize the influence of the surface water, two popular drainage systems were recommended by Koerner (2011), namely inlet and piping systems, shifted inlet and piping. The difference in these two techniques is their location. The former ones is positioned within the protected zone, while the shifted systems is placed behind the protected zone as illustrated in **Figure 2.18**

2.6.2 Methods to eliminate the effect of seepage flow

Recently, a number of alternatives have been initiated and exploited to deal with the influences of seepage water flow through the MSE walls, such as using free-draining materials, installing a vertical drainage system behind the front wall, placing inner drainage system within the protected zone. Among the alternative techniques, the use of permeable geosynthetic reinforcements may be particularly appropriate for MSE walls that utilize poorly draining materials, such as in-placed marginal soils, as fills due to its drainage capacities compared to others. Below is a brief description of those popular alternatives:

(a) Koerner (1998) reported that the increase in seepage pressure in the protected zone can be avoided using free-draining materials, such as sand or gravel. However, the use such good draining materials are not always available, especially in the tropical climate area where residual soils are normally found to be marginal lateritic soils.

(b) Positioning vertical drainage systems behind the facing element and the protected zone using free draining materials. However, these techniques have been reported to be not easy for installation such vertical draining path, also not be able to protect whole the protected zone (Shibuya et al., 2007).

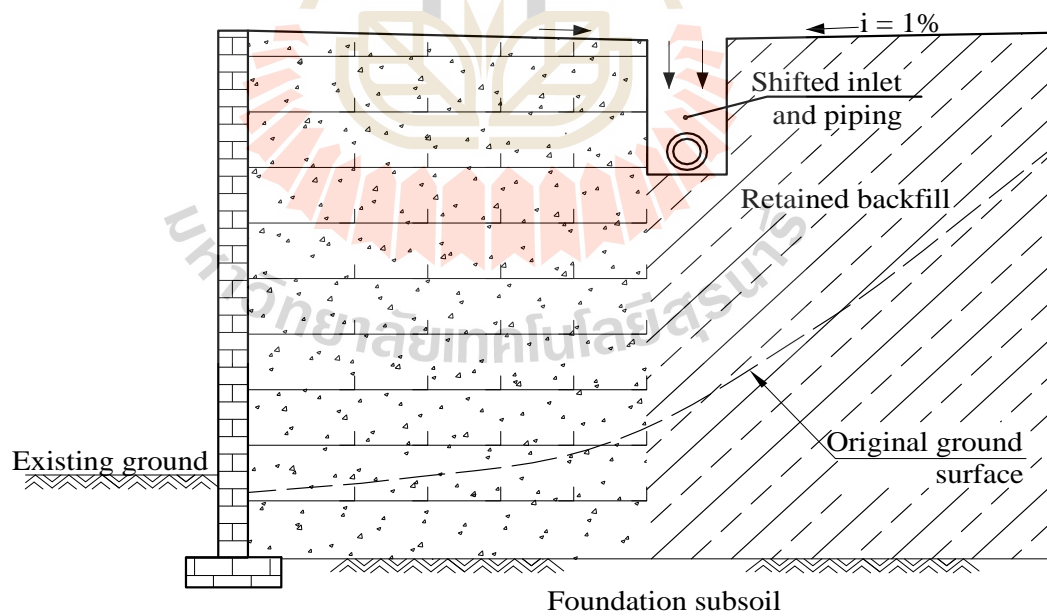
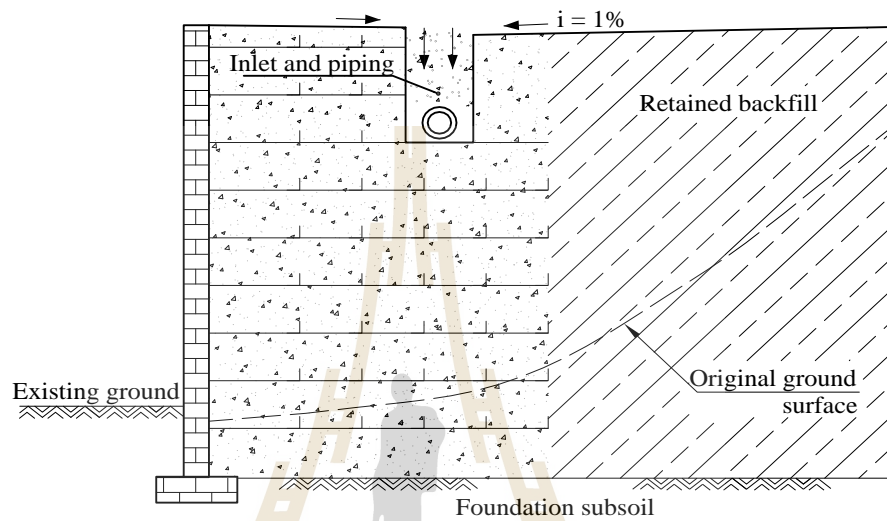
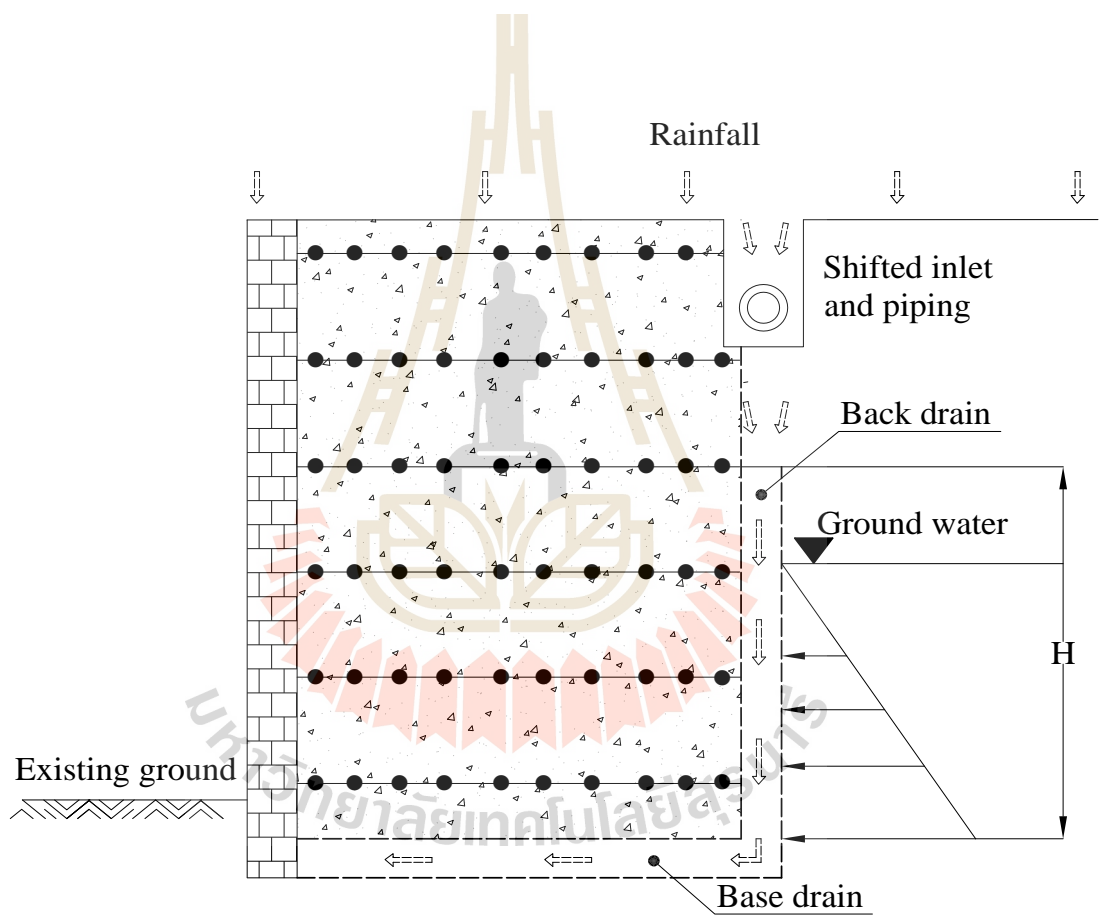


Table 2.7 Some recent approaches to minimize the effect of seepage flow

| No | Approaches | Advantages | Disadvantages | Proposed by |
|----|--|---|--|--|
| 1 | Use good draining soils, such as sand or gravel | <ul style="list-style-type: none"> ♦ High strength ♦ Compact easily ♦ Excess pore water pressures could be quickly decreased ♦ Avoid seepage pressure builds up | <ul style="list-style-type: none"> ♦ Costly ♦ Not be always available ♦ Not easy to construct a vertical drainage layer. | Koerner, 1998 |
| 2 | Increase length of protected zone | <ul style="list-style-type: none"> ♦ Be able to resist the seepage forces. | <ul style="list-style-type: none"> ♦ Increase in construction cost ♦ In-situ earthwork increases | n/a |
| 3 | Positioning an internal drainage system within the protected zone using geocomposite | <ul style="list-style-type: none"> ♦ High permeability ♦ Ease of transportation and placement ♦ Do not yield overloading due to its light weight ♦ Improved economy ♦ Consistent properties ♦ Reduce excavation | <p>Excessive chemical and biological clogging can significantly affect the filter and drain performance of geocomposite materials (FHWA, 1998; Wu, 2006)</p> | <p>Mitchell, 1995</p> <p>Zornberg, 1994</p> <p>Chen et al., 2007</p> |
| 4 | Provide suitable drainage beneath and behind the protected zone | <ul style="list-style-type: none"> ♦ Minimize the hydrostatic force ♦ Reduce downstream water level behind the protected zone | <p>Construction must be extensively instrumented to ensure the location, direction of the drainage system.</p> | n/a |



the body of the protected zone. The geocomposite materials generally comprise a core material of geonet which covered by two geotextile layers to avoid long term clogging.

2.6.2.2 Discontinuous back drain

The use of continuous back drain is necessary for several specific conditions, such as thawing phenomena, and when impervious soils are likely to yield an excessive amount of water in backfill and foundation soils. In other scenarios, discontinuous form should be considered and applied. The discontinuous form is similar to discrete “chimneys” or called as chimney drains as shown in **Figure 2.20** (Koerner, 2011).

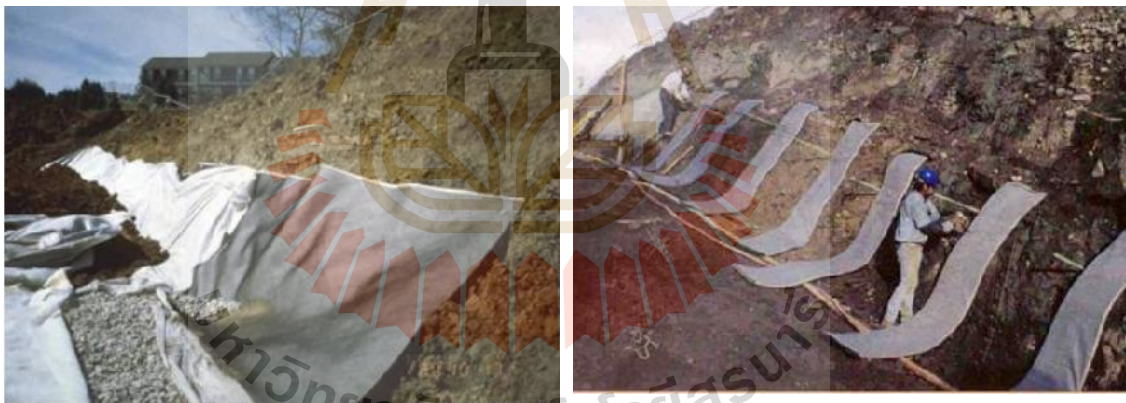


Figure 2.20 Use of continuous and intermittent geocomposite back drains (adopted from TenCate Geosynthetics, Inc).

2.6.2.3 Drainage within the protected zone

In the interior of the protected zone, the prime function of geosynthetics is obviously reinforcement. However, due to their engineering properties, geosynthetics function can be not only as soil reinforcements but also as

horizontal drains (Zornberg and Mitchell, 1994). The position of drainage system within the protected zone is essential for the case that the protected zone is fully filled with poorly draining materials, such as in-placed marginal soils. A typical form of this technique is that the permeable geosynthetics should be placed within the protected zone, so that the development of excess pore water pressure could be speedily eliminated.

2.7 Conceptual elucidation of the principal properties of unsaturated soil

MSE walls are generally made of compacted soils that are stated to be an unsaturated soil (Shibuya et al., 2007; Saito et al., 2008). The unique characteristic of unsaturated soil is its negative pore water pressure (Fredlund and Rahardjo, 1993). Due to the existence of negative pore water pressure which is commonly tensile, the behavior of unsaturated soils is significantly affected. Similar to conventional classic areas of soil mechanics, three prime categories are normally considered including shear strength, seepage or movement of water through unsaturated media and volume change behavior. The last one indicates a soil with its total volume may either increase (swelling) or decrease as the soil specimen absorbs water (the process of wetting). Within this section, the first two main categories are briefly elucidated.

2.7.1 Shear strength of unsaturated soils

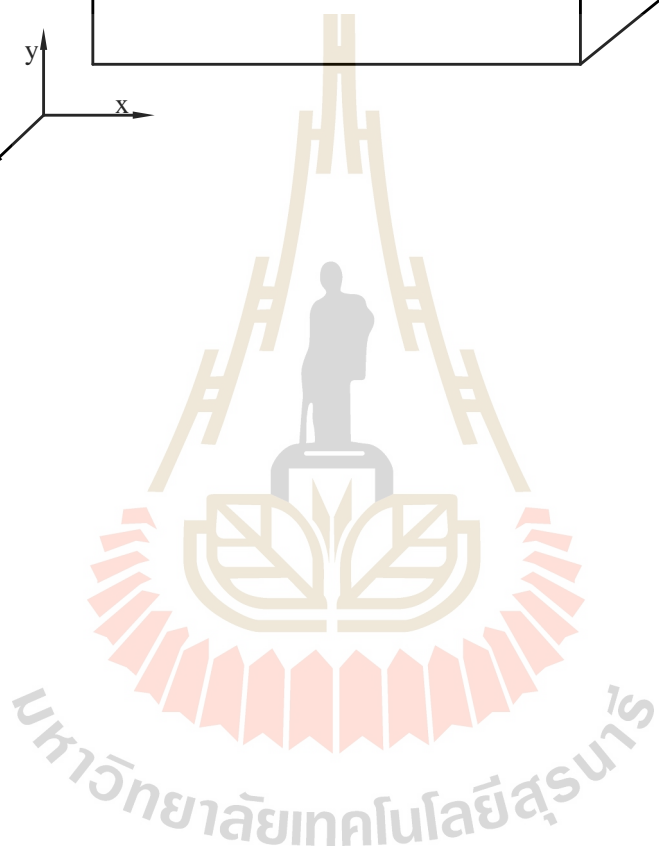
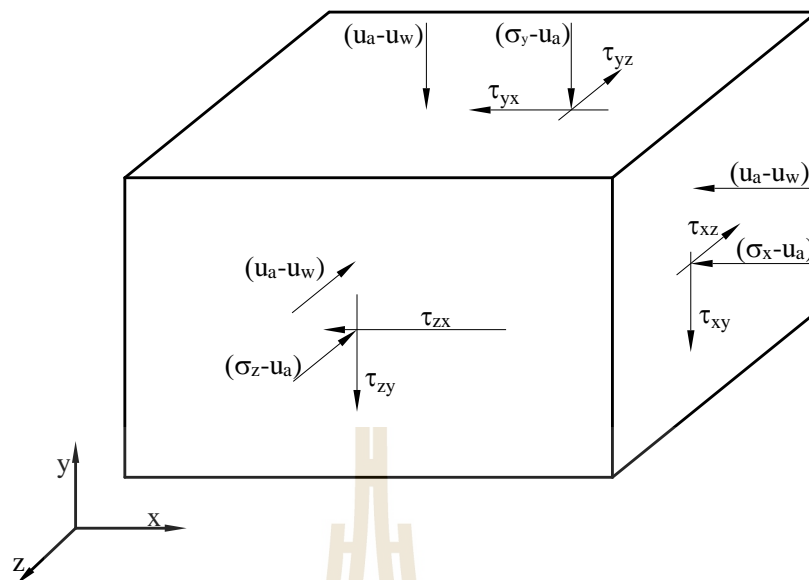
The term of shear strength of soil is to indicate soil's capacity to sustain the shearing stresses that a soil body might be exerted. When a shear force is exerted on a soil body, the shear stress develops and if it exceeds the limiting effective

shear stress, the shearing failure happens and forces the soil particles to slide or roll over each other. The stress state at which the failure happens is normally described based on the conventional soil failure criteria of Mohr-Coulomb and illustrated as following equation (Lambe and Whitman, 1969):

$$\tau = c' + (\sigma_n - u_w) \tan \phi' \quad (2.25)$$

where τ is the soil shear strength, c' is the effective cohesion, σ_n is the normal stress, u_w is the pore-water pressure, and ϕ' is the effective angle of internal friction. The term $(\sigma_n - u_w)$ is to indicate the saturated effective stress of soil (Terzaghi, 1943).

Considering a soil above a groundwater table, the u_w is negative pore water pressure and defined as matric suction (Fredlund and Rahardjo, 1993; Lu and Likos, 2004). In other words, throughout the concept of unsaturated soil, the pore phase is assumed to be fully filled with water and air. This is also a typical difference between these two types of soils. It is thus the state of stress for unsaturated soils differ from that described in saturated soil. A typical state of stress distribution at a point of unsaturated soil is illustrated in **Figure 2.21**.

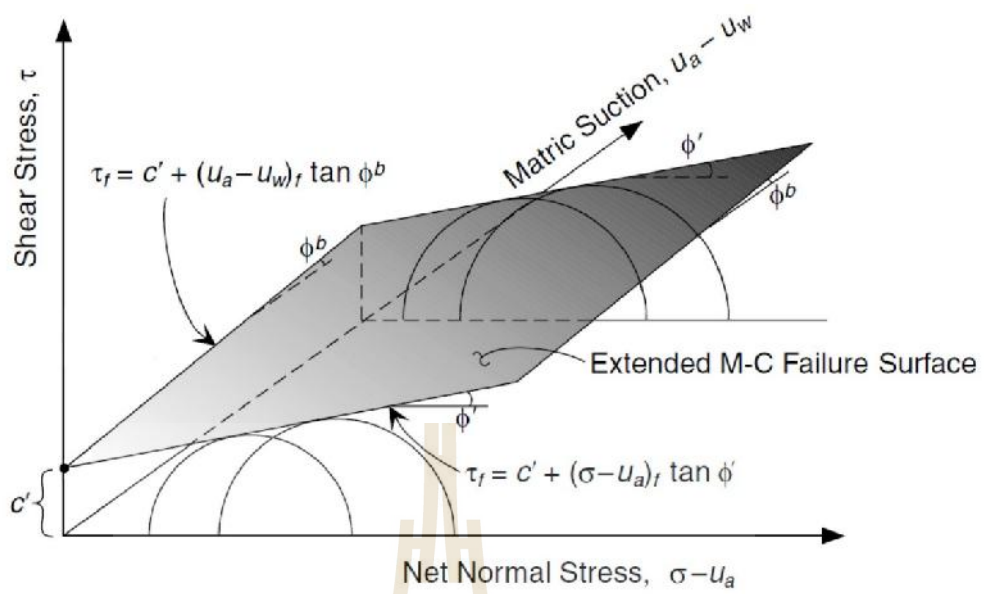


1977). This approach was formed/extended based on the Mohr-Coulomb (M-C) criteria, at which the shear stress is defined as:

$$\tau = c' + (\sigma_n - u_a) \tan \phi' + (u_a - u_w) \tan \phi^b \quad (2.26)$$

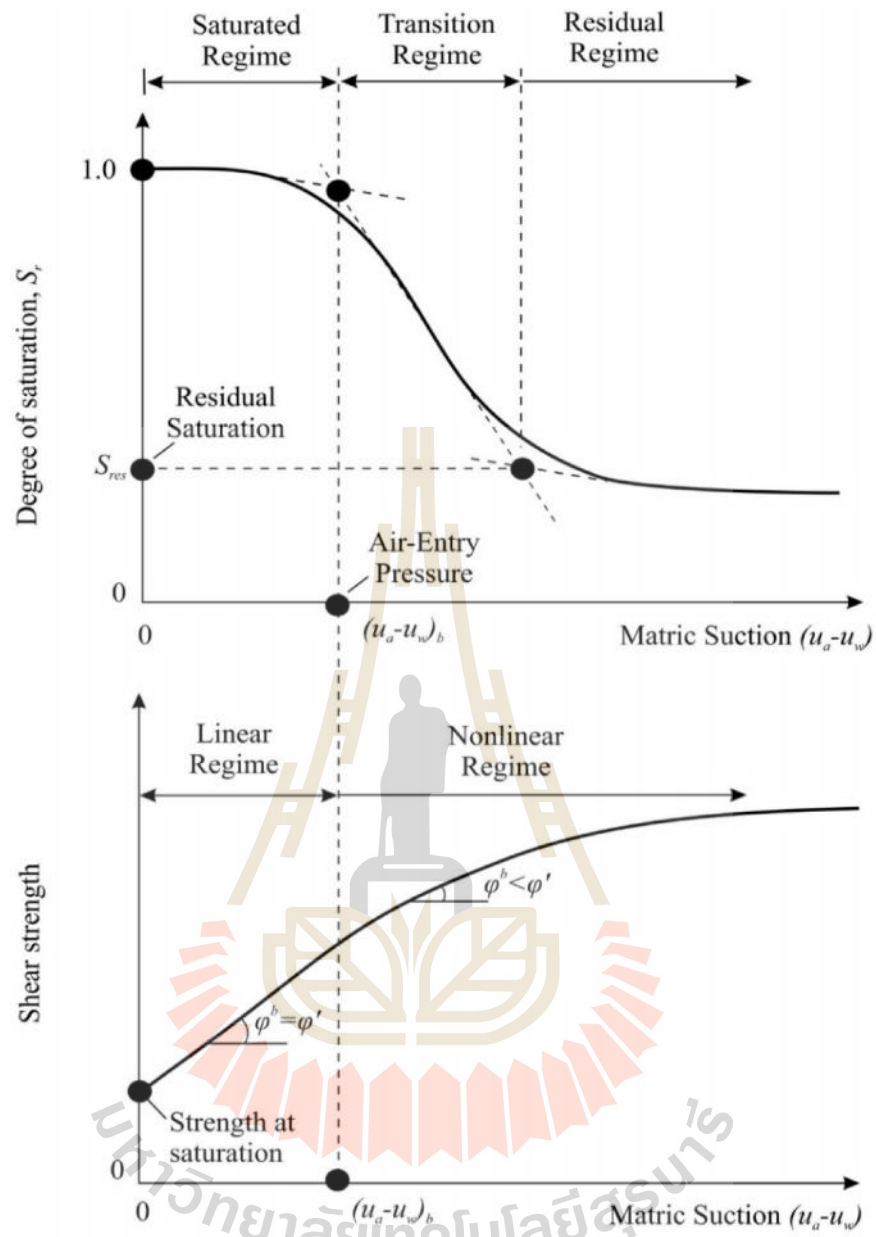
where u_a is the air-pore pressure, $(\sigma_n - u_a)$ is called the net normal stress, $(u_a - u_w)$ is matric suction, and ϕ^b is an additional variable to describe the influences of matric suction on the shear strength (Fredlund, Morgenstern et al., 1978).

The parameter ϕ^b was stated as a nonlinear function of soil suction (Gan and Fredlund, 1988; Escario et al., 1989; Vanapalli et al., 1996) and its magnitudes were varied from a value of being equal to or close to the internal friction angle ϕ' at level of zero soil suction (close to the saturation state) to about of 0° or even negative values for the suction level closed to the residual saturation state. The first two terms of equation (2.26) are to indicate the shear stress of saturated soil, while the third term is the distribution of shear stress of unsaturated soil which increases with increasing in soil suction. The extended Mohr-Coulomb failure surface based on independent stress variables was illustrated by Lu and Likos (2004) as shown in **Figure 2. 22**.



w^b

$\{'$



Throughout the M-C criteria, the effect of soil suction is ignored. Because the contribution of soil suction was not taken into consideration (Bishop, 1959; Bishop and Blight, 1963; Rahardjo et al., 1995), therefore Terzaghi effective concept was not applicable for explaining the stress state of unsaturated soil.

To work out the limitation of the concept of effective stress, Bishop (1959) had modified Terzaghi's effective stress concept and developed an equation to determine the effective stress of unsaturated soil which is described as:

$$\tau' = (\tau_n - u_a) + \tau(u_a - u_w) \quad (2.27)$$

where τ' is the effective stress of unsaturated soil, τ is the effective stress factor.

The term of soil suction is defined as the difference in pore air pressure and pore water pressure $\mathcal{E} = (u_a - u_w)$. Under the saturated condition, u_a is zero, u_w is positive, τ equals to one and the equation (2.27) become the Terzaghi's effective stress equation: $\tau' = (\tau_n - u_w)$. For completely dry soil, τ is equal to zero leading to the effective stress the net normal stress are equals to each other. Shear stress can be described by incorporating the single-valued effective stress expression into the classical Mohr–Coulomb failure criterion as:

$$\tau = c' + [(\tau_n - u_a) + \tau(u_a - u_w)] \tan \phi' \quad (2.28)$$

Based on the experimental data obtained from direct shear test, Bishop (1959) did suggest a nonlinear configuration of effective stress factor, τ , expressed as a function of the degree of saturation in **Figure 2.24**.

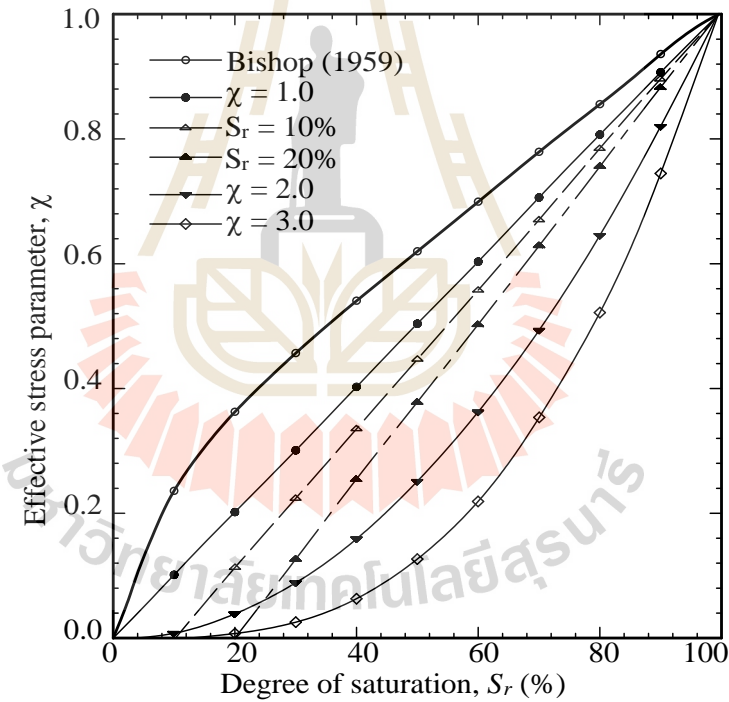
t

$$(u_a - u_w)/u_e$$

$$t = \left(\frac{u_a - u_w}{u_e} \right)^{-0.55} \qquad u_a - u_w > u_e$$

$$t = 1 \qquad u_a - u_w \leq u_e$$

$$u_e$$



t

2.7.1.3 Shear strength of unsaturated soil based on suction stress

approach

Because of the difficulties in the estimation of the effective stress factor $\bar{\sigma}$ in Bishop's approach as well as in the estimation of the material variable parameter of $\{^b$ explained in the independent stress variable method, Lu and Likos (2004, 2006) have utilized both the Terzaghi's effective stress concept and Bishop's effective stress to develop the suction stress characteristic curve to represent the state of stress in unsaturated soil.

Similar to the effective stress approach, the suction stress approach employs a single stress variable that is responsible for the mechanical behavior of earth materials. But, different from the Bishop's effective stress, the suction stress approach eliminates the need for defining the coefficient of effective stress $\bar{\sigma}$. The magnitude of effective stress based on the suction stress concept proposed by Lu and Likos (2006) is expressed as:

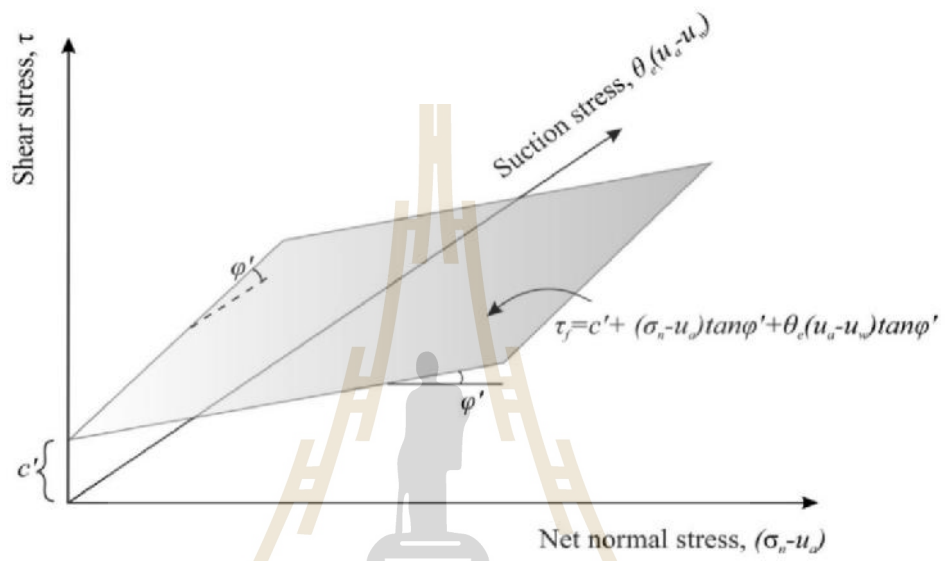
$$\bar{\sigma}' = (\bar{\sigma} - u_a) - \bar{\sigma}^s \quad (2.30)$$

where $\bar{\sigma}^s$ is the suction stress characteristic curve of soil, described as:

$$\bar{\sigma}^s = -(u_a - u_w) \quad \text{for} \quad u_a - u_w < 0 \quad (2.31 \text{ a})$$

$$\bar{\sigma}^s = f(u_a - u_w) \quad \text{for} \quad u_a - u_w \geq 0 \quad (2.31 \text{ b})$$

t



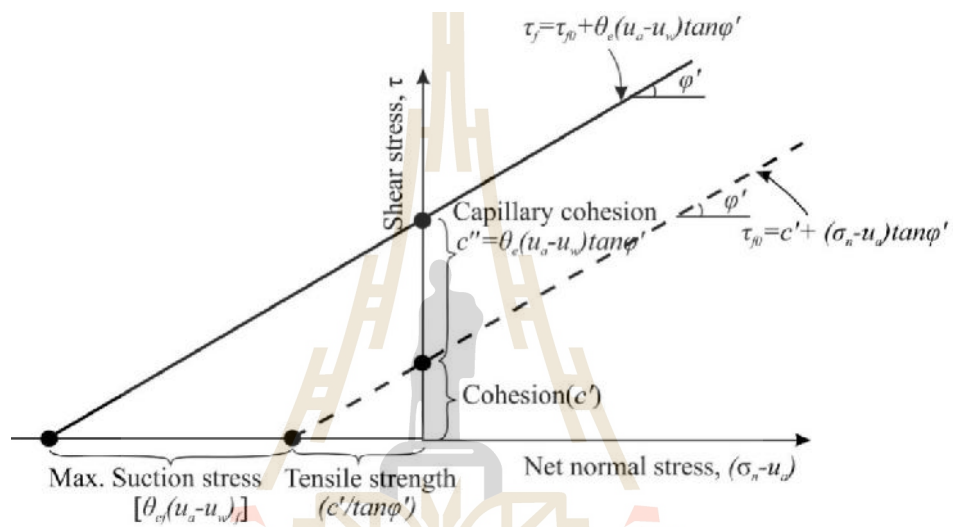
$$\dagger^s = -(u_a - u_w)_e = -(u_a - u_w) \left(\frac{n_r - n_{sat}}{n_r} \right)$$

$$\dagger = c' + (\dagger_n - u_a) \tan \phi' - (u_a - u_w) \left(\frac{n_r - n_{sat}}{n_r} \right) \tan \phi'$$

$$\tau = c' + c'' + (\sigma_n - u_a) \tan \phi'$$

$$c'' = -(u_a - u_w) \left(\frac{\sigma_{sat} - \sigma_r}{\sigma_{sat} - \sigma_r} \right) \tan \phi'$$

$$c' \quad c''$$



$$\tau = (\sigma_n - u_a) \tan \phi'$$

มหาวิทยาลัยเทคโนโลยีสุรนารี

2.7.2.1 Movement of moisture through unsaturated soil, flow equation

Playing an important role in many geo-environmental engineering problems, the principle of water flows through unsaturated geomaterials are more complex than those through saturated media due to the hydraulic conductivity of unsaturated soil is not constant with the change in moisture content, it varies with the level of water content or suction (Bouazza et al., 2013).

The unsaturated water flow was firstly presented by Richards in 1931. Richards stated that the prime difference in flow through the unsaturated and saturated condition is that under the latter condition the conductivity depends on the moisture content of the media and the pressure is expressed in term of capillary forces. However, the formulation of the partial differential flow equation for two conditions is found to be similar. To explain for water through unsaturated soils, a set of water mass balance equation is employed, and the governing differential equation is expressed as:

$$-\dots \left(\frac{\partial q_x}{\partial x} + \frac{\partial q_y}{\partial y} + \frac{\partial q_z}{\partial z} \right) = \frac{\partial (\dots)_v}{\partial t} \quad (2.37)$$

where \dots is the bulk density of water, q_x, q_y, q_z are water fluxes in the x, y , and z directions, respectively, t is the time, and $_v$ is the volumetric water content.

Buckingham (1907) generalized the Darcy's law for unsaturated flow by taking hydraulic conductivity into account as a function of suction head, with the magnitudes of water fluxes in each direction are described as:

$$q_x = -k_x(h_m) \frac{\partial h_m}{\partial x} \quad (2.38 \text{ a})$$

$$q_y = -k_y(h_m) \frac{\partial h_m}{\partial y} \quad (2.38 \text{ b})$$

$$q_z = -k_z(h_m) \frac{\partial h_m}{\partial z} \quad (2.38 \text{ c})$$

where h_m is matric suction head and $k(h_m)$ is the unsaturated hydraulic conductivity function. Combination equation (2.37) and (2.38 a, b, c) yields:

$$\frac{\partial}{\partial x} \left[k_x(h_m) \frac{\partial h_m}{\partial x} \right] + \frac{\partial}{\partial y} \left[k_y(h_m) \frac{\partial h_m}{\partial y} \right] + \frac{\partial}{\partial z} \left[k_z(h_m) \left(\frac{\partial h_m}{\partial z} + 1 \right) \right] = \frac{\partial \theta}{\partial t} \quad (2.39)$$

Applying the chain rule, the term $\partial \theta / \partial t$ in equation (2.39) can be represented in terms of the matric suction head:

$$\frac{\partial \theta}{\partial t} = \frac{\partial \theta}{\partial h_m} \frac{\partial h_m}{\partial t} \quad (2.40)$$

where $\partial \theta / \partial h_m$ is the specific soil water capacity (C):

$$C(h_m) = \frac{\partial \theta}{\partial h_m} \quad (2.41)$$

The governing equation of transient unsaturated flow could be withdrawn by substituting equations (2.40) and (2.41) into (2.39), and expressed as:

$$\frac{\partial}{\partial x} \left[k_x(h_m) \frac{\partial h_m}{\partial x} \right] + \frac{\partial}{\partial y} \left[k_y(h_m) \frac{\partial h_m}{\partial y} \right] + \frac{\partial}{\partial z} \left[k_z(h_m) \left(\frac{\partial h_m}{\partial z} + 1 \right) \right] = C(h_m) \frac{\partial h_m}{\partial t} \quad (2.42)$$

Applying the chain rule, Darcy's law can be expressed for each flow direction as follows:

$$q_x = -k_x(h_m) \frac{\partial h_m}{\partial x} = -k_x(h_m) \frac{\partial h_m}{\partial h_m} \frac{\partial h_m}{\partial x} = -D_x \frac{\partial h_m}{\partial x} \quad (2.43)$$

$$q_y = -k_y(h_m) \frac{\partial h_m}{\partial y} = -D_y \frac{\partial h_m}{\partial y} \quad (2.44)$$

$$q_z = -k_z(h_m) \left(\frac{\partial h_m}{\partial z} + 1 \right) = -D_z \frac{\partial h_m}{\partial z} - k_z(h_m) \quad (2.45)$$

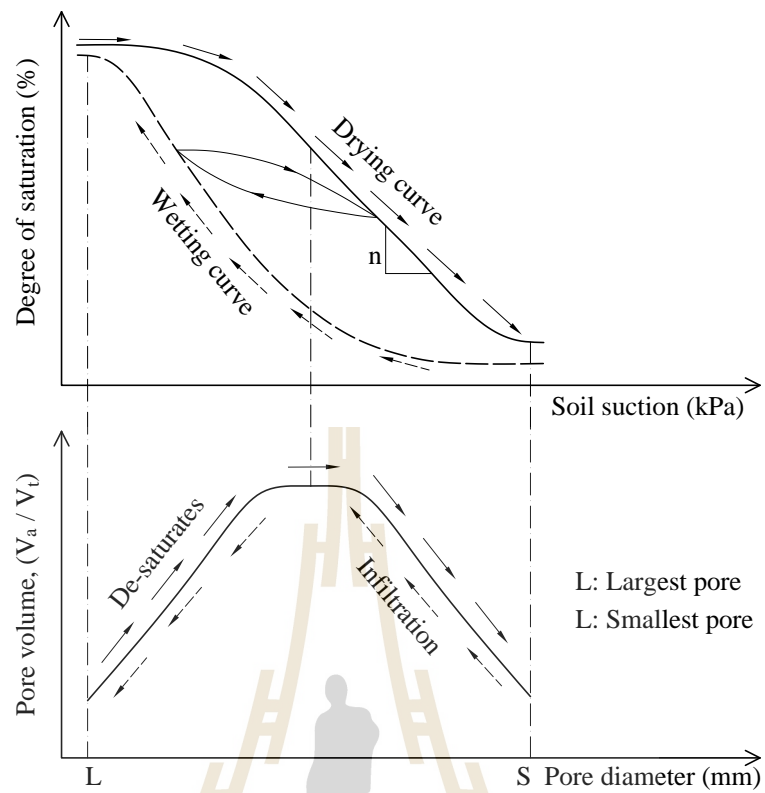
Applying equations of (2.43), (2.44), (2.45) into equation (2.39), obtains:

$$\frac{\partial}{\partial x} \left[D_x(h_m) \frac{\partial h_m}{\partial x} \right] + \frac{\partial}{\partial y} \left[D_y(h_m) \frac{\partial h_m}{\partial y} \right] + \frac{\partial}{\partial z} \left[D_z(h_m) \frac{\partial h_m}{\partial z} \right] + \frac{\partial k_z(h_m)}{\partial z} = \frac{\partial h_m}{\partial t} \quad (2.46)$$

where $D(h_m)$ is the ratio between the hydraulic conductivity of soil to its water capacity or defined as hydraulic diffusivity for unsaturated soil $D = k(h_m)/C(h_m)$.

Equations (2.39) and (2.46) are known as the Richards' equation expressed in term of pressure head and water content based equations. These two equations can be worked out using mathematical descriptions of SWCC and permeability function.

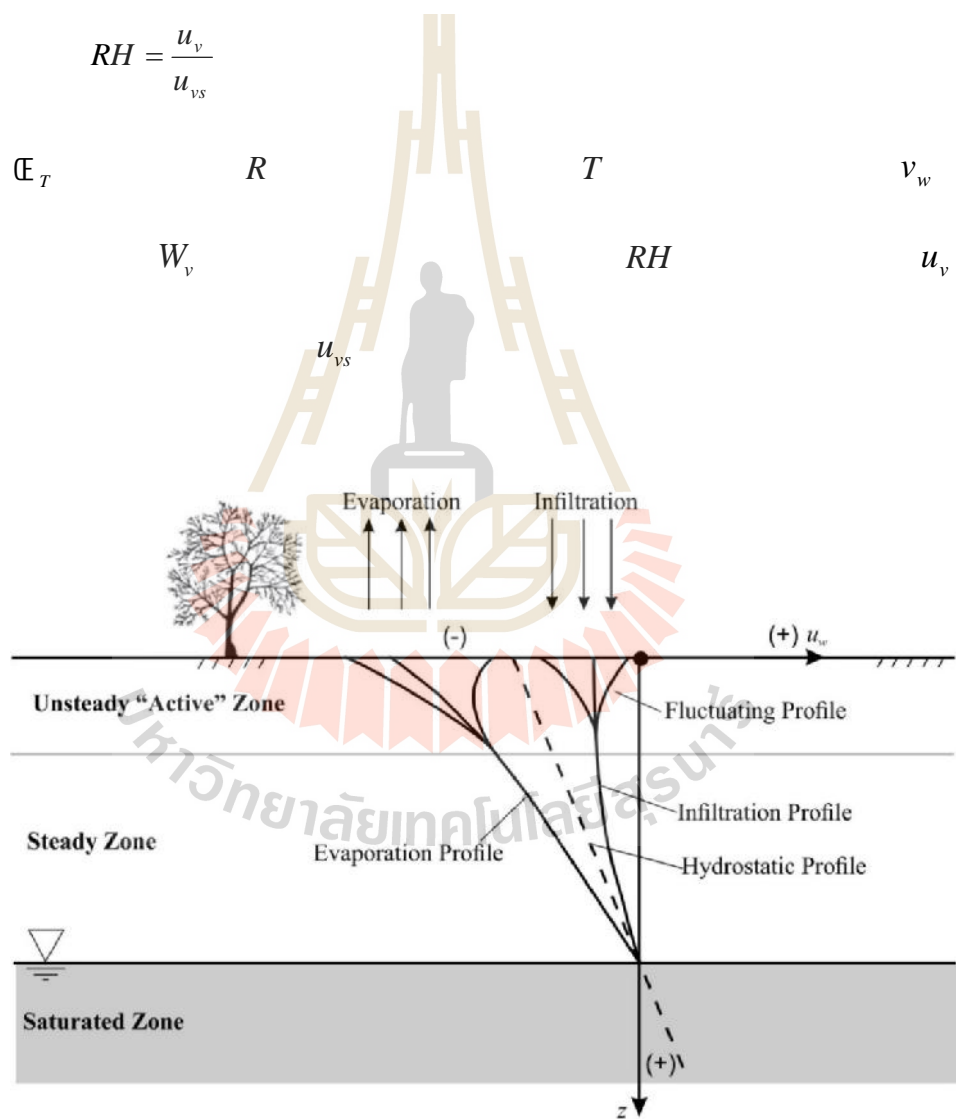
Theoretically, within the unsaturated zone, as the soil de-saturates the pore water pressure changes from positive (compressive) to negative (tensile) where the largest pores de-saturates first (**Figure 2.27**). The pore water pressure is negative and it affects the behavior of unsaturated zone significantly (Lu and Likos, 2004). The term of negative pore water pressure is known as suction, $u_a - u_w$. The magnitude of suction is dependent upon the magnitude of the radius of pore size of materials.



มหาวิทยาลัยเทคโนโลยีสุรนารี

$$\mathcal{E}_T = \frac{RT}{\epsilon_w W_v} \ln(RH)$$

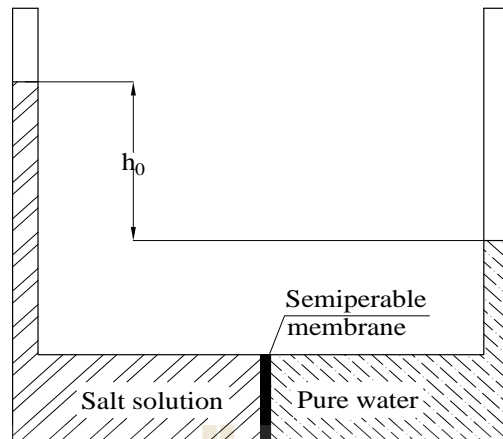
$$RH = \frac{u_v}{u_{vs}}$$



According to Fredlund and Rahardjo (1993), total soil suction comprises two components including matric suction ($\bar{U} = u_a - u_w$) and osmotic suction (f). The former one, \bar{U} , is mainly governed by the capillary rise due to the surface tension, whereas the latter is dependent upon the salt concentration in the pore water or because of the differences in salt concentration at different locations in the soil water.

The soil suction might be measured directly or indirectly. The fundamental concept of the first technique is to apply air pressure, resulting in increase or decrease of sample pore-water until the equilibrium state reaches, at which soil suction is equal to the imposed air pressure. When the equilibrium is reached, the resultant moisture content is unique to this soil at this suction. The basic concept of indirect method is based on thermodynamics, where the soil suction is computed from the measurement of relative humidity or heat dissipation. The details of soil suction measurement methodologies are not described in this thesis.

The magnitude of osmotic suction can be determined using squeezing technique. The key process of this technique is that distilled water adds to the soil specimen until the soil reaches near fluid consistent. Subsequently, the water is extracted from the soil specimen with fluid squeezer. The extracted water is then exerted to electrical conductivity test. Finally, the squeezed water is used to compute the osmotic suction of the soil specimen.



tension and the downward force due to the weight of the water in a tube reached (as shown in **Figure 2.30**).

Accordingly, the height of capillary rise h_c is

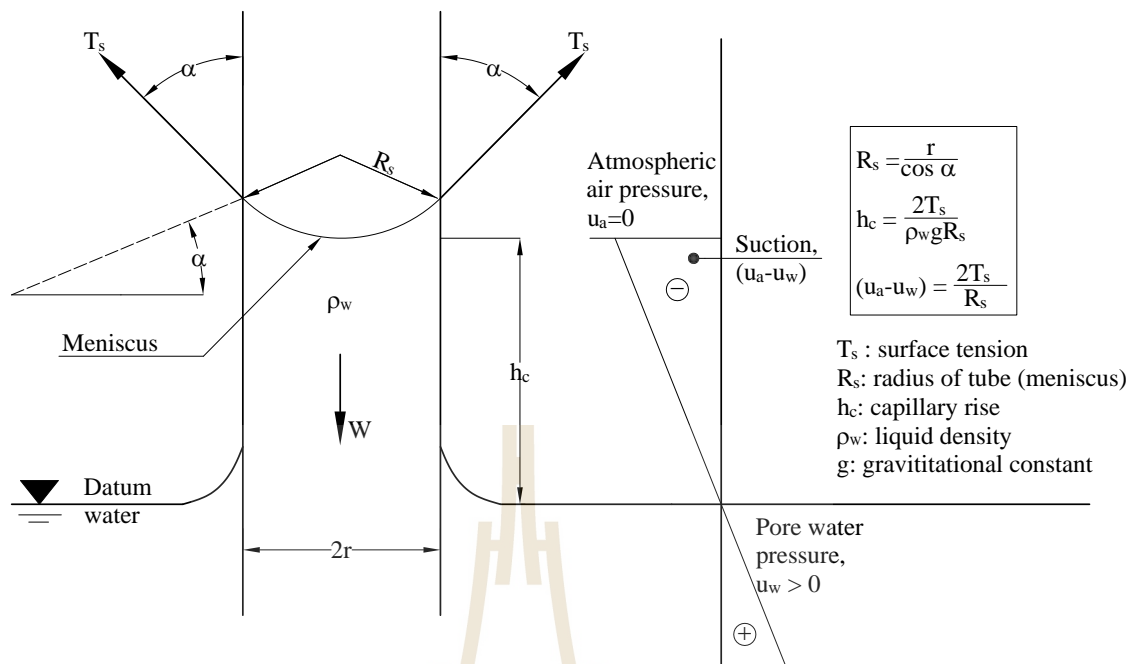
$$h_c = \frac{2T_s}{\gamma_w g r \cos \tilde{S}} \cong \frac{2T_s}{\gamma_w g R_s} \quad (2.49)$$

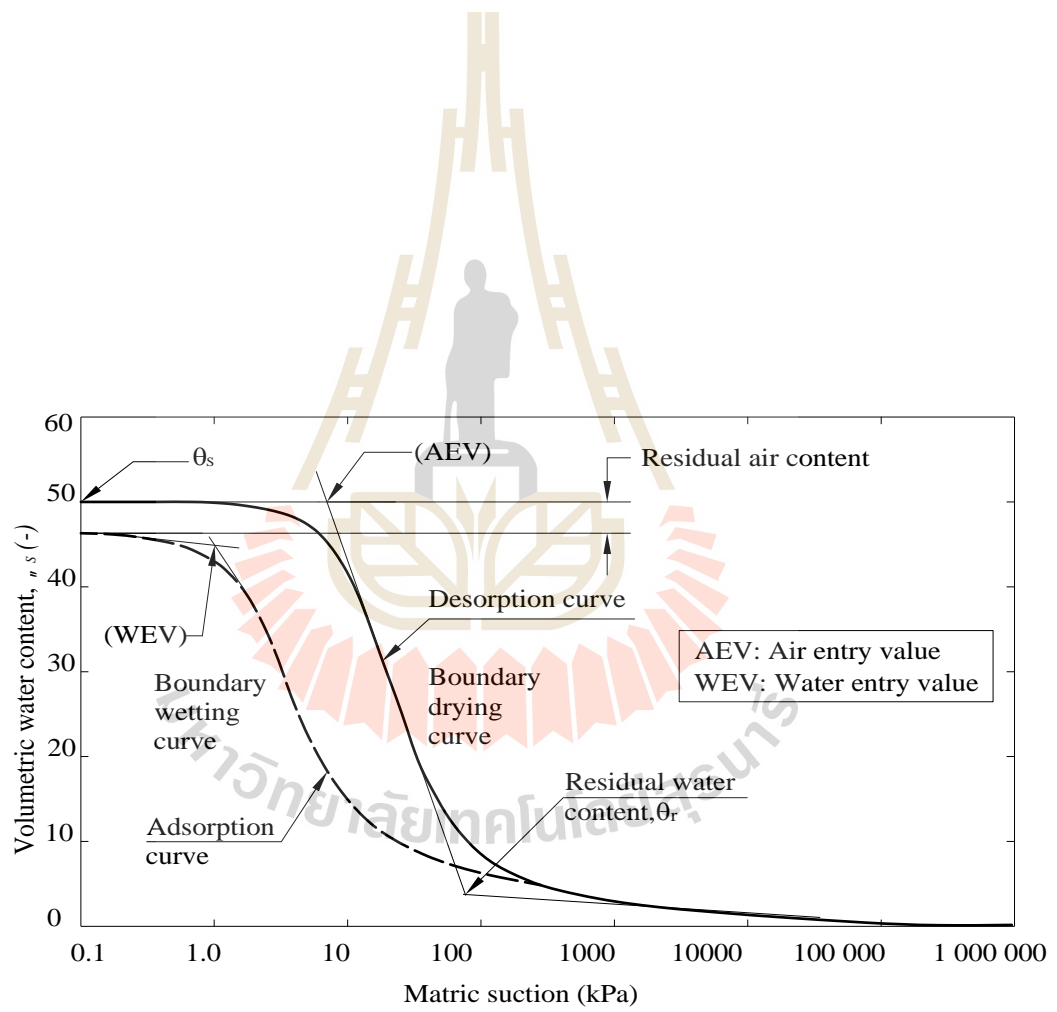
and the matric suction is defined as

$$u_a - u_w = \frac{2T_s}{r \cos \tilde{S}} \cong \frac{2T_s}{R_s} \quad (2.50)$$

where T_s is surface tension of the water-air interface, r is radius of the capillary tube, R_s is radius of curvature, \tilde{S} is contact angle.

Five possible contact angles in capillary tube were illustrated by Lu and Likos, (2004) including perfect wetting surface ($\tilde{S} = 0^\circ$), partial wetting surface ($0^\circ < \tilde{S} < 90^\circ$), neutral surface ($\tilde{S} = 90^\circ$), partial repellent surface ($90^\circ < \tilde{S} < 180^\circ$), perfectly repellent surface ($\tilde{S} = 180^\circ$)





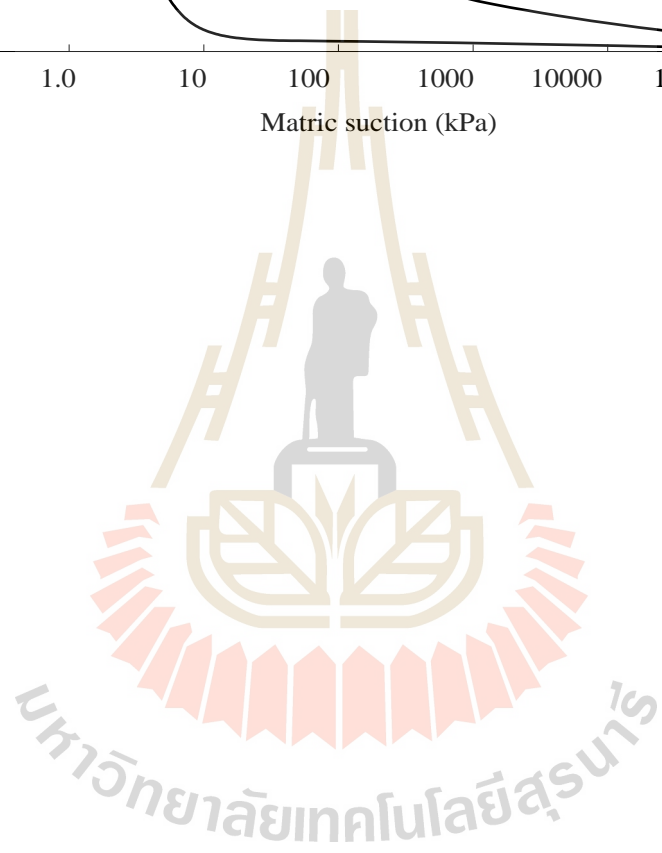
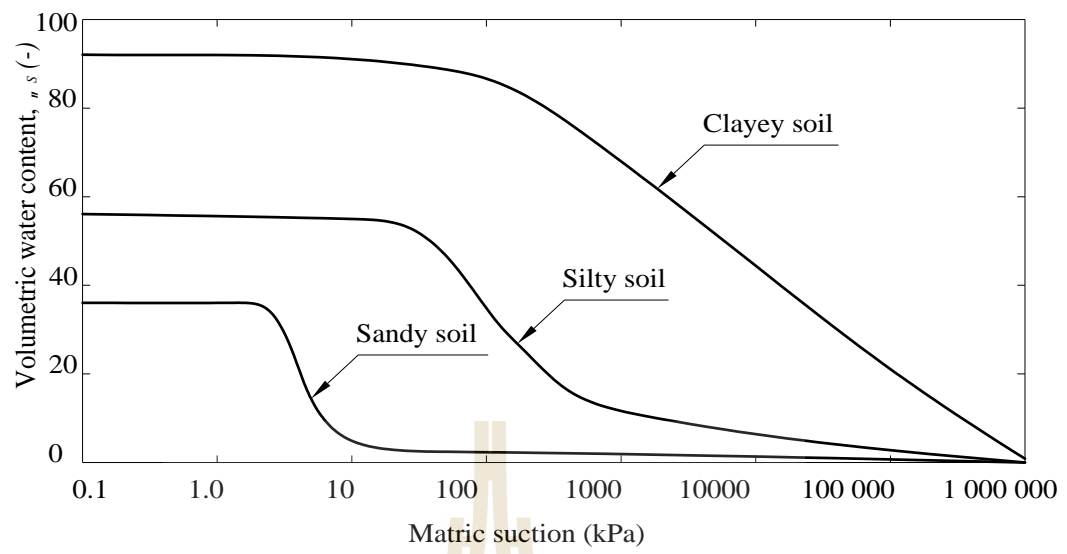


Table 2.8 Empirical mathematical equations for water retention characteristic curve (after Too et al., 2014)

| Authors | SWCC models | Parameters | Time |
|----------------|--|--|------|
| Gardner | $\theta(h) = \theta_r + (\theta_s - \theta_r)[1 + (\alpha h)^n]^{-1}$ | $\theta_r, \theta_s, \alpha, n$ | 1958 |
| Brooks-Corey | $\theta(h) = \theta_r + (\theta_s - \theta_r)(\alpha h)^{-\lambda}$ | $\theta_r, \theta_s, \alpha, \lambda$ | 1964 |
| Brutsaert | $\theta(h) = \theta_r + (\theta_s - \theta_r)[1/(1 + \frac{\alpha}{\theta_r})^n]$ | $\theta_r, \theta_s, \alpha, n$ | 1966 |
| Campbell | $\theta(h) = \theta_s (\alpha h)^{\lambda}$ | $\theta_s, \alpha, \lambda$ | 1974 |
| Van Genuchten | $\theta(h) = \theta_r + (\theta_s - \theta_r)[1 + (\alpha h)^n]^{-m}$ | $\theta_r, \theta_s, \alpha, n, m$ | 1980 |
| Tani | $\theta(h) = \theta_r + (\theta_s - \theta_r)[1 + (\alpha h)e^{-\alpha h}]$ | $\theta_r, \theta_s, \alpha$ | 1982 |
| Williams et al | $\ln \theta = a_1 + b_1 \ln \theta$ | a_1, b_1 | 1983 |
| Boltzman | $\theta(h) = \theta_r + (\theta_s - \theta_r) \exp(\frac{\alpha - \theta}{n})$ | $\theta_r, \theta_s, \alpha, n$ | 1984 |
| McKee | $\Theta = e^{\frac{\alpha - a_2}{b_2}}$ | a_2, b_2 | 1984 |
| Fermi | $\theta(h) = \theta_r + (\theta_s - \theta_r)(1/(1 + \exp(\frac{\alpha - \theta}{n})))$ | $\theta_r, \theta_s, \alpha, n$ | 1987 |
| McKee and Bumb | $\Theta = \frac{1}{1 + e^{\frac{\alpha - a_3}{b_3}}}$ | a_3, b_3 | 1987 |
| Fredlung-Xing | $\theta(h) = \theta_s + \frac{\theta_s - \theta_r}{[\ln(2.7183 + (\alpha h)^n)]^m}$ | $\theta_r, \theta_s, \alpha, n, m$ | 1994 |
| Ruso | $\theta(h) = \theta_r + (\theta_s - \theta_r)[(1 + 0.5\alpha h)e^{0.5\alpha h}]^{\frac{2}{2+n}}$ | $\theta_r, \theta_s, \alpha, n$ | 1998 |
| Kosugi | $\theta(h) = \theta_r + \frac{1}{2}(\theta_s - \theta_r) \operatorname{erfc}[\frac{\ln(h/h_m)}{\sqrt{2}}]$ | $\theta_r, \theta_s, \dagger, h_m$ | 1999 |
| Biexponential | $\theta(h) = \theta_r + (\theta_{s1}e^{-\alpha_1 h} + \theta_{s2}e^{-\alpha_2 h})$ | $\theta_{s1}, \theta_{s2}, \alpha_1, \alpha_2$ | 2009 |

$\Theta = \frac{\theta - \theta_r}{\theta_s - \theta_r}$ is normalized water content, θ_s is volumetric water content at saturation, θ_r is residual volumetric water content at high suction, λ is pore size distribution index, α is matric suction, h is suction head, α is soil parameter that which is related to AEV of the soil, $a_1, b_1, a_2, b_2, a_3, b_3, n, m$ are curve fitting parameters, n governs the slope of SWCC at the inflection point, which is related to the uniform of grain size, m represents the residual water content in soil

Gardner model

The first continuous function which used two fitting parameters, namely r and n proposed by **Gardner** (1958) has been adapted to model the SWCC. In term of the degree of saturation, the equation of the Gardner is defined as:

$$S = \frac{1}{1 + r\mathcal{E}^n} \quad (2.51)$$

where \mathcal{E} is soil suction, r and n are fitting parameters in which the r is related to the inverse of the AEV, and the n parameter is related to the pore size distribution. The normalized water content form of the Gardner model is described as:

$$\theta = \theta_r + (\theta_s - \theta_r) \left(\frac{1}{1 + r\mathcal{E}^n} \right) \quad (2.52)$$

Brooks and Corey model (B.C model)

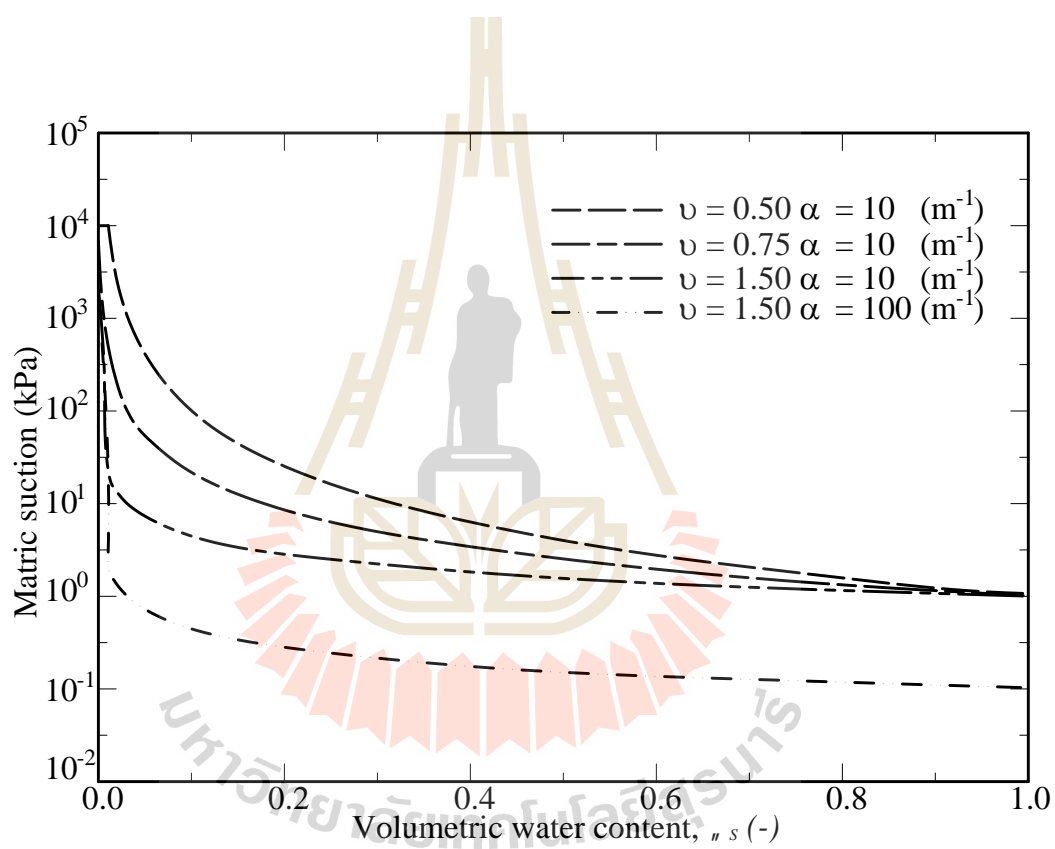
A SWCC model that assumed to be constant for suction less than the AEV was proposed by Brooks and Corey (1964). Throughout the Brooks and Corey model, only two fitting parameters were used including r and n , in which r parameter is related to AEV of the soil and the n parameter is to related to the soil pore size distribution. The Brooks & Corey (1964) model is illustrated as:

$$S_e = \left(\frac{\mathcal{E}}{r} \right)^{-n} = \frac{S - S_r}{S_{\max} - S_r} = (rh_c)^{-n} \quad \text{for } \mathcal{E} > \text{AEV or } rh_c > 1 \quad (2.53)$$

$$S_e = 1 \quad \text{for } \mathcal{E} \leq \text{AEV or } rh_c \leq 1$$

S_e
 S_{\max}
 S_r

$$\theta = \theta_r + (\theta_s - \theta_r) \left(\frac{h}{h_r} \right)^{-n}$$



soil is not well defined as using the model of B.C model leading to inaccuracy of evaluation of their behaviors. Although, all the model parameters used in Brooks and Corey model have physical meaning, the B.C model does not provide a continuous mathematical equation for the whole SWCC (Toll, 2001). Similarly, the Brooks and Corey model shows the discontinuity at the AEV.

Brutsaert model

Similar to the Gardner model, Brutsaert model was proposed in 1966. This is a type of continuous SWC models with meaningful parameters. This model provides a fit relationship between degree of saturation and soil suction data (Toll, 2001). Nevertheless, a decrease in the r parameter or an increase in the n parameter brings about the degree of saturation in low suction range, below 100% (Sillers et al., 2001), consequently, a restriction must be imposed on the relationship between the r and n parameters in order to ensure a reasonable function. The Brutsaert (1966) model is mathematically shown as:

$$S = 1 / (1 + (\frac{U}{r})^n) \quad (2.55)$$

The normalized water content form of this model is written as:

$$u = u_r + (u_s - u_r) (1 / (\frac{U}{r})^n) \quad (2.56)$$

van Genuchten model

A continuous SWCC model was proposed by **van Genuchten** (1980), namely van Genuchten model. The van Genuchten model consists of four independent parameters and three fitting parameters, namely n, m, r . The van Genuchten equation is described as:

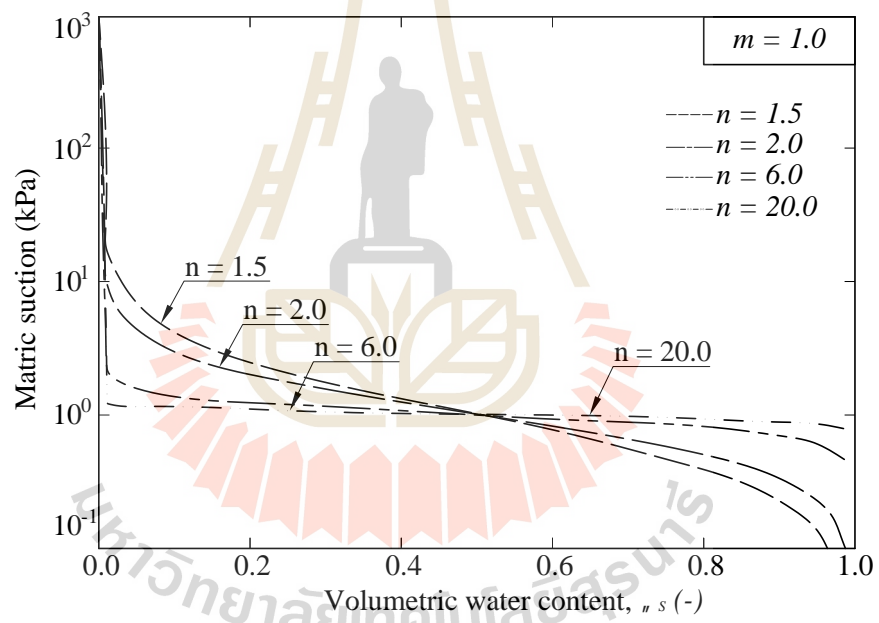
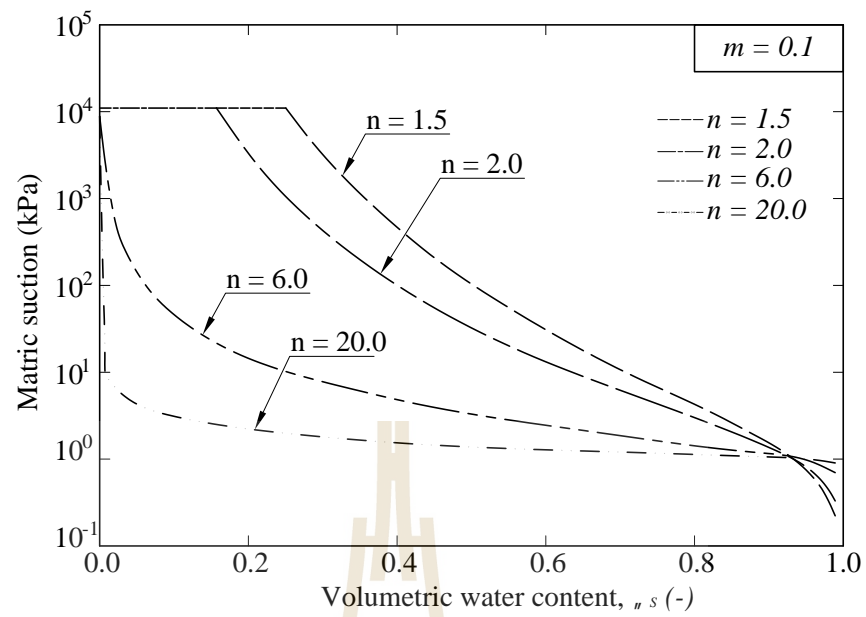
$$\theta = \theta_r + (\theta_s - \theta_r)[1 + (r h)^n]^{-m} \quad (2.57)$$

$$S_e = \frac{\theta(h) - \theta_r}{\theta_{sat} - \theta_r} = \left[\frac{1}{1 + (r h)^n} \right]^{1-\frac{1}{m}} \quad (2.58)$$

where θ is the volumetric water content, h is the pressure head, θ_s and θ_r represent the saturated and residual water content, respectively, S_e is the effective saturation, r , n and m are empirical shape parameters, r is defined as an inverse of the AEV.

In fact, the closed form equation proposed by van Genuchten model is found to be similar to that of the Brutsaert (1966) if value of m equals to 1, and the r parameter is inverted.

Figure 2.33 illustrates several SWCCs obtained from van Genuchten models for various magnitudes of the model parameters n and m . In term of physical meaning, the lower magnitude of the model parameter n implies the wider pore size distribution of a soil. The **Figure 2.33** indicates that if the magnitude of n is approaching infinity, the slope of SWCC curve is approaching zero.



similar to the van Genuchten According to the Fredlund and Xing model, when the distribution of pore size of a soil known, the corresponding SWCC of that soil could be determined from the following equation:

$$\theta = \theta_r + \frac{\theta_s - \theta_r}{[\ln(e + (h/a)^n)]^m} \quad (2.59)$$

2.7.2.4 Permeability function for unsaturated medium

To handle the seepage of water through unsaturated soil, a permeability function expressed in terms of suction of unsaturated soil is normally required. Compared to the permeability of saturated soils, k_s , which is a function of void ratio only. The permeability of unsaturated soils is primarily governed by both void ratio, e , and water content (Leong and Rahardjo, 1997). The hydraulic conductivity of unsaturated soils cannot be a constant due to the void ratio, water content, and the degree of saturation are tightly inter-related. Instead, the magnitude of permeability coefficient is a variable and defined as a function of the volumetric water content θ or the matric suction of the unsaturated soil U . Since the moisture content of unsaturated soil uniquely varies with suction, a logical conclusion follows that the unsaturated soil permeability is normally expressed in terms of suction and also possible to approximate from SWCC. Within the unsaturated zone, the number of flow paths decreases, then the permeability of the unsaturated soil is decreased with the degree of saturation in a nonlinear relation. In other words, under the unsaturated condition, the permeability coefficient is widely recognized to be a function of soil suction.

Recently, three categories of permeability function of an unsaturated soil have been illustrated including empirical equations, statistical models, and macroscopic models. Several measured permeability data are required to use empirical equation. A statistical model can be used to predict the permeability function when the saturated coefficient of permeability, k_s , and the SWCC are available.

a) Empirical equations

The empirical equations have been appeared due to the need for an equation to illustrate the changes in hydraulic conductivity with matric suction \mathbb{E} or volumetric water content w

$$\begin{cases} k_{\mathbb{E}} = f(\mathbb{E}) \\ k_{\mathbb{E}} = f(w) \end{cases} \quad (2.60)$$

To date, a number of empirical equations have been introduced to estimate the permeability function of unsaturated soils (**Table 2. 9**). Many soil parameters in the proposed equations come from estimated SWCCs with the equation from previous **Table 2. 8**.

Due to practical challenges, especially test procedure, empirical methods are hardly utilized. In addition, the unsaturated soil properties are normally estimated with presented fit functions. These functions are also commonly estimated with the statistical model based on typically quantified soil properties, such as gradation and Atterberg Limits.

Table 2. 9 A summary of experiential permeability equations $k(\xi)$ (after Fredlund, 1993)

| Functions | Literatures |
|---|----------------------------------|
| $k(\xi) = r\xi + b$ | Richards, 1931 |
| $k(\xi) = a \exp(b\xi)$ | Christensen, 1944 |
| $k_r = \Theta^n$ where $\Theta = (\theta - \theta_r)/(\theta_s - \theta_r)$ and $n = 3.5$ | Averyanov, 1950 |
| $k(\xi) = r\xi^{-n}$ | Wind, 1955 |
| $k_r = \exp(-r\xi)$ | Gardner, 1958 |
| $k(\xi) = k_s / (r\xi^n + 1)$ | |
| $k_r = (\xi / \xi_{aev})^{-n}$ for $\xi > \xi_{aev}$ | Brooks and Corey, 1964 |
| $k(\xi) = k_s$ for $\xi \leq \xi_{aev}$ | |
| $k(\xi) = k_s$ for $\xi \leq \xi_{aev}$ | Rijtema, 1965 |
| $k_r = k_s (\frac{\xi}{\xi_{aev}})^y$ for $\xi_{aev} \leq \xi \leq \xi_r, y = 2 + 3\}$ | |
| $k(\xi) = k_r (\frac{\xi}{\xi_r})^{-n}$ for $\xi > \xi_r$ | |
| $k(\xi) = \frac{k_s}{1 + r(\frac{\xi}{\xi_r})^b}$ | Arbhabhirama and Kridakorn, 1968 |
| $k(\xi) = k_s \exp[r(\theta - \theta_s)]$ | Davidson et al., 1969 |
| $k(\xi) = k_s (\frac{\theta - \theta_r}{\theta_s - \theta_r})^n$ | Campbell, 1974 |
| $k(\xi) = k_s \frac{[1 - (r\xi)^{n-1} + (1 + (r\xi)^n)^{-m}]^2}{[1 + (r\xi)^n]^{m/2}}$ | Mualem, 1986 |
| $k(\xi) = k_s \exp[b(\xi - \xi_b)]$ for $\xi > \xi_b$ | Philip, 1986 |
| $k(\xi) = k_s [\ln(e + (\frac{\xi}{r})^n)]^{-pm}$ | Leong and Rahardjo, 1997 |

r is diffusion coefficient, θ is pore size distribution index, θ_w is density of water, k_r is the coefficient of permeability at $\xi = \xi_r$, k_ξ is unsaturated soil permeability.

b) Statistical models

The fundamentals of the statistical models were based on three assumptions introduced by Mualem (1976), which was a combination of the Hagen-Poiseuille equation for fluid flow through the capillary tube and the knowledge of pore size distribution taken from the matric suction – moisture content relationship (Lu and Likos, 2004). Mualem (1976) proposed an equation to estimate the permeability of unsaturated soils as:

$$k_{rf} = (S_e)^1 [1 + (1 - S_e)^{1/m}]^m]^2 \quad (2.61)$$

The equation (2.61) is known as the van Genuchten-Mualem (VGM) model. In other words, this approach is based on the fact that both the permeability function and the SWCC are primarily estimated by the pore size distribution of the soil under consideration.

Figure 2.34 illustrates k-function curves obtained from van Genuchten model. It is obviously shown that the higher magnitude of the model parameter n yields the higher relative conductivity of the liquid phase found as shown in the **Figure 2.34 a**. This is due to the higher the value of model parameter n means the more uniformity the pore size distribution, and hence the easier the liquid flow through happens. The influence of model parameter m is illustrated in **Figure 2.34 b**. It shows that there is a slight influence of model parameter m on relative conductivity as the magnitude of m larger than 1.0.

c) Macroscopic models

The permeability function proposed by Mualem (1986) can be derived using the macroscopic models. All the microscopic models have the same following general forms:

$$k_r = S_e^u \quad (2.62)$$

$$S_e = \frac{S - S_r}{1 - S_r} \quad (2.63)$$

S and S_r are the degree of saturation and residual degree of saturation, respectively.

In fact, the influence of pore size distribution is not considered in all macroscopic models (Brooks and Corey, 1964). A general equation was then proposed to compute the value of δ by Brooks and Corey (1964) as:

$$u = (2 + 3\delta) / \delta \quad (2.64)$$

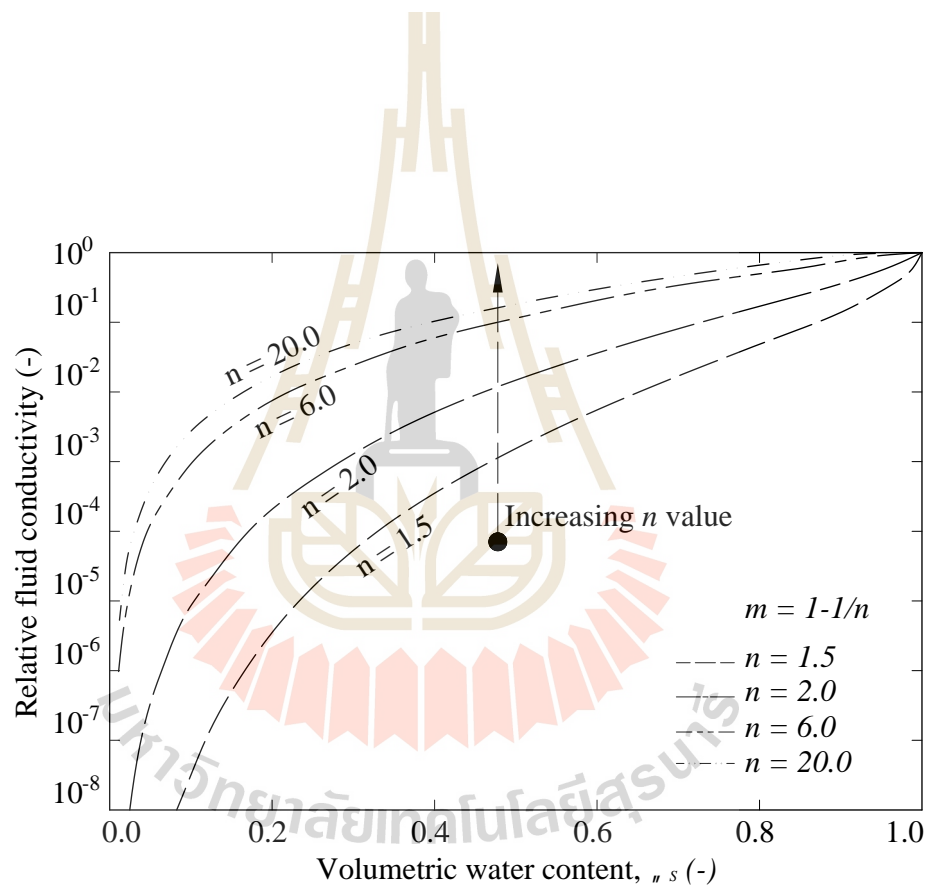
where δ is the positive pore size distribution index. Mualem (1976) also suggested that $u = 3 - 2m$, where m is soil water factor which is positive for granular material and negative for unstructured soils of fine texture. The magnitude of u is a constant depending on the assumption made as shown in **Table 2.10**.

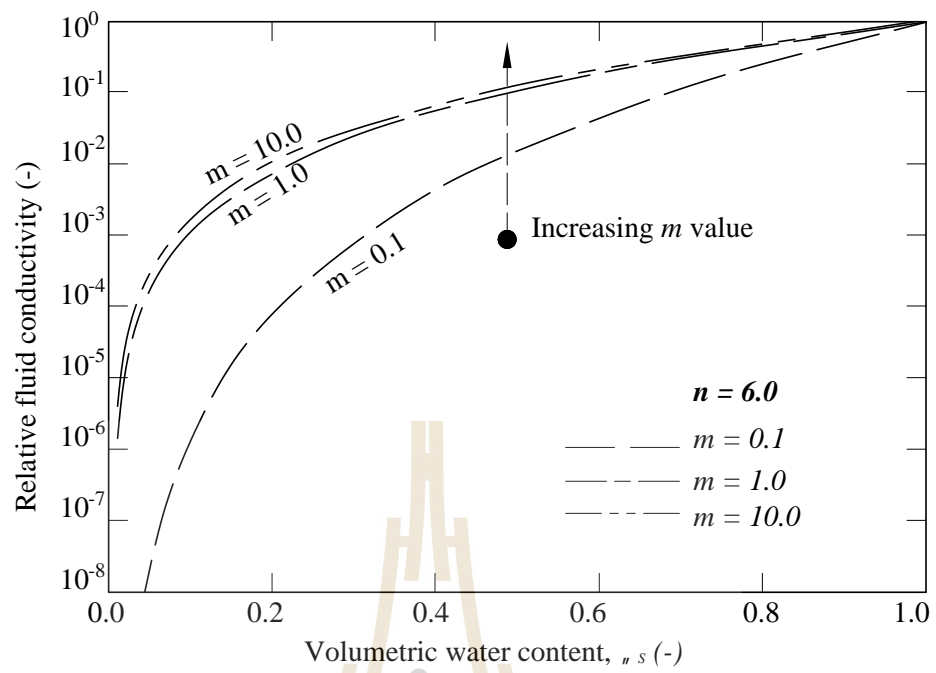
u

Magnitudes of $\frac{m}{n}$

Literatures

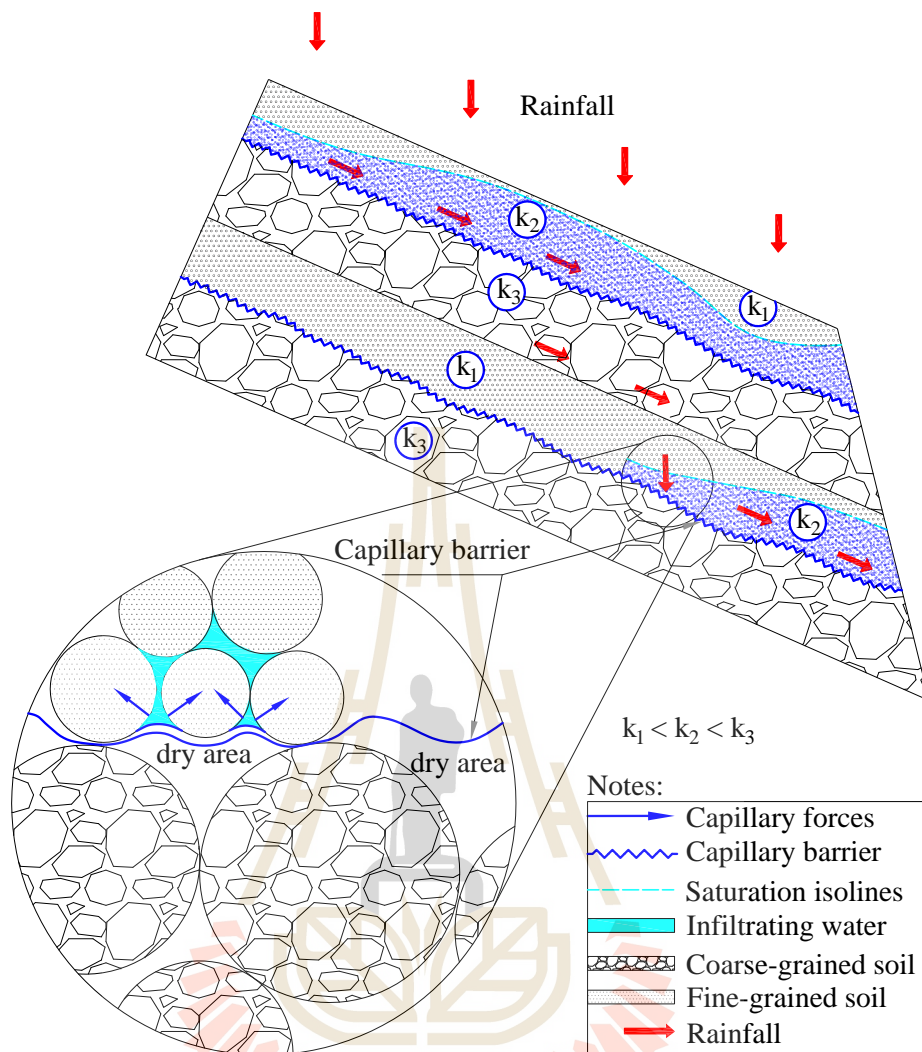
| | |
|----------|-------------------------------------|
| 3.5 | Averyanov, 1950 |
| 2 | Yuster, 1951 |
| 3 | Irmay, 1954; Brooks and Corey, 1964 |
| 4 | Corey, 1954 |
| 2.5-24.5 | Mualem, 1976 |



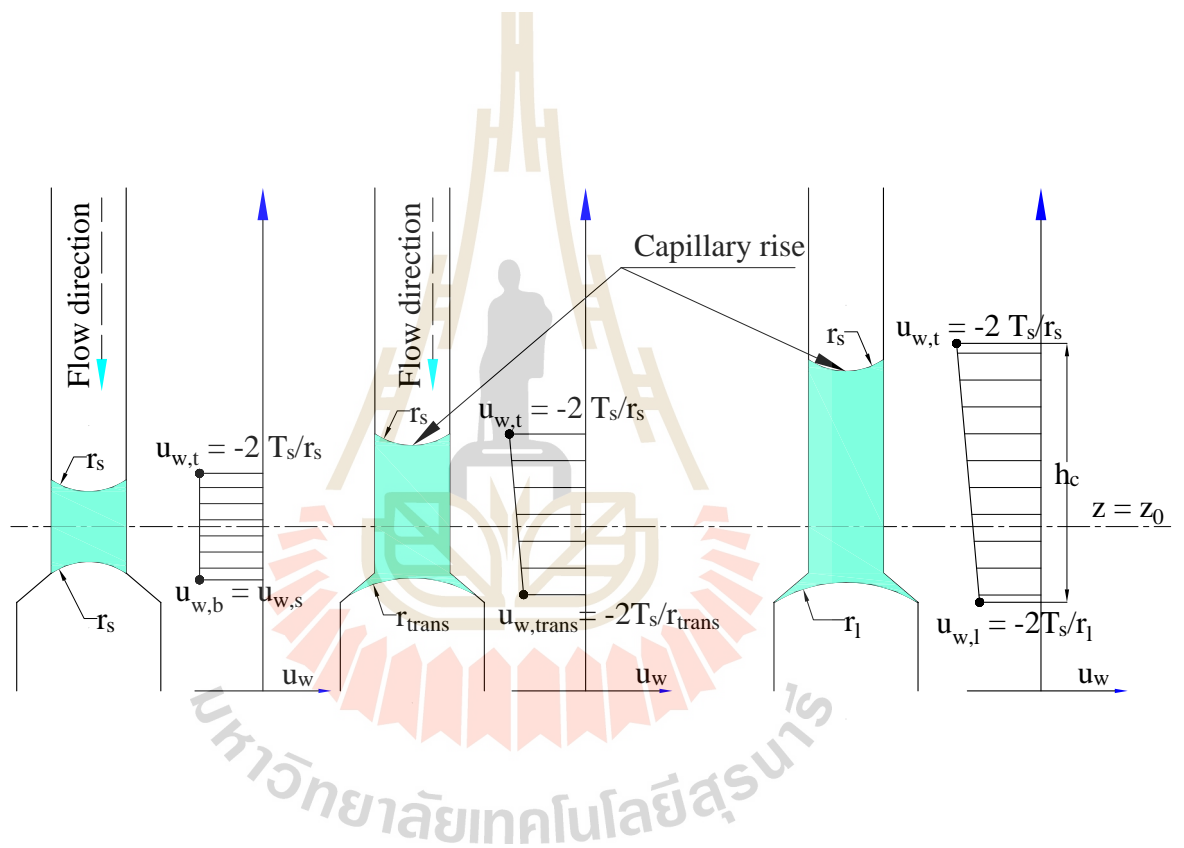


มหาวิทยาลัยเทคโนโลยีสุรนารี

on the unsaturated water flow is that the water might be obstructed at the interface between two materials have different hydraulic conductivity. The water is held due to suction forces and a capillary meniscus generates above the conductivity boundary. Subsequently, the degree of saturation in the smaller pore size soil layer will go up and result in a sufficient rise of the water column above the meniscus, this process (progressive accumulation of water) is continuously taken place until the moisture content or water pressure developed in the smaller pore size soil accomplishes a certain level such that the capillary barrier is broken (Mancarella et al., 2012). The breakthrough occurs only when the suction in the smaller pore size soil drops down to a level such that its value equals to the capillary pressure in the larger pore, known as water entry value (WEV) (Stormont and Anderson, 1999). Due to this moisture retaining behavior, the water infiltration into the larger pore size soil layer is limited or even restricted because of the capillary tension of smaller pore size (Shackelford et al., 1994; Tidwell et al., 2003; Stormont and Anderson, 1999). Khire et al., (2000) stated that the flow of water from smaller pore size through the larger pore size soil might not be taken place until low magnitudes of suction head are reached at the conductivity boundary.



มหาวิทยาลัยเทคโนโลยีสุรนารี



limiting/restricting infiltration into buried waste or preventing water rise into heave-sensitive soils or preventing the seepage of groundwater permeate through the protected zone of MSE walls. In order to comprehend the fundamentals of the capillary barrier, two capillary tubes having different diameters are often employed including a smaller diameter used to stand for the finer pore material, and the larger diameter tube is used to represent the coarser pore material (as shown in the **Figure 2.36**)

At the interface between air phase and water phase, the pore water pressure in the smaller radius tube, $u_{w,s}$, is estimated based on the Young-Laplace equation (Lu and Likos, 2004) as:

$$u_{w,s} = -\frac{2T_s}{r_s} \quad (2.65)$$

where T_s is the surface tension of the water phase, r_s is the radius of the smaller tube.

As the whole body of water lens is placed in the smaller tube, the magnitude of the water pressures at the top and that develops at the bottom of the water lens are equal. Because of gravitational force, the water lens tends to drop and the overlying water lens get thicker, leading to an increase in the total head. Finally, the pore water is then forced to move slightly into the transitional zone. As the bottom of the water lens moves forward to the transitional zone, the pore water pressure at the bottom of the lens becomes greater than that develops at the top and defined as (Lu and Likos, 2004):

$$u_{w,trans} = -\frac{2T_s}{r_{trans}} \quad (2.66)$$

where $u_{w,trans}$ is the pore water pressure at the transitional zone, r_{trans} is the radius of the tube at the transitional zone.

Because the pore water pressure generated at the bottom becomes larger than that at the top of the lens, the water lens tends to hang around at this place if no more water is infiltrated. In case that the infiltration from groundwater endures, the thickness of the water lens will build up gradually, hence pore water pressure at the bottom of the lens increases. Soon after the magnitude of pore water pressure equals to the WEV of the larger pore size materials, the wetting front will move forward to the location that is placed close to the end of the transition zone (**Figure 2.36c**). The maximum value of pore water pressure developed at the bottom of the lens with respect to the radius of the larger tube can be estimated as:

$$u_{w,l} = -\frac{2T_s}{r_l} \quad (2.67)$$

where $u_{w,l}$ is the pore water pressure at the larger radius tube, r_l is the radius of the larger tube.

The point at which water is able to flow through the interface defined as the breakthrough threshold, the capillary barrier is broken and the breakthrough head h_{br} can be estimated (Lu and Likos, 2004) as:

$$h_{br} \chi_w = u_{w,l} - u_{w,s} = \frac{2T_s}{r_s} - \frac{2T_s}{r_l} \quad (2.68)$$

$$h_{br} = \frac{2T_s}{\chi_w} \left(\frac{1}{r_s} - \frac{1}{r_l} \right) \quad (2.69)$$

In reality, the starting point of breakthrough is estimated based on the equality of unsaturated hydraulic conductivity at the interface between two porous materials having different pore size. A capillary barrier is normally generated at the interface of two unsaturated porous materials; particularly, when having an unsaturated fine-grained material is underlain by another unsaturated porous soil with relatively large pore size or higher conductivity at a given suction head that exists at their interface. Due to this, the water is unable to permeate through the underlying layer (higher conductivity) until a critical condition is reached.

2.8 In summary

As taking numerous advantages over the conventional concrete retaining walls, especially with tall walls and weak foundation conditions, the use of reinforced earth techniques has taken priority over all other forms of current retaining wall structures in terms of both economics and technics. The performance of MSE walls is mainly governed by the interaction between its constituents, particularly between backfill and reinforcing materials, which is dependent on the moisture responses taken place within reinforced soil mass. As a type of unsaturated soil mass, the MSE walls are normally stiff and strong when properly compacted due to the matric suction. However, matric suction might be significantly reduced as MSE walls subjected to rising of water table or under a heavy rain. Consequently, the MSE walls can be drastically moved, or even actual collapses. Among several drainage techniques that have also introduced to deal with the water flow through unsaturated MSE walls, the use of geocomposite which formed of a core material of geonet sandwiched by two layers of geotextile as an alternative drainage system has proven to be an appropriate

approach for MSE walls. According to previous published studies (Stormont et al., 1997; Lafleur et al., 2000; Stormont and Morris 2000; Iryo and Rowe, 2004; Nahlawi et al., 2007) they indicated that geotextiles oppose the water retention characteristic (WRC) that is similar to those of coarse-grained soils, such as gravels and sands. Hence, the WRC of nonwoven geotextile can affect the drainage capacities of geocomposite, but none of them incorporates WRC of geotextile to the simulation yet. The design of geocomposite drain in MSE walls does not include WRC of geotextile into consideration. Therefore, the initial aim of this research is to examine the influence of WRC of geotextile as well as of reinforced earth on flow behavior, which is necessary to allow more effective and applicable to use of geocomposite in MSE walls.

In addition, the current design section and illustration for MSE geosynthetic reinforced walls have assumed there is nonexistence of hydrostatic pressure, which implies that all water inside reinforced soil mass could be readily discharged around and/or through the reinforced soil mass and the wall facing. This condition is indeed to be desired but only if good draining backfills could be found. Practically, the use of in-placed marginal soils as backfill becomes more frequent, especially in tropical climate area where the residual soils are often found to be marginal lateritic soil. A number of previous researches have also reported that the performance of MSE walls utilized fine-grained marginal soils was good, there was no distress of reinforced structures observed if a proper drainage component installed. However, there have not many works pay attention to examine the influence of WRC of fine-grained marginal soils on the flow responses of MSE walls. Based on this, the second goal of this

research is to evaluate two feasible scenarios of MSE walls in which fine-grained marginal soils utilized as backfill materials.

2.9 References

- AASHTO., 2002. **Standard Specifications for Highway and Bridge**. American Association of State of Highway and Transportation Officials, Washington DC
- Abdolahzadeh, A. M., Vachon, B. L., Cabral, A. R., 2011. **Evaluation of the effectiveness of a cover with capillary barrier effect to control percolation into a waste disposal facility**. Canadian Geotechnical Journal 48(7): 996-1009.
- Aitchison, G., and Richards, B., 1965. **A broad-scale study of moisture conditions in pavement subgrades throughout Australia**, Butterworth & Company, for Division of Soil Mechanics, CSIRO.
- Alzamora, D. E., and Anderson, S., 2009. **Review of mechanically stabilized earth wall performance issues**. Transportation Research Board (TRB), 2009 Annual Meeting CD-ROM.
- Anderson, L. R., Nelson, K. J., Sampaco, C. L., 1995. **Mechanically Stabilized Earth Walls**. Transportation Research Circular (444): 17 pages
- Anderson, P. L., Gladstone, R. A., Sankey, J. E., 2012. **State of the practice of MSE wall design for highway structures**. Geotechnical Engineering State of the Art and Practice: Keynote Lectures from GeoCongress 2012: 443-463.
- Arbhabhirama, A., and Kridakorn, C., 1968. **Steady downward flow to a water table**. Water resources research 4(6): 1249-1257.

- Averyanov, S., 1950. **About permeability of subsurface soils in case of incomplete saturation.** English collection. The theory of ground water movement, 7, 19-21.
- Bathurst, R. J., and Simac, M. R., 1994. **Geosynthetic reinforced segmental retaining wall structures in North America.** Proceeding of the Fifth International Conference on Geotextiles, Geomembranes and Related Products, Singapore. 1-41
- Benson, C. H., and Khire, M. V., 1995. **Earthen covers for semi-arid and arid climates.** Geotechnical Special Publication, 53, 201-217.
- Berg, R., and Meyers, M., 1997. **Analysis of the collapse of a 6.7 m high geosynthetic-reinforced wall structure.** Proceedings of the Geosynthetics, 97, 85-104
- Bergado, D. T., Shivashankar, R., Alfaro, M. C., Chai, J.C., Balasubramaniam, A. S., 1993. **Interaction behaviour of steel grid reinforcements in a clayey sand.** Geotechnique 43(4): 589-603.
- Bergado, D. T., and Jin-Chun, C., 1994. **Pullout force/displacement relationship of extensible grid reinforcements.** Geotextiles and Geomembranes 13(5): 295-316.
- Bergado, D. T., Horpibulsuk, S., Teerawattanasuk, C., 2001. **Soil improvement by MSE – theoretical background.** Short course on mechanically stabilized earth. Asian Center for Soil Improvement and Geosynthetics, Asian Institute of Technology, Bangkok, Thailand
- Bishop, A. W., 1959. **The effective stress principle.** Teknisk Ukeblad, 39, 859-863.

- Bishop, A. W., 1954. **The use of pore-pressure coefficients in practice.** Geotechnique 4(4): 148-152.
- Bishop, A. W., and Blight, G., 1963. **Some aspects of effective stress in saturated and partly saturated soils.** Geotechnique 13(3): 177-197.
- Bouazza, A., Zornberg, J., McCartney, J. S., Singh, R. M., 2013. **Unsaturated Geotechnics Applied to Geoenvironmental Engineering Problems Involving Geosynthetics.** Engineering Geology, 165, 143-153.
- Brooks, R. H., and Corey, A. T., 1964. **Hydraulic properties of porous media and their relation to drainage design.** Colorado State University Hydrology Paper 27(3): 26-28.
- Brutsaert, W., 1966. **Probability laws for pore-size distributions.** Soil Science 101(2): 85-92.
- BS, B. S., 1995. **Code of Practice for Strengthened/Reinforced Soils and Other Fills.** British Standard Institution, London, UK.
- Buckingham, E., 1907. **Studies on the movement of soil moisture.** Government Printing Office, Bulletin 38, Washington, USA.
- Burwash, W., and Frost, J., 1991. **Case history of a 9 m high geogrid reinforced retaining wall backfilled with cohesive soil.** Geosynthetics Conference, Atlanta, Georgia, USA.
- Campbell, G. S., 1974. **A simple method for determining unsaturated conductivity from moisture retention data.** Soil Science 117(6): 311-314.
- Chai, J., 1992. **Interaction between grid reinforcement and cohesive-frictional soil and performance of reinforced wall/embankment on soft ground.** D. Engineering Dissertation. Asian Institute of Technology, Bangkok, Thailand.

- Chen, D. H., Nazarian, S., Bilyeu, J., 2007. **Failure Analysis of a Bridge Embankment with Cracked Approach Slabs and Leaking Sand**. Journal of Performance of Constructed Facilities 21(5): 375-381.
- Chinkulkijniwat, A., Hopibulsuk, S., Bui Van, D., Udomchai, A., Goodary, R., Arulrajah, A., 2016. **Influential factors affecting drainage design considerations for mechanical stabilised earth walls using geocomposite**. Geosynthetics International, 24 (3): 224-241.
- Christensen, H. R., 1944. **Permeability capillary potential curves for three prairie soils**. Soil Science 57(5): 381-390.
- Christopher, B. R., Gill, S. A., Giroud, J. P., Juran, I., Mitchell, J. K., Schlosser, F., Dunncliff, J., 1990. **Reinforced Soil Structures, volume 1. Design and Construction Guidelines**. U.S Department of Transportation Federation Highway Administration.
- Christopher, B. R., Zornberg, J. G., Mitchell, J. K., 1998. **Design guidance for reinforced soil structures with marginal soil backfills**. Proceedings of the Sixth International Conference on Geosynthetics, Atlanta, Georgia, US, 2, 797-804
- Christopher, B. R., 1993. **Deformation response and wall stiffness in relation to reinforced soil wall design**. Ph.D Dissertation, Purdue University, 352pp.
- Corey, A. T., 1954. **The interrelation between gas and oil relative permeabilities**. Producers monthly 19(1): 38-41.
- Davidson, J. M., Stone, L. R., Nielsen, D. R., Larue, M. E., et al. (1969). **Field Measurement and Use of Soil-Water Properties**. Water resources research 5(6): 1312-1321.

- De Bano, L. F., 2000. **The role of fire and soil heating on water repellency in wildland environments: a review**. Journal of Hydrology, 231, 195-206.
- Elias, V., Christopher, R., Barry, P. E., 2001. **Mechanically Stabilized Earth Walls and Reinforced Soil Slopes Design and Construction Guidelines**, Federal Highway Administration, US Department of Transportation., Publication No.FHWA NHI-00-043., 394 pages.
- Elias, V., and Swanson, P., 1983. **Cautions of reinforced earth with residual soils**, Transportation Research Record.
- Escario, V., Jucá, J. F., 1989. **Strength and deformation of partly saturated soils**. Proc. 12th ICSMFE, Rio de Janeiro, 2, 43-46.
- FHWA., 1998. **Geosynthetic Design and Construction Guidelines**. Federal Highway Administration, U.S Department of Transportation, Washington DC, USA.
- Fredlund, D. G., & Morgenstern, N. R. 1977. **Stress state variables for unsaturated soils**. ASCE, Journal of Geotechnical and Geoenvironmental Engineering, 103(5):447-466
- Fredlund, D. G., Morgenstern, N. R., Widger, R. A., 1978. **The shear strength of unsaturated soils**. Canadian Geotechnical Journal 15(3): 313-321.
- Fredlund, D. G., and Morgenstern, N. R., 1977. **Stress state variables for unsaturated soils**. Journal of Geotechnical and Geoenvironmental Engineering, 103
- Fredlund, D. G. and Rahardjo, H., 1993. **Soil mechanics for unsaturated soils**, John Wiley & Sons.

- Fredlund, D. G. and Xing, A., 1994. **Equations for the soil-water characteristic curve**. Canadian Geotechnical Journal 31(4): 521-532.
- Gan, K. J., and Fredlund, D. G., 1988. **Multistage direct shear testing of unsaturated soils**. American Society for Testing Materials, Geotechnical Testing Journal 11(2): 132-138.
- Gardner, W., 1958. **Mathematics of isothermal water conduction in unsaturated soil**. Highway research board special report, 40
- Horpibulsuk, S., and Niramitkornburee, A., 2010. **Pullout resistance of bearing reinforcement embedded in sand**. Soils and Foundations 50(2): 215-226.
- Horpibulsuk S., Suksiripattanapong, C., Niramitkornburee, A., Chinkulkijniwat, A., and Tangsutthinon, T., 2011. **Performance of an earth wall stabilized with bearing reinforcements**. Geotextiles and Geomembranes 29(5): 514-524.
- Hossain, M. S., Kibria, G., Khan, M. S., Hossain, J., Taufiq, T., 2011. **Effects of backfill soil on excessive movement of MSE wall**. Journal of Performance of Constructed Facilities 26(6): 793-802.
- Huang, C.C., 1994. **Report on three unsuccessful reinforced walls**. Recent Case Histories of Permanent Geosynthetic-Reinforced Soil Retaining Walls, (eds. Tatsuoka & Leshchinsky), Balkema, Rotterdam, 219-222.
- Ingold, T. S., 1982. **Reinforced Earth**, Thomas Telford, London.
- INDOT, 2013., **Indiana design manual, chapter 410**. Indiana Department of Transportation.
- Irmay, S., 1954. **On the hydraulic conductivity of unsaturated soils**. Eos, Transactions American Geophysical Union 35(3): 463-467.

- Iryo, T., and Rowe, R., 2004. **Numerical Study of Infiltration Into a Soil–Geotextile Column**. *Geosynthetics International* 11(5): 377-389.
- Jewell, R. A., 1984. **Interaction between soil and geogrids**. Proceedings of the Symposium on Polymer Grid Reinforcement in Civil Engineering, Thomas Telford Limited, London, UK, 22-23 March 1984, 11-17.
- Johnson, A., 2012. **Recommendations for Design and Analysis of Earth Structures Using Geosynthetic Reinforcements-EBGEO**. John Wiley & Sons
- Kerisel, J., 1993. **History of Retaining Wall Design**. Retaining Structures. Proceedings of the Conference Organized by the Institute of Civil Engineers and held on 20-23 July, 1992 at Robinson College, Cambridge, Thomas Telford, London.
- Khalili, N., and Khabbaz, M., 1998. **A unique relationship of χ for the determination of the shear strength of unsaturated soils**. *Geotechnique* 48(5).
- Khire, M. V., Benson, C. H., Bosscher, P. J., 2000. **Capillary barriers: design variables and water balance**. *Journal of Geotechnical and Geoenvironmental Engineering* 126(8): 695-708.
- Koerner, R. M., 1998. **Design with Geosynthetics**, Prentice Hall, 4th edition, New Jersey.
- Koerner, R. M., and Soong, T., 2000. **Design of Drainage Systems for Segmental Retaining Walls**. Proceedings of the 14th GRI Conference.
- Koerner, R. M., and Soong, T.-Y., 2001. **Geosynthetic Reinforced Segmental Retaining Walls**. *Geotextiles and Geomembranes* 19(6): 359-386.

- Koerner, R. M., 2005. **Designing with Geosynthetics**, Prentice Hall Publ Co, Englewood Cliffs, New Jersey.
- Koerner, R. M., Soong, T.-Y., Koerner, G. R., 2005. **Back drainage design and geocomposite drainage materials**, Proceeding of the 19th GRI conference: 51-86
- Koerner, R. M., and Koerner, G. R., 2011. **The Importance of Drainage Control for Geosynthetic Reinforced Mechanically Stabilized Earth Walls**. Journal of GeoEngineering 6(1): 3-13.
- Lafleur, J., Lebeau, M., Faure, Y. H., Savard, Y., Kehila, Y., 2000. **Influence of Matric Suction on the Drainage Performance of Polyester Geotextiles**. Proceedings 53rd Annual Conference of the Canadian Geotechnical Society, 1115-1122
- Lambe, T. W., and Whitman, V. R., 1969. **Soil Mechanics**. John Wiley and Sons: ISBN: 978-970-471-51192-51192.
- Lee, K. L., Adams, B. D., Vagneron, J. J., 1973. **Reinforced earth retaining walls**. Journal of Soil Mechanics & Foundations 99(sm10): 745-764.
- Leong, E. C., and Rahardjo, H., 1997. **Permeability functions for unsaturated soils**. Journal of Geotechnical and Geoenvironmental Engineering 123(12): 1118-1126.
- Long, R. P., 1995. **Mechanically Stabilized Earth Walls**. Transportation Research Board 74 Annual Meeting, Washington, D.C.
- Lu, N., and Godt, J., 2008. **Infinite slope stability under steady unsaturated seepage conditions**. Water resources research 44(11). doi:10.1029/2008WR006976

- Lu, N., Godt, J. W., Wu, D. T., 2010. **A closed-form equation for effective stress in unsaturated soil.** Water resources research 46(5). doi:10.1029/2009WR008646.
- Lu, N., and Likos, W. J., 2006. **Suction stress characteristic curve for unsaturated soil.** Journal of Geotechnical and Geoenvironmental Engineering 132(2): 131-142.
- Mahmood, T., 2009. **Failure Analysis of a Mechanically Stabilized Earth (MSE) wall using Finite Element Program PLAXIS,** The University of Texas at Arlington.
- Mancarella, D., Doglioni, A., Simeone, V., 2012. **On capillary barrier effects and debris slide triggering in unsaturated layered covers.** Engineering Geology, 147, 14-27.
- Marshall, T. J., Holmes, J. W., Rose, C. W., 1996. **Soil physics,** Cambridge University Press.
- McGown, A., Andrawes, K. Z., Prandhan, S., Khan, A. J 1998. **Limit state design of geosynthetic reinforced soil structures.** Proceedings of the Sixth International Conference on Geosynthetics, 144-179
- Meyerhof, G. G., 1963. **Some recent research on the bearing capacity of foundations.** Canadian Geotechnical Journal 1(1): 16-26.
- Mitchell, J., 1995. **Reinforced Soil Structures with Poorly Draining Backfills Part II: Case Histories and Applications.** Geosynthetics International 2(1): 265-307.
- Mitchell, J. K., and Villet, W. C., 1987. **Reinforcement of Earth Slopes and Embankments.** NCHRP Report, 290, Transportation Research Board, US

- Mualem, Y., 1976. **A new Model for Predicting the Hydraulic Conductivity of Unsaturated Porous Media**. Water Resour. Res 12(3): 513-522.
- Mualem, Y., 1986. **Hydraulic conductivity of unsaturated soils: prediction and formulas**. Methods of Soil Analysis: Part 1 - Physical and Mineralogical Methods (methodsofsoilan1): 799-823.
- Nahlawi, H., Bouazza, A., Kodikara, J., 2007. **Characterisation of Geotextiles Water Retention using a Modified Capillary Pressure Cell**. Geotextiles and Geomembranes 25(3): 186-193.
- Nand, K., 2005. **Concept and design of reinforced earth structures**. Report no.GE: R-73. Ministry of railways. Government of India.
- Narejo, D., and Ramsey, B., 2001. **MSE wall drainage alternatives Careful drainage design can prevent costly retaining-wall failures**. Geotechnical Fabrics Report 19(5): 26-29.
- NCMA., 1997. **Design Manual for Segmental Retaining Walls**. 2nd edition. National Concrete Masonry Association, Herndon, Virginia, USA.
- Nielsen, M. R., and Anderson, L. R., 1984. **Pullout resistance of wire mats embedded in soil**. Report Submitted to the Hilfiker Company.
- Ning, L., and Likos, W. J., 2004. **Unsaturated soil mechanics**. Jhon Wiley & Sons Inc, New Jersey.
- Okechukwu, S. I., Okeke, O. C., Akaolisa, C. C., Jack, L., Akinola, A. O., 2016. **Reinforced earth: Principles and Applications in engineering construction**. International Journal of Advanced Academic Research 2(6): 14-33

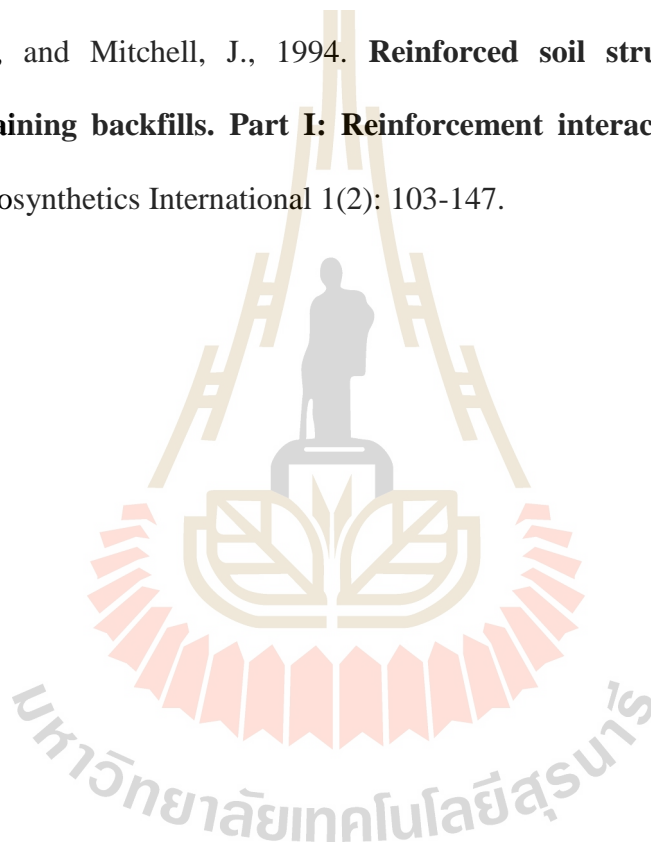
- Omuto, C., 2009. **Biexponential model for water retention characteristics.** Geoderma 149(3): 235-242.
- Philip, J. R., 1986. **Linearized unsteady multidimensional infiltration.** Water resources research 22(12): 1717-1727.
- Rahardjo, H., Lim, T. T., Chang, M. F., Fredlund, D. G., 1995. **Shear-strength characteristics of a residual soil.** Canadian Geotechnical Journal 32(1): 60-77.
- Rahardjo, H., Santoso, V. A., Leong, E. C., Ng, Y. S., Hua, C. J., 2011. **Performance of an instrumented slope covered by a capillary barrier system.** Journal of Geotechnical and Geoenvironmental Engineering 138(4): 481-490.
- Richards, L. A., 1931. **Capillary conduction of liquids through porous mediums.** Journal of Applied Physics 1(5): 318-333.
- Rijtema, P. E., 1965. **An analysis of actual evapotranspiration,** Center for Agricultural Publications and Documentation.
- Saito, M., Shibuya, S., Mitsui, J., & Hara, K. 2008. **L-shaped geodrain in embankment model test and numerical simulation.** In Geosynthetics in Civil and Environmental Engineering, Springer, Berlin, Heidelberg: 428-433
- Sandri, D., 1997. **A performance summary of reinforced soil structures in the greater Los Angeles area after the Northridge earthquake.** Geotextiles and Geomembranes 15(4): 235-253.
- Sankey, J. E., Soliman. A., 2004. **Tall wall mechanically stabilized earth applications.** Geotechnical Engineering for Transportation Projects, 2149-2158.

- Scarborough, J. A., 2005. **A tale of two walls: Case histories of failed MSE walls.** Proceedings of Geo-Frontiers, 2751-2762.
- Schlosser, F., and Long, N.-T., 1974. **Recent Results of French Research on Reinforced Earth.** Journal of the Construction Division 100(3): 223-237.
- Shackelford, C. D., Chang, C. K., Chiu, T. F., 1994. **The capillary barrier effect in unsaturated flow through soil barriers.** 1st ICEG Conference, Edmonton, CA, 789-793
- Shibuya, S., Kawaguchi, T., Chae, J., 2007. **Failure of Reinforced Earth as Attacked by Typhoon No. 23 in 2004.** Soils and Foundations 47(1): 153-160.
- Sillers, W. S., Fredlund, D. G., Zakerzadeh, N., 2001. **Mathematical attributes of some soil-water characteristic curve models.** Unsaturated soil concepts and their application in geotechnical practice, Springer, 243-283.
- Stormont, J., 1996. **The effectiveness of two capillary barriers on a 10% slope.** Geotechnical and Geological Engineering 14(4): 243-267.
- Stormont, J. C. and Anderson, C. E., 1999. **Capillary barrier effect from underlying coarser soil layer.** Journal of Geotechnical and Geoenvironmental Engineering 125(8): 641-648.
- Stormont, J. C., Henry, K. S., Evans, T. M., 1997. **Water Retention Functions of four Nonwoven Polypropylene Geotextiles.** Geosynthetics International 4(6): 661-672.
- Stormont, J. C., and Morris, C. E., 2000. **Characterization of Unsaturated Nonwoven Geotextiles.** Geotechnical Special Publication, 153-164.

- Stulgis, R., 2005. **Full-scale MSE Test Walls**. Proceedings of the Nineteenth Geosynthetic Research Institute Conference (GRI-19), Geosynthetics Institute, Las Vegas, NV, December, 14 – 16.
- Stulgis, R., 2005. **Selecting Reinforced Fill Materials for MSE Retaining Walls**. Geosynthetics Research and Development in Progress, ASCE, Geo-Frontiers Congress, Texas, US, January 24-26, 1-6
- Suksiripattanapong, C., Horpibulsuk, S., Chinkulkijniwat, A., and Chai, JC., 2013. **Pullout resistance of bearing reinforcement embedded in coarse-grained soils**. Geotextiles and Geomembranes 36: 44-54.
- Tensar., 1986. **Guidelines for the design of tensar geogrid reinforced soil retaining walls**. The Tensar corporation, Georgia, USA (Technical Note).
- Terzaghi, K., 1943. **Theoretical soil mechanics**. J. Wiley and Sons, inc.
- Tidwell, V. C., Glass, R. J., Chocas, C., Barker, G., Orear, L., 2003. **Visualization experiment to investigate capillary barrier performance in the context of a Yucca Mountain emplacement drift**. Journal of contaminant hydrology 62: 287-301.
- Toll, D. G., 2001. **Unsaturated Soil Concepts and Their Application in Geotechnical Practice**. Kluwer Academic Publishers.
- Too, V., Omuto, C., Biamah, E. and Obiero, J., 2014. **Review of Soil Water Retention Characteristic (SWRC) Models between Saturation and Oven Dryness**. Open Journal of Modern Hydrology, 4, 173-182
- van-Genuchten., 1980. **A closed-form Equation for Predicting the Hydraulic Conductivity of Unsaturated Soils**. Soil Science Society of America Journal 44(5): 892-898.

- Vanapalli, S. K., Fredlund, D. G., Pufahl, D. E., Clifton, A. W., 1996. **Model for the prediction of shear strength with respect to soil suction**. Canadian Geotechnical Journal 33(3): 379-392.
- Vanapalli, S. K., Sillers, W. S., Fredlund, M. D., 1998. **The meaning and relevance of residual state to unsaturated soils**. Proceedings of the 51st Canadian Geotechnical Conference, Alta, 4-7
- Vidal, H., 1969. **The Principle of Reinforced Earth**. Highway Research Record No. 282, Transportation Research Board: Washington, D.C.
- Voottipruex, P., Bergado, D. T., Kongkitkul, W., 2001. **Design of MSE wall using MSEXLS computer software**. Short course on mechanically stabilized earth. Asian Center for Soil Improvement and Geosynthetics, Asian Institute of Technology, Thailand, Nov 20th, 2001.
- Wind, G., 1955. **A field experiment concerning capillary rise of moisture in a heavy clay soil**. Netherlands Journal of Agricultural Science, 3, 60-69.
- Withiam, J. L., Voytko, E. P., Barker, R. M., Duncan, J. M., Kelly, B. C., Musser, S. C., Elias, V., 1998. **Load and Resistance Factor Design (LRFD) for Highway Bridge Substructures**, FHWA Publication No.FHWA HI-98-032. .
- Wu, J. T., 2006. **Design and construction guidelines for geosynthetic-reinforced soil bridge abutments with a flexible facing**, National Cooperative Highway Research Program (NCHRP) Report 556. Transportation Research Board.
- Yanful, E. K., 1993. **Oxygen diffusion through soil covers on sulphidic mine tailings**. Journal of Geotechnical Engineering 119(8): 1207-1228.

- Yubonchit, S., 2016. **Influence indices for rainfall - induced shallow slope failures in view of warning system implementation**. Ph.D dissertation., School of Civil Engineering, Suranaree University of Technology, Thailand.
- Yuster, S., 1951. **Theoretical considerations of multiphase flow in idealized capillary systems**. Proceedings of the 3rd World Petroleum Congress, Section II, The Hague.
- Zornberg, J., and Mitchell, J., 1994. **Reinforced soil structures with poorly draining backfills. Part I: Reinforcement interactions and functions**. Geosynthetics International 1(2): 103-147.



CHAPTER III

INFLUENTIAL FACTORS AFFECTING DRAINAGE

DESIGN CONSIDERATIONS FOR MECHANICAL

STABILISED EARTH WALLS USING

GEOCOMPOSITES

This part was established to examine a practical case of the use of reinforced earth structures as a retaining wall structure, in which the reinforced soil mass was fully filled with good draining materials. Initially, several crucial problems that inspired this part established is enlightened. Subsequently, an illustration of numerical and physical experiments that used throughout this research is displayed. After the successful calibration of the model the parametric was done by using Plaxis, the model calibration and its characters is presented in a section placed at the back of numerical and physical experiment section. Afterward, the computed results of parametric analysis are illustrated. The chapter is closed with an utmost elucidation of the influences of soil water characteristic on flow response presented in terms of effective saturation and phreatic surface is shown. In short, the results obtained from sensitivity analysis indicate that the flow response in both unreinforced and protected zone affected by soil water characteristic of geotextile, backfill materials, as well. The level of phreatic surface found in the protected zone was mainly governed by the ratio of hydraulic conductivity of geonet to that of backfill, the lower permeability the

higher phreatic surface inside the protected zone found. Another finding found was that the effect of capillary break phenomenon on the amount of water accumulated at the hydraulic conductivity boundary, hence the distribution of effective saturation.

3.1 Statement of problem

As described in the previous section, namely **Case studies of failed MSE walls**, there have been a number of MSE walls failures occurred, especially under a heavy rain. Most failures cases found were related to seepage water flow taken place within reinforced soil masses (Koerner and Soong, 2001; Narejo and Ramsey, 2001; Chen et al., 2007; Koerner and Koerner, 2011). A conclusion could be withdrawn from this is that whenever a reinforced earth structure is constructed adjacent to, or near to or subjected to a rising of the groundwater table, a proper drainage system must be addressed. In other words, any water ponding behind and beneath the protected zone must be properly collected, transmitted, and discharged. Special precautions should be taken for hillside constructions in particular due to the potential for seepage to occur through the retained soil. Several reinforced earth structures have also been designed and constructed based on design codes, the drainage was placed at the bottom of the wall, which was made of drainage pipes (Shibuya et al., 2007). It was, however, the drainage pipes did not extend to cover the area behind the wall. Hence, there was insufficient capacity in the drainage system. It was concluded that conventional drainage systems were not applicable in mountainous areas where there was a large amount and/or high level of ground water

The material conventionally used as the drainage medium for MSE walls is well-graded gravel. This desired strategy is becoming increasingly expensive, and

effective installation of this material as a vertical drainage layer is difficult in the field. An alternative to the use of well-graded gravel is to provide drainage with the use of geocomposites (Koerner and Soong, 2000; Koerner and Soong, 2005; Chen et al., 2007). It is broadly recognized that the use of geocomposites could provide numerous advantages over the conventional techniques. Geocomposites comprise a core material with a large flow channel (e.g., geonet), which is covered by two nonwoven geotextile layers. Stormont et al., (1997) stated that geocomposites could provide a hydraulic conductivity approximately 10 to 100 times higher than that of compacted backfills. Due to its specific hydraulic properties, non-woven geotextiles could function as both drainage and capillary barrier (Stormont and Morris, 2000). Geocomposites are light and do not add significantly to the weight of soil in the backfill. Furthermore, geocomposites allow for quick and easy installation compared with conventional drains using gravel. McKean and Inouye (2001) reported a successful field case study of using geocomposites to prevent water flowing behind a retaining wall. This geocomposite was reported to have performed successfully for a period of 14 years.

Although there have been many reported case studies on the successful implementation of geocomposites in drainage systems, there have been limited numerical simulations of drainage for MSE walls using geocomposites (Koerner and Soong, 2005; Yoo and Jung, 2006). In addition, there is no known work that incorporates the water retention characteristic (WRC) of geotextiles in these reported numerical simulations. Previous studies indicate that geotextiles' water retention characteristics are similar to those of coarse-grained soils, such as gravels and sands (Lafleur et al., 2000; Morris, 2000; Stormont and Morris, 2000; Iryo and Rowe, 2003;

Bathurst, 2007; Nahlawi et al., 2007). Various methods have been introduced to determine the WRC of geotextiles, including a hanging column test by Stormont and Morris (2000); a capillary rise test approach in which a geotextile sheet was immersed in water at its base by Lebeau et al., (2000); an outflow capillary pressure cell by Knight and Kotha (2001); a modified outflow capillary pressure cell by Nahlawi et al., (2007); and a suction plate apparatus based on the hanging column test procedure by Bathurst et al., (2009). Currently, the design of geocomposite drains in MSE wall does not incorporate the WRC of geotextiles. A fundamental understanding of the effect of WRC of geotextiles on flow response is necessary to allow for a more effective and appropriate use of geocomposites in MSE walls.

This part was done by carrying out a large scale flow test through an MSE wall in which an L-shape geocomposite drain was installed. Instruments were installed for monitoring flow and deformation responses during the tests. The instruments consisted of four standpipe piezometers, 10 time domain reflectometer (TDR) probes and 10 surface settlements plates. Numerical analyses were subsequently conducted using the Plaxis 2D finite element modelling software to investigate the effect of the hydraulic properties on the water flow taking place in the MSE wall.

The initial goal of this part is to figure out the most important aspects that affect drainage design considerations for MSE walls using geocomposites as an artificial drainage system, subsequently, it may lead to a better understanding of the various parameters that affect the performance of the geocomposite drain and will facilitate the selection of suitable geocomposite drains for implementation in MSE walls.

3.2. Materials used in this study

The soil used in this investigation was a sandy soil consisting of 10% gravel, 87.3% sand, and 2.7% silt. The particle size distribution of the sand is presented in the upper right corner of **Figure 3.1**. This sand was classified as poorly graded sand (SP), according to the Unified Soil Classification System (USCS), with a specific gravity of 2.74. The compaction characteristics under standard Proctor energy was the optimum water content (OWC) of 5.7% and maximum dry unit weight $\gamma_{d\max}$ of 16.7 kN/m³. The saturated hydraulic conductivity of the soil was $k_{sat} = 17$ m/day. Generally, well-graded materials are commonly used as backfill materials due to their high efficiency in field compaction. However, uniform sand was used in this investigation to ensure consistency of the soil compacted in the large-scale physical model. Determinations of the WRC of the soil were conducted along the drying and wetting paths. The drying phase WRC was obtained using a pressure plate apparatus and the wetting phase WRC was obtained from the double-walled triaxial cell. The relationships between volumetric water content and matric suction of the soil along wetting and drying paths are presented in **Figure 3.1**

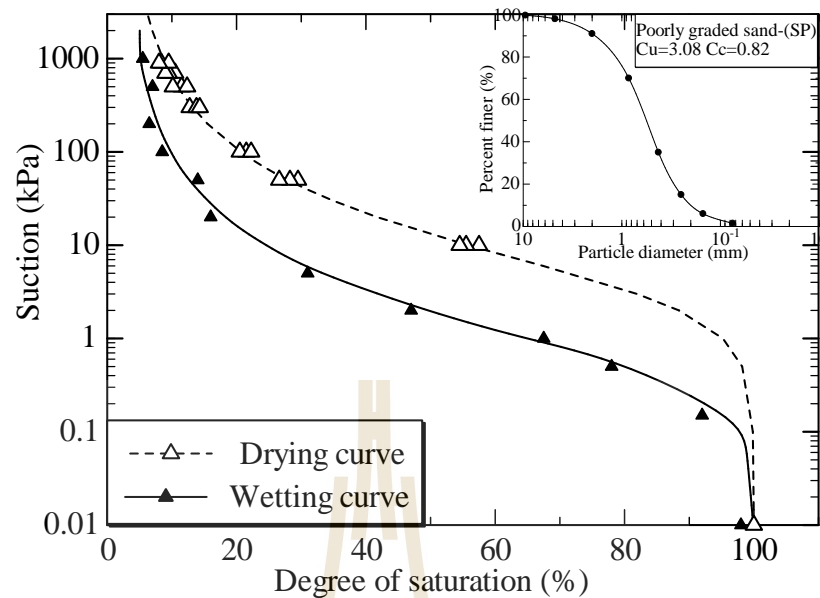


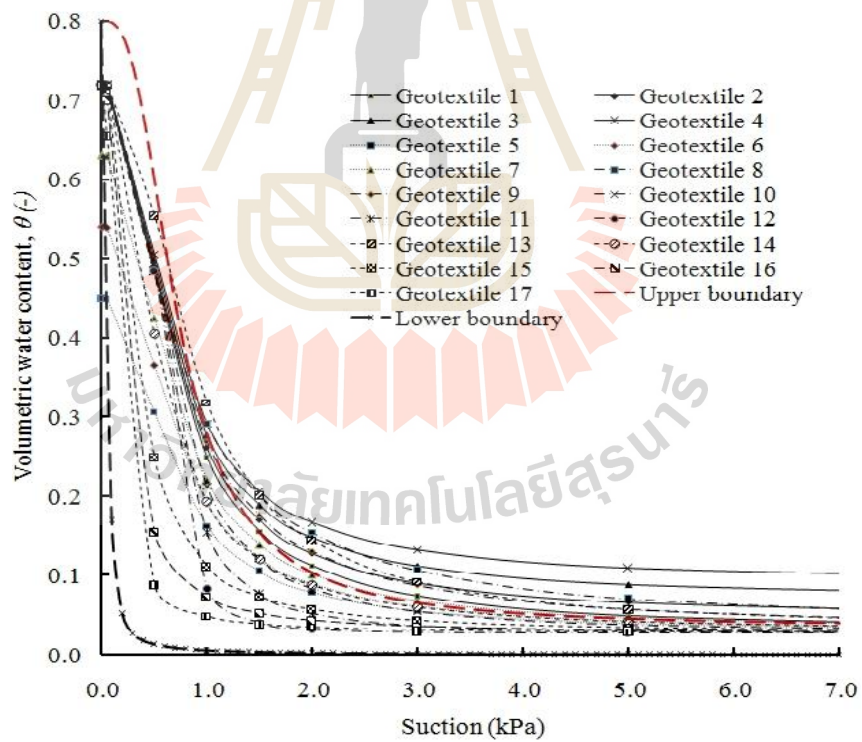
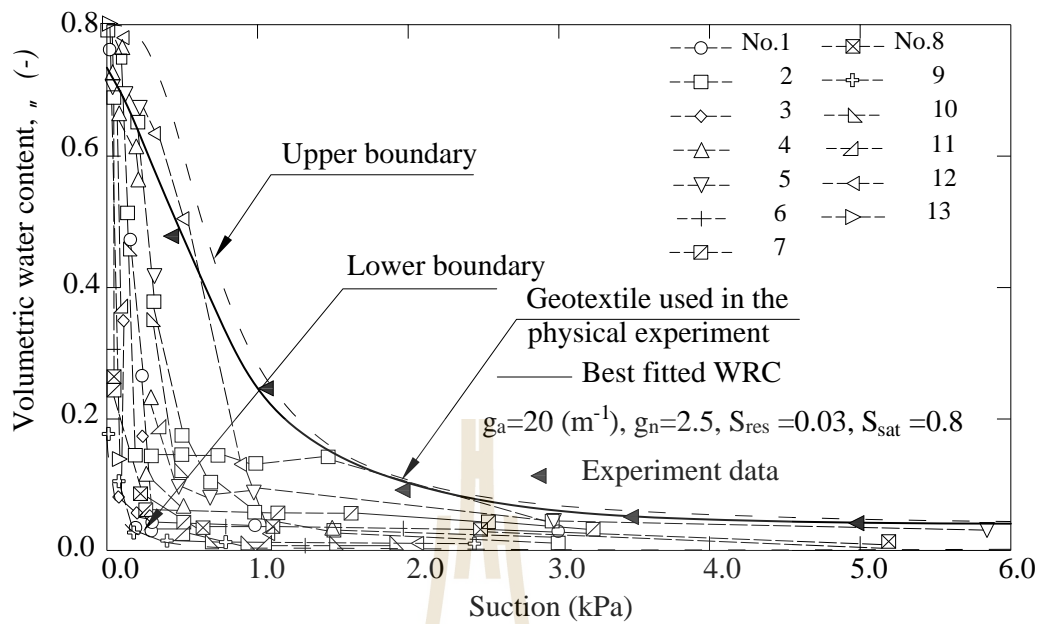
Figure 3.1 Water retention characteristic curves and grain-size distribution of the soil used in this part

The non-woven needle-punched polyester geotextile used in this study had an average thickness of 0.25 cm, an apparent opening size of 0.075 mm and a porosity of 0.90. The hydraulic properties of the geotextile are shown in **Table 3.1**. The transmissivity of the geonet was $0.004 \text{ m}^2/\text{sec}$ and this was converted to a saturated hydraulic conductivity of 69120 m/day. The WRC of the geotextile was conducted along the wetting path using a capillary rise test (Lafleur et al., 2000), which was conducted by hanging a 25 cm x 300 cm strip of geotextile vertically and placing the lower end of the strip in the reservoir water. The strip was covered with plastic wrap to prevent evaporation and allowed to equilibrate for 72 h. The sample was then cut into small strips to determine the volumetric water content. The volumetric water content was measured at different positions above the water surface by cutting the

specimen into 50 mm long segments and weighing the samples before and after oven drying. The relationships between the volumetric water content and matric suction of the geotextile are presented with the other WRC curves in **Figure 3.2**. The VG model was used to describe the relationship between volumetric water content and matric suction for the soil and the geotextile. The parameters used to fit the model to the test results for the soil and the geotextile in summarized in **Table 3.1**.

Table 3.1 VG and VGM model parameters and saturated hydraulic conductivity of the materials used in the physical test.

| VG and VGM parameters | | Sandy soil | Geotextile | Geonet |
|--|-------------------|------------|------------|--------|
| g_a | $[\text{m}^{-1}]$ | 20 | 20 | 600 |
| g_n | $[-]$ | 1.5 | 2.5 | 40 |
| S_{res} | $[-]$ | 0.03 | 0.03 | 0.00 |
| S_{sat} | $[-]$ | 1.00 | 0.80 | 1.00 |
| Geotextile: saturated hydraulic conductivity | | | | |
| $K_{lateral}$ | $[\text{m/day}]$ | 17 | 320 | 69120 |
| $K_{longitudinal}$ | $[\text{m/day}]$ | 17 | 2000 | 69120 |



3.3. Establishment for numerical and physical experiments

3.3.1 Numerical background

Numerical analysis of moisture flow through unsaturated soil is mostly performed through the solution of Richards' equation which is a parabolic partial differential equation. The quality of numerical solution of moisture flow through unsaturated soil is mainly governed by precisely estimated unsaturated soil properties include soil water characteristic, and unsaturated soil permeability (Dye, 2008). Based on the primary target of this research work, a range of SWCC and $k(h)$ was considered for two sensitivity studies: 1) varied SWCC, 2) varied hydraulic conductivity.

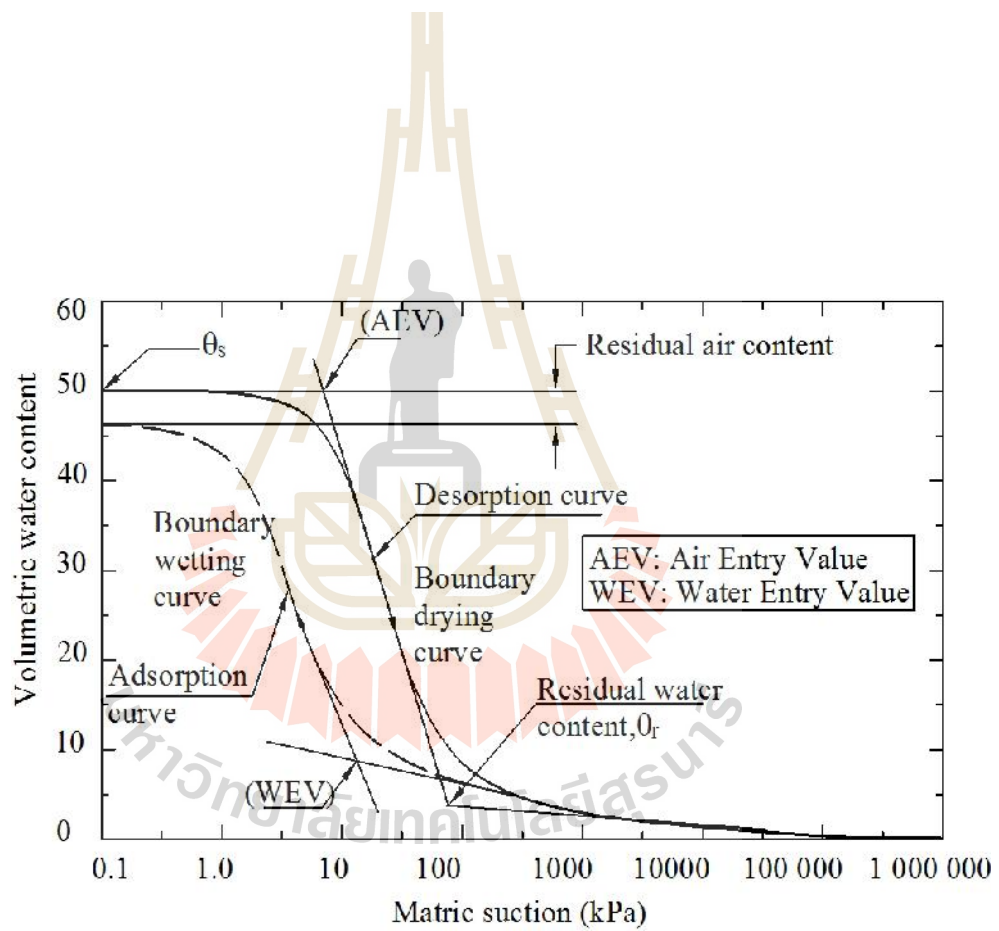
The governing equation for transient water flow in a two-dimensional homogeneous anisotropic material within an unsaturated porous medium is as follows:

$$\frac{\partial \theta}{\partial t} = k_x \frac{\partial^2 h}{\partial x^2} + k_y \frac{\partial^2 h}{\partial y^2} \quad (3.1)$$

where θ is volumetric water content, h is the total head, k_x and k_y are the unsaturated coefficients of permeability in the x- and y- directions, and t is time. To solve Equation 1, constitutive equations related to θ , k_x , and k_y to h are required. Iryo and Rowe (2003, 2004) concluded that there was considerable evidence to suggest that (van-Genuchten, 1980) and van Genuchten-Mualem (VGM) models, which combines the van Genuchten and Mualem hypotheses (Mualem, 1976) are applicable to nonwoven geotextiles. Thus, both of these constitutive equations are employed to approximate WRC and permeability functions for both the soil and the nonwoven geotextile.

$$S_e = \frac{S - S_{res}}{S_{sat} - S_{res}} = \left[1 + (g_a |h_p|)^{g_n} \right]^{g_c}$$

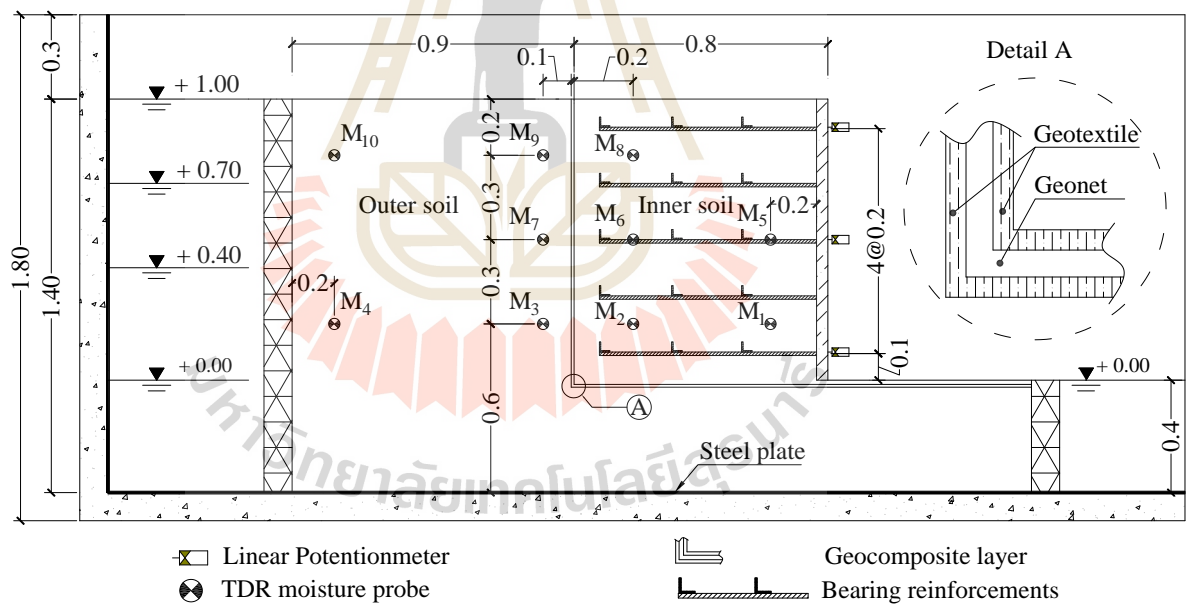
$$k_r(S_e) = S_e^{0.5} [1 - (1 - S_e^{-1/g_c})^{-g_c}]^2$$



(AEV), bulk water begins to drain away. Similarly to the AEV, when a soil is wetted, the degree of saturation increases markedly when the suction decreases to attain a suction value termed the water-entry value (WEV). The parameter g_a is a fitting parameter that reflects the inflection point on the WRC curve generated by **Equation 3.2a** and the largest pore size in the material. The parameter g_n reflects the steepness of the WRC curve in the desaturation zone, and a small value of g_n yields a steep WRC curve in the de-saturation zone and is hence related to the pore size distribution.

3.3.2 Physical Experiments

Large-scale physical experiments for a wall height of 1.0 m (as shown in **Figure 3.4**) were conducted to simulate an MSE wall under a high ground water level. The bottom, left and right sides of the physical model were established as an impervious boundary. Ground water flows during the tests were controlled by water levels in the upstream and downstream water tanks. The water level in the downstream water tank was kept constant at the toe of the wall (+0.0 m) using a control weir. The water level in the upstream tank was increased stepwise from heights of +0.0 m, +0.4 m, +0.7 m, and +1.0 m. The upstream water level was increased after reaching a steady state in which there was no change in the water content values, read from the TDR probes, for a period equal to or greater than 24 hours. This configuration was established to simulate the most severe situation in which the groundwater level behind an MSE wall is very high, similar to the situation that may occur in mountainous areas during heavy rainfalls. The shallow soil layer was assumed to be underlain by a bedrock layer such that inundation might occur during a heavy rainstorm (**Figure 3. 4b**).



Although the MSE wall base was always submerged, the distance between the MSE wall base and the bottom impervious boundary was likely to affect the seepage response. To exclude the effect of the distance between the MSE wall base to the bottom impervious boundary, the bottom boundary should be located far enough away that its location would not affect the seepage response. Numerical modelling results undertaken at various distances from the base of the MSE wall to the bottom boundary were used to justify the location of the bottom boundary in the physical experiments. The required depth of the impervious boundary, at a location that did not affect the seepage response, was no less than 0.4 m from the base of the MSE wall.

In practice, additional considerations such as the potential to scour beneath the wall, wave action effects and destabilizing forces due to hydrostatic pressure must be taken into account if an MSE wall is to be partly submerged in a body of water. This study aimed to investigate only the effect of geocomposite drains on the seepage water flow in an MSE wall; so, the above mentioned considerations were not considered.

The tank was filled with compacted soil to a height of 1.4 m. Compaction was carried out with a hand compactor in layers measuring 0.2 m in thickness to a density of 90% of the standard Proctor density at a water content of 5.7%. The degree of compaction and water contents were checked at 3 points for each compacted layer. These points were located along a longitudinal line close to the centre line near the wall facing, the geocomposite drain, and the porous concrete upstream wall. Wherever the degree of compaction was found to be inadequate, additional compaction was undertaken until the targeted density was achieved. The wall facing was made of an acrylic plate with 5 layers of “bearing reinforcement” (Horpibulsuk

and Niramitkornburee, 2010) with equal lengths of 0.7 m (equal to $0.8H$, where H is the wall height), which conforms with AASHTO recommendations (AASHTO, 2002). The bearing reinforcement was composed of a longitudinal member and transverse (bearing) members. The longitudinal member was a steel deformed bar, and the transverse members were a set of angle steels. The longitudinal and transverse members were welded to each other. A sketch of the bearing reinforcement is shown in **Figure 3. 4c**. The vertical and horizontal spacing between each reinforcement layer were fixed at 0.20 m and 0.25 m, respectively.

The MSE wall was extensively instrumented. Locations of the instruments are illustrated in **Figure 3.4**. Four standpipe piezometers, 10 surface settlement plates and 10 TDR probes were installed to measure water levels, settlements and volumetric water contents during seepage flow, respectively. The piezometers were installed along the centre line of the tank (**Figure 3.4 a**). Settlements were measured by precise levelling with reference to a benchmark. Three linear potentiometers were installed at the wall facing panel to measure lateral wall movements at different points during seepage. Data read from TDR probes and piezometers were considered and are presented in this paper.

Two physical experiments were conducted: without geocomposite drain installation (case I) and with geocomposite drain installation (case II). For the experiment with a geocomposite drain, the geocomposite was installed at a distance of 0.8 m from the wall facing.

3.3.3 Numerical modeling

A series of numerical experiments were subsequently conducted to investigate the effect of the relevant material properties on the ground water flow through the MSE wall, with a geocomposite drain installed, using the finite element code Plaxis 2D. The models were verified with the results taken from the physical experiments introduced in the previous section. The MSE wall model without geocomposite installation was verified prior to the MSE wall model with geocomposite installation.

The properties that predominantly affect the hydraulic behaviours of the MSE wall with geocomposite installation were the hydraulic conductivity of the geocomposite, the variation in the hydraulic conductivity with the degree of saturation, the water retention characteristics of the soil and the geocomposite components (geotextile and geonet). As the geonet has a very open structure, VG and VGM models with the following considerations were assigned to the geonet:

1. *The geonet has a large and single pore size attribution.*
2. *The geonet can be completely dried and saturated under suitable magnitudes of suction.*

With respect to the first consideration, high values of g_a and g_n reflect a large pore size and a more uniform pore size distribution, respectively. Hence, high g_a and g_n values were assigned to the geonet. Parametric studies indicated that assigning magnitudes of g_a greater than 600 [m^{-1}] and magnitudes of g_n greater than 40 resulted in no changes in the calculation results. As such, the geonet parameters g_a and g_n were assigned values of 600 [m^{-1}] and 40, respectively. Based on the second consideration, the geonet parameters S_{res} and S_{sat} were set to 0.00 and 1.00, respectively. The

parameters for the hydraulic constitutive equations VG and VGM for the soil, the geotextile and the geonet assigned to the models are summarized in **Table 3.1**.

Data from the wetting phase WRC of 13 geotextiles reported by Iryo and Rowe, (2003) were utilized as the reference data in the selection of parameters for the numerical experiment by the VG and VGM models. The basic properties of these 13 nonwoven geotextiles are shown in **Table 3.2**, and the WRC of these, together with their upper and lower bounds (long dash lines) are presented in **Figure 3.2 a**. The ranges of the VG and VGM model parameters of the geotextile were varied such that their WRC curves were inside this boundary (**Figure 3.2 b**). Seventeen sets of VG and VGM model parameters of geotextile were used as shown in **Table 3.3**. These parameters were varied based on the VG and VGM model parameters of the geotextile used in the physical experiment (**Table 3.1**), i.e., $g_a = 20 \text{ [m}^{-1}\text{]}$, $g_n = 2.5$, $S_{res} = 0.03$, and $S_{sat} = 0.80$. In total, 61 numerical simulations were conducted in this study. The parameter values assigned to every case are shown in **Table 3.4**. The assigned parameters as well as type of calculation models are shown in the **Table 3.5**

Table 3.2 Properties of thirteen nonwoven geotextiles reported by Iryo and Rowe
(2003)

| No. | Mass per unit area (g/m ²) | Apparent Opening Size (mm) | Porosity | Saturated transmissivity (m ² /s) |
|-----|---|-------------------------------|----------|---|
| 1 | 339 | 0.15 | 0.88 | - |
| 2 | 543 | 0.15 | 0.84 | - |
| 3 | 340 | 0.18 | 0.87 | - |
| 4 | 540 | 0.15 | 0.88 | - |
| 5 | 266 | 0.04 | 0.89 | 6.80 x 10 ⁻⁶ |
| 6 | 340 | 0.18 | 0.94 | 3.90 x 10 ⁻⁵ |
| 7 | - | 0.15 | 0.88 | 2.93 x 10 ⁻⁵ |
| 8 | 543 | 0.15 | 0.87 | 1.65 x 10 ⁻⁵ |
| 9 | - | - | 0.96 | 3.90 x 10 ⁻⁵ |
| 10 | 154 | - | 0.94 | - |
| 11 | 333 | - | 0.93 | - |
| 12 | 276 | - | 0.91 | - |
| 13 | 468 | - | 0.86 | 5.5 x 10 ⁻⁶ |

Table 3.3 VG and VGM model parameters of the geotextiles assigned in the numerical experiment.

| Material | van Genuchten Parameters | | | |
|---------------|---|-------------------------|---------------------------------|---------------------------------|
| | $\frac{1}{g^a(\sigma)} \text{ (l}^{-1}\text{)}$ | $\frac{1}{g^n(\sigma)}$ | $\frac{h}{s_{sat}} \text{ (-)}$ | $\frac{1}{s_{res}} \text{ (-)}$ |
| Geotextile 1 | 20 | 2.5 | 0.8 | 0.03 |
| Geotextile 2 | 20 | 2.5 | 0.8 | 0.05 |
| Geotextile 3 | 20 | 2.5 | 0.8 | 0.08 |
| Geotextile 4 | 20 | 2.5 | 0.8 | 0.10 |
| Geotextile 5 | 20 | 2.5 | 0.5 | 0.03 |
| Geotextile 6 | 20 | 2.5 | 0.6 | 0.03 |
| Geotextile 7 | 20 | 2.5 | 0.7 | 0.03 |
| Geotextile 8 | 20 | 2.0 | 0.7 | 0.03 |
| Geotextile 9 | 20 | 2.2 | 0.7 | 0.03 |
| Geotextile 10 | 20 | 3.0 | 0.7 | 0.03 |
| Geotextile 11 | 20 | 4.0 | 0.7 | 0.03 |
| Geotextile 12 | 20 | 6.0 | 0.7 | 0.03 |
| Geotextile 13 | 16 | 2.5 | 0.8 | 0.03 |
| Geotextile 14 | 25 | 2.5 | 0.8 | 0.03 |
| Geotextile 15 | 40 | 2.5 | 0.8 | 0.03 |
| Geotextile 16 | 60 | 2.5 | 0.8 | 0.03 |
| Geotextile 17 | 100 | 2.5 | 0.8 | 0.03 |

Table 3.4 VG and VGM model parameters assigned to every case in the numerical experiment.

| Sandy soil | | | | | | Geotextile | | | | | | Geonet | | | | | | Remarks |
|-----------------|-----------------|-------------|-------------------------------|-------------|---------|-----------------|-----------------|-------------|-------------------------------|-------------|---------|-----------------|-----------------|-------------|-------------------------------|-------------|---------|---------|
| \bar{s}_{res} | \bar{s}_{sat} | \bar{g}^n | $\frac{\bar{s}_y}{\bar{g}^a}$ | \bar{k}^x | k_y | \bar{s}_{res} | \bar{s}_{sat} | \bar{g}^n | $\frac{\bar{s}_y}{\bar{g}^a}$ | \bar{k}^x | k_y | \bar{s}_{res} | \bar{s}_{sat} | \bar{g}^n | $\frac{\bar{s}_y}{\bar{g}^a}$ | \bar{k}^x | k_y | |
| (-) | (-) | (-) | (m ⁻¹) | (m/day) | (m/day) | (-) | (-) | (-) | (m ⁻¹) | (m/day) | (m/day) | (-) | (-) | (-) | (m ⁻¹) | (m/day) | (m/day) | |
| 0.03 | | | | | | | | | | | | | | | | | | Case 1 |
| 0.05 | 1.0 | 1.5 | 20 | 17 | 17 | 0.03 | 0.8 | 2.5 | 20 | 320 | 2000 | 0 | 1.0 | 40 | 600 | 6.9E4 | 6.9E4 | Case 2 |
| 0.08 | | | | | | | | | | | | | | | | | | Case 3 |
| 0.1 | | | | | | | | | | | | | | | | | | Case 4 |
| 0.7 | | | | | | | | | | | | | | | | | | Case 5 |
| 0.03 | 0.8 | 1.5 | 20 | 17 | 17 | 0.03 | 0.8 | 2.5 | 20 | 320 | 2000 | 0 | 1.0 | 40 | 600 | 6.9E4 | 6.9E4 | Case 6 |
| 0.9 | | | | | | | | | | | | | | | | | | Case 7 |
| | 1.8 | | | | | | | | | | | | | | | | | Case 8 |
| 0.03 | 1.0 | 2.0 | 20 | 17 | 17 | 0.03 | 0.8 | 2.5 | 20 | 320 | 2000 | 0 | 1.0 | 40 | 600 | 6.9E4 | 6.9E4 | Case 9 |
| | | 2.5 | | | | | | | | | | | | | | | | Case 10 |
| | | 3.0 | | | | | | | | | | | | | | | | Case 11 |
| | | 5.0 | | | | | | | | | | | | | | | | Case 12 |
| 0.03 | 1.0 | 1.5 | 10 | 17 | 17 | 0.03 | 0.8 | 2.5 | 20 | 320 | 2000 | 0 | 1.0 | 40 | 600 | 6.9E4 | 6.9E4 | Case 13 |
| | | | 25 | | | | | | | | | | | | | | | Case 14 |

| | | | | | | | | | | | | | | | | | | |
|-----|--|--|--|--|--|--|--|--|--|--|--|--|--|--|--|--|--|---------|
| 30 | | | | | | | | | | | | | | | | | | Case 15 |
| 1.7 | | | | | | | | | | | | | | | | | | Case 16 |
| 100 | | | | | | | | | | | | | | | | | | Case 17 |
| 170 | | | | | | | | | | | | | | | | | | Case 18 |
| 200 | | | | | | | | | | | | | | | | | | Case 19 |
| 320 | | | | | | | | | | | | | | | | | | Case 20 |
| 500 | | | | | | | | | | | | | | | | | | Case 21 |

Table 3.4 VG and VGM model parameters assigned to every case in the numerical experiment (continued).

| Sandy soil | | | | | | Geotextile | | | | | | Geonet | | | | | | Remarks |
|------------|-----------|-----|--------------------|---------|---------|------------|-----------|-----|--------------------|---------|---------|-----------|-----------|-----|--------------------|---------|---------|---------|
| s_{res} | s_{sat} | s | g^a | k^x | k_y | s_{res} | s_{sat} | s | g^a | k^x | k_y | s_{res} | s_{sat} | s | g^a | k^x | k_y | |
| (-) | (-) | (-) | (m ⁻¹) | (m/day) | (m/day) | (-) | (-) | (-) | (m ⁻¹) | (m/day) | (m/day) | (-) | (-) | (-) | (m ⁻¹) | (m/day) | (m/day) | |
| | | | | | | 0.05 | | | | | | | | | | | | Case 22 |
| 0.03 | 1.0 | 1.5 | 20 | 17 | 17 | 0.08 | 0.8 | 2.5 | 20 | 320 | 2000 | 0 | 1.0 | 40 | 600 | 6.9E4 | 6.9E4 | Case 23 |
| | | | | | | 0.1 | | | | | | | | | | | | Case 24 |
| | | | | | | 0.7 | | | | | | | | | | | | Case 25 |
| 0.03 | 1.0 | 1.5 | 20 | 17 | 17 | 0.03 | 0.6 | 2.5 | 20 | 320 | 2000 | 0 | 1.0 | 40 | 600 | 6.9E4 | 6.9E4 | Case 26 |
| | | | | | | 0.5 | | | | | | | | | | | | Case 27 |

| | | | | |
|-----------------------|------------------------|--------------------------|------|---------|
| 0.03 1.0 1.5 20 17 17 | 0.03 0.8 3 20 320 2000 | 0 1.0 40 600 6.9E4 6.9E4 | 2 | Case 28 |
| | | | 2.2 | Case 29 |
| | | | 4 | Case 30 |
| | | | 6 | Case 31 |
| | | | | Case 32 |
| 0.03 1.0 1.5 20 17 17 | 0.03 0.8 2.5 320 2000 | 0 1.0 40 600 6.9E4 6.9E4 | 16 | Case 33 |
| | | | 20 | Case 34 |
| | | | 25 | Case 35 |
| | | | 40 | Case 36 |
| | | | 60 | Case 37 |
| | | | 100 | Case 38 |
| 0.03 1.0 1.5 20 17 17 | 0.03 0.8 2.5 20 2000 | 0 1.0 40 600 6.9E4 6.9E4 | 50 | Case 39 |
| | | | 100 | Case 40 |
| | | | 200 | Case 41 |
| | | | 500 | Case 42 |
| | | | 1000 | Case 43 |
| | | | 2000 | Case 44 |

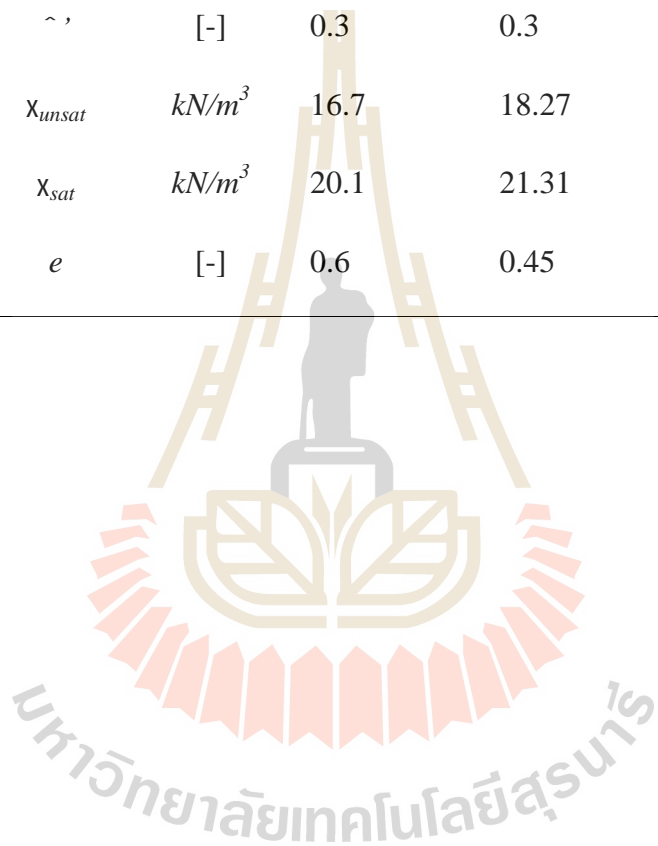
Table 3.4 VG and VGM model parameters assigned to every case in the numerical experiment (continued).

| Sandy soil | | | | | | Geotextile | | | | | | Geonet | | | | | | Remarks |
|------------------------|------------------------|--------------------|---|------------------------|------------------|------------------------|------------------------|--------------------|---|------------------------|------------------|------------------------|------------------------|--------------------|---|------------------------|------------------|---------|
| \bar{s}_{res} (-) | \bar{s}_{sat} (-) | \bar{g}^n (-) | $\frac{\bar{s}}{\bar{g}^a}$ (m ⁻¹) | \bar{k}^x (m/day) | k_y (m/day) | \bar{s}_{res} (-) | \bar{s}_{sat} (-) | \bar{g}^n (-) | $\frac{\bar{s}}{\bar{g}^a}$ (m ⁻¹) | \bar{k}^x (m/day) | k_y (m/day) | \bar{s}_{res} (-) | \bar{s}_{sat} (-) | \bar{g}^n (-) | $\frac{\bar{s}}{\bar{g}^a}$ (m ⁻¹) | \bar{k}^x (m/day) | k_y (m/day) | |
| 0.03 | 1.0 | 1.5 | 20 | 17 | 17 | 0.03 | 0.8 | 2.5 | 20 | 320 | 17 | 0 | 1.0 | 40 | 600 | 6.9E4 | 6.9E4 | Case 45 |
| | | | | | | | | | | | 34 | | | | | | | Case 46 |
| | | | | | | | | | | | 50 | | | | | | | Case 47 |
| | | | | | | | | | | | 320 | | | | | | | Case 48 |
| | | | | | | | | | | | 1000 | | | | | | | Case 49 |
| | | | | | | | | | | | 4000 | | | | | | | Case 50 |
| | | | | | | | | | | | 5000 | | | | | | | Case 51 |
| 0.03 | 1.0 | 1.5 | 20 | 17 | 17 | 0.03 | 0.8 | 2.5 | 20 | 320 | 2000 | 0 | 1.0 | 40 | 600 | 2.0E3 | 2.0E3 | Case 52 |
| | | | | | | | | | | | | | | | | 5.0E3 | 5.0E3 | Case 53 |
| | | | | | | | | | | | | | | | | 1.0E4 | 1.0E4 | Case 54 |
| | | | | | | | | | | | | | | | | 1.5E4 | 1.5E4 | Ca |
| | | | | | | | | | | | | | | | | 2.0E4 | 2.0E4 | Ca |
| | | | | | | | | | | | | | | | | 2.5E4 | 2.5E4 | Ca |
| | | | | | | | | | | | | | | | | 3.0E4 | 3.0E4 | Case 58 |
| | | | | | | | | | | | | | | | | 4.0E4 | 4.0E4 | Case 59 |
| | | | | | | | | | | | | | | | | 8.0E4 | 8.0E4 | Case 60 |
| | | | | | | | | | | | | | | | | 1.0E5 | 1.0E5 | Case 61 |

Table 3.5 Input data for numerical simulation (based cases)

| Parameters | Symbol | Units | Materials | | | | Remarks |
|------------------------------|-----------|------------|--------------|----------------|------------|--------|---------|
| | | | Sandy soil | Lateritic soil | Geotextile | Geonet | |
| Material models | | | | | | | |
| Mechanical model | Model | | Mohr-Coulomb | | | | |
| Type of material behavior | | | Drained | | | | |
| Cohesion | c' | kPa | 1 | 19 | 1 | 1 | |
| Friction angle | ϕ' | $degree$ | 40 | 30.75 | 40 | 40 | |
| Hydraulic model | Model | | van Genuchen | | | | |
| Permeability | k | $m/days$ | 17 | 0.3456 | | 69120 | |
| Lateral direction | k_x | | | | 320 | | |
| Longitudinal direction | k_y | | | | 2000 | | |
| van Genuchen parameter g_a | g_a | $[m^{-1}]$ | 20 | 0.8 | | 600 | |
| van Genuchen parameter g_n | g_n | $[-]$ | 1.5 | 1.4 | | 40 | |
| Residual moisture content | S_{res} | $[-]$ | 0.03 | 0.2 | 0.03 | 0 | |
| Saturated moisture content | S_{sat} | $[-]$ | 1.0 | 1.0 | 1.0 | 1.0 | |

| | | | | | | |
|---------------------------------|------------------|----------|------|-------|------|------|
| Deformation parameters | | | | | | |
| Effective modulus of elasticity | E' | kPa | 50E3 | 50E3 | 50E3 | 50E3 |
| Effective Poisson's ratio | ν' | [-] | 0.3 | 0.3 | 0.3 | 0.3 |
| Dry unit weight | γ_{unsat} | kN/m^3 | 16.7 | 18.27 | 5 | 5 |
| Total unit weight | γ_{sat} | kN/m^3 | 20.1 | 21.31 | 12 | 12 |
| Void ratio | e | [-] | 0.6 | 0.45 | 0.9 | 0.98 |



3.4 Results and Discussions

3.4.1 Experimental results

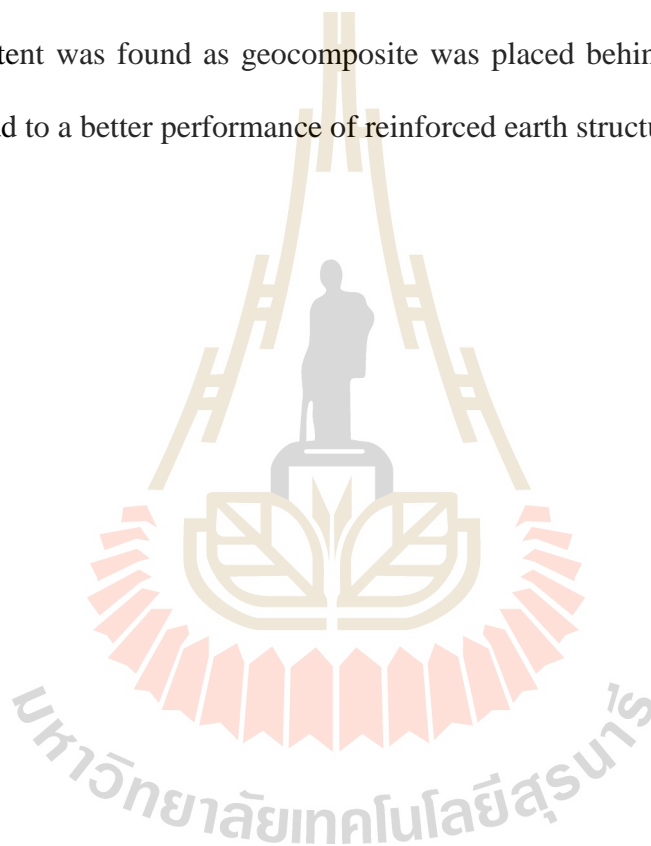
Figure 3.5 a presents the change in level of the phreatic surface were measured using three standpipe piezometers as depicted in **Figure 3.4 a** at 18 days, 21 days, and 23 days, with represent the end times of rising of upstream water tables of +0.4 m, +0.7 m, and +1.0 m, respectively. Due to the head loss, the height of the phreatic surface was decreased through the wall facing as water permeating through the protected zone. The experimental results of variation of the level of phreatic surface inside reinforced earth mass also proved that the high permeable geocomposite can collect the water inside the unreinforced zone and drain it out at the drainage wall. Inside protected zone, the phreatic surface significantly drops and was found to be close to the base of MSE wall.

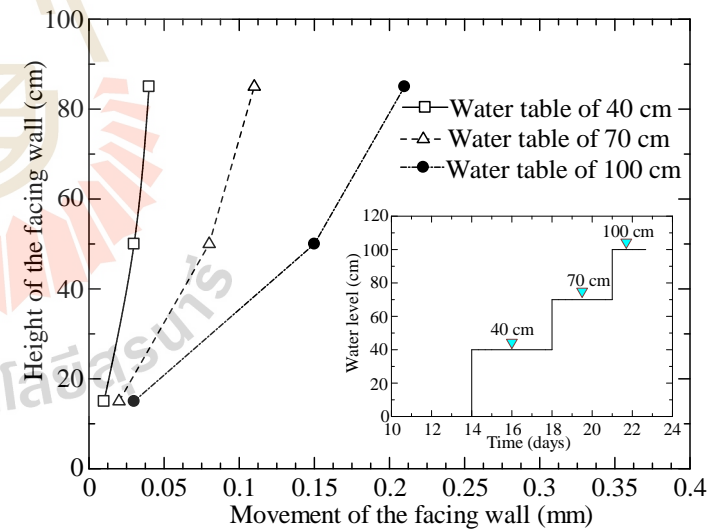
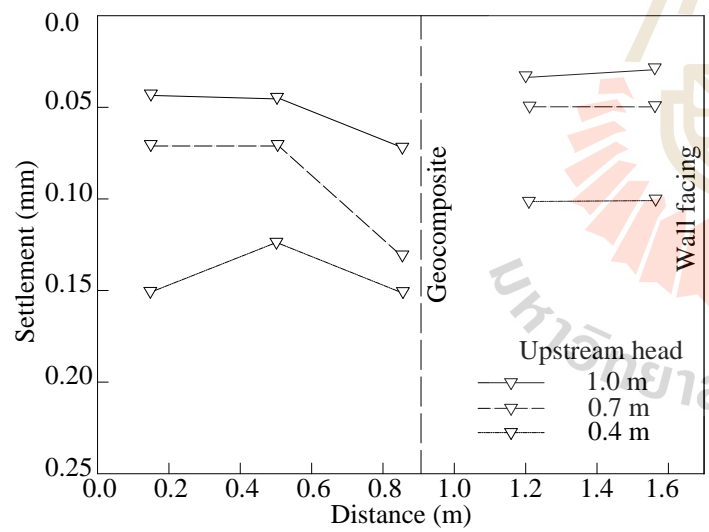
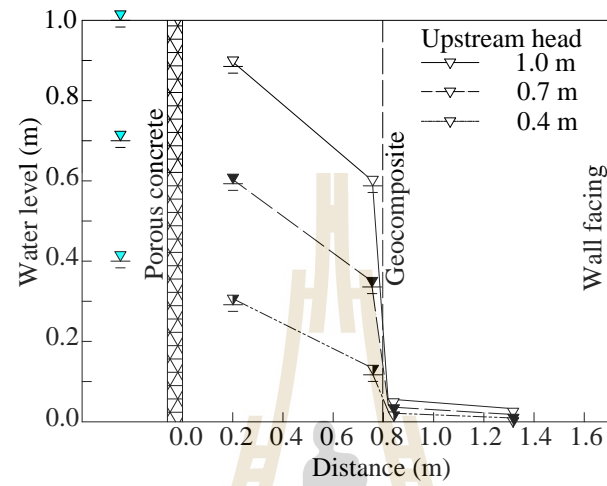
Figure 3.5 b and c present the surface settlements along the longitudinal direction and the horizontal wall movement, respectively, after reaching steady state at each upstream water level. Since compaction control near the geocomposite was difficult, a greater surface settlement was found outside the protected zone close to the geocomposite at each upstream water level. Although the height of the inner phreatic surfaces of all upstream water levels was very low and almost identical, greater surface settlement inside the protected zone and a greater wall movement were recorded with increasing height of the upstream water.

Figure 3.6 illustrates the measured moisture obtained from ten TDR moisture probes with their locations are depicted in the **Figure 3.4 b**. The measurement results show that the moisture content behind the drainage wall (inside the protected zone) was found to be lower than that found in front of the drainage wall (inside the

unreinforced zone). Similarity, the moisture content measured at each TDR moisture probe for the case without (solid lines) drainage system installed was found much higher than that for the case of drainage wall installed (dashed lines).

A conclusion could be withdrawn from the experimental results is that the use of such kind of base and vertical drain geocomposite could eliminate the influences of seepage water flow on the performance of reinforced earth structures. The lower moisture content was found as geocomposite was placed behind the protected zone, this might lead to a better performance of reinforced earth structure.





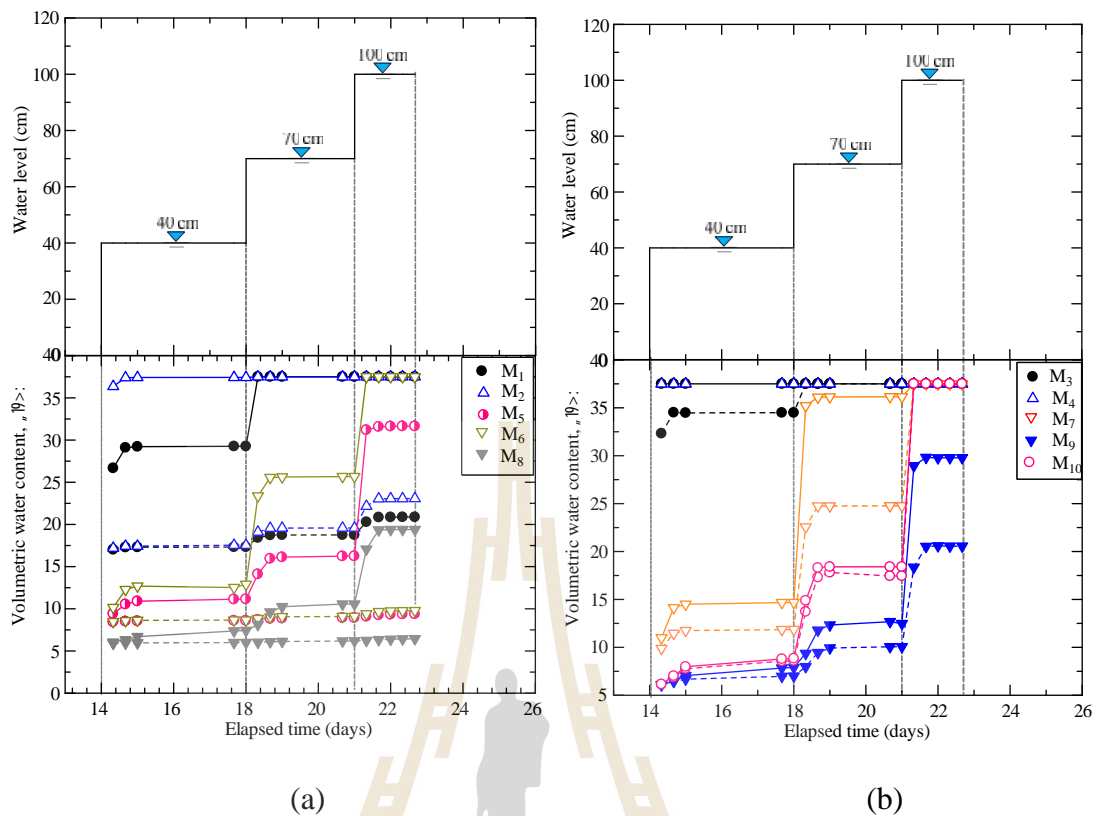


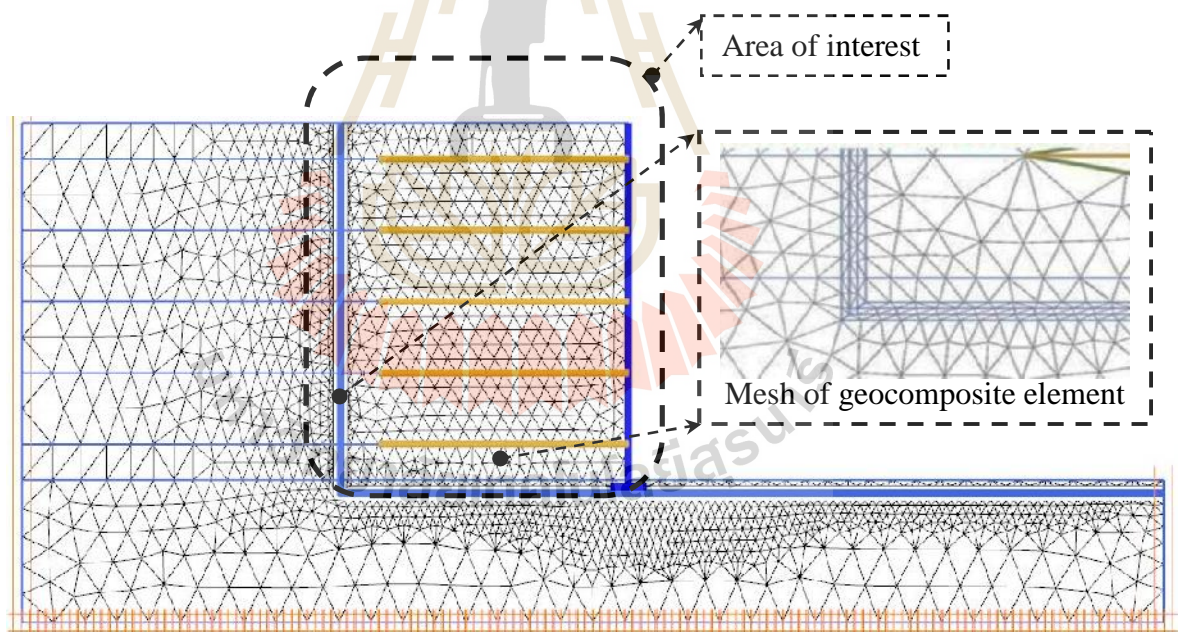
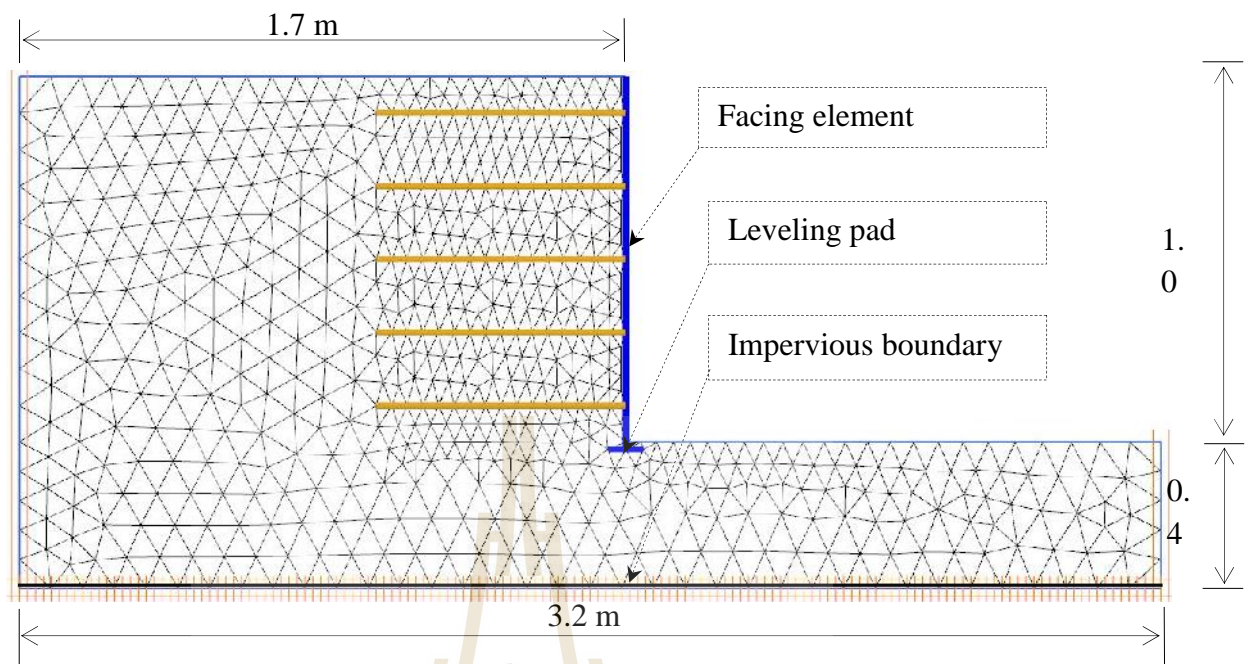
Figure 3.6 (a) measured moisture content s in protected zone, and (b) in unreinforced zone for case I (without geocomposite drain installed, solid lines) and case II (with geocomposite drain installed, dashed lines)

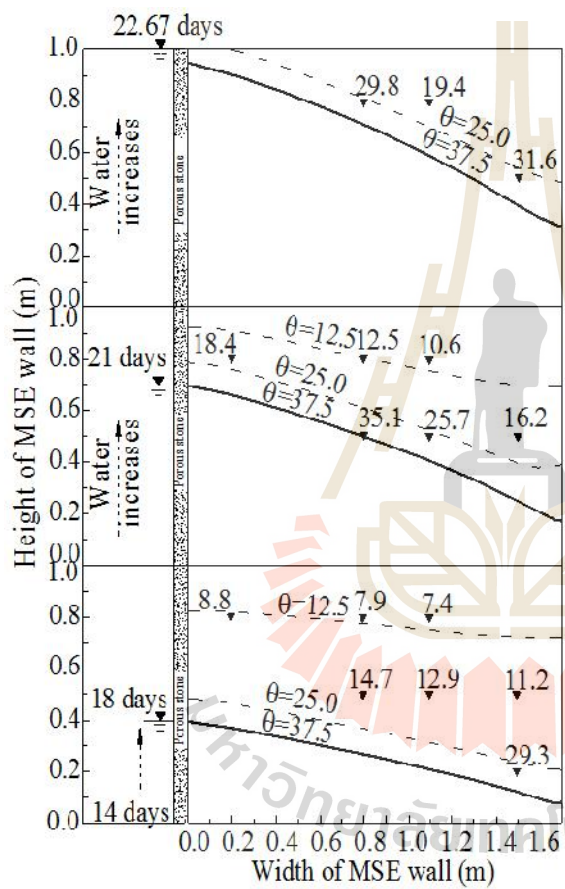
3.4.2 Model Calibration

Model calibrations were conducted prior to the parametric studies. The models were developed in the Plaxis environment to simulate the physical modelling studies. These models incorporated soil characteristics, structural components (reinforcements and acrylic facing), and drainage components (geotextile and geonet). As the model of the MSE wall with the geocomposite is complex, given the thin layers of geotextiles and geonets installed, verification of the MSE wall without the

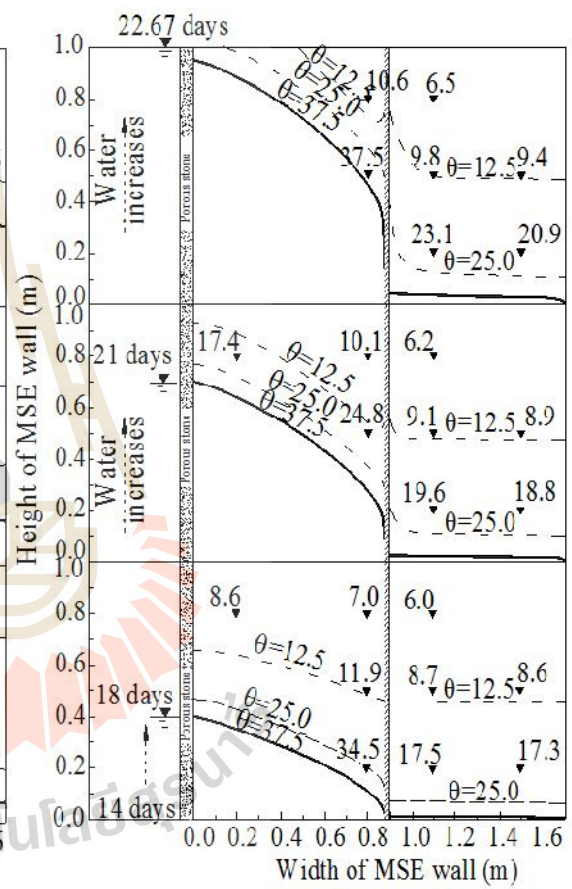
geocomposite was conducted prior to that of the MSE wall with the geocomposite. Material properties assigned to the models are presented in **Table 3.1**.

The discretized plane strain finite element mesh is shown in **Figure 3.7 a** and **3.7 b** for the MSE wall without and with geocomposite drain installation, respectively. A triangular mesh was used in the model. Although a rectangular mesh is commonly adopted in water flow models, it has been reported that the calculated results do not depend on the type of mesh because the interpolation function in flow problems is linear (Potts et al., 2001). In Plaxis, there are two types of triangular elements: 6-node triangles and 15-node triangles. In this study, 15-node triangles were assigned to the models. The use of 15-node triangles yields more accurate calculation results than that of 6-node triangles. A fine mesh with an average element size of 0.033 m was assigned. A finer mesh was also assigned to the geotextile and the geonet. The initial conditions of the model were defined based on the controlled density and water content during the placement of compacted soil in the physical box. Dirichlet boundary conditions with prescribed pressures were imposed on the left, right, and upper boundaries of the model. The bottom boundary of the model was defined as impermeable. In Plaxis, the time steps were assigned automatically for steady-state calculation. At each time step, a modified Newton-Raphson model was used to solve the relevant equations iteratively. At each iteration, increments of the groundwater head were calculated from the imbalance in the nodal discharges and added to the active head. This process was continued until the norm of the unbalances vector, i.e., the error in the nodal discharges, was smaller than that of the tolerated error of 0.01 (or 1%).





▼ Measured water content from physical experiment
 — Phreatic surface obtained from FEM



— Geocomposite layer
 $\theta=12.5$ Water content obtained from FEM

(a)

(b)

Figure 3.8 presents the measured (with symbols) and calculated (with lines) water levels and volumetric water contents for the various upstream water levels for tests without (**Figure 3.8 a**) and with (**Figure 3.8 b**) geocomposite installation. The water levels and the volumetric water contents presented in **Figure 3.8** were measured at 18 days, 21 days, and 23 days, which represent the end times of upstream water levels of +0.4 m, + 0.7 m, and + 1.0 m, respectively. At any upstream water level height, the water level decreases through the wall face. The measured water level data for case I (no geocomposite) were compared with those for case II (with geocomposite). The comparisons show that the highly permeable geocomposite can effectively prevent water flow to the protected zone, as it collects the water in the unreinforced zone and drains it at the wall face.

Figure 3.9 shows volumetric water contents measured at various times from TDR moisture probes M_2 , M_6 and M_8 (as shown in **Figure 3.4 b**). These probes were located at a horizontal distance of 0.6 m from the wall facing, i.e., at 0.2 m horizontally from the geocomposite drain for the MSE wall case II. Higher water contents were found at the lower TDR probes. The water contents in the protected zone with geocomposite installation were much lower than those without geocomposite. In the installation without geocomposite, the volumetric water content read from the probe M_2 rose from 0.05 ($S_l = 20\%$) to 0.40 ($S_l = 100\%$) when the upstream water level was raised from 0.2 m to 1.0 m. The volumetric water content with the geocomposite was found to be only half of that in the case without the geocomposite. At probe M_6 , the volumetric water content rose from 0.05 to final values of 0.38 and 0.12 for the case without and with the geocomposite, respectively. Even at the location of probe M_8 , where the water content exhibited the weakest effect

on the rise in the upstream water level, the difference between the final water contents for the case without and with the geocomposite was significant.

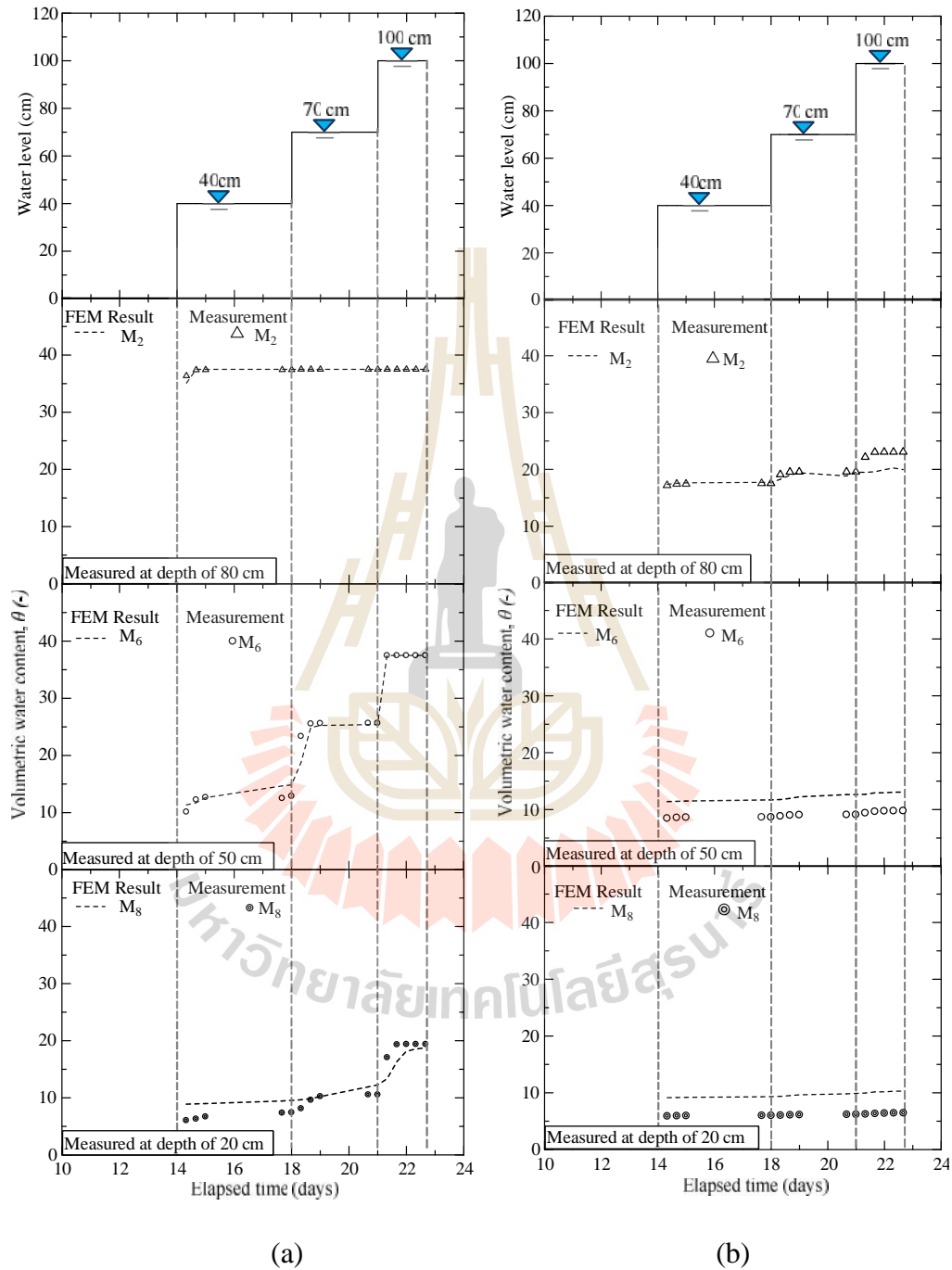


Figure 3.9 Time series plot for the water content for MSE wall case I (without geocomposite drain installed) (a), and (b) case II (with geocomposite drain installed).

3.5 Parametric Study

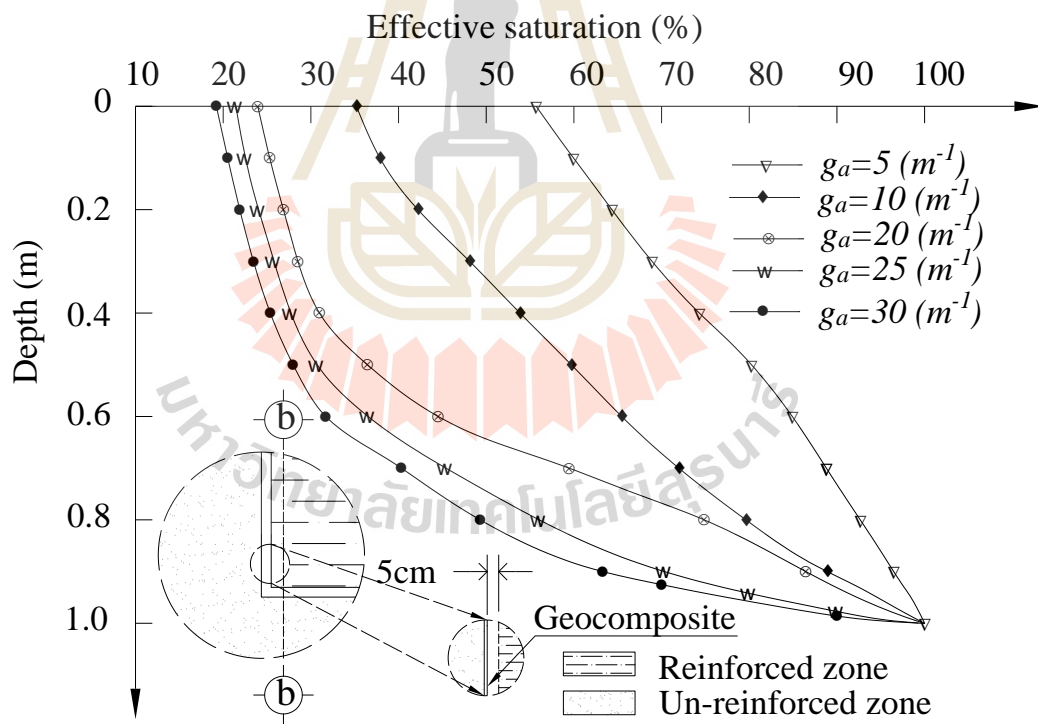
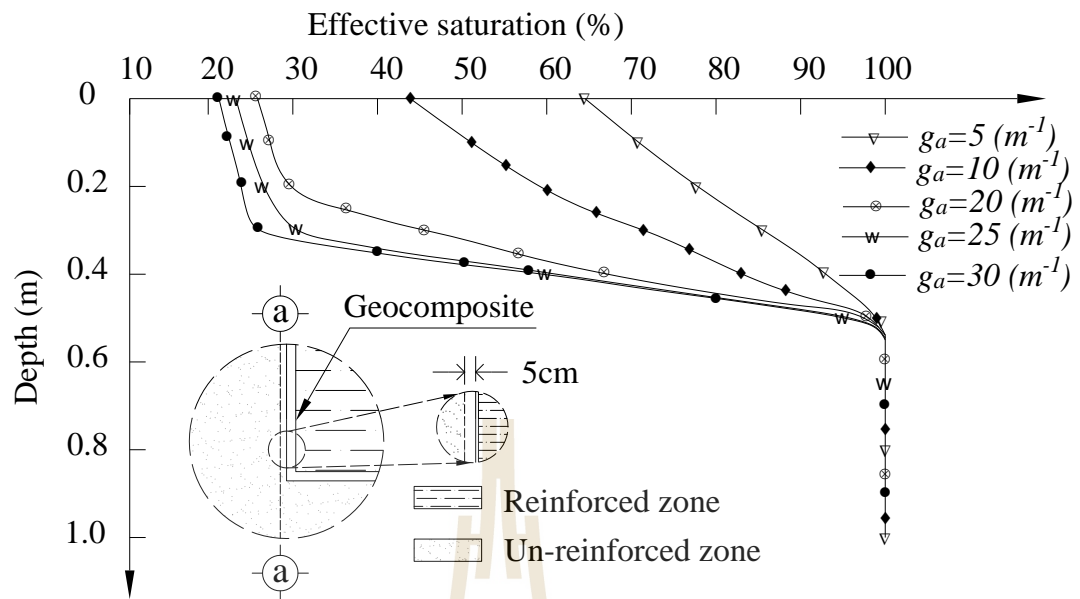
The hydraulic response, including the effective saturation and phreatic surface, determined from numerical experiments are presented and discussed in this section. The effects of the hydrological properties of the soil and the geotextile on the hydraulic response were evaluated using 1) van Genuchten parameters (S_{res} , S_{sat} , g_a , g_n) and 2) the corresponding saturated permeability. For the hydrological properties of the geonet, only the saturated hydraulic conductivity of the geonet was evaluated.

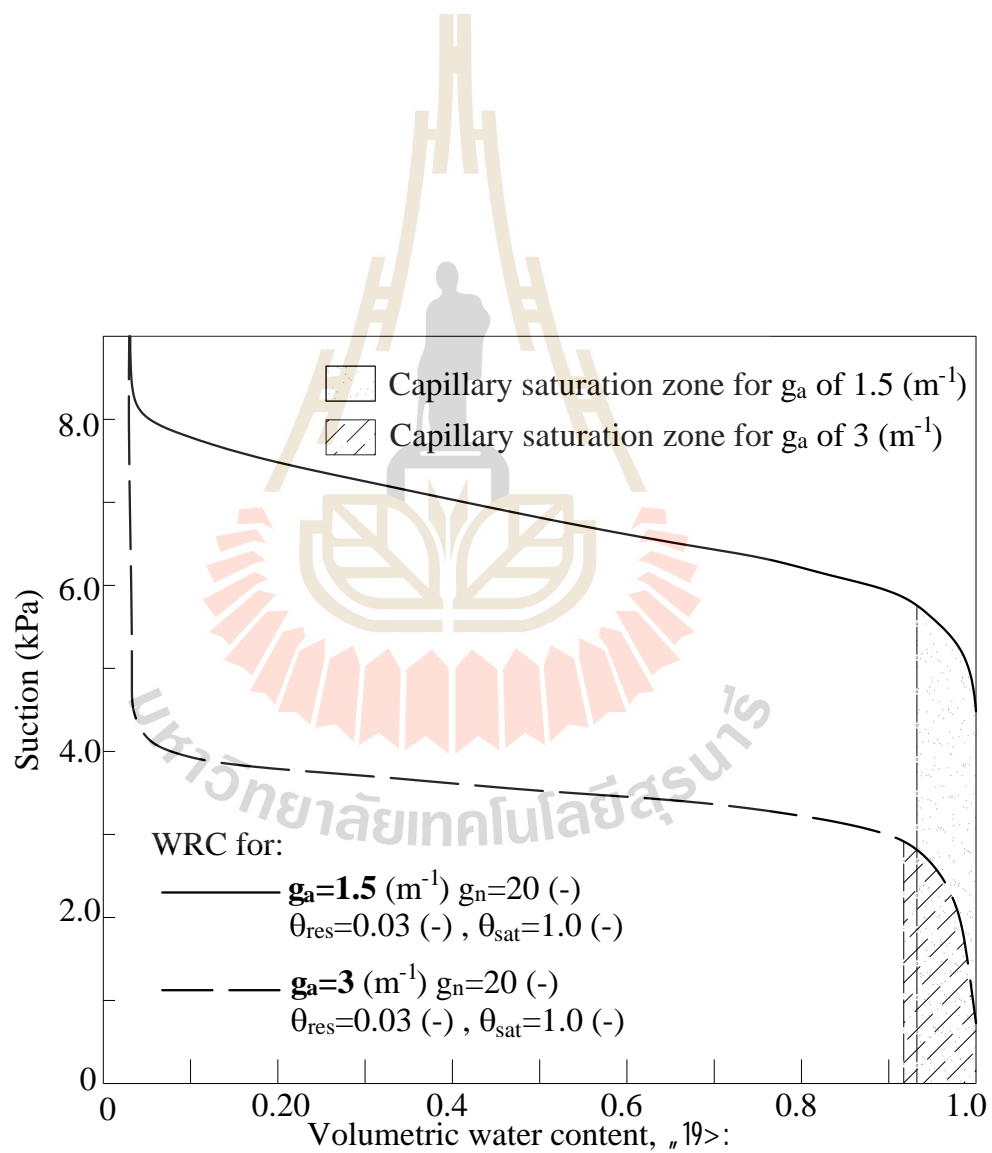
The numerical results are mainly illustrated in terms of effective saturation and phreatic surface. In general, it was found that the phreatic surface outside of the protected zone does not change notably within the range of parameters indicated in **Table 3.3**. The phreatic surface in the protected zone and the distribution of effective saturation were affected by some of the parameters, as discussed throughout this section.

3.5.1 Effect of van Genuchten parameters of the backfill

3.5.1.1 The van Genuchten parameter g_a

Figures 3.10a and 3.10b present the effective saturation profiles along sections *a-a* and *b-b*, respectively, for various magnitudes of g_a . The alignment of these sections is vertical and located at 0.05 m to the left and right from the geocomposite drainage. At a certain depth above the phreatic surface, the soil with a low g_a value exhibits high saturation. The degree of saturation is found to decrease when decreasing the magnitude of g_a . In short, the wet zone spreads more widely for the low g_a soil than for the high g_a soil.



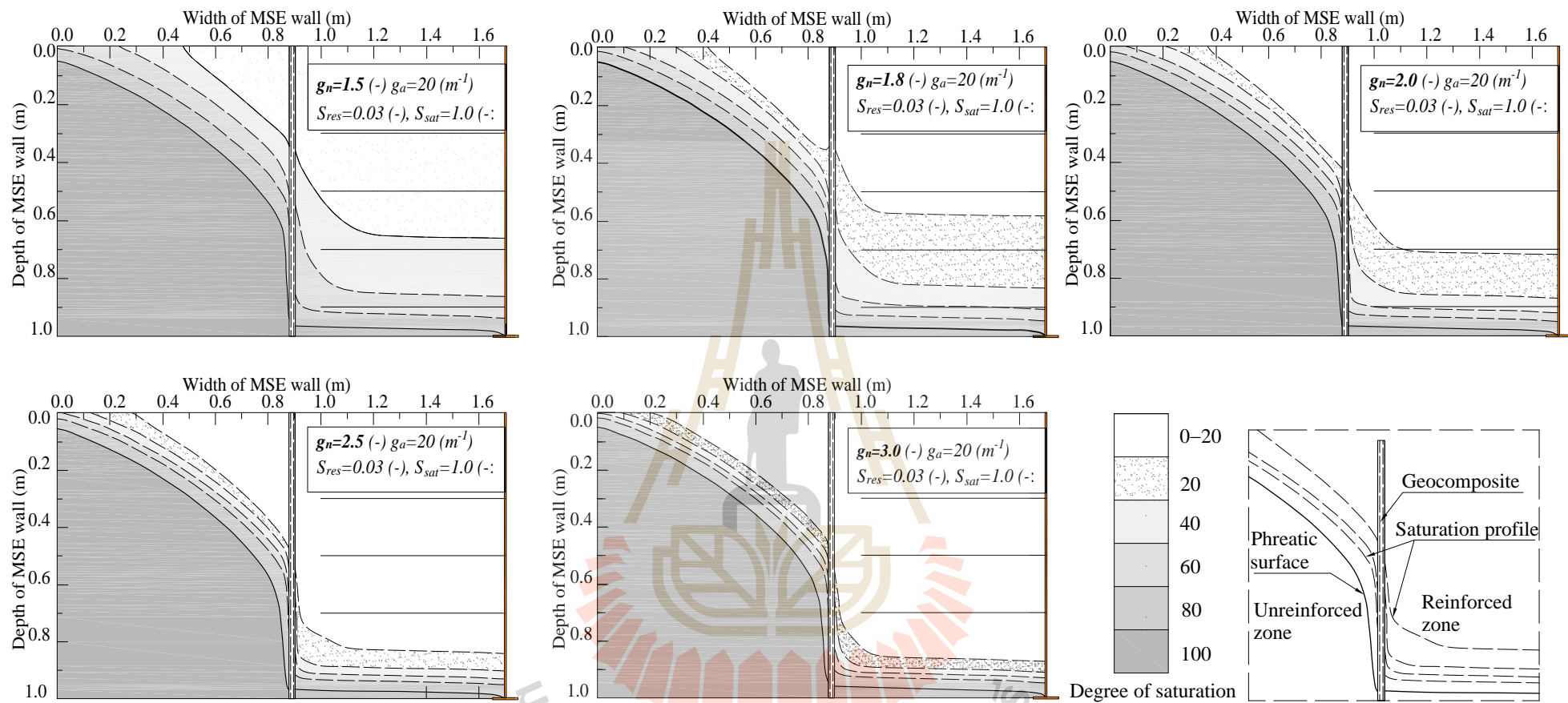


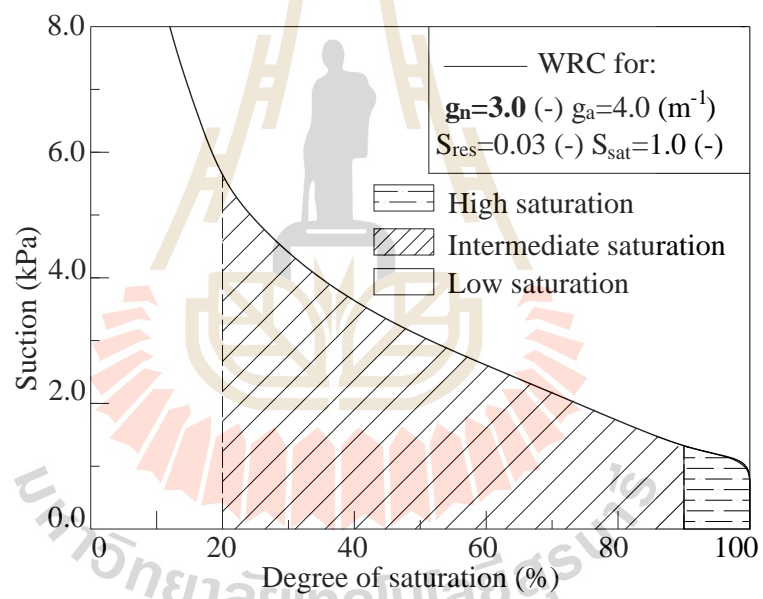
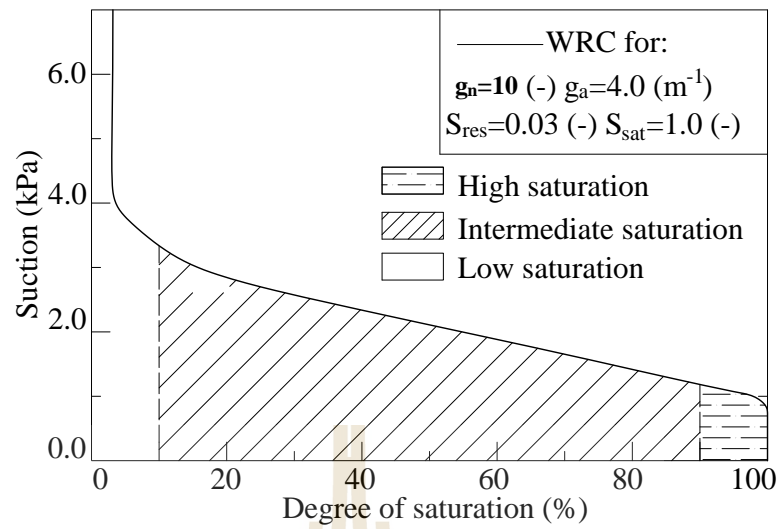
The magnitude of g_a represents the largest pore size present in the soil. Soil with a large g_a value has large pore sizes. Theoretically, at the interface of two materials with different largest pore sizes, the capillary barrier phenomenon (Ross, 1990) can occur when water does not readily flow from smaller to larger pore materials. The wide range of the capillary saturation zone plays a dominant role in the distribution of saturation in these experiments, and hence, the capillary barrier effect is negligible.

3.5.1.2 The van Genuchten Parameters g_n

Figure 3.12 presents phreatic surface and effective saturation profiles on the MSE wall model calculated at various magnitudes of g_n of the soil. The results show that effective saturation (both inside and outside the protected zone) between 20 and 80% clearly depends on the magnitude of g_n . A greater magnitude of g_n yields narrower effective saturation contours in the 20% to 80% range.

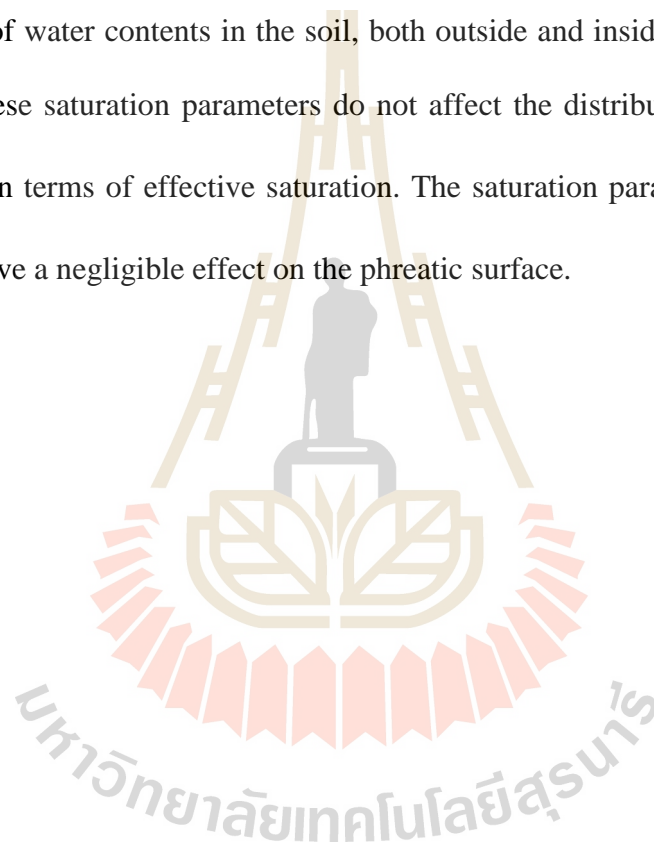
The magnitude of g_n reflects the steepness of the WRC curve in the desaturation zone as a smaller g_n yields a steeper curve. **Figure 3.13** compares the WRC curves of two soils having both high and low values of g_n . In the high saturation range, these WRC curves are similar. Within this range, a similar change in suction for both soils results in approximately similar saturation changes. As such, the width between the contours of 80% and 100% effective saturation as shown in **Figure 3.12** are similar for different values of g_n . For the intermediate saturation range, the soil with the higher g_n exhibits a narrower range of suction change (as shown in **Figure 3.13**). Thus, the contour width for 20% to 80% effective saturation is found to be narrower in a higher g_n soil than that in a lower g_n soil (**Figure 3.13**).

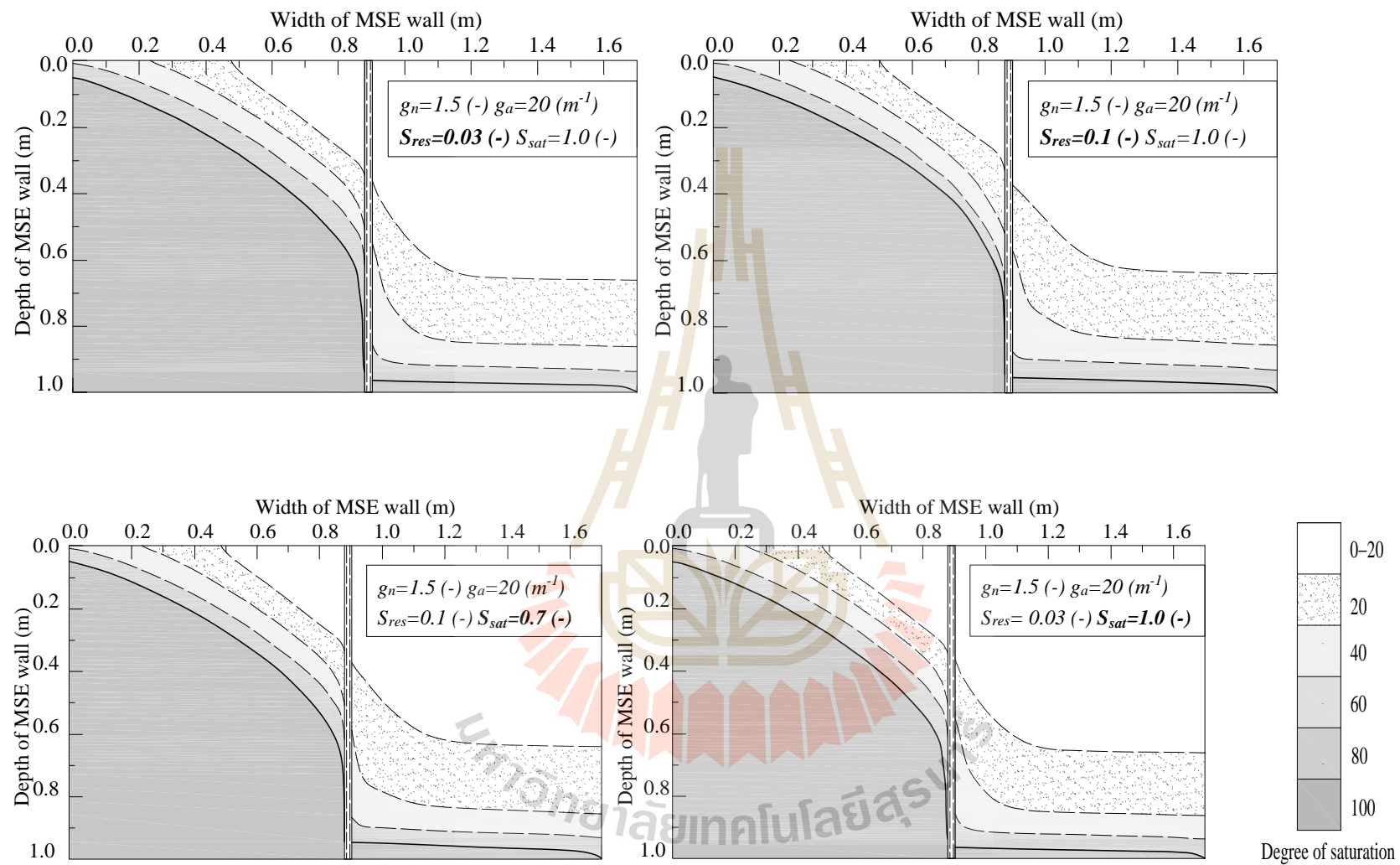




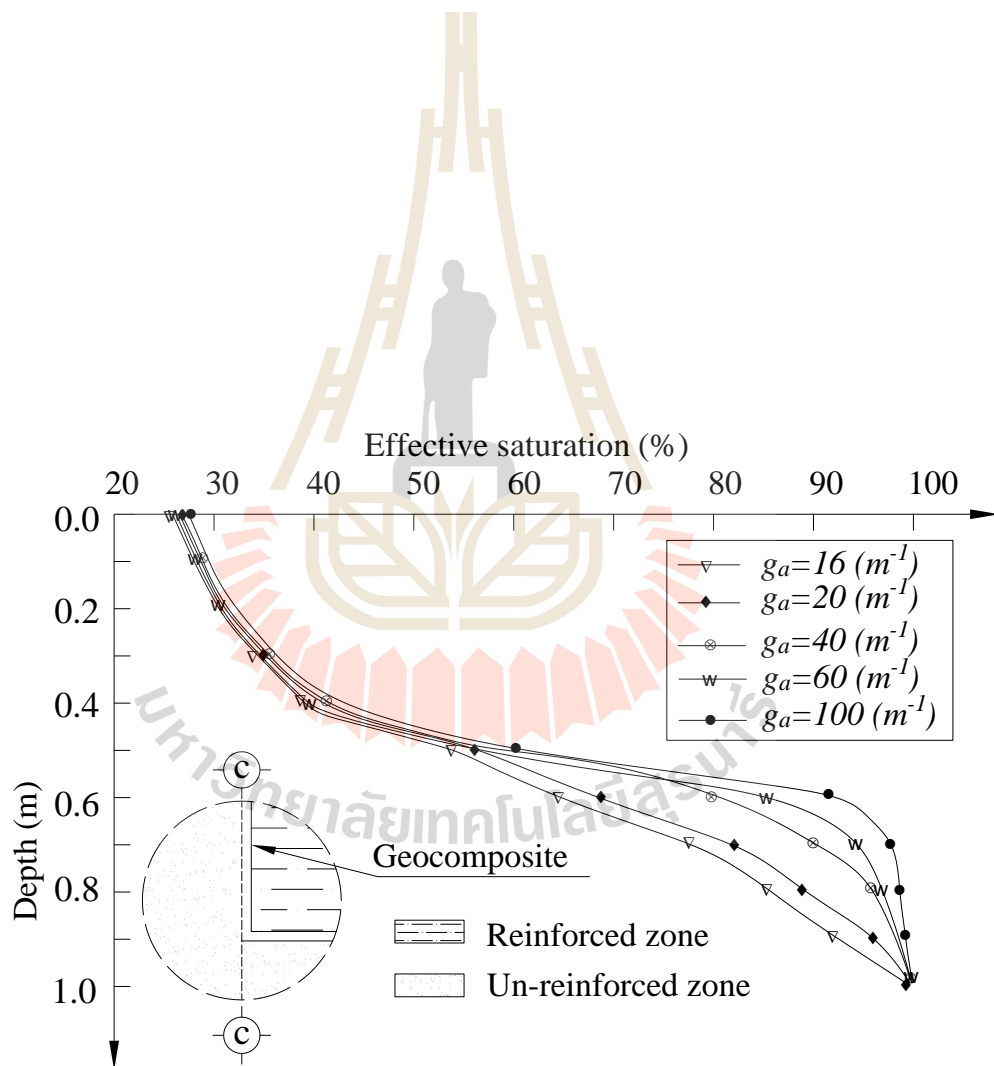
3.5.1.3 The saturation parameters S_{sat} and S_{res}

Figures 3.14 a and 3.14 b present phreatic surface and effective saturation profiles on the MSE wall model calculated at the lowest and the highest magnitudes of S_{res} (0.03, 0.05, 0.08, and 0.10) and S_{sat} (0.7, 0.8, 0.9, and 1.0), respectively. The saturation parameters S_{sat} and S_{res} of the soil might affect the distribution of water contents in the soil, both outside and inside the protection zone. However, these saturation parameters do not affect the distribution of water content represented in terms of effective saturation. The saturation parameters S_{sat} and S_{res} of the soil have a negligible effect on the phreatic surface.



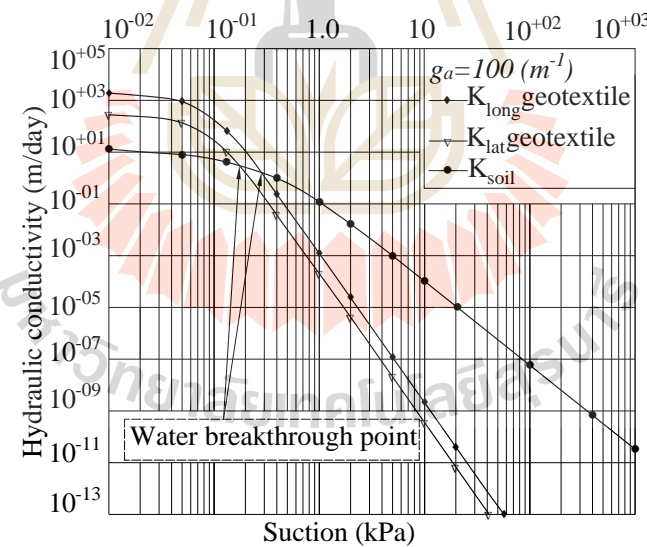
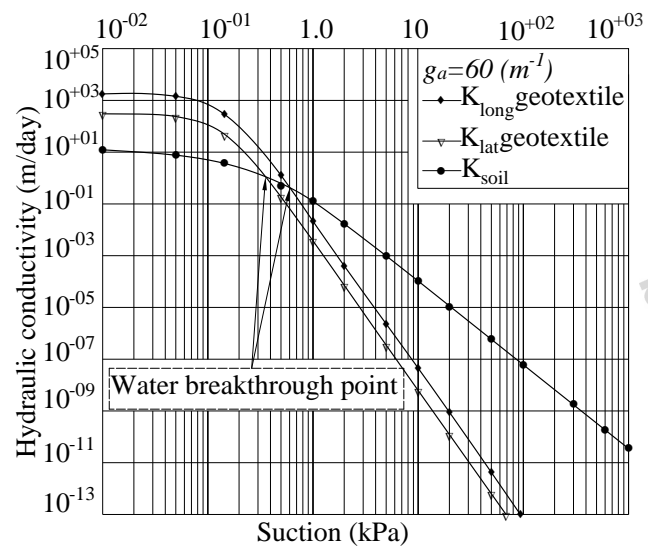
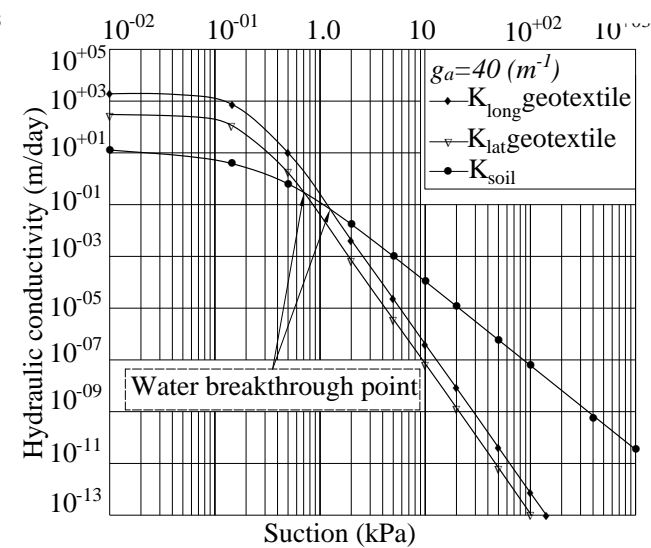
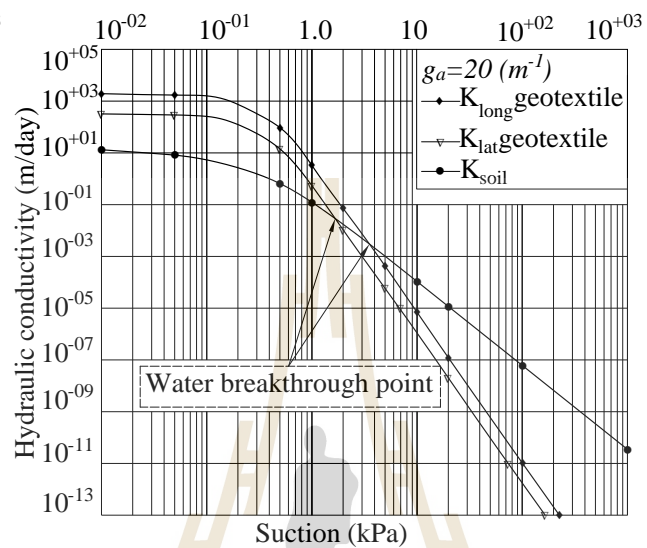
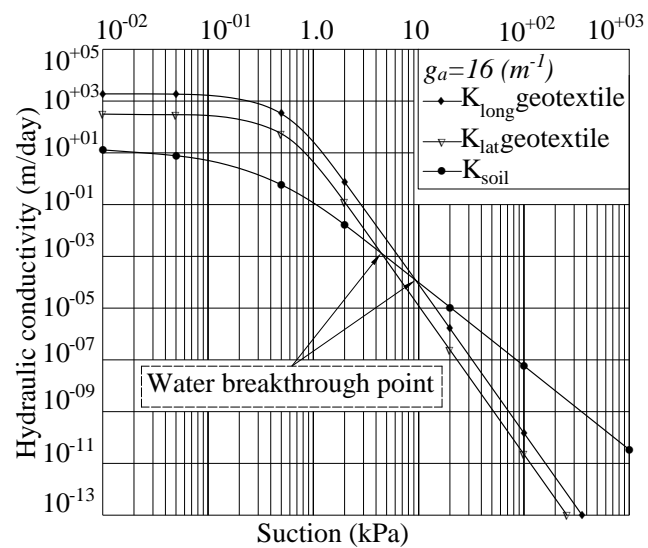


g_a



The capillary barrier phenomenon plays an important role in the degree of saturation at the soil-geotextile interface. Previous studies, i.e., (Stormont et al., 1997; Henry and Holtz, 2001; Iryo and Rowe, 2003; Bathurst, 2007; Bathurst et al., 2009; Bouazza et al., 2013), reported that geotextiles may act as coarse grain soil and can either facilitate or obstruct drainage flow depending on the saturation conditions of the soil and geotextiles. Under unsaturated conditions, the flow of water from smaller to larger pore size materials is obstructed by the capillary break phenomena, and hence, water accumulates at the interface. This phenomenon occurs until the magnitude of suction at the interface decreases to a critical suction level. At this point, the hydraulic conductivities of the two materials reach the same value, and water breaks through the interface.

Figure 3.16 presents the hydraulic conductivity functions of the soil and geotextile at various g_a values of the geotextile. The magnitudes of the critical suction for all cases are low, with water found not to permeate through the interface at high suction levels. Thus, the saturation profiles at high suction levels are not appreciably different among all cases (**Figure 3.15**). Although the critical suction in all cases is found to be low, the magnitudes vary between cases (**Figure 3.16**). A high g_a value of the geotextile yields a low magnitude of critical suction and subsequently results in a higher saturation at high saturation levels.



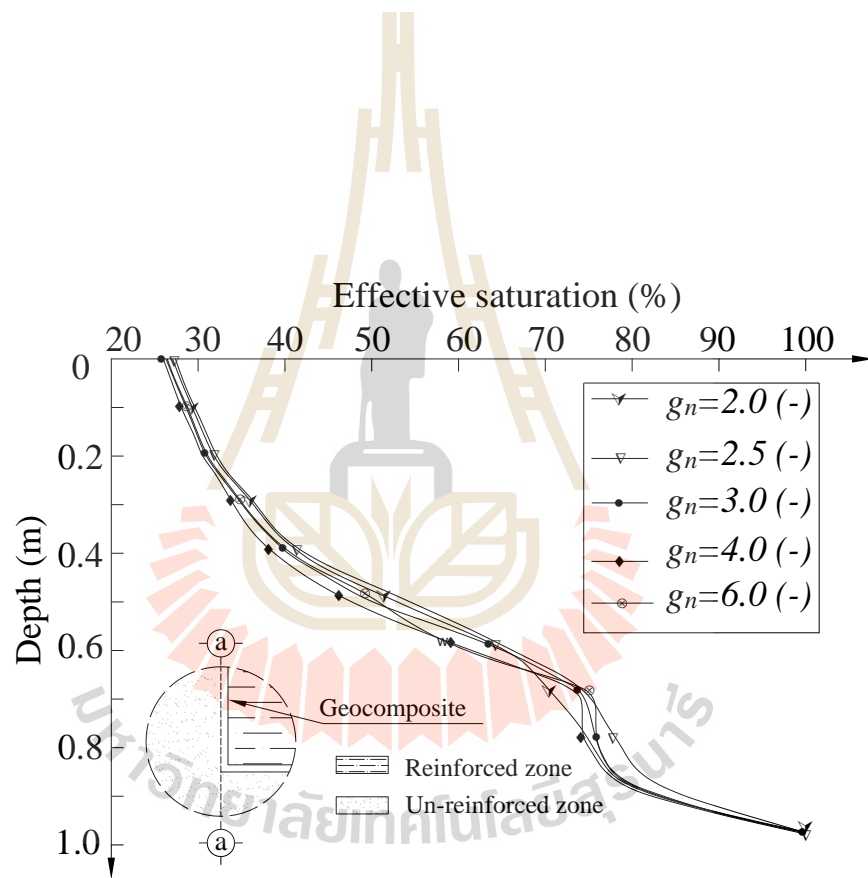
g_n

g_n

g_n

g_n

g_n

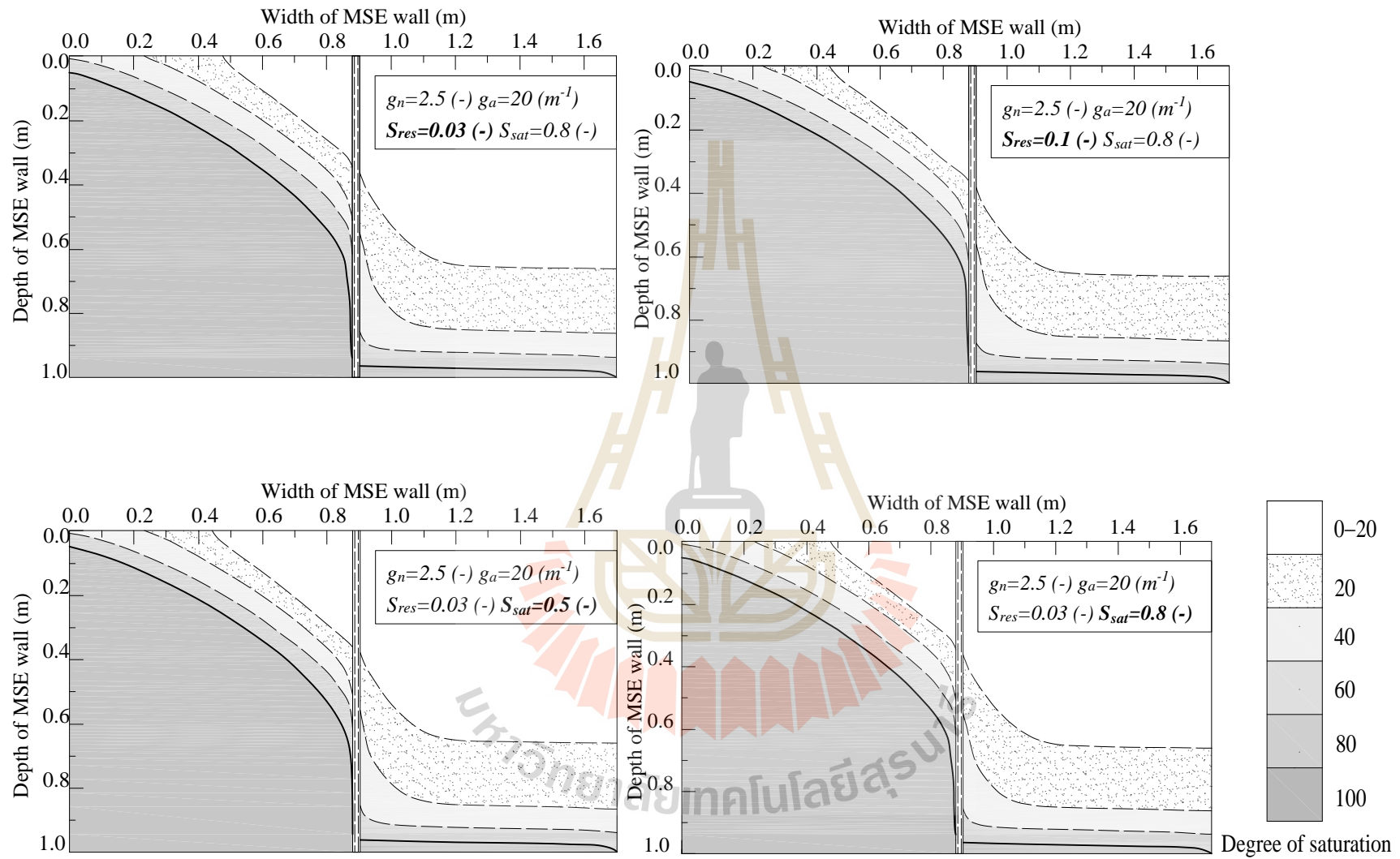


3.5.2.3 The saturation parameters S_{sat} and S_{res}

Figures 3.18 a and 3.18 b present phreatic surface and effective saturation profiles on the MSE wall model calculated at the lowest and highest magnitudes of S_{res} (0.03, 0.05, 0.08, and 0.10) and S_{sat} (0.5, 0.6, 0.7, and 0.8), respectively. Similar to the saturation parameters S_{sat} and S_{res} of the soil, the saturation parameters S_{sat} and S_{res} of the geotextile do not affect the distribution of water content and the location of the phreatic surface. In fact, the variation of S_{sat} and S_{res} may affect the distribution of the degree of soil saturation. It is, however, the computation results were presented in terms of effective saturation, S_e , which is defined as:

$$S_e = \frac{S - S_{res}}{S_{sat} - S_{res}} \quad (3.3)$$

The equation (3.3) implies that the degree of saturation does not change as S_{sat} or S_{res} change. For example, two soils have S_{res} equals to 0.9 and 0.7 will have S_e value under the phreatic surface of 1.0



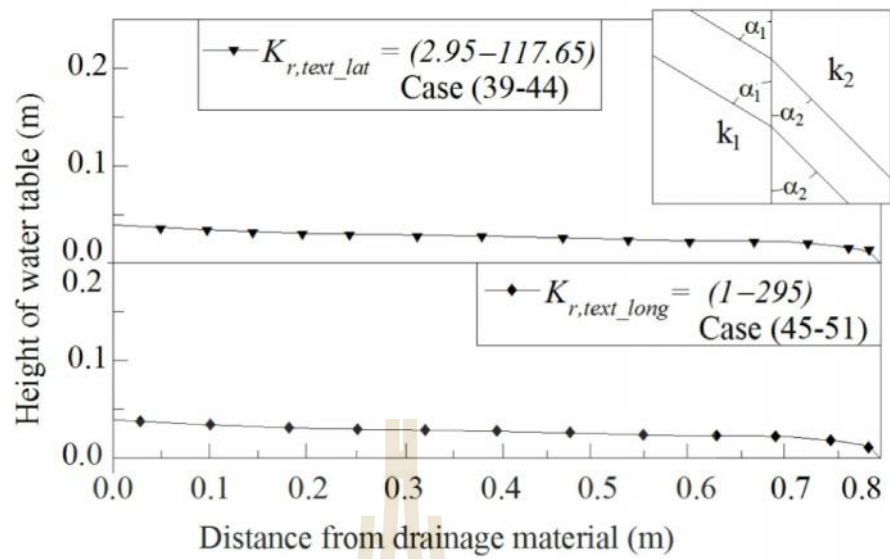
3.5.3 Effect of hydraulic conductivity ratio

The level of the phreatic surface inside the protected zone is vital to the stability of the MSE wall. The lower the phreatic surface level results in a lower water content inside the protected zone and hence leads to higher stability for the wall. In most of the simulation cases, the phreatic surface level inside the protected zone drops close to the bottom-most part of this zone. However, a higher the phreatic surface levels are still found in some cases. It is known that flow across a boundary between two materials of different hydraulic conductivities might result in a refraction of the flow direction, as shown in the top right of **Figure 3.19**.

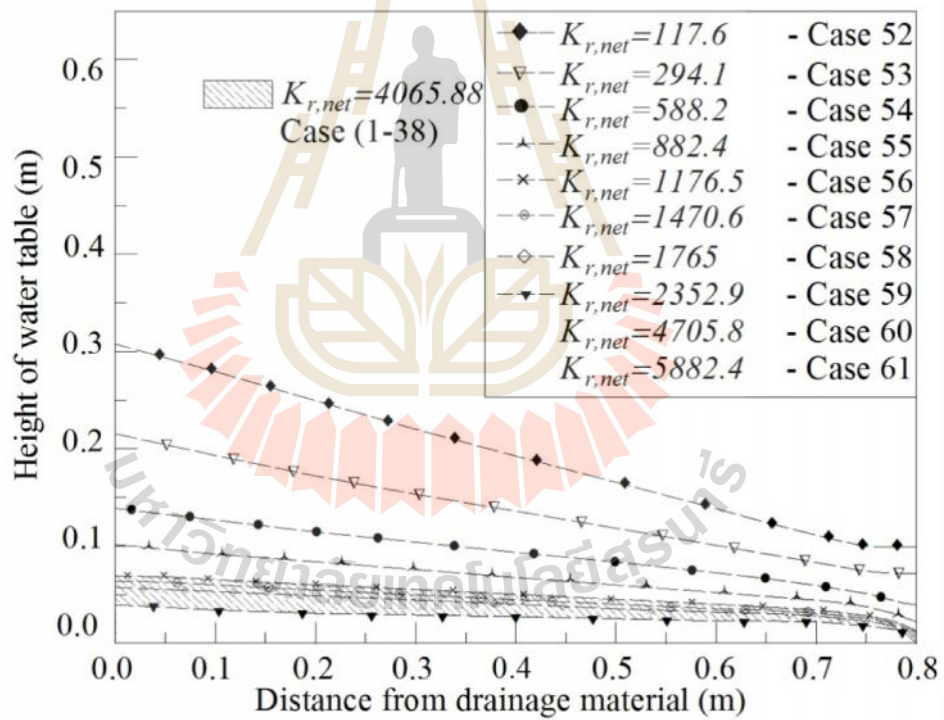
The relationship between the reflected angles and the hydraulic conductivity of the materials is written as

$$\frac{\tan r_1}{\tan r_2} = \frac{k_1}{k_2} \quad (3.4)$$

In other words, the ratio of the hydraulic conductivity of geocomposite materials to that of soil may affect the phreatic surface in the protected zone. **Figures 3.19 a** and **3.19 b** show the phreatic surface in the protected zone for various ratios between the hydraulic conductivity of the geotextile and that of soil and ratios between the hydraulic conductivity of the geonet and that of soil, respectively. As the geotextile exhibits anisotropic behaviour in drainage functions, the effect of the hydraulic conductivity of the geotextile, both in the lateral and longitudinal directions, on the phreatic surface in the protected zone must be investigated. Hence, the ratio between the hydraulic conductivity of the geotextile in the lateral direction and that of soil ($K_{r, \text{text}_{-lat}}$) and the ratio between the hydraulic conductivity of the geotextile in the longitudinal direction and that of soil ($K_{r, \text{text}_{-long}}$) were taken into consideration.



(a)



(b)

The phreatic surface plots shown in **Figure 3.19 a** indicate that $K_{r, \text{text_lat}}$ and $K_{r, \text{text_long}}$ do not affect the phreatic surface in the protected zone.

Figure 3.19 b presents the effect of the ratio between the hydraulic conductivity of the geonet and that of soil ($K_{r, \text{net}}$) on the phreatic surface in the protected zone. A large $K_{r, \text{net}}$ value is found at the lower phreatic surface level in the protected zone. Further reduction of the phreatic surface level is not observed when the magnitude of $K_{r, \text{net}}$ is greater than 1765. The variation of the phreatic surface level due to the effect of other parameters studied (Cases 1-38) is indicated by the grey shaded area in **Figure 3.19 b**. The small band in the grey shaded area indicates that there is little variation in the phreatic surface level in the protected zone due to any change in the other studied parameters. These results clearly indicate that the phreatic surface level in the protected zone is mainly governed by the magnitude of $K_{r, \text{net}}$.

3.6 Conclusions

The drainage ability of geocomposites, which consists of a core material with a large flow channel (geonet) sandwiched by two nonwoven geotextile layers, was investigated through large-scale MSE wall model tests. The experimental results indicate that the geocomposite studied effectively prevents the flow of water into the protected zone by collecting water in the unreinforced zone and draining it in front of the wall face. Comparisons between the deformations of the MSE wall models with and without geocomposite installation indicate that the MSE wall with a geocomposite is far superior to that without a geocomposite. Numerical models were

established to conduct parametric studies. The following conclusions can be drawn as a result of this research:

- 1) The WRC of the soil reflects the distribution of effective saturation in the soil both inside and outside the protected zones. The WRC of the geotextile reflects the distribution of effective saturation in the soil both inside and outside the protected zone.
- 2) The “capillary barrier” phenomenon plays a role in the distribution of effective saturation at the soil-geotextile interface. The lower magnitude of suction where the water permeates through the interface results in a greater amount of water accumulation at this interface.
- 3) The phreatic surface in the protected zone is governed by the ratio between the hydraulic conductivity of the geonet and that of the soil ($K_{r,net}$). The lower magnitude of $K_{r,net}$ results in a higher phreatic surface level in the protected zone. As the phreatic surface level in the protected zone is vital for the stability of the MSE wall, a proper magnitude of permeability for the geonet must be used such that the water table level inside the protected zone is low and close to the base of the protected zone. This approach is similar to the conventional design method in which candidate materials are selected for collecting and transmitting seepage water whose transmissivity must be greater than the required flow rate.

3.7 References

- AASHTO., 2002. **Standard Specifications for Highway and Bridge**. American Association of State of Highway and Transportation Officials, Washington DC
- Bathurst, R., et al., 2009. **Experimental investigation of infiltration ponding in one-dimensional sand–geotextile columns**. *Geosynthetics International* 16(3): 158-172.
- Bathurst, R., 2007. **Geosynthetics Classification**. IGS Leaflets on Geosynthetics Applications, IGS Education Committee, available at www.geosyntheticssociety.org.
- Bouazza, A., et al., 2013. **Unsaturated Geotechnics Applied to Geoenvironmental Engineering Problems Involving Geosynthetics**. *Engineering Geology*, 165, 143-153.
- Chen, D.-H., et al., 2007. **Failure Analysis of a Bridge Embankment with Cracked Approach Slabs and Leaking Sand**. *Journal of Performance of Constructed Facilities* 21(5): 375-381.
- Dye, H. B., 2008. **Moisture movement through expansive soil and impact on performance of residential structures**, Arizona State University.
- Henry, K. S., and Holtz, R. D., 2001. **Geocomposite Capillary Barriers to Reduce Frost Heave in Soils**. *Canadian Geotechnical Journal* 38(4): 678-694.
- Horpibulsuk, S., and Niramitkornburee, A., 2010. **Pullout resistance of bearing reinforcement embedded in sand**. *Soils and Foundations* 50(2): 215-226.
- Iryo, T., and Rowe, R., 2004. **Numerical Study of Infiltration Into a Soil–Geotextile Column**. *Geosynthetics International* 11(5): 377-389.

- Iryo, T., and Rowe, R., 2003. **On the Hydraulic Behavior of Unsaturated Nonwoven Geotextiles.** *Geotextiles and Geomembranes* 21(6): 381-404.
- Knight, M., and Kotha, S., 2001. **Measurement of Geotextile-Water Characteristic Curves Using a Controlled Outflow Capillary Pressure Cell.** *Geosynthetics International* 8(3): 271-282.
- Koerner, R., and Soong, T.-Y., 2000. **Design of Drainage Systems for Segmental Retaining Walls.** *Proceedings of the 14th GRI Conference*, 323-351
- Koerner, R. M., and Koerner, G. R., 2011. **The Importance of Drainage Control for Geosynthetic Reinforced Mechanically Stabilized Earth Walls.** *Journal of GeoEngineering* 6(1): 3-13.
- Koerner, R. M., and Soong, T.-Y., 2001. **Geosynthetic Reinforced Segmental Retaining Walls.** *Geotextiles and Geomembranes* 19(6): 359-386.
- Koerner, R. M., and Soong, T.-Y., 2005. **Analysis and Design of Veneer cover Soils.** *Geosynthetics International* 12(1): 28-49.
- Lafleur, J., et al., 2000. **Influence of Matric Suction on the Drainage Performance of Polyester Geotextiles.** *Proceedings 53rd Annual Conference of the Canadian Geotechnical Society*, 1115-1122
- McKean, J., and Inouye, K., 2001. **Field evaluation of the long-term performance of geocomposite sheet drains.** *Geotextiles and Geomembranes* 19(4): 213-234.
- Morris, C. E., 2000. **Unsaturated flow in nonwoven geotextiles.** *GeoEng 2000: International Conference on Geotechnical and Geological Engineering*, Melbourne, Australia, 19-24 Nov, 2000, Technomic, Lancaster, PA, USA.

- Mualem, Y., 1976. **A new Model for Predicting the Hydraulic Conductivity of Unsaturated Porous Media**. Water Resour. Res 12(3): 513-522.
- Nahlawi, H., et al., 2007. **Characterisation of Geotextiles Water Retention using a Modified Capillary Pressure Cell**. Geotextiles and Geomembranes 25(3): 186-193.
- Narejo, D., and Ramsey, B., 2001. **MSE wall drainage alternatives Careful drainage design can prevent costly retaining-wall failures**. Geotechnical Fabrics Report 19(5): 26-29.
- Potts, D. M., et al., 2001. **Finite element analysis in geotechnical engineering: application**, Thomas Telford.
- Ross, B., 1990. **The diversion capacity of capillary barriers**. Water resources research 26(10): 2625-2629.
- Shibuya, S., et al., 2007. **Failure of Reinforced Earth as Attacked by Typhoon No. 23 in 2004**. Soils and Foundations 47(1): 153-160.
- Stormont, J. C., et al., 1997. **Water Retention Functions of four Nonwoven Polypropylene Geotextiles**. Geosynthetics International 4(6): 661-672.
- Stormont, J. C., and Morris, C. E., 2000. **Characterization of Unsaturated Nonwoven Geotextiles**. In Advances in Unsaturated Geotechnics, ASCE, 153-164.
- van-Genuchten., 1980. **A closed-form Equation for Predicting the Hydraulic Conductivity of Unsaturated Soils**. Soil Science Society of America Journal 44(5): 892-898.

Yoo, C., and Jung, H.-Y., 2006. **Case history of Geosynthetic Reinforced Segmental Retaining Wall Failure**. Journal of Geotechnical and Geoenvironmental Engineering 132(12): 1538-1548.



CHAPTER IV

SEEPAGE RESPONSES IN MSE WALLS UTILIZE IN-PLACED MARGINAL SOILS AS FILL MATERIALS WITH GEOCOMPOSITES FOR DRAINAGE

This chapter aimed to imitate two feasible scenarios of MSE walls, in which in-placed marginal soils utilized as backfill materials. The prime target of this initiative was to assess potential influence of each unsaturated hydraulic parameters of in-placed marginal backfills on the seepage responses in MSE walls drained by geocomposite. To fulfill this part, a series of parametric studies were executed using computer program Plaxis 2D. The parametric study results indicate that the use of in-placed marginal soils, which exhibit high fine-grained particles, may result in a wide-spread high water content area inside the MSE wall, even when the geocomposite was properly installed and the water behind and beneath the backfill zone was apparently to be properly collected and drained. In addition, the fine particle content in the in-placed marginal soils affects the hydraulic conductivity of the backfill. The hydraulic conductivity of the in-placed marginal soils in the upstream side has a significant effect on the level of the phreatic surface inside the protected zone (or the inner phreatic surface). Furthermore, the hydraulic conductivity of the soil inside the protected zone noticeably affects the inner phreatic surface, particularly when the

capacity of the drainage medium is insufficient for collecting all the water flowing from the upstream side.

Another finding was found from severe cases, in which the upstream water flow rate is greater than the drainage capacity of the drainage medium, a high saturated hydraulic conductivity backfill material can limit the height of the phreatic surface inside the protected zone.

This chapter is organized as follows: Firstly, an extensive problem on the use of in-placed marginal soils with high fine-grained particles as backfill is presented. Subsequently, some basic and relevant properties of materials used in this part are displayed. Next, the results obtained from parametric studies are illustrated. Close to the end of this chapter, a discussion section is established to discourse upon the obtained results with the aim of pointing out how the each hydraulic property of in-placed marginal soils affects the seepage responses in MSE walls. The chapter closes with some conclusions which are withdrawn from this part of the research.

Throughout this chapter, the term of in-placed marginal soils is used, which is combined from two labels including “in-placed” and “marginal”, the first label is to indicate a soil that exists in its natural state or its original position where the MSE wall is placed on, the second label is to represent for a kind of high fine-grained soils.

4.1 Statement of problem

Due to the scarcity of granular materials or known as good draining materials, the in-placed local soils have been widely utilized as backfill materials, especially in the tropical climate area where the residual soils are normally found to be marginal lateritic soils. Moreover, in order to pursue the strategy of enhancing the economics of

MSE walls, the use of such low permeability materials which extends beyond the characteristics accepted by AASHTO/FHWA or NCMA as shown in **Table 4.1**, is being a top priority. Previous researchers have found that most MSE walls constructed using in-placed marginal soils with high fine-grained particles often instrumented during and after construction process (Zornberg and Mitchell, 1994; Mitchell, 1995). The overall long-term performance of these MSE walls, such as lateral displacement and vertical settlement, was reported to be excellent (Zornberg and Mitchell, 1994; Mitchell, 1995; Zornberg and Bueno, 2006).

Table 4.1 Soil characteristics for use within protected zone (Sandri, 2005)

| Feature | AASHTO <i>(obligated)</i> | NCMA <i>(suggested)</i> | Marginal soils |
|-------------------------|-------------------------------------|-----------------------------------|-----------------------|
| Percent pass sieve #5 | 100 | 75-100 | - |
| Percent pass sieve #4 | - | 20-100 | - |
| Percent pass sieve #40 | 0-60 | 0-60 | - |
| Percent pass sieve #200 | 0-15 | 0-35 | >35 |
| Plasticity Index | 6 | 20 | >20 |

Besides a number of successful cases of utilizes of in-placed marginal soils as fill in MSE walls, a number of failure cases have also reported (Zornberg and Mitchell, 1994; Mitchell, 1995). Koerner and Soong (2001) documented 26 case histories of MSE wall failures in the United States, 17 of which were related to low permeability soil backfills. They concluded that if marginal soils or high fine-grained soils were used in the protected zone, any water ponding that occurs behind or

beneath the protected zone must be properly collected and discharged. Good performance of MSE walls is mainly governed by the seepage responses within the MSE walls. In other words, the use of in-placed marginal soils as backfills could yield both economic and even environmental benefits. A list of MSE walls that utilized marginal soils as backfill is shown in **Table 4.2**.

Table 4.2 MSE walls utilized high fine-grained soils as backfill (after Mitchell, 1995)

| Place of construction | Function of MSE wall | Fill materials | Reinforcing materials | Time | Literatures |
|---|-------------------------|-----------------------------------|-------------------------------------|------|----------------|
| Autoroute A15, Rouen, France | Embankment | Weathered chalk, silt | Nonwoven geotextile | 1971 | Mitchell, 1995 |
| Illinois River wall, Oregon, USA | River wall | Silty sand | Nonwoven geotextile | 1974 | |
| Barrage de Maraval, Pierrefeu, France | Dam spillway weir | Compacted clay | Woven geotextile | 1976 | |
| TRRL experimental wall, Crowthorne, UK | Reinforced earth wall | Silty clay, sandy clay | Steel and plastic strips | 1978 | |
| Yokohama residential complex, Tokyo, Japan | Retaining wall | Volcanic clay | Metal strips | 1978 | |
| Chemie Linz embankment, Austria | Reinforced earth wall | Silty sand | Nonwoven geotextile | 1984 | |
| Annan by pass retaining wall, U.K | Retaining wall | Clayey till | Concrete half discs used as anchors | 1989 | |
| Calgary parking lot, Alberta, Canada | Retaining wall | Low plastic clay till | Geogrid | 1984 | |
| Cannon Creek embankment, Arkansas, USA | Highway embankment | Highly plastic and expansive clay | Geogrid | 1988 | |
| Reinforced slopes, Taiwan | Reinforced slopes | Clayey silt | Geogrid | n/a | Zornberg, 2006 |
| Reinforced steep slope, highway SP-123, Sao Paulo, Brazil | Reinforced steep slope, | Sandy silt | Woven and nonwoven geotextile | 1984 | |

Table 4.2 MSE walls utilized high fine-grained soils as backfill (after Mitchell, 1995)

(continued)

| Place of construction | Function of MSE wall | Fill materials | Reinforcing materials | Time | Literatures |
|--|----------------------|---------------------------------|-----------------------------|------|--------------------------|
| Retaining wall, California, USA | Retaining wall | High plasticity silts and clays | Geogrid | 2000 | Sandri, 2000 |
| MSE wall, Dallas Avenue of SH342, Texas, USA | MSE wall | Clayey sand | Steel wire meshes | 2004 | Hossain et al., 2011 |
| Ramp Struck wall, Mae Moh mine, Thailand | Ramp struck wall | Red clay | Steel bearing reinforcement | 2016 | Horpibulsuk et al., 2016 |

In spite of its extensive use in MSE walls, no reliable design methodology for MSE walls utilizes high fine-grained marginal soils as backfills have been built. Very few studies have paid attention to the influence of seepage responses on the performance of MSE walls. Similarly, moisture susceptibility is even a major concern in MSE walls that are filled with high fine-grained marginal soils, but no previous research has conducted a parametric study to gain a better understanding of this critical point, particularly when the protected zone is well encapsulated with a drainage system.

It is, thus, the finding from this part could contribute to as well as reinforce the knowledge of seepage responses in MSE wall utilizes in-placed fine-grained marginal soils as fill materials.

4.2 A brief literature on geotechnical properties of in-placed marginal soils

The in-placed marginal soils are generally found in tropical climate area, particularly in the mountainous area. In reality, the term of “marginal laterite” or “marginal” is normally employed to describe a wide variety of tropical soils. Previous researchers have reported that the geotechnical behavior of marginal soils is predominantly affected by several factors, such as their mineralogical constituents, environment conditions (Oyelami and Van Rooy, 2016). Due to direct formation from their parent rocks, the marginal soils can be inherent several characteristics of the parent rocks.

The distribution of grain size of reported marginal soils has been found to be rich in sand and gravel contain, contains less than 30% silt. Liquid limit of marginal soils varies between 25 and 63, and plasticity indices are in the range of (5-42) (Badmus, 2010; Quadri et al., 2012; Eluozo and Nwaobakata, 2013). **Figure 4.1** illustrates the location of marginal soil depicted in Casagrande’s chart (Biswal, Sahoo et al., 2016).

Previous researchers (Alao, 1983; Omotoso et al., 2012; Horpibulsuk et al., 2013) have found that the optimum moisture content of marginal clays, marginal soils, and marginal gravels are laid in range of (9-19%), its maximum dry density varies between 1.3 tons/m³ to 2.4 tons/m³. The compressive strengths of marginal soils have been reported and it falls within the range of (0.5-1.5MPa) (Oyelami and Van Rooy, 2016). Townsend (1985) reported that the effective angle of marginal clays varies between 20 and 30°, and 30 to 40° for marginal gravels. The cohesion of marginal soils have also examined by Omotoso et al., (2012) with its magnitude

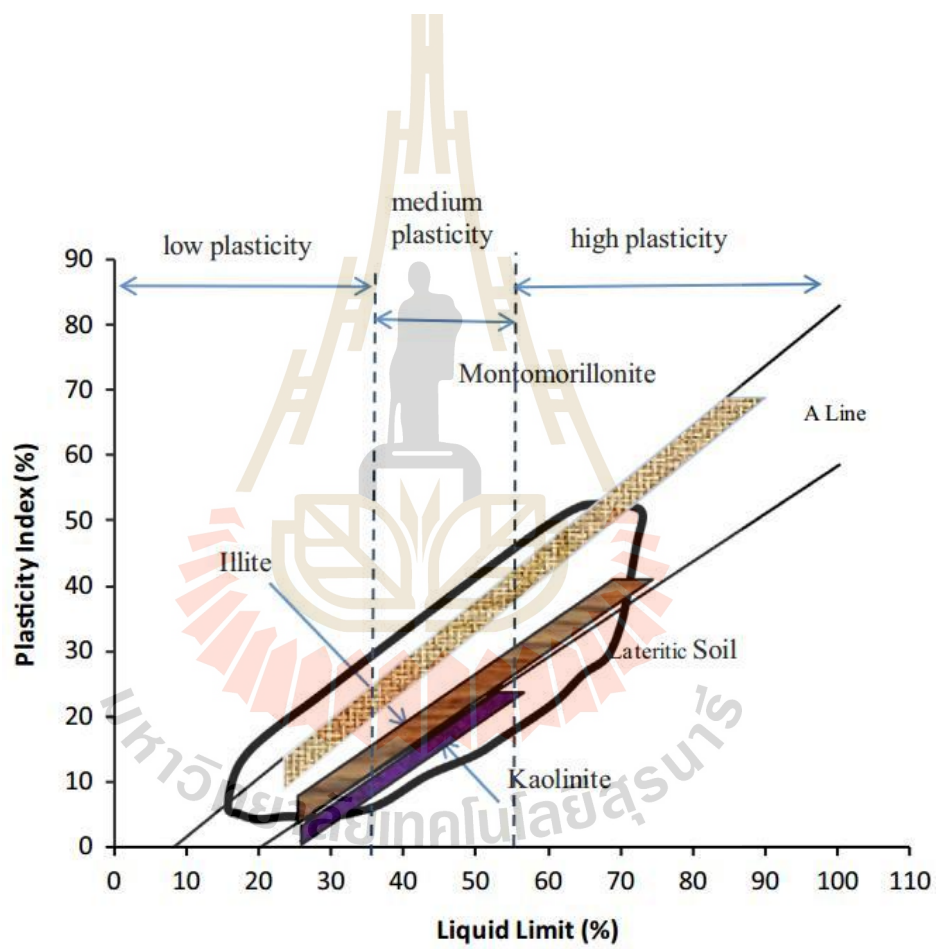


Table 4.3 Summary of typical geotechnical engineering properties of marginal lateritic soils

| No | Characteristic | Unit | Values |
|----|--------------------------|------------------|----------|
| 1 | Liquid limit (LL) | % | 25-63 |
| 2 | Plasticity Index (PI) | % | 5-42 |
| 3 | Optimum moisture content | % | 9-12 |
| 4 | Maximum dry density | ton/m^3 | 1.3-2.4 |
| 5 | Compressive strength | MPa | 0.5-1.5 |
| 6 | Effective friction angle | degree | 20-40 |
| 7 | Cohesion | kPa | 70-100 |
| 8 | Hydraulic conductivity | m/day | 0.01-400 |

4.3 Materials

The materials involved in this part were a sandy soil, a marginal soil, and a geocomposite, which comprises the geotextile and geonet. Among these materials, sandy soil, geosynthetic materials were utilized from the first main part that presented in the Chapter 3. The marginal soil was classified as clayey sand (SM-SC) according to the USCS. The soil comprises 26% fine particles (0.075 mm) with a PI of 16%. According to AASHTO (2002), this soil fails to meet the requirement for backfill materials, which limits the fine particles to no greater than 15%. The hydraulic conductivity of the marginal soil at the saturated state was found to be 0.34 m/day. Since the marginal soil comprises very fine pores, determining its wetting phase WRC using a double-wall triaxial cell was difficult, time-consuming, as well. Instead of directly determining the wetting phase WRC, the drying phase WRC of the marginal

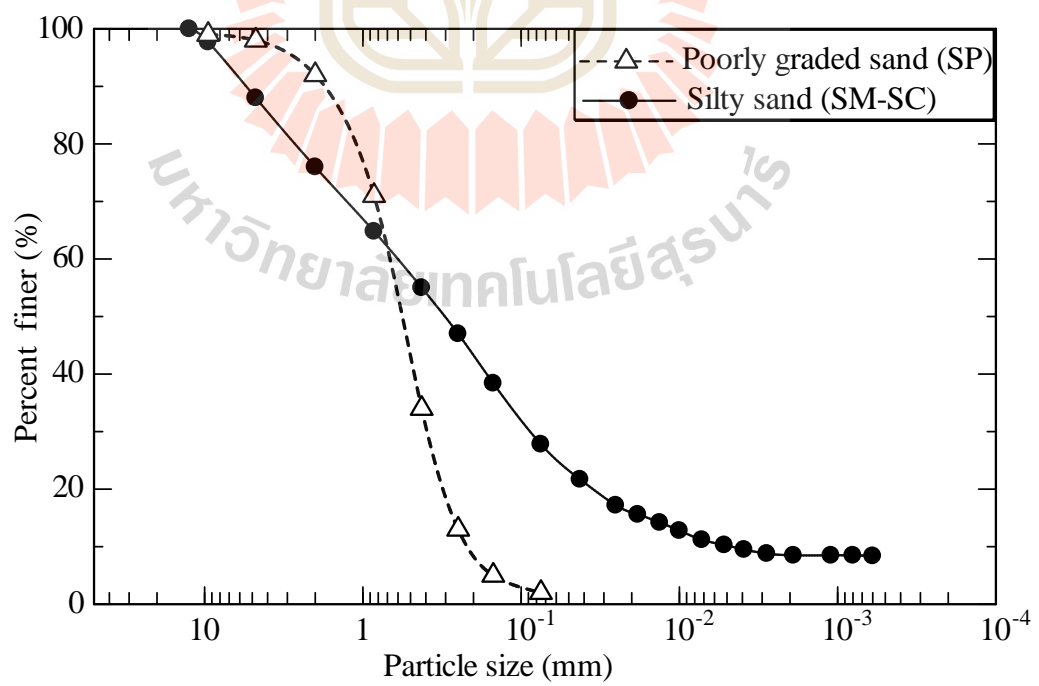
soil was obtained from a pressure plate apparatus (ASTM, 2008). Sequential nonlinear regression was employed to fit the VG model (Eq. 3.2 a – Chapter 3) to the measured WRC and to provide the best-fit VG model parameter values for the drying phase WRC of the marginal soil. The VG model parameter values for the wetting phase WRC are the same as those for the drying phase WRC except for the parameter, g_a , which is twice as high as that for the drying phase WRC (Kool and Parker, 1987)

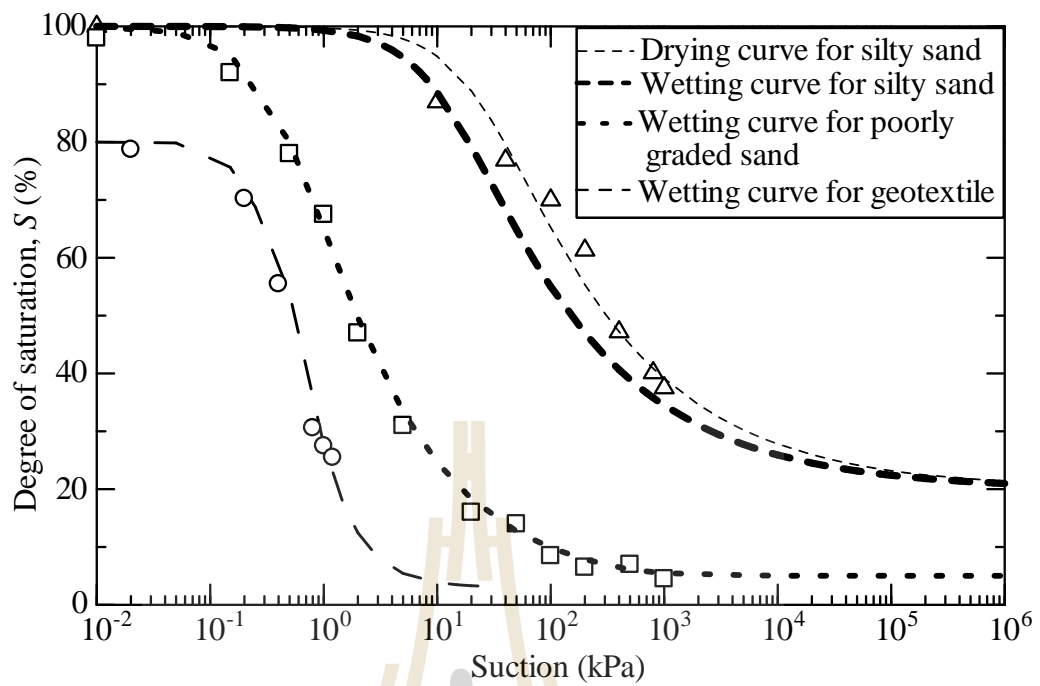
Figure 4.2 a presents the particle size distribution of the sandy soil along with that of the marginal soil. **Figure 4.2b** presents the measured (indicated by symbols) and calculated (indicated by lines) wetting phase WRC of the sandy soil, the marginal soil, and the geotextile. The VG model parameter values used to fit the model to the test results for the soil and the geotextile are summarized in **Table 4.4**. The wetting phase WRC of the marginal soil was plotted from the VG model (Eq. 3.2 a) with the parameter values obtained from the process mentioned above, these parameter values are presented in **Table 4.4**.

Table 4.4 van Genuchten model parameters of the materials used in this study

| Materials | VG-VGM model parameters | | | | |
|---------------|---------------------------|-----------|---------------|---------------|-------------------------|
| | g_a [m^{-1}] | g_n [-] | S_{res} [-] | S_{res} [-] | k [m/day] |
| Sandy soil | 20 | 1.5 | 0.03 | 1 | 17 |
| Marginal soil | 0.8 | 1.4 | 0.2 | 1.0 | 0.3456 |
| Geotextile | 20 | 1.5 | 0.03 | 0.8 | 2000 (320) ^a |
| Geonet | 600 | 40 | 0 | 1 | 69120 |

^a: Hydraulic conductivity of geotextile in lateral direction





| Materials | VG-VGM model parameters (Case No. 1) | | | | |
|-------------------------|--------------------------------------|-----------|---------------|---------------|-------------------------|
| | g_a [m^{-1}] | g_n [-] | S_{res} [-] | S_{res} [-] | k [m/day] |
| Compacted sandy soil | 20 | 1.5 | 0.03 | 1 | 17 |
| Compacted marginal soil | 0.8 | 1.4 | 0.2 | 1 | 0.3456 |
| Geotextile | 20 | 1.5 | 0.03 | 0.8 | 2000 (320) ^a |
| Geonet | 600 | 40 | 0 | 1 | 69120 |

| Case No. | Materials | | Varied parameters | Values |
|----------|------------------------|-------------------------|-------------------|--------|
| | Inside protection zone | Outside protection zone | | |

Table 4.5 Model parameters for each case in the L-S scenario (continued)

| | | | | |
|----------------|-----------------|-----------------|--------------------------|--------------------|
| 2, 3, 4, 5 | CS | NL ^b | g_a [m ⁻¹] | 0.5, 1.0, 3.0, 5.0 |
| 6, 7, 8, 9 | | | g_n [-] | 1.3, 1.5, 1.6, 1.7 |
| 10, 11, 12 | | | S_{res} [-] | 0.1, 0.25, 0.3 |
| 13, 14, 15 | | | S_{sat} [-] | 0.85, 0.9, 0.95 |
| 16, 17 | | | k [m/day] | 0.03456, 3.456 |
| 18, 19, 20, 21 | CS ^b | NL | k [m/day] | 1.7, 85, 170, 340 |
| A, B, C | CS | CS ^b | k [m/day] | 340, 170, 85 |
| D | CS ^b | NL | k [m/day] | 85 |

CS: Compacted sandy soil,

NL: Native marginal soil,

^a: Hydraulic conductivity of geotextile in lateral direction,

^b: Varied material.

Table 4.6 Model parameters for each case in the L-L scenario

| Materials | VG-VGM model parameters (Case No. 1 [*]) | | | | |
|--------------------------------|--|-----------|---------------|---------------|-------------------------|
| | g_a [m ⁻¹] | g_n [-] | S_{res} [-] | S_{sat} [-] | k [m/day] |
| Native in-placed marginal soil | 0.8 | 1.4 | 0.3 | 1 | 0.3456 |
| Compacted marginal soil | 0.8 | 1.4 | 0.2 | 1 | 0.3456 |
| Geotextile | 20 | 1.5 | 0.03 | 0.8 | 2000 (320) ^a |
| Geonet | 600 | 40 | 0 | 1 | 69120 |

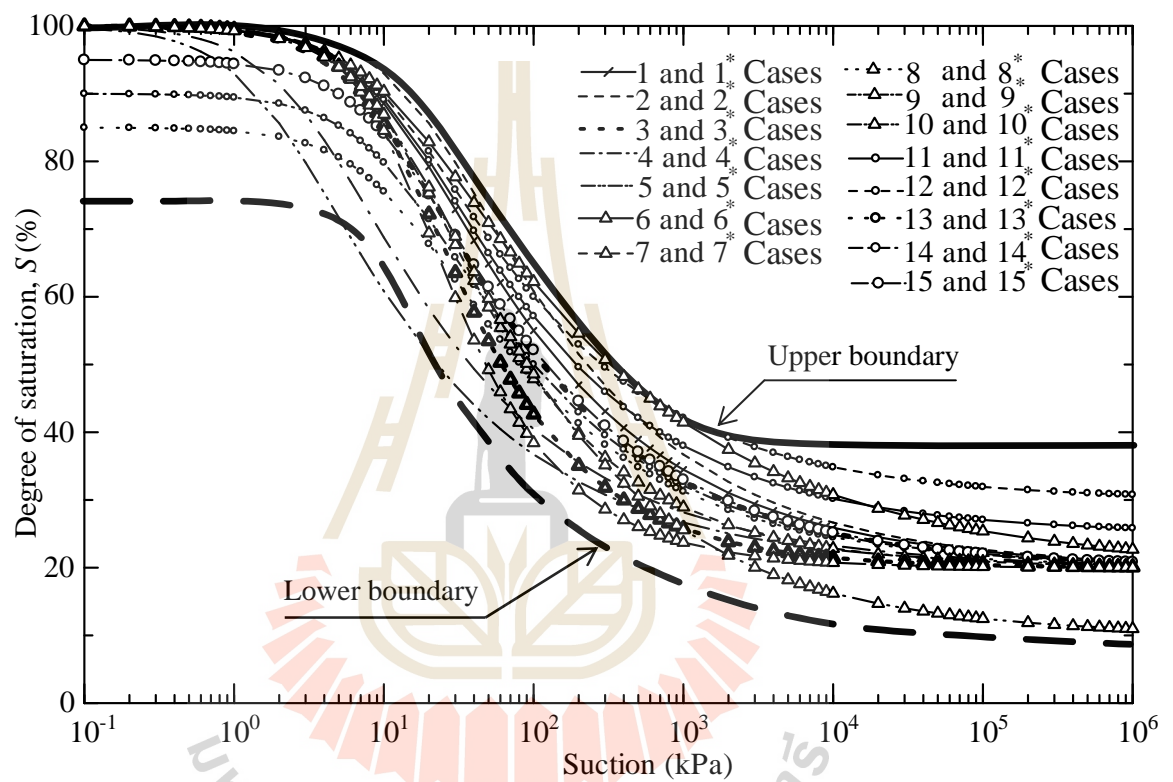
| Case No. | Materials | | Varied parameters | Values |
|---|------------------------|-------------------------|--------------------------|--------------------|
| | Inside protection zone | Outside protection zone | | |
| 2 [*] , 3 [*] , 4 [*] , 5 [*] | CL ^b | NL | g_a [m ⁻¹] | 0.5, 1.0, 3.0, 5.0 |
| 6 [*] , 7 [*] , 8 [*] , 9 [*] | | | g_n [-] | 1.3, 1.5, 1.6, 1.7 |
| 10 [*] , 11 [*] , 12 [*] | | | S_{res} [-] | 0.1, 0.25, 0.3 |
| 13 [*] , 14 [*] , 15 [*] | | | S_{sat} [-] | 0.85, 0.9, 0.95 |

CL: Compacted marginal soil,

NL: Native in-placed marginal soil,

^a: Hydraulic conductivity of geotextile in lateral direction,

^b: varied material.



(a)

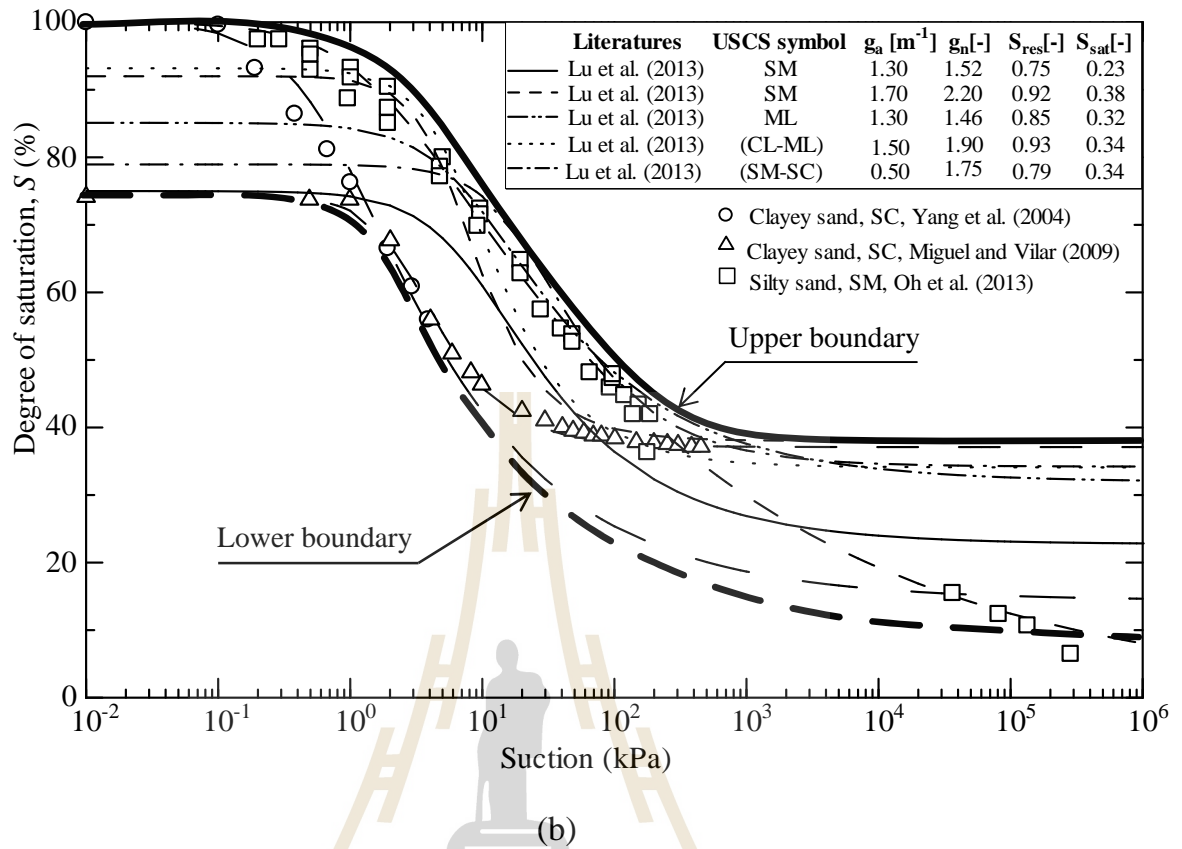


Figure 4.3 (a) WRC curves of the considered marginal soils and (b) WRC curves for different types of marginal soils obtained from previous studies.

4.4 Parametric study results

4.4.1 Seepage responses in the L-S scenario

The L-S scenario was intended to imitate a possible scenario, in which native in-placed marginal soil was located outside the protected zone and sandy soil was used as the backfill material in the protected zone. The first main goal of the L-S scenario was to examine the effect of the unsaturated flow properties of the marginal soils outside the protected zone on the seepage responses. The effect of the ratio of the saturated hydraulic conductivity of the geonet to that of the soil outside the protected zone, namely, K^{outer} , was assessed through a series of numerical cases (as shown in

Table 4.5). The calculation results obtained from the numerical sensitivity analysis from the twenty-five cases indicated that the seepage responses in the protected zone are slightly affected by the unsaturated flow properties of the soil outside the protected zone. The permeability ratio K^{outer} greatly affects the level of the inner phreatic surface. The details of the calculation results are as follows:

4.4.1.1 Effect of the g_a of in-placed soils outside the protected zone

Figure 4.4a presents the variation in the effective saturation (S_e) in the soils along the vertical lines located (a) 0.05 m to the left (outside the protected zone) and (b) 0.05 m to the right (inside the protected zone) of the geocomposite-soil interface as the g_a of the native marginal soil varies from 0.5 to 5.0 [m^{-1}] (cases 1-5). The S_e outside the protected zone for cases 1-3 ($g_a = 0.5, 0.8,$ and 1.0 [m^{-1}], respectively) remained greater than 90% for the entire height. However, the S_e outside the protected zone for $g_a = 3.0$ and 5.0 [m^{-1}] above the mid-height wall level significantly decreased, reaching $S_e = 70\%$ and 60% , respectively. The variation in the g_a of the marginal soil had a little effect on the effective saturation inside the protected zone.

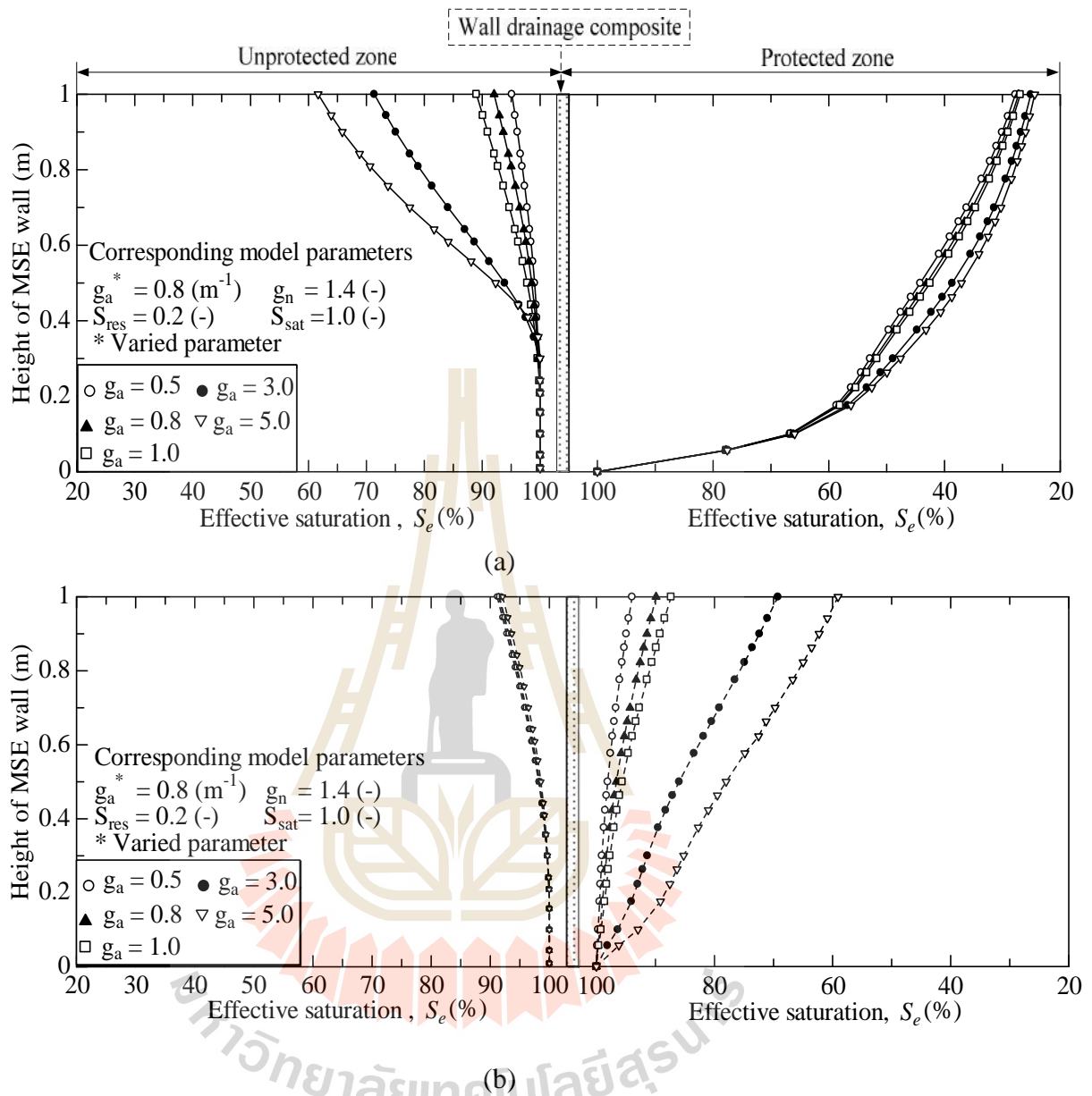
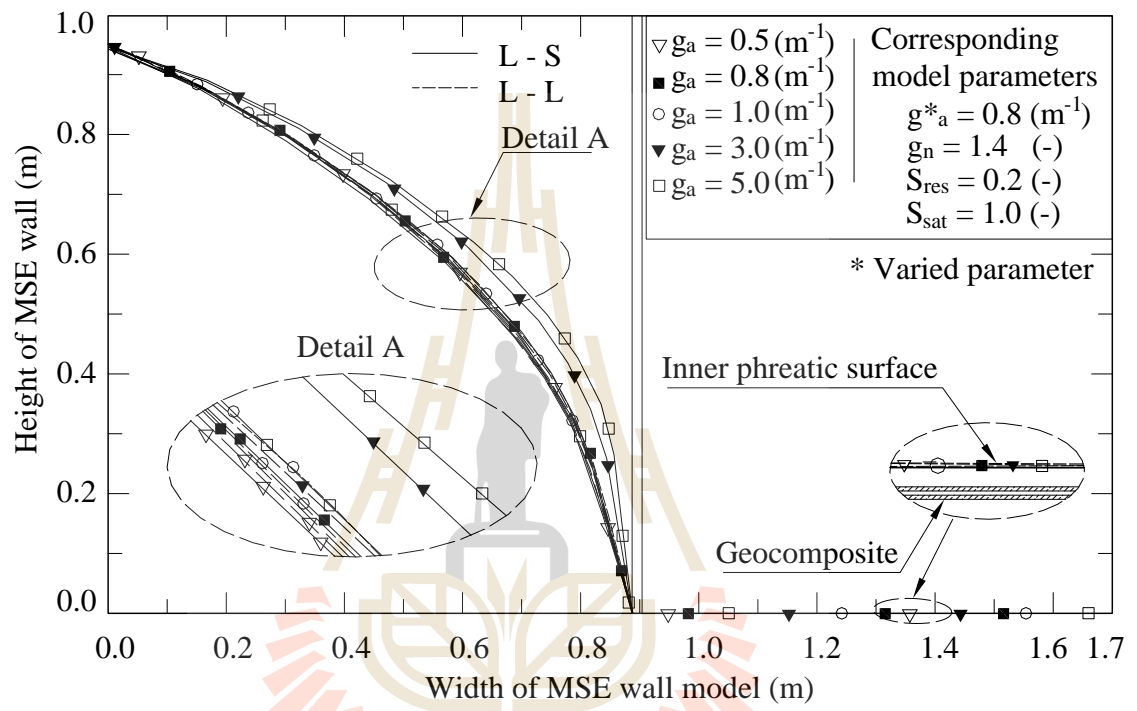


Figure 4.4 (a) Effective saturation profiles along the vertical sections located at 5cm apart to either side of the soil-geocomposite interface, outside and inside the protected zone, for varying g_a values of the native in-placed marginal soil for L-S scenario and (b) varying g_a values of the compacted marginal soil for L-L scenario.

g_a

g_a

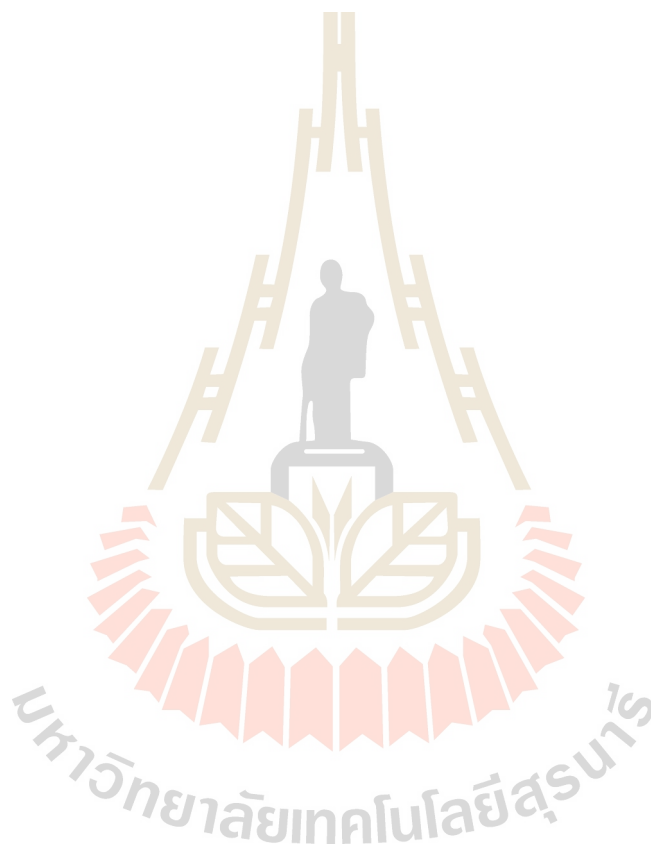


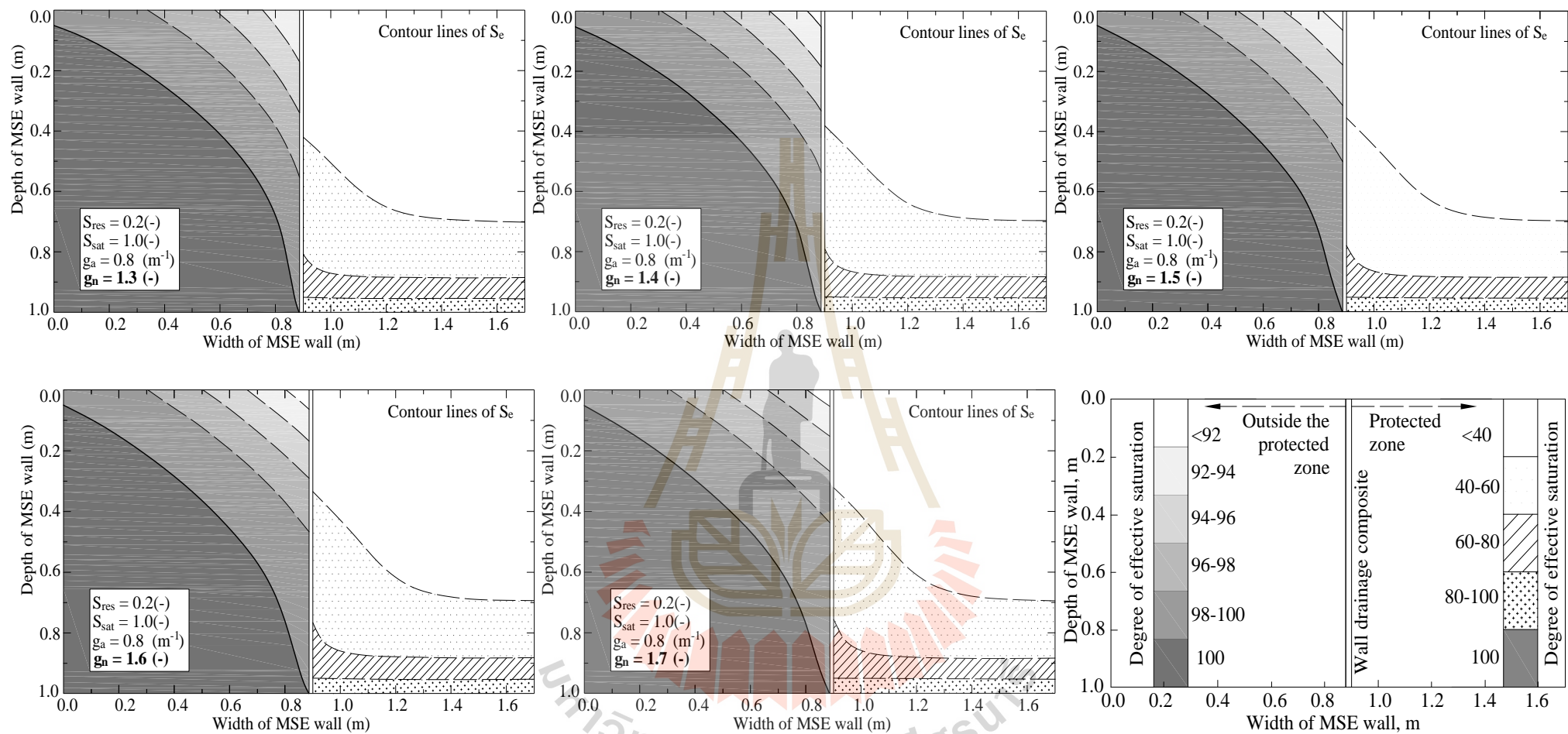
g_a

g_n

g_n

and 6-9). The outer phreatic surface was flatter for the soil with a lower g_n . The lower g_n value resulted in a wider distribution of the effective saturation in the soil outside the protected zone. Again, the distribution of the effective saturation inside the protected zone exhibited a little change as the g_n value of the soil outside the protected zone increased.

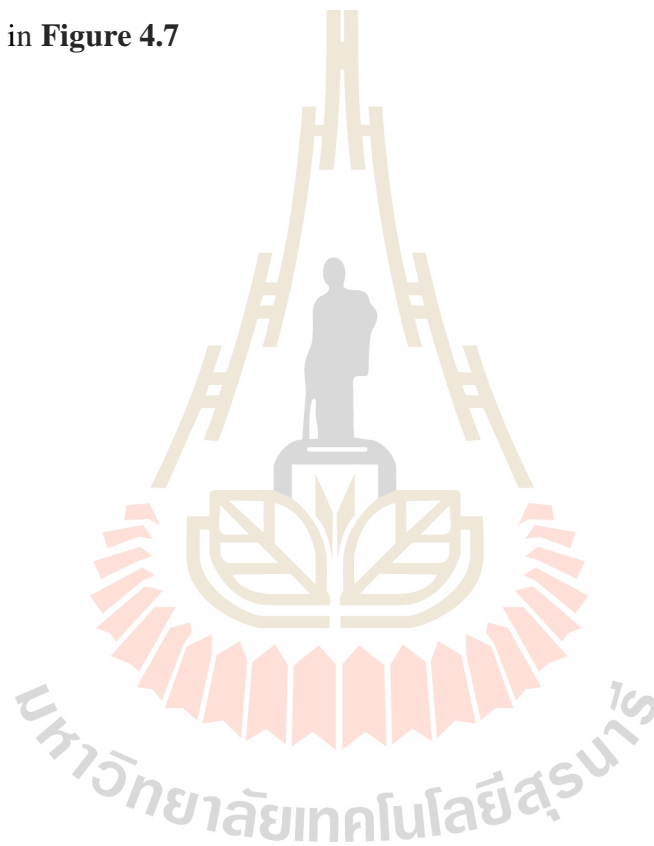


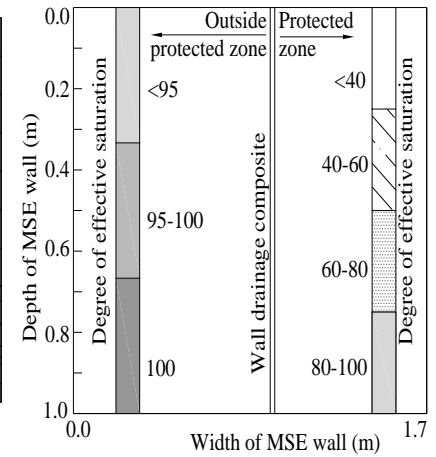
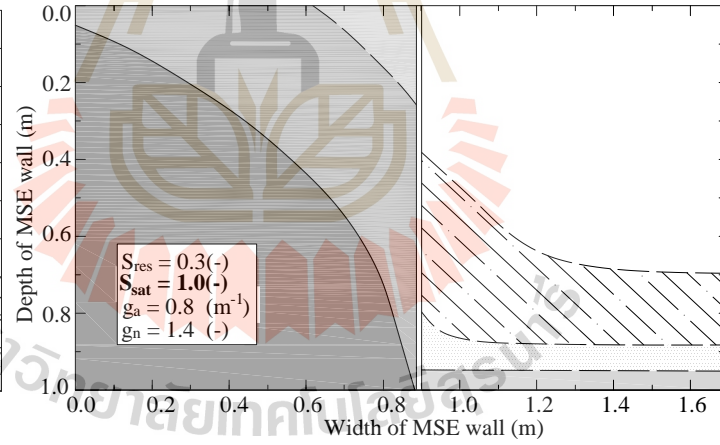
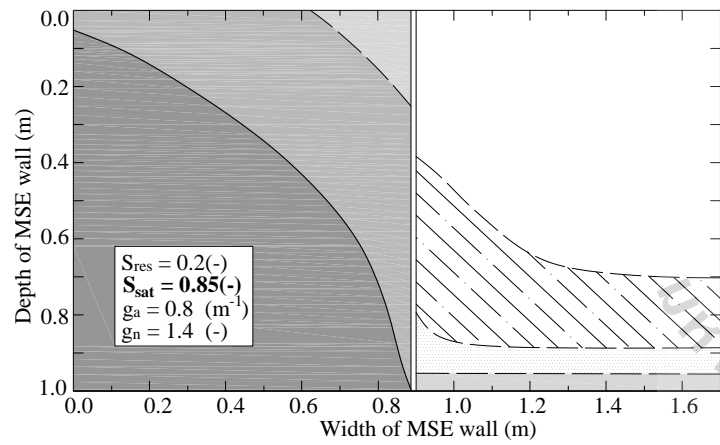
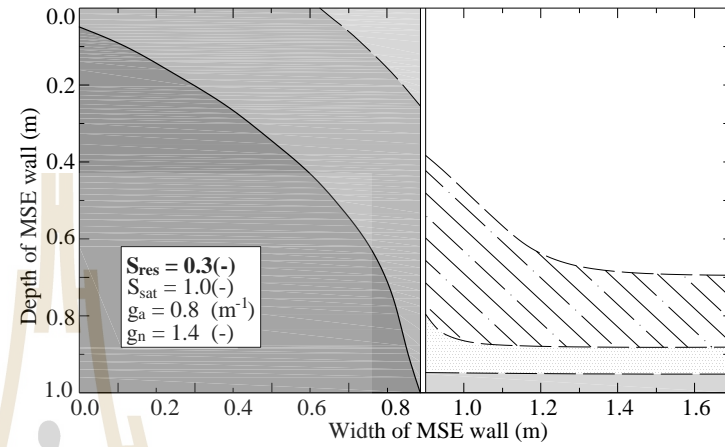
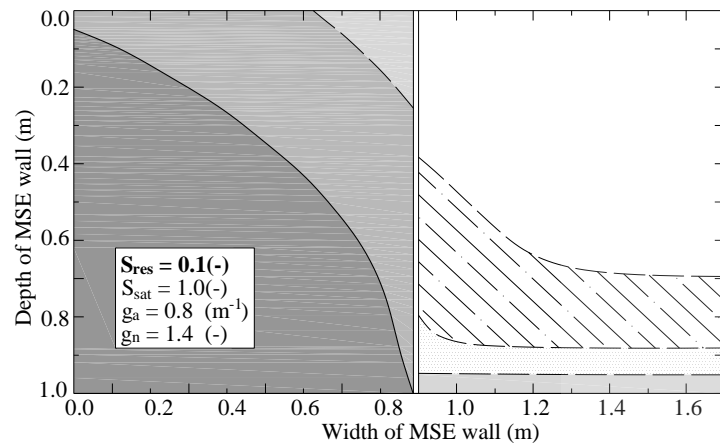


g_n

4.4.1.3 Effect of S_{res} and S_{sat} of native in-placed marginal soils outside the protected zone

The effects of the S_{res} and S_{sat} parameters were investigated through simulation cases 10-12 and 13-15, respectively. The simulation results revealed that the S_{sat} and S_{res} parameters for the marginal soils outside the protected zone did not affect the distribution of the effective saturation or the locations of the inner and outer phreatic surfaces as shown in **Figure 4.7**





S_{res}

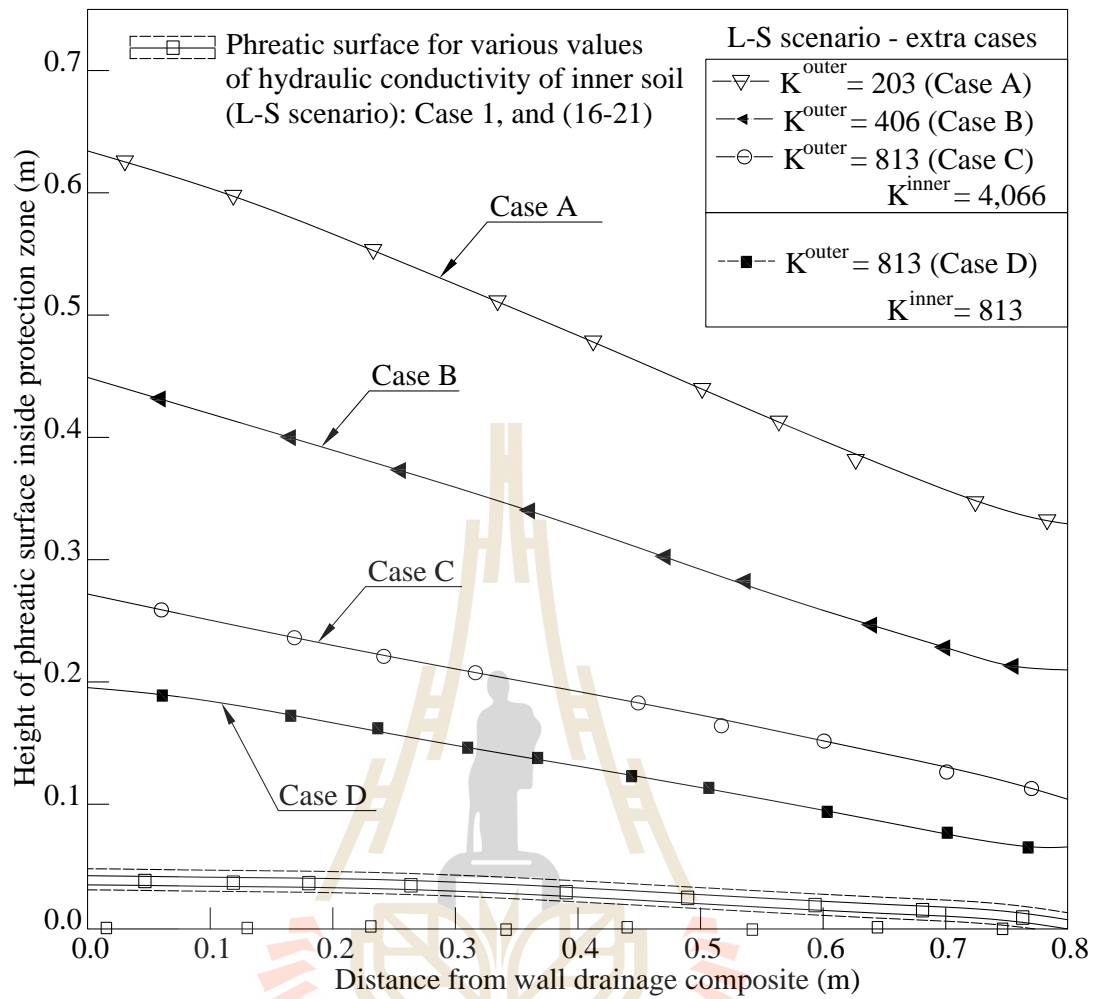
S_{sat}

4.4.1.4 Effect of the hydraulic conductivity ratio

This section examines the influence of the hydraulic conductivity of the geonet relative to that of the soil outside the protected zone and that of the soil inside the protected zone on the inner phreatic surface. The comparisons of the hydraulic conductivity of the geonet to that of the soil are expressed in terms of the hydraulic conductivity ratio. The ratio of the hydraulic conductivity of the geonet to that of the soil outside the protected zone is K^{outer} , and the ratio of the hydraulic conductivity of the geonet to that of the soil inside the protected zone is K^{inner} .

4.1.1.4.1 Effect of K^{outer}

Figure 4.8 presents the variation in the inner phreatic surface for cases 1, 16, and 17. In these cases, the magnitude of K^{outer} varied starting from greater than 20,000, while the magnitude of K^{inner} was kept constant at a value of 4,066. The magnitudes of both K^{outer} and K^{inner} were greater than 1,765, which is the critical value at which further reductions in the hydraulic conductivity ratio substantially increase the inner phreatic surface (Chinkulkijniwat et al., 2016). Therefore, the level of the inner phreatic surface was clearly low for all these cases.



K^{outer}

K^{inner}

K^{outer}

K^{outer}

higher level of the inner phreatic surface. This comparison confirms the key role of K^{outer} in the level of the inner phreatic surface.

4.4.1.4.2 Effect of K^{inner}

Figure 4.8 presents the variation in the inner phreatic surface for cases 1 and 18-21. In these cases, K^{inner} varied from 203 to 4,066, while K^{outer} was kept constant at 200,000. If K^{inner} affected the level of the inner phreatic surface, then the level of this surface would be high since some cases have a K^{inner} value that is less than the critical value. The calculation results show that the level of the inner phreatic surface was low for all these cases. Therefore, when the magnitude of K^{outer} is greater than the critical value, the magnitude of K^{inner} has a negligible effect on the inner phreatic surface.

The effect of K^{inner} when K^{outer} is less than the critical value can be determined by comparing the levels of the inner phreatic surface for cases *C* and *D*, as shown in **Figure 4.8**. Cases *C* and *D* both have K^{outer} values of 813 but have different magnitudes of K^{inner} . The magnitude of K^{inner} was 4,066 for case *C* and 813 for case *D*. Both cases showed a high level of the inner phreatic surface since K^{outer} is lower than the critical value of 1,765. The level of the inner phreatic surface for case *C* is higher than that for case *D*. This result differs from that for cases 1 and 18-21, in which K^{inner} has a negligible effect on the level of the inner phreatic surface. When the geonet capacity is not sufficient to drain all of the water flowing to the geocomposite (K^{outer} is lower than the critical value), K^{inner} affects the inner phreatic surface, and a lower K^{inner} resulted in a lower level of the inner phreatic surface, which is related to the high permeability of soil placed in the protected zone.

4.4.2 Seepage responses in the L-L scenario

The L-L scenario was designed to simulate a practical case in which in-placed marginal soils are used as the backfill materials for an MSE wall with adjacent native marginal soils. The seepage responses, represented by the degree of effective saturation and the level of the phreatic surface, were investigated through parametric study analyses (from case 1* to 15*) with varying unsaturated flow parameters of the compacted marginal soils inside the protected zone, as shown in **Table 4.6**. The computed results show that the moisture content in the protected zone was always higher for the L-L scenario than for the L-S scenario. The variation in the unsaturated flow properties of the soil inside the protected zone negligibly affects the seepage responses outside the protected zone. The details of the calculation results are as follows:

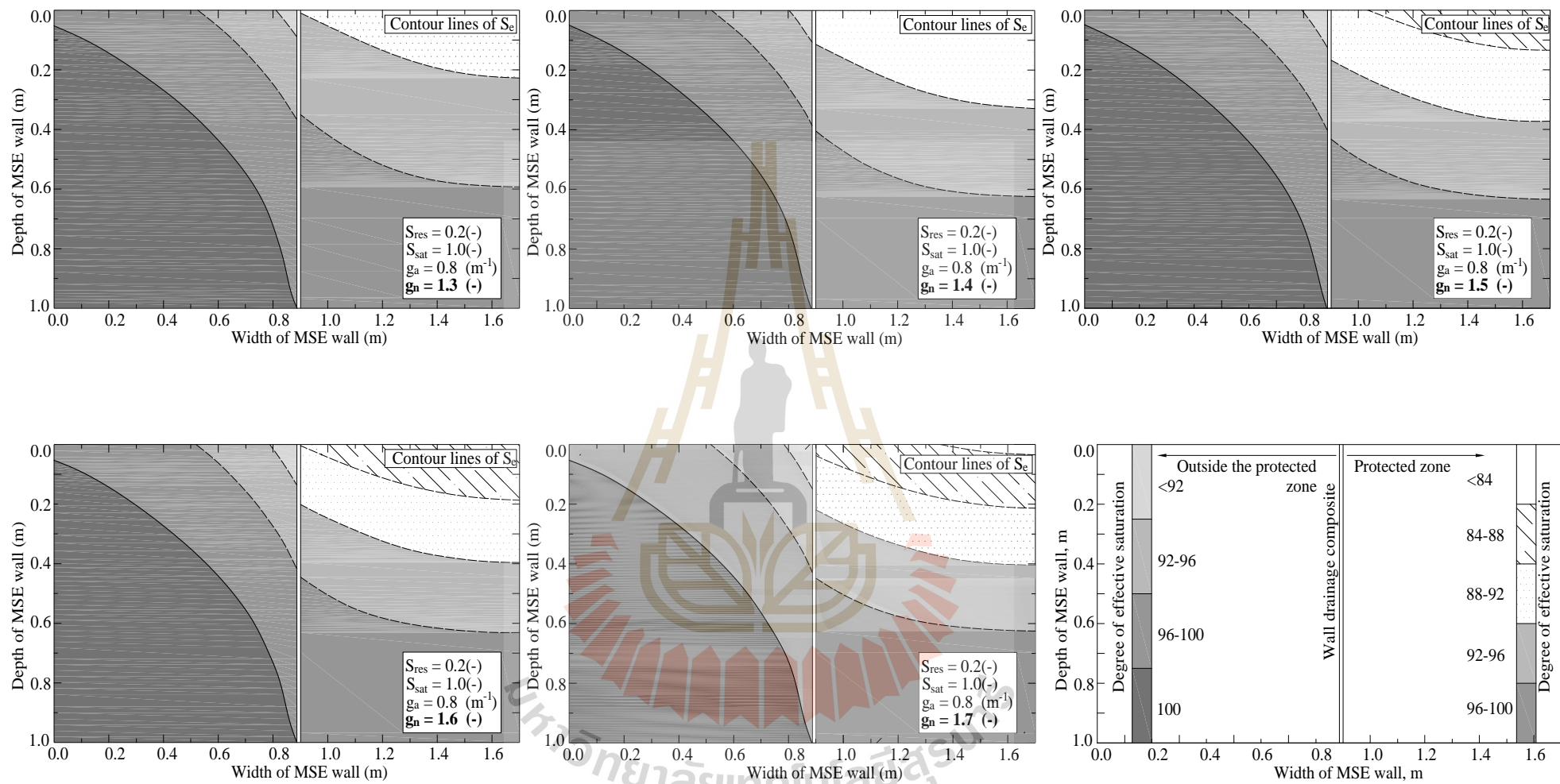
4.2.2.1 Effect of the g_a of the compacted marginal soil inside the protected zone

Figure 4.4 b shows the variation in S_e along the vertical lines located 0.05 m to the left (outside the protected zone) and 0.05 m to the right (inside the protected zone) of the geocomposite-soil interface as the g_a of the marginal soil varied from 0.5 to 5.0 [m^{-1}] (cases 1*-5*). The effective saturation outside the protected zone did not obviously vary with g_a , whereas the effective saturation inside the protected zone did. The S_e inside the protected zone remained greater than 80% for cases 1*-3* ($g_a = 0.5, 0.8, \text{ and } 1.0$), whereas S_e was less than 50% for cases 1-5 in the L-S scenario.

Figure 4.5 presents the variation in the outer phreatic surface as the g_a of the compacted marginal soil varies from 0.5 to 5.0 [m^{-1}] (dashed lines). The variation in the g_a of the soil inside the protected zone has a negligible effect on the outer phreatic surface.

4.2.2.2 Effect of the g_n of the compacted marginal soil inside the protected zone

Figure 4.9 presents the phreatic surface and the effective saturation contour lines as the g_n of the compacted marginal soil varies from 1.3 to 1.7 (cases 1* and 6* to 9*). A lower g_n value resulted in a wider distribution of the effective saturation both inside and outside of the protected zone. Again, the variation in the g_n of the soil inside the protected zone has a negligible effect on the seepages of the soil outside the protected zone.



g_n

4.2.2.3 Effect of S_{res} and S_{sat} of the compacted marginal soil inside the protected zone

The effects of the parameters S_{res} and S_{sat} were investigated through simulation cases 1* and 10*-12* and cases 1* and 13*-15*, respectively. Similar to that obtained in the L-S scenario, the S_{sat} and S_{res} parameters of the soil do not affect the effective saturation distribution or the locations of the inner and outer phreatic surfaces.

4.5 Discussions

4.5.1 Distribution of the water content

The g_a value reflects the inflection point of the WRC curve (as shown in **Figure 4.10**). Therefore, the g_a value affects the distribution of the water content in the high saturation zone. A soil with a lower g_a represents a wider range of suction in the capillary saturation (CS) zone and therefore a wider area of the high saturation zone within the same suction range. The g_n value reflects the steepness of the WRC in the desaturation (DS) zone (as shown in **Figure 4. 10**). Therefore, g_n affects the distribution of the water content in the intermediate saturation range. A soil with a smaller g_n exhibits a wider range of suction variability and therefore a wider area of the intermediate saturation zone. In marginal soil, which possesses a low g_a value, the high saturation zone covers almost the entire body of the marginal soil. Therefore,

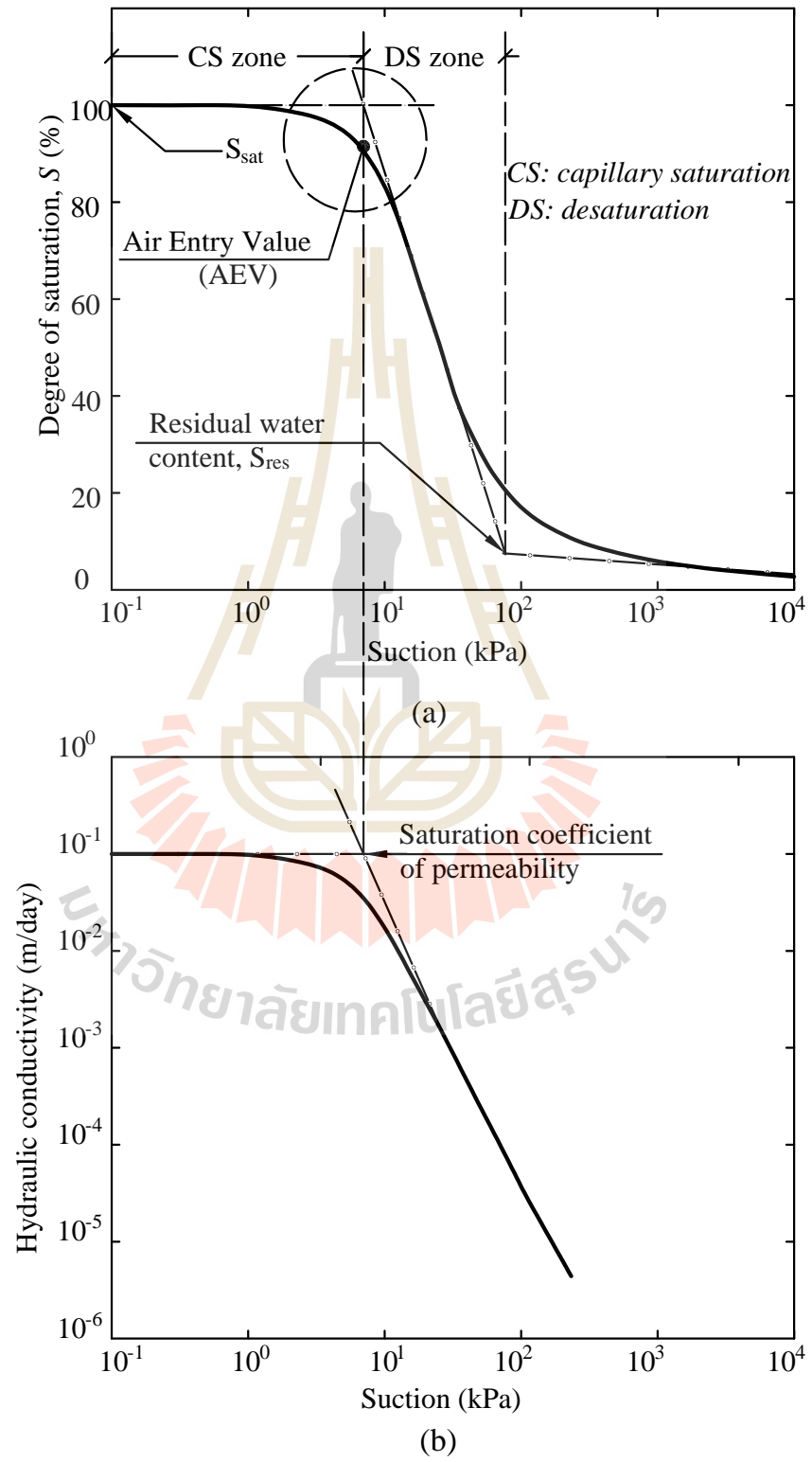


Figure 4.10 (a) Typical water retention characteristic curve, (b) typical k-function curve

4.5.2 Location of the outer phreatic surface

The g_a and g_n values of the soil outside the protected zone affect the level of the outer phreatic surface. Wise et al., (1994) investigated the effect of g_a and g_n on the height of the phreatic surface in a soil subjected to varying upstream and downstream water levels. Wise et al., (1994) reported that lower g_a and g_n values reflect a relative abundance of smaller pores. Consequently, the height of the phreatic surface was lower since more water was retained in the vadose zone.

This study reported different effect of g_a and g_n on the height of the outer phreatic surface than those reported by Wise et al., (1994). A lower g_a decreased the height of the phreatic surface, while a lower g_n increased the level of the phreatic surface. The capillary barrier at the interface between the soil and the geotextile prevents water from flowing from the soil into the drainage system (geotextile and then geonet). This barrier disappears when the suction at the interface decreases to a critical suction level. At this point, the hydraulic conductivity of the two materials equals to each other. Hence, the water was able to pass through the interface. As the soil started at a dry condition and became wet during the seepage process, the smaller magnitude of the suction at the critical suction point made it more difficult for the water to break through the interface, thus decreasing the phreatic surface level.

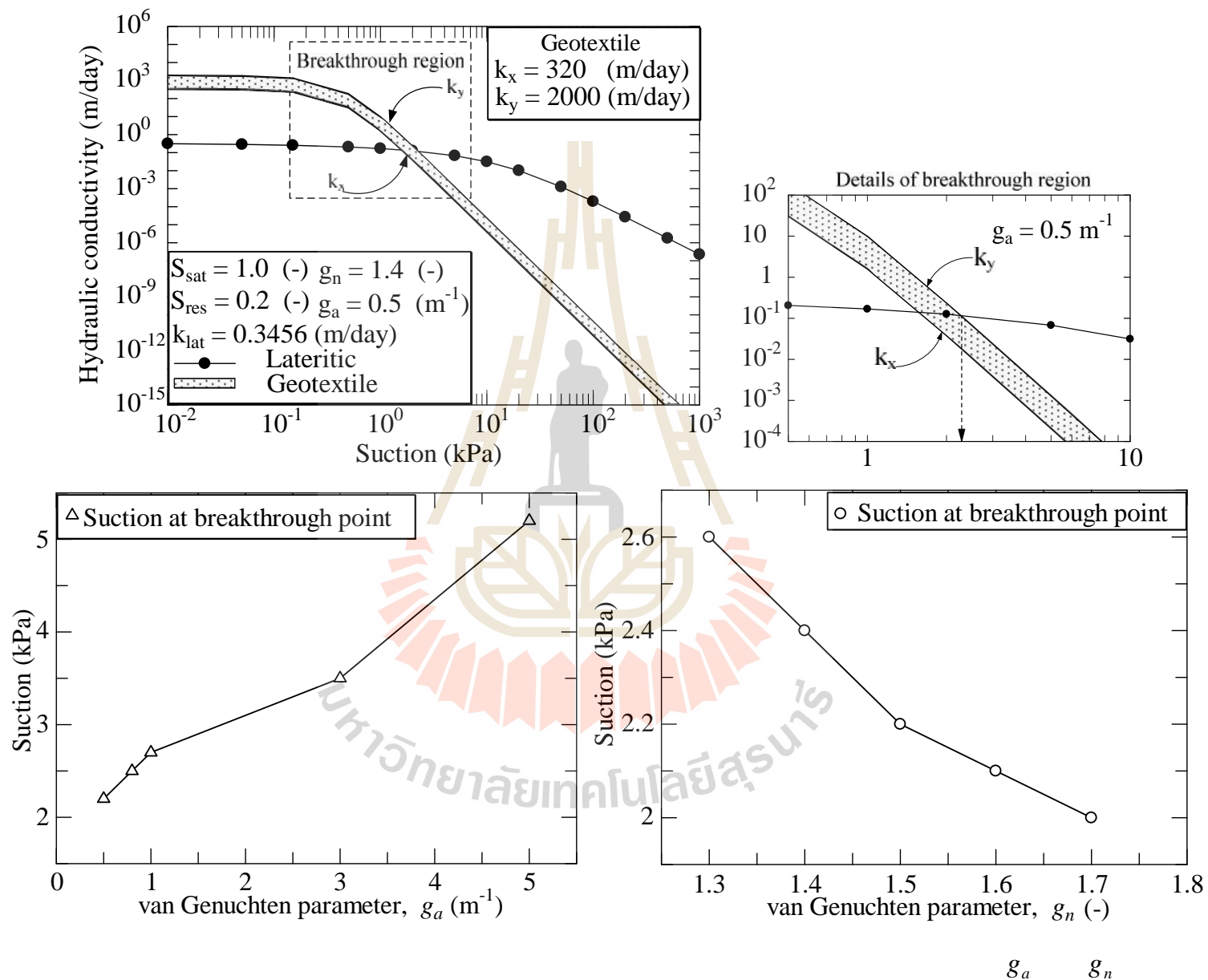


Figure 4.11 plots the k-function curves of the geotextile and the soil for varying magnitudes of g_a and g_n of the soil. Although not considerably different, the magnitude of suction at the breakthrough point increases with g_a but decreases with increasing of g_n . This effect indicates why a lower g_a results in a lower phreatic surface while a lower g_n results in a higher phreatic surface. Chinkulkijniwat et al., (2016) reported that the location of the outer phreatic surface did not clearly change within the variation range of the parameters, which could be due to low variation in the critical suction at the breakthrough point (similar to this study). Furthermore, the soil studied by Chinkulkijniwat et al., (2016) was sandy soil, and the high saturation zone did not spread widely. In contrast, the soil studied in this research was marginal soil with a low g_a value, which resulted in a large high saturation zone spreading over the entire body of the soil. Within the high saturation zone, a small change in the suction value at the breakthrough point has an important effect on the location of the phreatic surface.

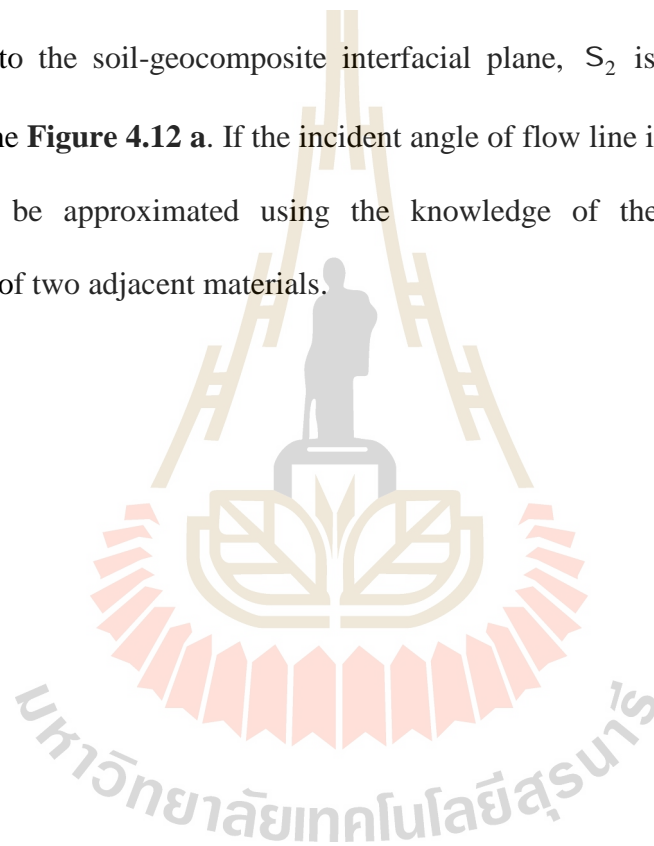
4.5.3 Level of the inner phreatic surface

If the drainage capacity of the geonet is sufficiently high that all of the water flowing from the upstream side is properly collected and drained, no increase in the inner phreatic surface is observed. The drainage capacity of the geonet can be characterized by its thickness and the ratio of the saturated hydraulic conductivity of the geonet to that of the soil outside the protected zone, K^{outer} . As discussed by Chinkulkijniwat et al., (2016), the saturated hydraulic conductivity ratio between two adjacent media asserts a flow reflection path, as described in Eq. 4.1 (see also **Figure**

4.12 a). Furthermore, a greater gradient of the flow path in the drainage medium results in a lower phreatic surface level flowing out of the drainage medium and thus a lower inner phreatic surface.

$$\frac{\tan S_1}{\tan S_2} = \frac{k_1}{k_2} \quad (4.1)$$

where S_1 is an incident angle which is an angle between an incident flow line and a line normal to the soil-geocomposite interfacial plane, S_2 is a reflected angle as depicted in the **Figure 4.12 a**. If the incident angle of flow line is known, the reflected angle could be approximated using the knowledge of the saturated hydraulic conductivity of two adjacent materials.



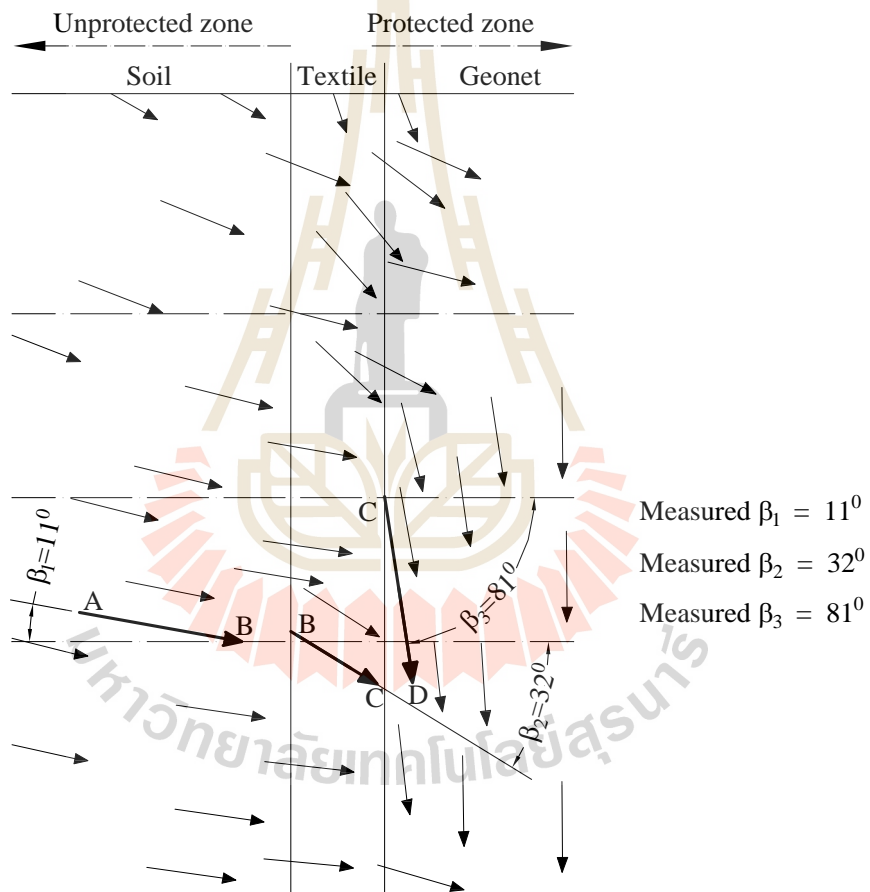
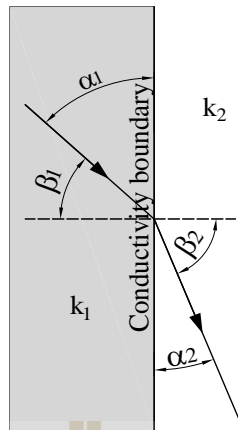


Figure 4.12 b presents flow vectors at the soil-geocomposite interfaces extracted from the calculation case A in L-S scenario. With the incident angle S_1 of 11° , the approximated reflected angle in geotextile S_2 is 25° corresponded to $k_1 = 340 \text{ m/day}$ and $k_2 = \sqrt{320 \times 2000} = 800 \text{ m/day}$. Reminding that the geotextile possesses hydraulic conductivity anisotropy, with lateral and longitudinal saturated hydraulic conductivity of 320, and 2000 m/day, respectively. Similarly, the approximated angle of flow line in geonet S_3 is 87° corresponded to saturated hydraulic conductivity of the geonet of 69120 m/day. These angle values agree rather well with the angles S_2 and S_3 directly measured from the corresponding flow vectors.

If the drainage capacity of the geonet is not sufficient, the inner phreatic surface will be observable. In this case, the greater rate of water flowing to the drainage medium results in a higher inner phreatic surface level. The rate of water flowing to the drainage medium is characterized by the saturated hydraulic conductivity of the soil at the upstream side and the height of the upstream water table.

Although the rate of water flowing to the geocomposite is the main factor that affects the level of the inner phreatic surface, the calculation results show that the saturated hydraulic conductivity of the backfill material also affects the inner phreatic surface (Ref. cases C and D), particularly when the drainage capacity of the geonet is not sufficiently high to collect all the upstream water that flows to the protected zone. As shown in **Eq. 4.1**, water flow across a boundary between two materials with different hydraulic conductivities causes a refraction of the flow direction. Taking the

geocomposite as material #1 and the backfill material as material #2, **Eq. 4.1** shows that a greater k_2 yields a greater S_2 and therefore a lower level of the inner phreatic surface. Comparing cases C and D, which have the same K^{outer} but different values of K^{inner} , the level of the inner phreatic surface of case C is higher than that of case D.

4.6. Conclusions

Examining the case of a high level of upstream groundwater flowing towards an MSE wall with a geocomposite, the following conclusions can be drawn from this study:

1. The WRCs of a soil outside the protected zone has a negligible effect on the seepage responses of the soil inside the protected zone, and vice versa.
2. A greater fine particle content (lower g_a and g_n values) in the soil outside the protected zone results in a wider distribution of the high-water-content area. Careful geocomposite installation is required for this soil type, since increasing water content results in the loss of suction forces and therefore decreased interface strength.
3. Although a suitable geocomposite was installed to prevent water from permeating into the protected zone, using soil with the considered fine particle content as the backfill material could result in a large high-water-content area. Care must be taken when using this type of soil as the backfill material, since the protected zone might experience a high water content, which will directly affect the pullout resistance of the reinforcement. For example, Mitchell (1995) suggested using a permeable

reinforced geosynthetic in MSE walls with a cohesive backfill material to provide both reinforcement and lateral drainage along the soil-reinforcement interface.

4. The ratio of the hydraulic conductivity of the geonet to that of the soil outside the protected zone (K^{outer}) has a significant effect on the level of the inner phreatic surface. If the geocomposite possesses insufficient drainage capacity (low K^{outer}), using a backfill material with a lower hydraulic conductivity could increase the severity of the rising of the inner phreatic surface.
5. The capillary barrier affects the level of the outer phreatic surface, particularly if the soil outside the protected zone has high fine particle content.
6. A wider pore size distribution (lower g_n value) soil outside the protected zone results in a wider high-water-content distribution and a flatter phreatic surface level in the soil outside the protected zone.

4.7 References

- AASHTO., 2002. **Standard Specifications for Highway and Bridge**. American Association of State of Highway and Transportation Officials, Washington DC.
- Alao, D. A., 1983. **Geology and engineering properties of laterites from Ilorin, Nigeria**. Engineering Geology 19(2): 111-118.
- ASTM., 2008. **Standard Test Methods for Determination of the Soil Water Characteristic Curve for Desorption Using a Hanging Column**,

- Pressure Extractor, Chilled Mirror Hygrometer, and/or Centrifuge. D6836, ASTM International.
- Badmus, B., 2010. **Plasticity and compressibility characteristics of lateritic soil from Southwestern Nigeria.** Journal of Natural Sciences Engineering and Technology 9(1): 14-22.
- Biswal, D. R., Sahoo, U. C., Dash, S. R., 2016. **Characterization of granular lateritic soils as pavement material.** Transportation Geotechnics, 6, 108-122.
- Bonsor, H. C., MacDonald, A. M., & Davies, J., 2014. **Evidence for extreme variations in the permeability of laterite from a detailed analysis of well behaviour in Nigeria.** Hydrological processes, 28(10), 3563-3573.
- Chinkulkijniwat, A., Horpibulsuk, S., Bui Van, D., Udomchai, A., Goodary, R., Arulrajah, A., 2016. **Influential factors affecting drainage design considerations for mechanical stabilised earth walls using geocomposites.** Geosynthetics International, 24 (3): 224-241.
- Eluozo, S. N., and Nwaobakata, C., 2013. **Predictive models to determine the behavior of plastic and liquid limit of Lateratic soil for Raod construction at Egbema: Imo state of Nigeria.** International Journal of Engineering & Technology 2(1): 25-31.
- Horpibulsuk, S., Suddeepong, A., Chamket, P., Chinkulkijniwat, A., 2013. **Compaction behavior of fine-grained soils, lateritic soils and crushed rocks.** Soils and Foundations 53(1): 166-172.
- Horpibulsuk, S., Udomchai, A., Joongklang, A., Mavong, N., Nikompakdi, P., Arulrajah, A., & Disfani, M. M. 2016. **Pullout mechanism of the bearing**

- reinforcement embedded in claystone soil of Mae Moh mine.** Japanese Geotechnical Society Special Publication, 2(65): 2204-2208.
- Hossain, M. S., Kibria, G., Khan, M. S., Hossain, J., & Taufiq., T. 2011. **Effects of backfill soil on excessive movement of MSE wall.** Journal of Performance of Constructed Facilities, 26(6): 793-802.
- Koerner, R. M., and Soong, T.-Y., 2001. **Geosynthetic Reinforced Segmental Retaining Walls.** Geotextiles and Geomembranes 19(6): 359-386.
- Kool, J. B., and Parker, J. C., 1987. **Development and evaluation of closed-form expressions for hysteretic soil hydraulic properties.** Water resources research 23(1): 105-114.
- Lu, N., Kaya, M., Collins, B. D., Godt, J. W., 2012. **Hysteresis of unsaturated hydromechanical properties of a silty soil.** Journal of Geotechnical and Geoenvironmental Engineering 139(3): 507-510.
- Miguel, M. G. and Vilar, O. M., 2009. **Study of the water retention properties of a tropical soil.** Canadian Geotechnical Journal 46(9): 1084-1092.
- Mitchell, J., 1995. **Reinforced Soil Structures with Poorly Draining Backfills Part II: Case Histories and Applications.** Geosynthetics International 2(1): 265-307.
- Oh, S., and Lu, N., 2014. **Uniqueness of the suction stress characteristic curve under different confining stress conditions.** Vadose Zone Journal 13(5). doi:10.2136/vzj2013.04.0077
- Omotoso, O. A., Ojo, O. J., Adetolaju, E. T., 2012. **Engineering properties of lateritic soils around Dall Quarry in Sango area, Ilorin, Nigeria.** Earth Science Research 1(2): 71-81. DOI: <http://dx.doi.org/10.5539/esr.v1n2p71>

- Oyelami, C., and Van Rooy, J. L., 2016. **A review of the use of lateritic soils in the construction/development of sustainable housing in Africa: A geological perspective.** Journal of African Earth Sciences, 119, 226-237.
- Prescott, J. A., and Pendleton, R. L., 1952. **Laterite and, Lateritic Soils**, LWW.
- Quadri, H. A., Adeyemi, O. A., Olafusi, O. S., 2012. **Investigation of the Geotechnical Engineering Properties of Laterite as a Subgrade and Base Material for Road Constructions in Nigeria.** Civil and Environmental Research 2(8): 23-31.
- Sandri, D., Silver, G., & Trazo, R. 2000. **Design, Construction, and Monitoring of a 14.9 m High Geosynthetic Reinforced Segmental Retaining Wall in a Seismically Active Region.** In Advances in Transportation and Geoenvironmental Systems Using Geosynthetics: 244-256.
- Sandri, D., 2005. **Drainage recommendations for MSE walls constructed with marginal fills.** Proceedings of North American Geo-synthetics Conference (NAGS2005), Las Vegas, Nevada, USA, GRI-19 (CD-volume).
- Townsend, F. C., 1985. **Geotechnical characteristics of residual soils.** Journal of Geotechnical Engineering 111(1): 77-94.
- Wise, W. R., Clement, T. P., Molz, F. J., 1994. **Variably saturated modeling of transient drainage: sensitivity to soil properties.** Journal of Hydrology 161(1): 91-108.
- Yang, H., Rahardjo, H., Leong, E. C., Fredlund, D.G., 2004. **Factors affecting drying and wetting soil-water characteristic curves of sandy soils.** Canadian Geotechnical Journal 41(5): 908-920.

Zornberg, J., and Mitchell, J., 1994. **Reinforced soil structures with poorly draining backfills. Part I: Reinforcement interactions and functions.**

Geosynthetics International 1(2): 103-147.

Zornberg, J. G., and Bueno, B. S., 2006. **Use of Poor-Draining Soils in Reinforced Soil Structures in Brazil.** Transportation Research Board 85th Annual Meeting. No. 06-1719



CHAPTER V

CONCLUSIONS AND RECOMMENDATIONS

5.1 Summary and conclusions

To fulfill the aim of examining the seepage responses of MSE walls, two key parts were executed throughout this dissertation. The first part was to examine the performance of MSE wall since an alternative drainage geocomposite employed. Initially, the physical models of MSE walls were performed under two working conditions. They were with geocomposite exploited and without installation of geocomposite. To cope with the time-consuming since carrying out physical experiments, the computer program, Plaxis 2D, was then employed to conduct a series of parametric studies after good agreement results between numerical and physical model obtained. The computation results obtained from the numerical analysis were exploited to investigate the foremost unsaturated hydraulic factors that govern the seepage responses of MSE walls induced by rising of the upstream water table. All the numerical computation results were predominantly illustrated in terms of effective saturation and the phreatic surface that were supposed to represent the moisture response in MSE walls.

The second main part was established to evaluate two feasible scenarios of the use of MSE walls, in which high fine-grained in-placed marginal soils were utilized as fill materials. The well-validated numerical model obtained from the first part was

utilized to perform a series of parametric studies. Consequently, the computed results of each scenario were analyzed to assess the influence of unsaturated hydraulic characteristic of fine-grained soil on seepage responses of MSE walls.

5.1.1 Foremost factors affect the hydrological responses in MSE walls fully filled with good draining material

In the scenario that the models were fully filled with good draining backfill materials, the experimental results indicated that the moisture content illustrated in terms of effective saturation and phreatic surface in the protected zone was drastically diminished due to the appearance of geocomposite layer. Similarly, the horizontal movement and settlement of surface of the model with geocomposite installed were found to be lower than that without installation of geocomposite. Consequently, a good performance of MSE walls could be gained as the development of pore water pressure lessened. Numerical parametric studies using finite element method illustrated that the seepage responses of MSE wall were predominantly dominated by the WRC of the fill as well as of the geotextiles. The permeability ratio, termed, $K_{r,net}$, between geotnet and backfill also play a vital role in the level of the phreatic surface inside the protected zone. The lower value of $K_{r,net}$ brings about the higher phreatic surface inside the protected zone, hence the instability of MSE wall might be transpired. One more finding from this part was the influence of capillary break phenomenon which is normally appeared at the hydraulic conductivity boundary. At the interface between two materials have different hydraulic conductivities, the distribution of effective saturation could be affected due to this phenomenon, the lower magnitude of breakthrough suction at the interface where

water tends to permeate through the interface, the greater amount of water accumulation along the interface found.

5.1.2 Seepage responses in MSE walls utilize fine-grained marginal soils as fills

This part was established to assess two feasible scenarios of MSE walls, in which the local materials that possess good engineering properties but just fails to meet the requirement due to presenting a large amount of fine particle or low permeability. Results obtained from the first scenario, namely L-S scenario, generally illustrate that the soil placed outside the protected zone does not significantly affect the moisture content inside the protected zone. Instead, it markedly affects the moisture profile in the unprotected zone. The greater amount of fine particles (lower g_a and g_n values) of the soil outside the protected zone causes the wider distribution of high moisture content in the unprotected zone, hence yielding a larger pore water pressure that acts to the protected zone. In the case that the drainage capacity of geocomposite is not sufficient enough to drain the incident water out, the use of high fine-grained soil might cause a higher level of the phreatic surface in the protected zone. Another finding was found from this scenario was the influence of permeability ratio of geonet to that of the soil placed outside the protected zone, termed K^{outer} , on the rising of the phreatic surface in the protected zone. The lower permeability ratio, the higher phreatic in the protected zone might be taken place. It was also found that the permeability ratio between geonet and the soil placed inside the protected zone, termed as K^{inner} , affected the level of phreatic surface inside the protected zone, if the magnitude K^{inner} of less than the critical value of 1765. The lower K^{inner} results in a

lower phreatic surface in the protected zone, which might be related to high permeability of the soil placed in the protected zone.

The computed results obtained from the second scenario, namely L-L, also described that the use of high fine-grained marginal soils may cause a wider distribution of high water content both inside and outside the protected zone, that was not found in the first of L-S scenario due to the protected zone was fully filled with good draining material.

5.2 Limitations and recommendations for future works

- A mini scale of MSE wall was built and undertaken a series of parametric studies to examine the seepage responses, it was thus the finding of critical permeability ratio of around of 1765 was apparently to be valid for corresponding to the model depicted in this dissertation. Due to the head loss, the magnitude of critical permeability ratio might be varied with the geometry of the model. More investigation should be performed to figure out the typical magnitude of critical permeability ratio with respect to the specific model geometry. Throughout this research, typical hydraulic conductivity coefficients of considered materials assigned to models were mainly obtained from corresponding laboratory tests for soils, and from specification for geocomposite materials, however, care must be also paid to the numerical errors that can be occurred due to high anisotropic permeability ratio that assigned to the numerical model by examining the moisture profile such as saturation contour lines, phreatic surface, and pore water pressure.

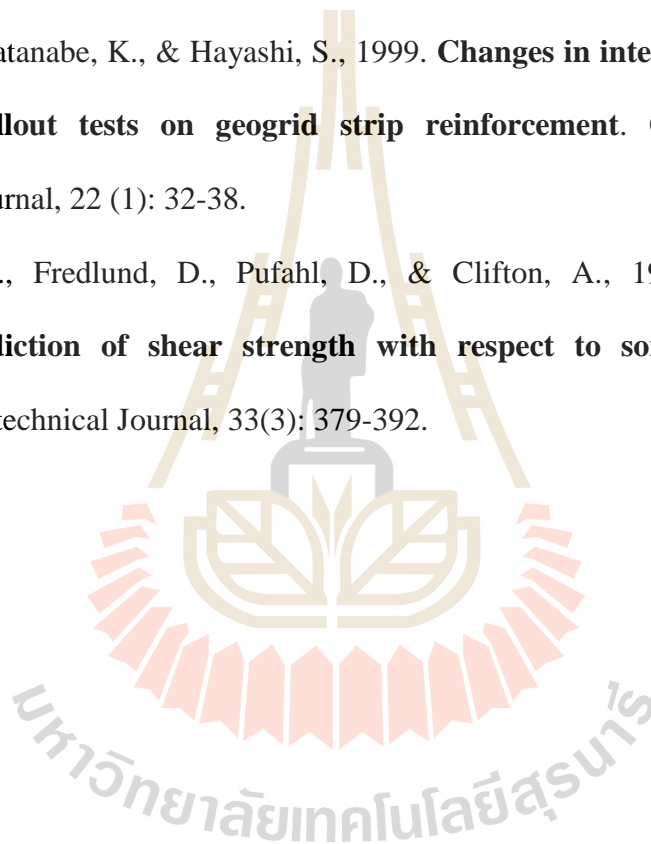
- Currently, several methods have been developed for predicting the pullout resistance of soil reinforcement, especially for inextensible steel reinforcement. However, all the proposed methods have been based on the saturated shear strength parameters (AASHTO, 2002; Alfaro and Pathak, 2005; Bergado et al., 1992; Horpibulsuk and Niramitkornburee, 2010; Jewell et al., 1984; Shahu et al., 1999), while in reality MSE walls are usually built above the ground water table where the backfill material is typically in a state of unsaturated condition. Previous studies show that the shear strength of soils under unsaturated condition varied with capillary stresses or the matric suction (Cunningham et al., 2003; Khalili and Khabbaz, 1998; Vanapalli et al., 1996). Hence, affecting the bearing capacity of unsaturated soils. As the pullout bearing resistance of the bearing reinforcements is estimated based on that assumption, the effect of matric suction is not yet taken into account. It is then using the conventional methods may not be reliable and lead to an uneconomical design. It would be interesting if a new method that incorporated unsaturated properties could be developed.
- The performance of geocomposite is believed to be affected by several factors such as clogging of geocomposite layer, long-term deformation of geotextiles under constant tensile stress known as creep of geosynthetic, effect of jointing of geocomposite section and of compressive stress on the hydraulic properties of geocomposite. These relevant factors were not taken into account throughout this dissertation.

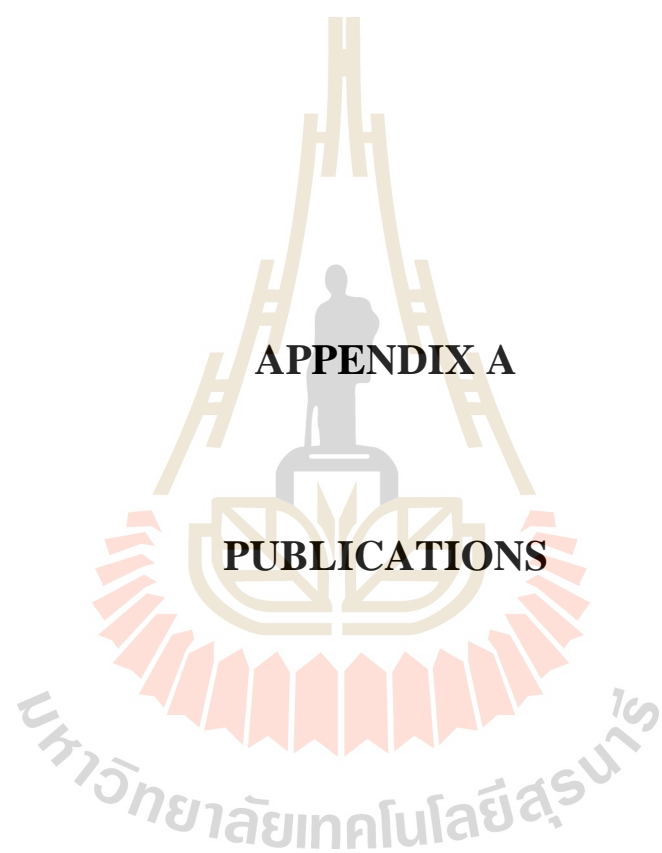
- The geocomposite drain was assumed as continuous back geocomposite drain placed behind the reinforced zone, this condition is not always necessitous, even costly. It is thus the use of the discontinuous form of geocomposite drain is likely to be more appropriate. More investigation on the determination of effective spacing of geocomposite drain may be necessary.

5.3 References

- AASHTO., 2002. **Standard Specifications for Highway and Bridge**. American Association of State of Highway and Transportation Officials, Washington DC
- Alfaro, M., & Pathak, Y., 2005. **Dilatant stresses at the interface of granular fills and geogrid strip reinforcements**. Geosynthetics International, 12(5): 239-252.
- Bergado, D., Chai, J., & Balasubramaniam, A., 1992. **Interaction between grid reinforcement and cohesive-frictional soil**. Proceedings of Earth Reinforcement Practice, 34.
- Cunningham, M., Ridley, A., Dineen, K., & Burland, J., 2003. **The mechanical behaviour of a reconstituted unsaturated silty clay**. Geotechnique, 53(2): 183-194.
- Horpibulsuk, S., & Niramitkornburee, A., 2010. **Pullout resistance of bearing reinforcement embedded in sand**. Soils and Foundations, 50(2): 215-226.

- Jewell, R. A., 1984. **Interaction between soil and geogrids**. Proceeding of the Symposium on Polymer Grid Reinforcement in Civil Engineering, Thomas Telford Limited, London, UK, 22-23 March 1984, 11-17.
- Khalili, N., & Khabbaz, M., 1998. **A unique relationship of χ for the determination of the shear strength of unsaturated soils**. Geotechnique, 48(5).
- Shahu, J., Watanabe, K., & Hayashi, S., 1999. **Changes in interface stresses during pullout tests on geogrid strip reinforcement**. Geotechnical Testing Journal, 22 (1): 32-38.
- Vanapalli, S., Fredlund, D., Pufahl, D., & Clifton, A., 1996. **Model for the prediction of shear strength with respect to soil suction**. Canadian Geotechnical Journal, 33(3): 379-392.





List of Publications

INTERNATIONAL JOURNAL PAPERS

Chinkulkijniwat A., Horpibulsuk S., Bui Van D., Udomchai A., Goodary A and Arulrajah A (2016). **Influential factors affecting drainage design considerations for mechanical stabilised earth walls using geocomposites.** Geosynthetics International, 24 (3): 224-241.

INTERNATIONAL CONFERENCES

Bui Van D., Chinkulkijniwat A., Horpibulsuk S., et al (2016). **Influence of nonwoven geotextile on the hydraulic response of mechanical stabilized earth wall.** The sixth International Conference on Geotechnique, Construction Materials & Environment, GEOMATE, Bangkok, Thailand, 14-16 November 2016. Best paper award

Bui Van D., Yubonchit S., Udomchai A., Chinkulkijniwat A., et al (2017). **Water retention characteristics of in placed soil on moisture condition inside and outside the reinforced soil structures.** The 11th South East Asean Technical University Consortium Symposium, Ho Chi Minh city, Vietnam, 13-15 March 2017



Geosynthetics International

ISSN 1072-6349 | E-ISSN 1751-7613

Volume 24 Issue 3, June, 2017, pp. 224-241

[Next >](#)

Influential factors affecting drainage design considerations for mechanical stabilised earth walls using geocomposites

Authors: A. Chinkulkijniwat¹ S. Horpibulsuk² D. Bui Van³ A. Udomchai⁴ R. Goodary⁵ A. Arulrajah⁶
Associate Professor Professor and Director PhD Scholar Post-graduate researcher Lecturer and
Dean of the Faculty of Sustainable Development and Engineering Professor



[Author Affiliations](#)

<https://doi.org/10.1680/jgein.16.00027>

Published Online: May 31, 2017

Keywords: Geosynthetics Geocomposite drain Mechanical stabilised earth wall Seepage flow through unsaturated media

DOI: 10.1680/jgein.16.00027

Influential factors affecting drainage design considerations for mechanical stabilised earth walls using geocomposites

A. Chinkulkijniwat¹, S. Horpibulsuk², D. Bui Van³, A. Udomchai⁴, R. Goodary⁵ and A. Arulrajah⁶

¹Associate Professor, Center of Excellence in Civil Engineering, School of Civil Engineering, Suranaree University of Technology, 111 University Avenue, Muang District, Nakhon Ratchasima 30000 Thailand, E-mail: avirun@sut.ac.th (corresponding author)

²Professor and Director, Center of Excellence in Innovation for Sustainable Infrastructure Development, Chair of School of Civil Engineering, Suranaree University of Technology, 111 University Avenue, Muang District, Nakhon Ratchasima 30000, Thailand, E-mail: suksorn@sut.ac.th

³PhD Scholar, School of Civil Engineering, Suranaree University of Technology, 111 University Avenue, Muang District, Nakhon Ratchasima 30000, Thailand, E-mail: buivanduc@hung.edu.vn

⁴Post-graduate researcher, Center of Excellence in Innovation for Sustainable Infrastructure Development, School of Civil Engineering, Suranaree University of Technology, 111 University Avenue, Muang District, Nakhon Ratchasima 30000, Thailand, E-mail: artitai@sut.ac.th

⁵Lecturer and Dean of the Faculty of Sustainable Development and Engineering, Faculty of Sustainable Development and Engineering, Université des Mascareignes, Mauritius, E-mail: rgoodary@udm.ac.mu

⁶Professor, Swinburne University of Technology, Melbourne, Australia, E-mail: arulrajah@swin.edu.au

Received 05 January 2016, revised 11 May 2016, accepted 07 September 2016

ABSTRACT: Mechanically stabilised earth (MSE) walls are made of unsaturated soil that is strengthened with artificial materials. They have been widely used over the past three decades; however, occasional failures due to inadequate drainage during heavy rainfall have been encountered. Essentially, the reinforced zone of the MSE wall must be protected from water inflow for the system to work satisfactorily. Recent studies have reported on the alternative use of geocomposites to replace the conventional drainage system in MSE walls, typically comprising well-graded gravel. Geocomposites comprise a core material with a large flow channel, which is covered by a nonwoven geotextile. Although it is widely recognised that geotextiles possess a water retention characteristic (WRC), only a few studies have examined the effect of WRC on the seepage responses of MSE walls. In this research, large-scale physical model tests for seepage flow through an MSE wall were undertaken with and without an L-shaped geocomposite drain. Comparisons indicate that the MSE wall with a geocomposite is superior to that without a geocomposite installed. A series of numerical experiments was conducted with finite element software to investigate the effects of the hydrologic properties of the soil, geotextile, and geonet on the seepage responses in the MSE wall. The seepage responses, including effective saturation and phreatic surface, were found to be primarily governed by the WRC of the soil and the ratio between the saturate hydraulic conductivity of the geonet and that of the soil. The 'capillary barrier' phenomenon was found to play a secondary role in determining the effective saturation along the interface between the soil and the geocomposite.

KEYWORDS: Geosynthetics, Geocomposite drain, Mechanical stabilised earth wall, Seepage flow through unsaturated media

REFERENCE: Chinkulkijniwat, A., Horpibulsuk, S., Bui Van, D., Udomchai, A., Goodary, R. and Arulrajah, A. (2016). Influential factors affecting drainage design considerations for mechanical stabilised earth walls using geocomposites. *Geosynthetics International*, [http://dx.doi.org/10.1680/jgein.16.00027]

1. INTRODUCTION

Failures of mechanically stabilised earth (MSE) walls in mountainous areas where seasonally heavy rainfall is encountered is often attributed to ineffective drainage

systems. Koerner and Soong (2001) documented 26 case histories of MSE wall failures in the United States, with most of these attributed to excessive deformation (serviceability) and actual collapse. Seventeen of the 26 cases were related to low permeability soil backfills, which led

to the conclusion that if fines (silts and/or clays) are allowed in the reinforced zone backfill soil, any water ponding behind and beneath the reinforced zone must be properly collected, transmitted, and discharged. Special precautions should be taken for hillside constructions in particular due to the potential for seepage to occur through the retained soil.

Shibuya *et al.* (2007) reported on results from a catastrophic failure of a reinforced earth wall in Yabu, Japan, in 2004, after a typhoon. Although the reinforced earth wall was designed and constructed based on design codes, the drainage was constructed at the bottom of the wall from drainage pipes, and it did not extend to cover the area behind the wall; hence, there was insufficient capacity in the drainage system. It was concluded that conventional drainage systems were not applicable in mountainous areas where there was a large amount and/or high level of groundwater (Shibuya *et al.* 2007).

The material conventionally used as the drainage medium for MSE walls is well-graded gravel. This is becoming increasingly expensive, and effective installation of this material as a vertical drainage layer is difficult in the field. An alternative to the use of well-graded gravel is to provide drainage through the use of geocomposites (Koerner and Soong 2000; Koerner 2005; Chen *et al.* 2007). Geocomposites provide a hydraulic conductivity approximately 10 to 100 times higher than that of compacted backfills. Geocomposites comprise a core material with a large flow channel (e.g., geonet), which is covered by a nonwoven geotextile that acts as both a filter and a separator. Geocomposites offer numerous advantages over the conventional method of drainage for MSE walls using gravel. Transport and installation of geocomposites are much easier than for conventional drains. Geocomposites are light and do not add significantly to the weight of the soil in the backfill. Furthermore, geocomposites allow for quick and easy installation compared with conventional drains using gravel. McKean and Inouye (2001) reported a successful field case study using geocomposites to prevent water flowing behind a retaining wall. This geocomposite was reported to have performed successfully for a period of 14 years.

Although there have been many reported case studies on the successful implementation of geocomposites in drainage systems, there have been limited numerical simulations of drainage for MSE walls using geocomposites (Koerner 2005; Yoo and Jung 2006). In addition, there is no known work that incorporates the water retention characteristic (WRC) of geotextiles in these reported numerical simulations. Previous studies indicate that geotextiles' water retention characteristics are similar to those of coarse-grained soils such as gravels and sands (Stormont *et al.* 1997; Lafleur *et al.* 2000; Morris 2000; Stormont and Morris 2000; Knight and Kotha 2001; Iryo and Rowe 2003, 2004; Bouazza *et al.* 2006; Bathurst *et al.* 2007, 2009; Nahlawi *et al.* 2007). Various methods have been introduced to determine the WRC of geotextiles, including a hanging column test by Stormont and Morris (2000); a capillary rise test approach in which a geotextile

sheet was immersed in water at its base by Lafleur *et al.* (2000); an outflow capillary pressure cell by Knight and Kotha (2001); a modified outflow capillary pressure cell by Nahlawi *et al.* (2007); and a suction plate apparatus based on the hanging column test procedure by Bathurst *et al.* (2009). To date, the design of geocomposite drains in MSE walls does not incorporate the WRC of geotextiles. A fundamental understanding of the effect of WRC of geotextiles on flow response is necessary to allow for a more effective and appropriate use of geocomposites in MSE walls.

This research was conducted using a large-scale flow test through an MSE wall in which an L-shape geocomposite drain was installed. Instruments were installed for monitoring flow and deformation responses during the tests. The instruments consisted of four standpipe piezometers, 10 time domain reflectometer (TDR) probes and 10 surface settlement plates. Numerical analyses were subsequently conducted using the Plaxis-2D finite element modelling software to investigate the effect of the hydraulic properties on the water flow taking place in the MSE wall.

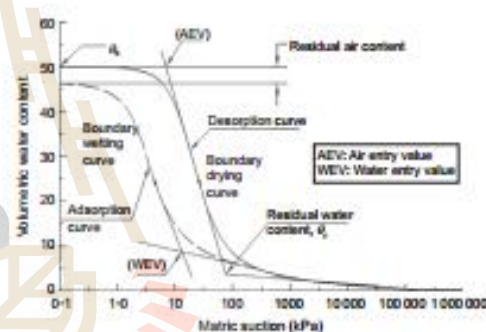


Figure 1. Schematic diagram of water retention characteristic curve

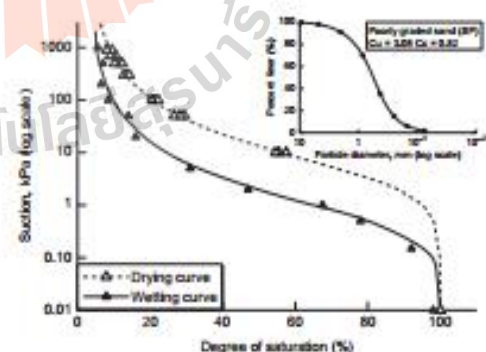


Figure 2. Water retention characteristic curves of the soil used in the physical test. The dry curve was obtained using a pressure plate apparatus, and the wetting curve was obtained using a double-walled triaxial cell

This research will lead to a better understanding of the various parameters that affect the performance of the geocomposite drain, and will facilitate the selection of suitable geocomposite drains for implementation in MSE walls.

Table 1. VG and VGM model parameters and saturated hydraulic conductivity of the materials used in the physical test

| VG and VGM parameters | Sandy soil | Geotextile | Geonet |
|--|------------|------------|--------|
| ρ_s [m ⁻³] | 20 | 20 | 600 |
| ρ_w [-] | 1.5 | 2.5 | 40 |
| S_{sat} [-] | 0.03 | 0.03 | 0.00 |
| S_{sat} [-] | 1.00 | 0.80 | 1.00 |
| Geotextile: saturated hydraulic conductivity | | | |
| $K_{lateral}$ [m/day] | 17 | 320 | 69 120 |
| $K_{longitudinal}$ [m/day] | 17 | 2000 | 69 120 |

2. SET-UP FOR NUMERICAL EXPERIMENT AND PHYSICAL EXPERIMENTS

2.1. Numerical background

The governing equation for transient water flow in a two-dimensional homogeneous anisotropic material within an unsaturated porous medium is as follows

$$\frac{\partial \theta}{\partial t} = k_x \frac{\partial^2 h}{\partial x^2} + k_y \frac{\partial^2 h}{\partial y^2} \quad (1)$$

where θ is the volumetric water content, h is the total head, k_x and k_y are the unsaturated coefficients of permeability in the x - and y -directions, and t is time. To solve Equation 1, constitutive equations related to θ , k_x , and k_y to h are required. Iryo and Rowe (2003, 2004) concluded that there is considerable evidence to suggest

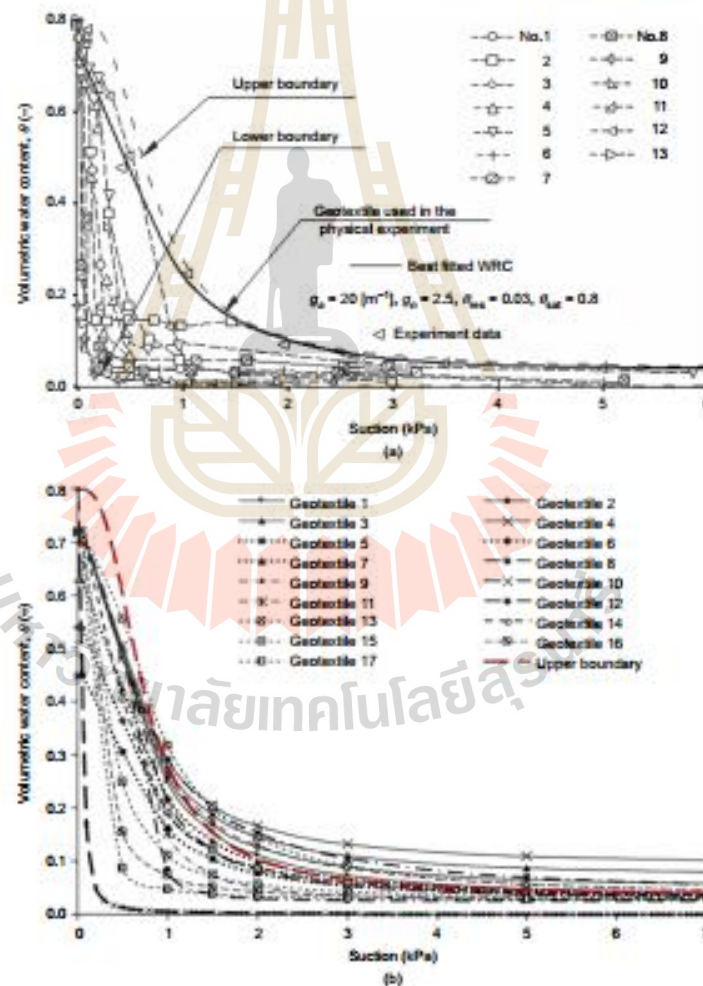


Figure 3. (a) Wetting phase WRC curves of 13 geotextiles reported by Iryo and Rowe (2003) and of the geotextile used in the physical test, and (b) WRC curves of all geotextiles assigned to the numerical experiment



that van Geuchten (VG) (van Genuchten, 1980) and van Genuchten-Mualem (VGM) models, which combine the van Genuchten and Mualem hypotheses (Mualem 1976), are applicable to nonwoven geotextiles. Thus, both of these constitutive equations were employed to approximate WRC and permeability functions for both the soil

$$S_e = \frac{S - S_{\text{res}}}{S_{\text{est}} - S_{\text{res}}} = [1 + (g_e |h_p|)^{k_e}]^{\lambda_e} \quad (2a)$$

$$k_r(S_e) = S_e^{0.5} [1 - (1 - S_e^{-1/6})^{-6}]^2 \quad (2b)$$

where S_e is the effective degree of saturation, S is the degree of saturation, S_{res} is the residual saturation at a very high value of suction, S_{sat} is the saturation of saturated soil, h_p is the matric suction head, k_r is the relative permeability coefficient, g_u [m^{-1}], g_e and g_a are fitting parameters, and according to the Mualem hypothesis (Mualem 1976), g_e is assigned a value of $1/g_a - 1$.

Figure 1 presents a typical plot of a WRC curve. For the drying phase, pore water tends to migrate as suction increases, and when the value reaches the air-entry value (AEV), bulk water begins to drain away. Similarly to the AEV, when a soil is wetted, the degree of saturation increases markedly when the suction decreases, to attain a suction value termed the water-entry value (WEV). The parameter g_u is a fitting parameter that reflects the inflection point on the WRC curve generated by Equation 2a and the largest pore size in the material. The parameter g_a reflects the steepness of the WRC curve in the desaturation zone, and a small value of g_u yields a steep WRC curve in the desaturation zone and is hence related to the wide pore size distribution.

2.2. Materials

The soil used in this investigation is a sandy soil consisting of 10% gravel, 87.3% sand, and 2.7% silt. The particle size distribution of the sand is presented in the upper right corner of Figure 2. This sand is classified as poorly graded sand (SP), according to the Unified Soil Classification System (USCS), with a specific gravity of 2.74. The compaction characteristics under standard Proctor energy are an optimum water content (OWC) of 5.7% and maximum dry unit weight γ_{dmax} of 16.7 kN/m³. The saturated hydraulic conductivity of the soil is $k_{sat} = 17$ m/day. Well-graded materials are generally used as backfill materials due to their high efficiency in field compaction. However, uniform sand was used in this investigation to ensure consistency of the soil compacted in the large-scale physical model. Determinations of the WRC of the soil were conducted along the drying and wetting paths. The drying phase WRC was obtained using a pressure plate apparatus, and the wetting phase WRC was obtained from the double-walled triaxial cell. The relationships between volumetric water content and matric suction of the soil along wetting and drying paths are presented in Figure 2.

The non-woven needle-punched polyester geotextile used in this study had an average thickness of 0.25 cm, an apparent opening size of 0.075 mm and a porosity of 0.90. The hydraulic properties of the geotextile are shown in Table 1. The transmissivity of the geonet was 0.004 m²/s, and this was converted to a saturated hydraulic conductivity of 69 120 m/day. The WRC of the geotextile was conducted along the wetting path using a capillary rise test (Lafleur *et al.* 2000), which was conducted by hanging a 25 cm × 300 cm strip of geotextile vertically and placing the lower end of the strip in the reservoir water. The strip was covered in plastic wrap to prevent evaporation and allowed to equilibrate for 72 h. The sample was then cut into small strips to determine the volumetric water content. The volumetric water

content was measured at different positions above the water surface by cutting the specimen into 50 mm long segments and weighing the samples before and after oven drying. The relationships between the volumetric water content and matric suction of the geotextile are presented with the other WRC curves in Figure 3. The VG model was used to describe the relationship between volumetric water content and matric suction for the soil and the geotextile. The parameters used to fit the model to the test results for the soil and the geotextile are summarised in Table 1.

2.3. Physical experiments

Large-scale physical experiments for a wall height of 1.0 m (Figure 4) were conducted to simulate an MSE wall under a high groundwater level. The bottom, left and right sides of the physical model were established as an impervious boundary. Groundwater flows during the

Table 2. Properties of 13 nonwoven geotextiles reported by Iryo and Rowe (2003)

| No. | Mass per unit area (g/m ²) | Apparent opening size (mm) | Porosity volume ratio | Saturated transmissivity (m ² /h) |
|-----|--|----------------------------|-----------------------|--|
| 1 | 339 | 0.15 | 0.88 | — |
| 2 | 543 | 0.15 | 0.84 | — |
| 3 | 340 | 0.18 | 0.87 | — |
| 4 | 540 | 0.15 | 0.88 | — |
| 5 | 266 | 0.04 | 0.89 | 6.80×10^{-6} |
| 6 | 340 | 0.18 | 0.94 | 3.90×10^{-3} |
| 7 | — | 0.15 | 0.88 | 2.93×10^{-3} |
| 8 | 543 | 0.15 | 0.87 | 1.65×10^{-3} |
| 9 | — | — | 0.96 | 3.90×10^{-3} |
| 10 | 154 | — | 0.94 | — |
| 11 | 333 | — | 0.93 | — |
| 12 | 276 | — | 0.91 | — |
| 13 | 468 | — | 0.86 | 5.5×10^{-6} |

Table 3. VG and VGM model parameters of the geotextiles assigned in the numerical experiment

| Material | van Genuchten parameters | | | |
|---------------|--------------------------|-----------|---------------|---------------|
| | g_u (m ⁻¹) | g_a (—) | S_{sat} (—) | S_{res} (—) |
| Geotextile 1 | 20 | 2.5 | 0.8 | 0.03 |
| Geotextile 2 | 20 | 2.5 | 0.8 | 0.05 |
| Geotextile 3 | 20 | 2.5 | 0.8 | 0.08 |
| Geotextile 4 | 20 | 2.5 | 0.8 | 0.10 |
| Geotextile 5 | 20 | 2.5 | 0.5 | 0.03 |
| Geotextile 6 | 20 | 2.5 | 0.6 | 0.03 |
| Geotextile 7 | 20 | 2.5 | 0.7 | 0.03 |
| Geotextile 8 | 20 | 2.0 | 0.7 | 0.03 |
| Geotextile 9 | 20 | 2.2 | 0.7 | 0.03 |
| Geotextile 10 | 20 | 3.0 | 0.7 | 0.03 |
| Geotextile 11 | 20 | 4.0 | 0.7 | 0.03 |
| Geotextile 12 | 20 | 6.0 | 0.7 | 0.03 |
| Geotextile 13 | 16 | 2.5 | 0.8 | 0.03 |
| Geotextile 14 | 25 | 2.5 | 0.8 | 0.03 |
| Geotextile 15 | 40 | 2.5 | 0.8 | 0.03 |
| Geotextile 16 | 60 | 2.5 | 0.8 | 0.03 |
| Geotextile 17 | 100 | 2.5 | 0.8 | 0.03 |

Table 4. VG and VGM model parameters assigned to every case in the numerical experiment

| Sandy soil | | | | | | Geotextile | | | | | | Geomat | | | | | | Remarks |
|--------------|--------------|-----------|--------------------------|---------------|---------------|--------------|--------------|-----------|--------------------------|---------------|---------------|--------------|--------------|-----------|--------------------------|-------------------|-------------------|---------|
| S_{vm} (-) | S_{vm} (-) | g_v (-) | g_v (m ⁻¹) | k_v (m/day) | k_v (m/day) | S_{vm} (-) | S_{vm} (-) | g_v (-) | g_v (m ⁻¹) | k_v (m/day) | k_v (m/day) | S_{vm} (-) | S_{vm} (-) | g_v (-) | g_v (m ⁻¹) | k_v (m/day) | k_v (m/day) | |
| 0.03 | 1.0 | 1.5 | 20 | 17 | 17 | 0.03 | 0.8 | 2.5 | 20 | 320 | 2000 | 0 | 1.0 | 40 | 600 | 6.9×10^4 | 6.9×10^4 | Case 1 |
| 0.05 | | | | | | | | | | | | | | | | | | Case 2 |
| 0.08 | | | | | | | | | | | | | | | | | | Case 3 |
| 0.1 | | | | | | | | | | | | | | | | | | Case 4 |
| 0.03 | 0.7 | 1.5 | 20 | 17 | 17 | 0.03 | 0.8 | 2.5 | 20 | 320 | 2000 | 0 | 1.0 | 40 | 600 | 6.9×10^4 | 6.9×10^4 | Case 5 |
| | 0.8 | | | | | | | | | | | | | | | | | Case 6 |
| | 0.9 | | | | | | | | | | | | | | | | | Case 7 |
| 0.03 | 1.0 | 1.8 | 20 | 17 | 17 | 0.03 | 0.8 | 2.5 | 20 | 320 | 2000 | 0 | 1.0 | 40 | 600 | 6.9×10^4 | 6.9×10^4 | Case 8 |
| | 2.0 | | | | | | | | | | | | | | | | | Case 9 |
| | 2.5 | | | | | | | | | | | | | | | | | Case 10 |
| | 3.0 | | | | | | | | | | | | | | | | | Case 11 |
| 0.03 | 1.0 | 1.5 | 5.0 | 17 | 17 | 0.03 | 0.8 | 2.5 | 20 | 320 | 2000 | 0 | 1.0 | 40 | 600 | 6.9×10^4 | 6.9×10^4 | Case 12 |
| | 10 | | | | | | | | | | | | | | | | | Case 13 |
| | 25 | | | | | | | | | | | | | | | | | Case 14 |
| | 30 | | | | | | | | | | | | | | | | | Case 15 |
| 0.03 | 1.0 | 1.5 | 20 | 1.7 | 1.7 | 0.03 | 0.8 | 2.5 | 20 | 320 | 2000 | 0 | 1.0 | 40 | 600 | 6.9×10^4 | 6.9×10^4 | Case 16 |
| | | | | 100 | 100 | | | | | | | | | | | | | Case 17 |
| | | | | 170 | 170 | | | | | | | | | | | | | Case 18 |
| | | | | 200 | 200 | | | | | | | | | | | | | Case 19 |
| | | | | 320 | 320 | | | | | | | | | | | | | Case 20 |
| | | | | 500 | 500 | | | | | | | | | | | | | Case 21 |
| 0.03 | 1.0 | 1.5 | 20 | 17 | 17 | 0.05 | 0.8 | 2.5 | 20 | 320 | 2000 | 0 | 1.0 | 40 | 600 | 6.9×10^4 | 6.9×10^4 | Case 22 |
| | | | | | | 0.08 | | | | | | | | | | | | Case 23 |
| | | | | | | 0.1 | | | | | | | | | | | | Case 24 |
| 0.03 | 1.0 | 1.5 | 20 | 17 | 17 | 0.03 | 0.7 | 2.5 | 20 | 320 | 2000 | 0 | 1.0 | 40 | 600 | 6.9×10^4 | 6.9×10^4 | Case 25 |
| | | | | | | 0.6 | | | | | | | | | | | | Case 26 |
| | | | | | | 0.5 | | | | | | | | | | | | Case 27 |
| 0.03 | 1.0 | 1.5 | 20 | 17 | 17 | 0.03 | 0.8 | 2 | 20 | 320 | 2000 | 0 | 1.0 | 40 | 600 | 6.9×10^4 | 6.9×10^4 | Case 28 |
| | | | | | | 2.2 | | | | | | | | | | | | Case 29 |
| | | | | | | 3 | | | | | | | | | | | | Case 30 |
| | | | | | | 4 | | | | | | | | | | | | Case 31 |
| | | | | | | 6 | | | | | | | | | | | | Case 32 |
| 0.03 | 1.0 | 1.5 | 20 | 17 | 17 | 0.03 | 0.8 | 2.5 | 16 | 320 | 2000 | 0 | 1.0 | 40 | 600 | 6.9×10^4 | 6.9×10^4 | Case 33 |
| | | | | | | | | | 20 | | | | | | | | | Case 34 |
| | | | | | | | | | 25 | | | | | | | | | Case 35 |
| | | | | | | | | | 40 | | | | | | | | | Case 36 |
| | | | | | | | | | 60 | | | | | | | | | Case 37 |
| | | | | | | | | | 100 | | | | | | | | | Case 38 |

[illegible]

tests were controlled by water levels in the upstream and downstream water tanks. The water level in the downstream water tank was kept constant at the toe of the wall (+0.0 m) using a control weir. The water level in the upstream tank was increased stepwise from heights of +0.0 m, +0.4 m, +0.7 m, and +1.0 m. The upstream water level was increased after reaching a steady state in which there was no change in the water content values, read from the TDR probes, for a period equal to or greater than 24 h. This configuration was established to simulate the most severe situation in which the groundwater level behind an MSE wall is very high, similar to the situation that may occur in mountainous areas during heavy rainfalls. The shallow soil layer was assumed to be underlain by a bedrock layer, such that inundation might occur during a heavy rainstorm (Figure 4b).

Although the MSE wall base was always submerged, the distance between the MSE wall base and the bottom impervious boundary is likely to affect the seepage response. To exclude the effect of the distance between the MSE wall base and the bottom impervious boundary, the bottom boundary should be located far enough away that its location would not affect the seepage response. Numerical modelling results undertaken at various distances from the base of the MSE wall to the bottom boundary were used to justify the location of the bottom boundary in the physical experiments. The required depth of the impervious boundary, at a location that did not affect the seepage response, was no less than 0.4 m from the base of the MSE wall.

In practice, additional considerations such as the potential to scour beneath the wall, wave action effects and destabilising forces due to hydrostatic pressure must be taken into account if an MSE wall is to be partly submerged in a body of water. This study aimed to investigate only the effect of geocomposite drains on the seepage water flow in an MSE wall, so the abovementioned considerations were not considered.

The tank was filled with compacted soil to a height of 1.4 m. Compaction was carried out with a hand compactor in layers measuring 0.2 m in thickness to a density of 90% of the standard Proctor density at a water content of 5.7%. The degree of compaction and water contents were checked at 3 points for each compacted layer. These points were located along a longitudinal line close to the centre line near the wall facing the geocomposite drain, and the porous concrete upstream wall. Wherever the degree of compaction was found to be inadequate, additional compaction was undertaken until the targeted density was achieved. The wall facing was made of an acrylic plate with 5 layers of 'bearing reinforcement' (Horpibulsuk *et al.* 2011) with equal lengths of 0.7 m (equal to $0.8H$, where H is the wall height), which conforms with AASHTO recommendations (AASHTO 2002). The bearing reinforcement was composed of a longitudinal member and transverse (bearing) members. The longitudinal member was a steel deformed bar, and the transverse members were a set of angle steels. The longitudinal and transverse members were welded to each other. A sketch of the bearing reinforcement is shown in Figure 4c.

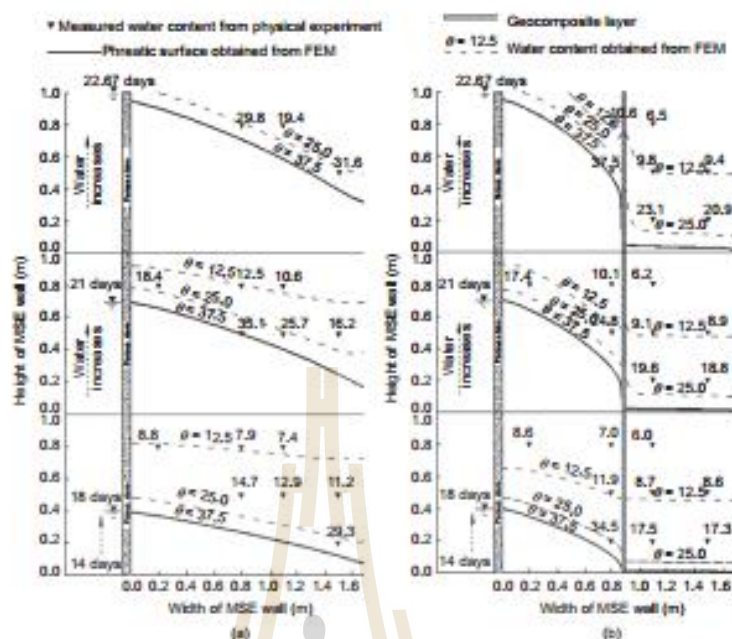


Figure 5. Measured and calculated phreatic surfaces and water contents for MSE wall (a) case I (without geocomposite drain installed) and (b) case II (with geocomposite drain installed).

The vertical and horizontal spacings between each reinforcement layer were fixed at 0.20 m and 0.25 m, respectively.

The MSE wall was extensively instrumented. Locations of the instruments are illustrated in Figure 4. Four standpipe piezometers, 10 surface settlement plates and 10 TDR probes were installed to measure water levels, settlements and volumetric water contents during seepage flow, respectively. The piezometers were installed along the centre line of the tank (Figure 4a). Settlements were measured by precise levelling with reference to a benchmark. Three linear potentiometers were installed at the wall facing panel to measure lateral wall movements at different points during seepage. Data read from TDR probes and piezometers were considered and are presented in this paper.

Two physical experiments were conducted: without geocomposite drain installation (case I) and with geocomposite drain installation (case II). For the experiment with a geocomposite drain, the geocomposite was installed at a distance of 0.8 m from the wall facing.

2.4. Additional numerical experiment

A series of numerical experiments was subsequently conducted to investigate the effect of the relevant material properties on the groundwater flow through the MSE wall, with a geocomposite drain installed, using the finite element code Plaxis 2D. The models were verified with the results taken from the physical experiments explained in the previous section. The MSE wall model without

geocomposite installation was verified prior to the MSE wall model with geocomposite installation.

The properties that predominantly affect the hydraulic behaviours of the MSE wall with geocomposite installation are the hydraulic conductivity of the geocomposite, the variation in the hydraulic conductivity with the degree of saturation, the water retention characteristics of the soil and the geocomposite components (geotextile and geonet). As the geonet has a very open structure, VG and VGM models with the following considerations were assigned to the geonet

- (1) The geonet has a large and single pore size attribution.
- (2) The geonet can be completely dried and saturated under suitable magnitudes of suction.

With respect to the first consideration, high values of g_a and g_s reflect a large pore size and a more uniform pore size distribution, respectively. Hence, high g_a and g_s values were assigned to the geonet. Parametric studies indicated that assigning magnitudes of g_a greater than 600 [m^{-1}] and magnitudes of g_s greater than 40 resulted in no changes in the calculation results. As such, the geonet parameters g_a and g_s were assigned values of 600 [m^{-1}] and 40, respectively. Based on the second consideration, the geonet parameters S_{res} and S_{sat} were set to 0.00 and 1.00, respectively. The parameters for the hydraulic constitutive equations VG and VGM for the soil, the geotextile and the geonet assigned to the models are summarised in Table 1.

Data from the wetting phase WRC of 13 geotextiles reported by Iryo and Rowe (2003) were used as the reference data in the selection of parameters for the numerical experiment by the VG and VGM models. The basic properties of these 13 nonwoven geotextiles are shown in Table 2, and the WRC of these, together with their upper and lower bounds (long dash lines), are presented in Figure 3a. The ranges of the VG and VGM model parameters of the geotextile were varied such that their WRC curves were inside this boundary (Figure 3b). Seventeen sets of VG and VGM model parameters of geotextile were used as shown in Table 3. These parameters were varied based on the VG and VGM model parameters of the geotextile used in the physical experiment (Table 1), i.e., $g_w = 20 \text{ [m}^{-1}\text{]}$, $g_a = 2.5$, $S_{\text{sat}} = 0.03$, and $S_{\text{sat}} = 0.80$. In total, 61 numerical simulations were conducted in this study. The parameter values assigned to every case are shown in Table 4.

3. RESULTS AND DISCUSSION

3.1. Large-scale flow through MSE wall test results

Figure 5 presents the measured (with symbols) and calculated (with lines) water levels and volumetric water contents for the various upstream water levels for tests without (Figure 5a) and with (Figure 5b) geocomposite installation. The water levels and the volumetric water contents presented in Figure 5 are those measured at 18 days, 21 days, and 23 days, which represent the end times of upstream water levels of +0.4 m, +0.7 m, and +1.0 m, respectively. At any upstream water level height, the water level decreases through the wall face. The measured water level data for case I (no geocomposite) are compared with those for case II (with geocomposite). The comparisons show that the highly permeable geocomposite can effectively prevent water flow to the reinforced zone (or protected zone), as it collects the

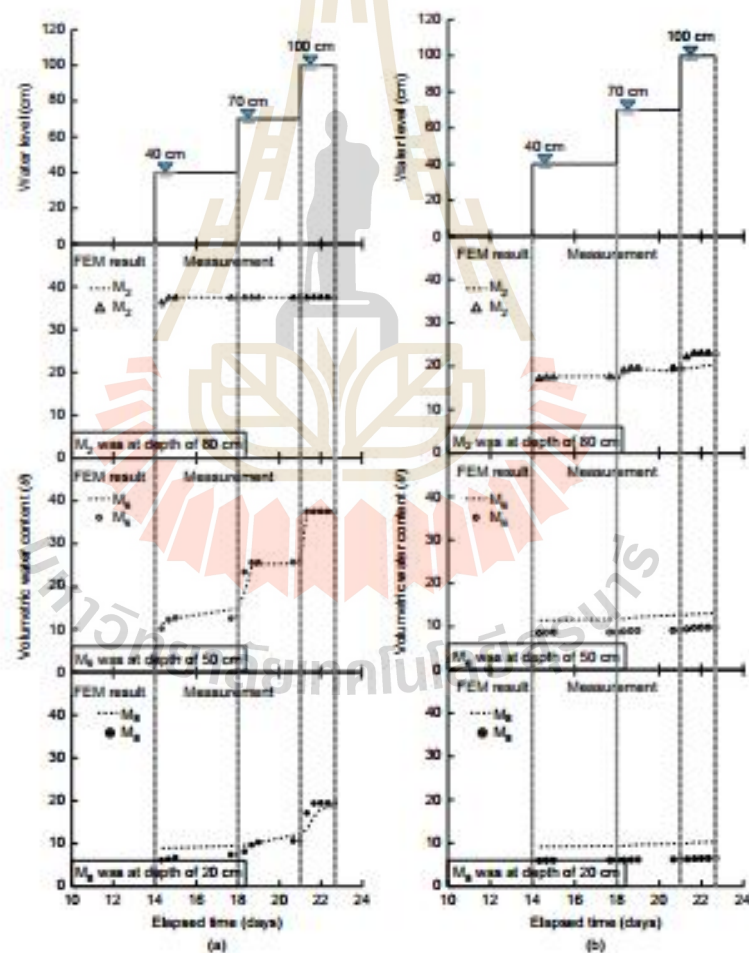


Figure 6. Time series plot of the water content for MSE wall case I (without geocomposite drain installed) and case II (with geocomposite drain installed)

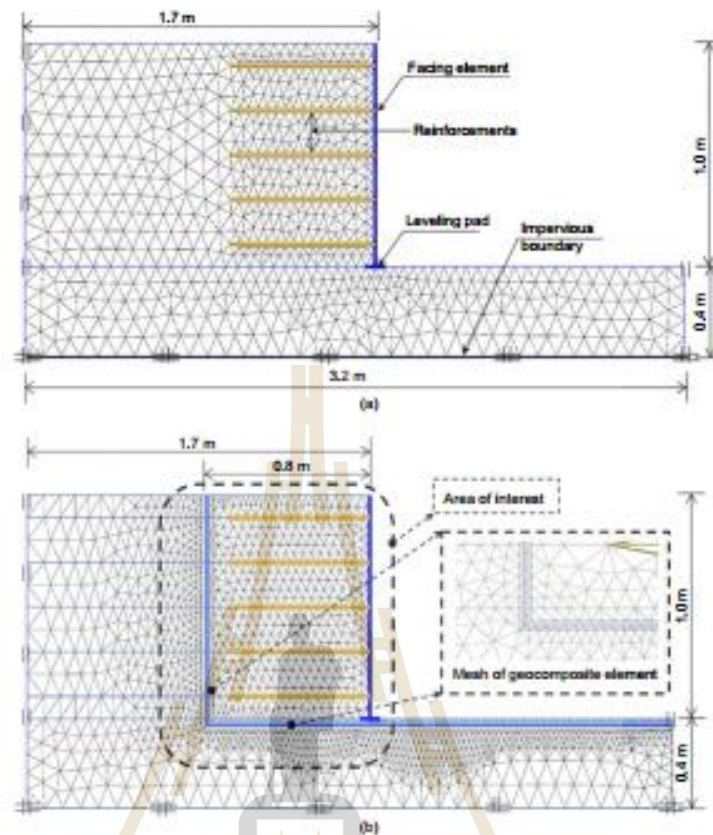


Figure 7. Mesh discretisation of the models (a) without and (b) with geocomposite installation

water in the unreinforced zone and drains it at the wall face.

Figure 6 shows volumetric water contents measured at various times from TDR probes M_2 , M_6 and M_8 (see Figure 4). These probes were located at a horizontal distance of 0.6 m from the wall facing, i.e., at 0.2 m horizontally from the geocomposite drain for the MSE wall case II. Higher water contents were found at the lower TDR probes. The water contents in the reinforced zone with geocomposite installation were much lower than those without geocomposite. In the installation without geocomposite, the volumetric water content read from the probe M_2 rose from 0.05 ($S_r = 20\%$) to 0.40 ($S_r = 100\%$) when the upstream water level was raised from 0.2 m to 1.0 m. The volumetric water content with the geocomposite was found to be only half of that in the case without the geocomposite. At probe M_6 , the volumetric water content rose from 0.05 to final values of 0.38 and 0.12 for the case without and with the geocomposite, respectively. Even at the location of probe M_8 , where the water content exhibited the weakest effect on the rise in the upstream water level, the difference between the final water contents for the case without and with the geocomposite was significant.

3.2. Model calibration

Model calibrations were conducted prior to the parametric studies. The models were developed in the Plaxis environment to simulate the physical modelling studies. These models incorporated soil characteristics, structural components (reinforcements and acrylic facing), and drainage components (geotextile and geonet). As the model of the MSE wall with the geocomposite is complex, given the thin layers of geotextiles and geonets installed, verification of the MSE wall without the geocomposite was conducted prior to that of the MSE wall with the geocomposite. Material properties assigned to the models are presented in Table 1.

The discretised plane strain finite element mesh is shown in Figures 7a and 7b for the MSE wall without and with geocomposite drain installation, respectively. A triangular mesh was used in the model. Although a rectangular mesh is commonly adopted in water flow models, it has been reported that the calculated results do not depend on the type of mesh because the interpolation function in flow problems is linear (Potts and Zdravkovic 2001).

In Plaxis, there are two types of triangular elements: 6-node triangles and 15-node triangles. In this study,

15-node triangles were assigned to the models. The use of 15-node triangles yields more accurate calculation results than that of 6-node triangles. A fine mesh with an average element size of 0.033 m was assigned. A finer mesh was also assigned to the geotextile and the geonet. The initial conditions of the model were defined based on the controlled density and water content during the placement of compacted soil in the physical box. Dirichlet boundary conditions with prescribed pressures were imposed on the left, right, and upper boundaries of the model. The bottom boundary of the model was defined as impermeable. In Plaxis, the time steps were assigned automatically for steady-state calculation. At each time step, a modified Newton-Raphson model was used to solve the relevant equations iteratively. In each iteration, increments of the groundwater head were calculated from the imbalance in the nodal discharges and added to the active head. This process was continued until the norm of the unbalance vector, i.e., the error in the nodal discharges, was smaller than that of the tolerated error of 0.01 (or 1%).

Figures 5 and 6 compare the measured and calculated phreatic surface, distribution and time series of volumetric water content at various heights of the upstream water level. The numerical model yields a variation in the phreatic surface similar to that measured in the tests. Fair agreement between the measurements and the corresponding calculations for the two cases was found.

4. PARAMETRIC STUDY

The hydraulic response, including the effective saturation and phreatic surface, determined from numerical experiments are presented and discussed in this section. The effect of the hydrological properties of the soil and the geotextile on the hydraulic response was evaluated using (1) van Genuchten parameters (S_{res} , S_{sat} , g_a , g_n) and (2) the corresponding saturated permeability. For the hydrological properties of the geonet, only the saturated hydraulic conductivity of the geonet was evaluated.

In general, it was found that the phreatic surface outside the protected zone does not change notably within the range of parameters indicated in Table 3. The phreatic surface in the protected zone and the distribution of effective saturation were affected by some of the parameters, as discussed in this section.

4.1. Effect of the van Genuchten parameters of the soil material

4.1.1. The van Genuchten parameter g_a

Figures 8a and 8b present the effective saturation profiles along sections *a-a* and *b-b*, respectively, for various magnitudes of g_a . The alignment of these sections is vertical and located at 0.05 m to the left and right from the geocomposite drainage. At a certain depth above the phreatic surface, the soil with a low g_a value exhibits high saturation. The degree of saturation is found to decrease when the magnitude of g_a decreases. In short, the wet zone spreads more widely for the low g_a soil than for the high g_a soil.

The magnitude of g_a reflects the inflection point of the wetting cycle WRC curve and hence the capillary saturation zone of the wetting cycle WRC curve. Figure 9 compares two WRC curves of two soils with high and low values of g_a . The lower g_a soil yields a wider range of suction in the capillary saturation zone, and hence a wider spread of the high saturation zone within the same suction range. Within the capillary saturation zone and in a zone slightly beyond the capillary saturation zone, there is little change in the saturation such that the rate of saturation

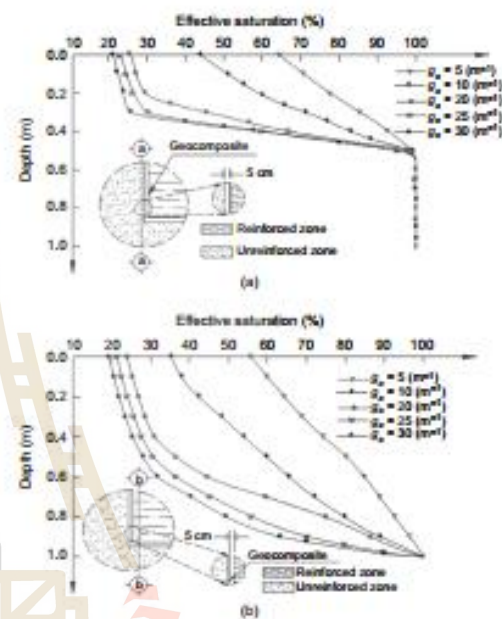


Figure 8. Effective saturation profile along vertical sections located (a) 5 cm left and (b) 5 cm right of the geocomposite for various magnitudes of g_a of soil

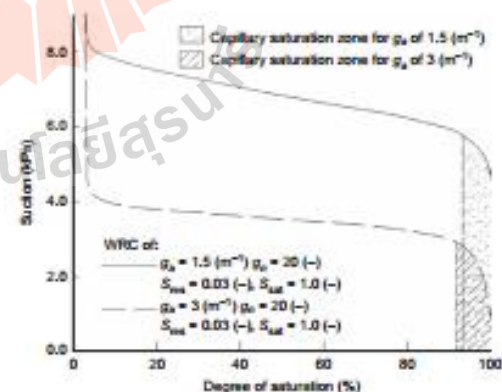


Figure 9. Typical water retention characteristic curve with low and high g_a values

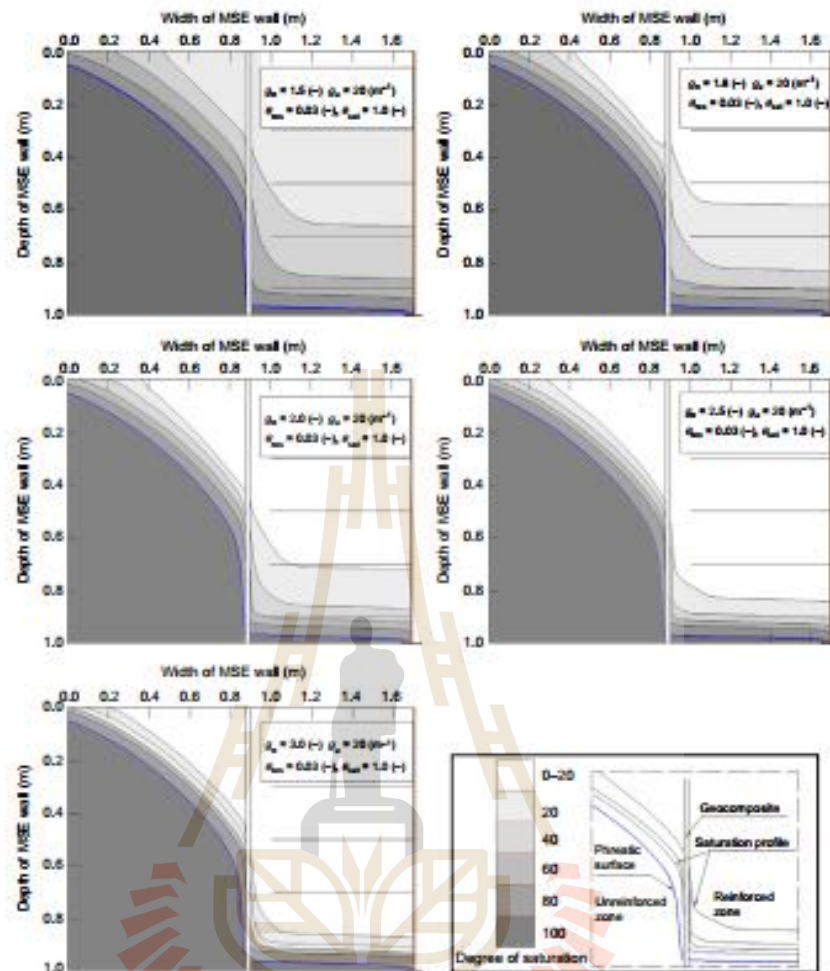


Figure 10. Phreatic surface (bold line) and effective saturation profiles in the MSE model for various magnitudes of g_a of soil

change in these zones is lower than that in the other zones. Thus, the rate of saturation change is found to be lower in the lower g_a soil.

The magnitude of g_a represents the largest pore size present in the soil. Soil with a large g_a value has large pore sizes. Theoretically, at the interface of two materials with different largest pore sizes, the capillary barrier phenomenon (Ross 1990) can occur when water does not readily flow from smaller to larger pore materials. The wide range of the capillary saturation zone plays a dominant role in the distribution of saturation in these experiments, and hence, the capillary barrier effect is negligible.

4.1.2. The van Genuchten parameters g_a

Figure 10 presents phreatic surface and effective saturation profiles on the MSE wall model calculated at various magnitudes of g_a of the soil. The results show

that effective saturation (both inside and outside the protected zone) between 20 and 80% clearly depends on the magnitude of g_a . A greater magnitude of g_a yields narrower effective saturation contours in the 20% to 80% range.

The magnitude of g_a reflects the steepness of the WRC curve in the desaturation zone, as a smaller g_a yields a steeper curve. Figure 11 compares the WRC curves of two soils having both high and low values of g_a . In the high saturation range, these WRC curves are similar. Within this range, a similar change in suction for both soils results in approximately similar saturation changes. As such, the width between the contours of 80% and 100% effective saturation as shown in Figure 10 are similar for different values of g_a . For the intermediate saturation range, the soil with the higher g_a exhibits a narrower range of suction change (see Figure 11). Thus, the contour width for 20%

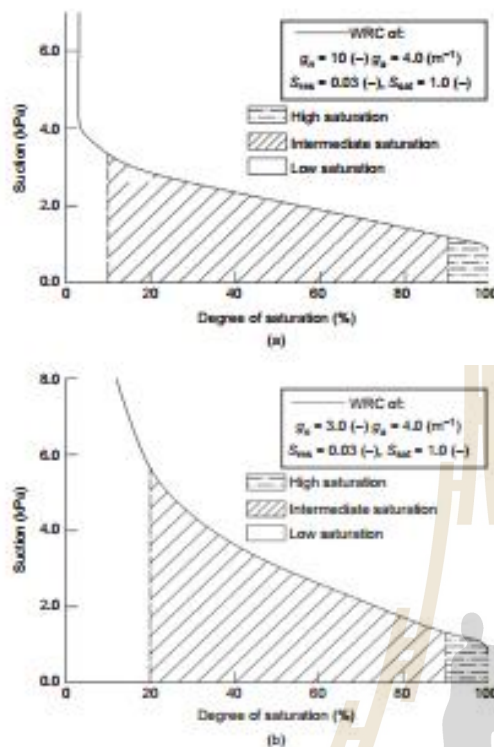


Figure 11. Typical water retention characteristic curve for low (a) and high (b) g_a values

to 80% effective saturation is found to be narrower in a higher g_a soil than that in a lower g_a soil (Figure 11).

4.1.3. The saturation parameters S_{res} and S_{sat}

Figures 12a and 12b present phreatic surface and effective saturation profiles on the MSE wall model calculated at the lowest and the highest magnitudes of S_{res} (0.03, 0.05, 0.08, and 0.10) and S_{sat} (0.7, 0.8, 0.9, and 1.0), respectively. The saturation parameters S_{sat} and S_{res} of the soil might affect the distribution of water contents in the soil, both outside and inside the protection zone. However, these saturation parameters do not affect the distribution of water content represented in terms of effective saturation. The saturation parameters S_{sat} and S_{res} of the soil have a negligible effect on the phreatic surface.

4.2. Effect of the van Genuchten parameters of the geotextile

4.2.1. The van Genuchten parameter g_a

Figure 13 presents the effective saturation profiles along the soil-geotextile interface for various magnitudes of g_a of the geotextile. This interface is outside the protected zone. The effective saturation profiles along the interfacial section increase with depth for all g_a values, and are found to reach full saturation at a depth of 1.0 m below the surface. It is clearly shown that an increase in g_a reflects an

increase in the degree of saturation along the interfacial section. The saturation profiles at shallow depth are found to be slightly different from each other, but the saturation profiles at greater depth become notable depending on the parameter g_a .

The capillary barrier phenomenon plays an important role in the degree of saturation at the soil-geotextile interface. Previous studies, i.e., Stormont *et al.* (1997); Henry *et al.* (2001); Iryo and Rowe (2003); Iryo and Rowe (2004); Bathurst *et al.* (2007, 2009); Siemens and Bathurst (2010); Zornberg *et al.* (2010) and Bouazza *et al.* (2013), reported that geotextiles may act as coarse grain soil and can either facilitate or obstruct drainage flow depending on the saturation conditions of the soil and geotextiles. Under unsaturated conditions, the flow of water from smaller to larger pore size materials is obstructed by capillary break, and hence, water accumulates at the interface. This phenomenon occurs until the magnitude of suction at the interface decreases to a critical suction level. At this point, the hydraulic conductivities of the two materials reach the same value, and water breaks through the interface.

Figure 14 presents the hydraulic conductivity functions of the soil and geotextile at various g_a values of the geotextile. The magnitudes of the critical suction for all cases are low, with water found not to permeate through the interface at high suction levels. Thus, the saturation profiles at high suction levels are not appreciably different between all cases (Figure 13). Although the critical suction in all cases is found to be low, the magnitudes vary between cases (Figure 14). A high g_a value of the geotextile yields a low magnitude of critical suction and subsequently results in a higher saturation at high saturation levels.

4.2.2. The van Genuchten parameter g_s

Figure 15 presents the effective saturation profiles along the soil-geotextile interface for various magnitudes of g_s . This interface is outside the protected zone. It is evident that the g_s parameter has little effect on the effective saturation profile along the soil-geotextile interface. The parameter g_s does not affect the pore size of the material and thus the capillary barrier, resulting in a slight difference in the degree of saturation at the interface for various magnitudes of g_s .

4.2.3. The saturation parameters S_{res} and S_{sat}

Figures 16a and 16b present phreatic surface and effective saturation profiles on the MSE wall model calculated at the lowest and highest magnitudes of S_{res} (0.03, 0.05, 0.08, and 0.10) and S_{sat} (0.5, 0.6, 0.7, and 0.8), respectively. Similarly to the saturation parameters S_{sat} and S_{res} of the soil, the saturation parameters S_{sat} and S_{res} of the geotextile do not affect the distribution of water content and the location of the phreatic surface.

4.3. Effect of hydraulic conductivity ratio

The level of the phreatic surface inside the protected zone is vital to the stability of the MSE wall. The lower phreatic surface level results in a lower water content inside the

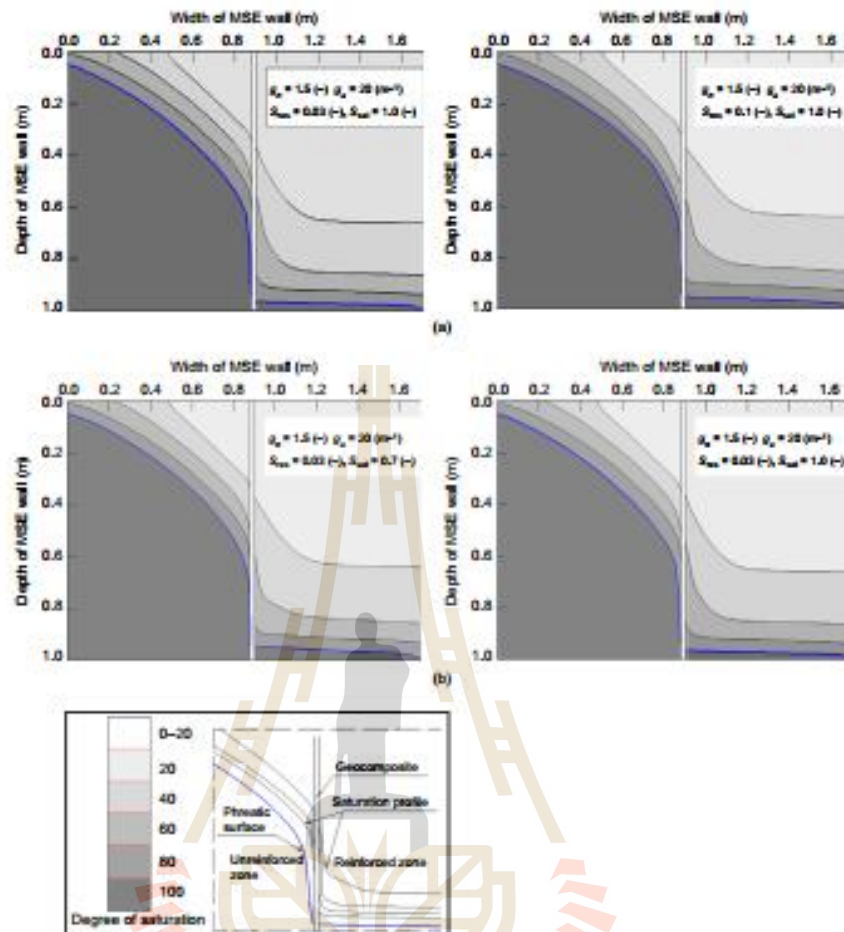


Figure 12. Phreatic surfaces (bold line) and effective saturation profiles in the MSE model for the lowest and highest values of S_{sat} (a) and S_{sat} (b) of soils assigned in the numerical experiment

protected zone and hence leads to higher stability for the wall. In most of the simulation cases, the phreatic surface level inside the protected zone drops close to the bottom-most part of this zone. However, higher phreatic surface levels are still found in some cases. It is known that flow across a boundary between two materials of different hydraulic conductivities might result in a refraction of the flow direction, as shown in the top right of Figure 17. The relationship between the reflected angles and the hydraulic conductivity of the materials is written as

$$\frac{\tan \alpha_1}{\tan \alpha_2} = \frac{k_2}{k_1} \quad (3)$$

In other words, the ratio of the hydraulic conductivity of geocomposite materials to that of soil may affect the phreatic surface in the protected zone. Figures 17a and 17b show the phreatic surface in the protected zone for various ratios between the hydraulic conductivity of the geotextile and that of soil and ratios between the hydraulic

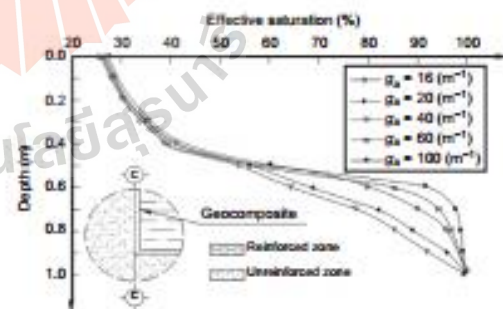
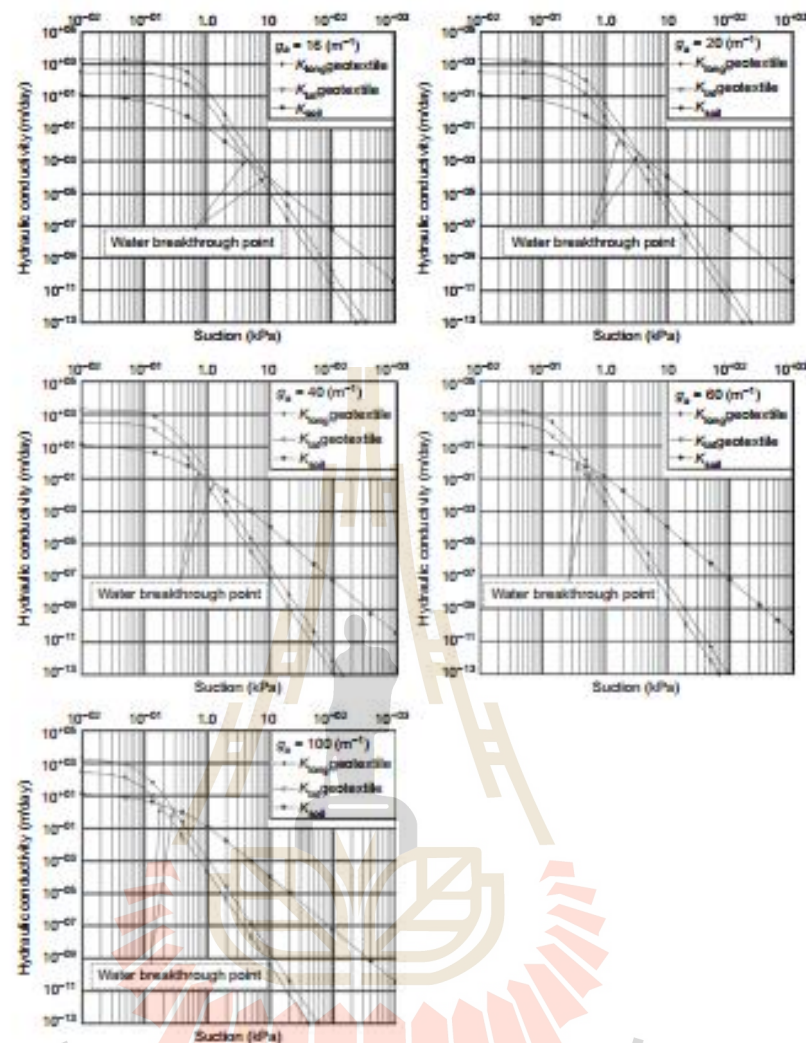


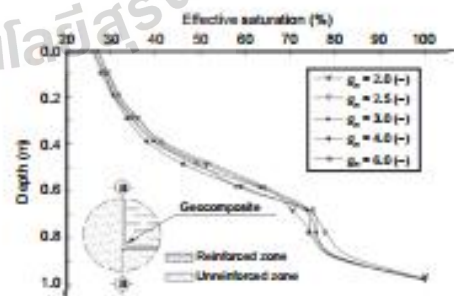
Figure 13. Effective saturation profiles along the soil-geotextile interface for various magnitudes of g_a of geotextile

conductivity of the geonet and that of soil, respectively. As the geotextile exhibits anisotropic behaviour in drainage functions, the effect of the hydraulic conductivity of the geotextile, both in the lateral and longitudinal directions,


 Figure 14. Hydraulic conductivity functions of the soil and geotextile with various magnitudes of g_s of the geotextile

on the phreatic surface in the protected zone must be investigated. Hence, the ratio between the hydraulic conductivity of the geotextile in the lateral direction and that of soil ($K_{r,soil,lat}$) and the ratio between the hydraulic conductivity of the geotextile in the longitudinal direction and that of soil ($K_{r,soil,long}$) were taken into consideration. The phreatic surface plots shown in Figure 17a indicate that $K_{r,soil,lat}$ and $K_{r,soil,long}$ do not affect the phreatic surface in the protected zone.

Figure 17b presents the effect of the ratio between the hydraulic conductivity of the geonet and that of soil ($K_{r,soil}$) on the phreatic surface in the protected zone. A large $K_{r,soil}$ value is found at the lower phreatic surface level in the protected zone. Further reduction of the


 Figure 15. Effective saturation profiles along the soil–geotextile interface for various magnitudes of g_s of geotextile

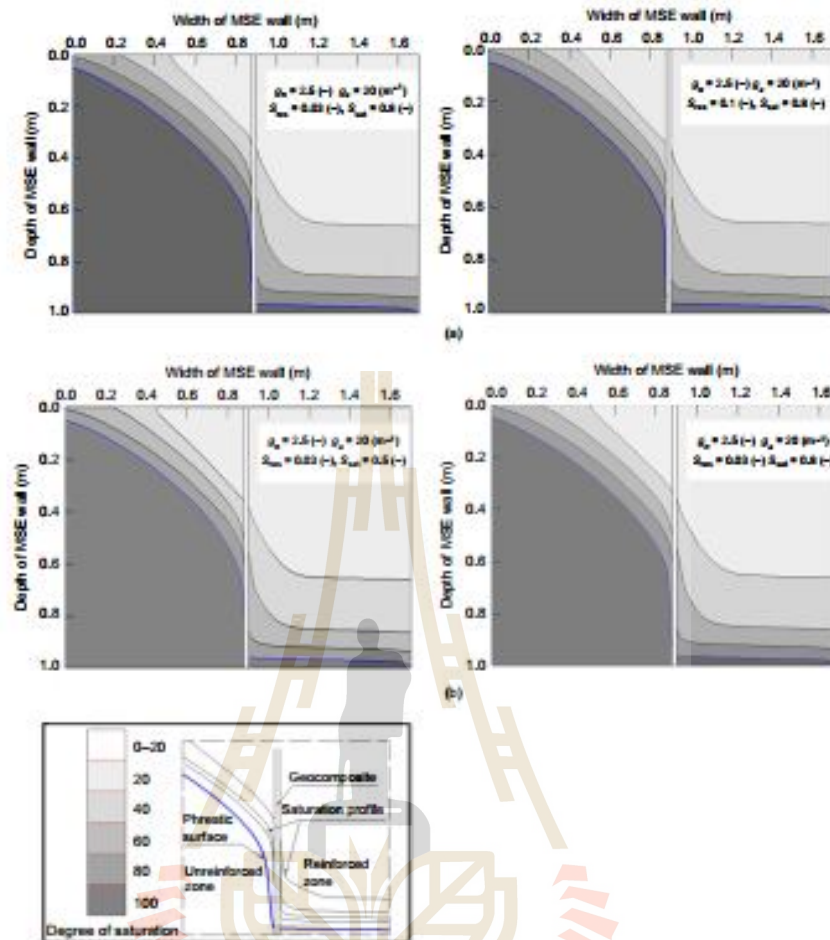


Figure 16. Phreatic surfaces (bold line) and effective saturation profiles in the MSE model for the lowest and highest values of S_{wet} (a) and S_{wet} (b) of geotextiles assigned in the numerical experiment

phreatic surface level is not observed when the magnitude of K_{wet} is greater than 1765. The variation of the phreatic surface level due to the effect of other parameters studied (Cases 1–38) is indicated by the grey shaded area in Figure 17b. The small band in the grey shaded area indicates that there is little variation in the phreatic surface level in the protected zone due to any change in the other studied parameters. These results clearly indicate that the phreatic surface level in the protected zone is mainly governed by the magnitude of K_{wet} .

5. CONCLUSIONS

The drainage ability of geocomposites, which consists of a core material with a large flow channel (geonet) sandwiched by two nonwoven geotextile layers, was investigated through large-scale MSE wall model tests. The

experimental results indicate that the geocomposite studied effectively prevents the flow of water into the reinforced zone by collecting water in the unreinforced zone and draining it in front of the wall face. Comparisons between the deformations of the MSE wall models with and without geocomposite installation indicate that the MSE wall with a geocomposite is far superior to that without a geocomposite. Numerical models were established to conduct parametric studies. The following conclusions can be drawn as a result of this research.

- (1) The WRC of the soil reflects the distribution of effective saturation in the soil both inside and outside the protected zones. The WRC of the geotextile reflects the distribution of effective saturation in the soil both inside and outside the protected zone.
- (2) The 'capillary barrier' phenomenon plays a role in the distribution of effective saturation at the

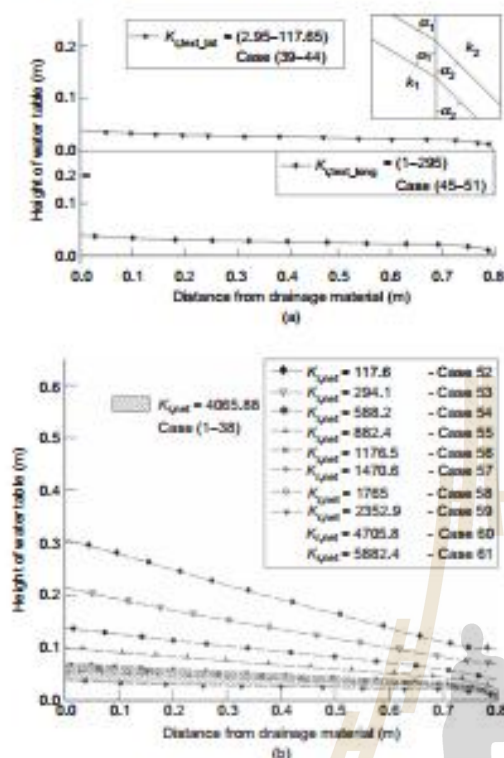


Figure 17. Variation in phreatic surface in the protected zone for (a) various ratios between the hydraulic conductivity of the geotextile and that of soil and (b) various ratios between the hydraulic conductivity of the geonet and that of soil

soil-geotextile interface. The lower magnitude of suction where the water permeates through the interface results in a greater amount of water accumulation at this interface.

- (3) The phreatic surface in the protected zone is governed by the ratio between the hydraulic conductivity of the geonet and that of the soil ($K_{r,net}$). The lower magnitude of $K_{r,net}$ results in a higher phreatic surface level in the protected zone. As the phreatic surface level in the protected zone is vital for the stability of the MSE wall, a proper magnitude of permeability for the geonet must be used such that the water table level inside the protected zone is low and close to the base of the protected zone. This approach is similar to the conventional design method in which candidate materials are selected for collecting and transmitting seepage water, whose transmissivity must be greater than the required flow rate.

ACKNOWLEDGEMENTS

This work was financially supported by Thailand Research Fund (TRF) Grant No. MRG5480240,

TRF Senior Research Scholar Program Grant No. RTA5980005, and the Thailand Toray Science Foundation.

NOTATION

Basic SI units are given in parentheses.

| | |
|------------------|---|
| G_g | specific gravity (–) |
| g_w | fitting parameter (m^{-1}) |
| g_e | fitting parameter (–) |
| g_w | fitting parameter (–) |
| h | total head (m) |
| h_p | suction head (m) |
| $K_{r,net}$ | ratio between the hydraulic conductivity of geonet and that of soil (–) |
| $K_{r,net,lat}$ | ratio between the hydraulic conductivity of geotextile in longitudinal direction and that of soil (–) |
| $K_{r,net,long}$ | ratio between the hydraulic conductivity of geotextile in longitudinal direction and that of soil (–) |
| k | saturated hydraulic conductivity (m/s) |
| k_r | relative hydraulic conductivity (–) |
| k_x | hydraulic conductivity in the x direction (m/s) |
| k_y | hydraulic conductivity in the y direction (m/s) |
| S | degree of saturation (–) |
| S_o | effective degree of saturation (–) |
| S_{res} | degree of saturation at residual water content (–) |
| S_{sat} | degree of saturation at zero suction (–) |
| t | time (s) |
| α | reflected angle (°) |
| γ_{dmax} | maximum dry unit weight (N/m^3) |

REFERENCES

- AASHTO (American Association of State of Highway and Transportation Officials) (2002). *Standard Specifications for Highway and Bridge*, 1st edn. American Association of State of Highway and Transportation Officials, Washington, DC, USA.
- Bathurst R. J., Ho A. F. & Siemens G. (2007). A column apparatus for investigation of 1-D unsaturated-saturated response of sand-geotextile systems. *ASTM Geotechnical Testing Journal*, 30, No. 6, 433–441.
- Bathurst R. J., Siemens G. & Ho F. (2009). Experimental investigation of infiltration ponding in one-dimensional sand-geotextile columns. *Geosynthetics International*, 16, No. 3, 158–172.
- Bouazza A., Freund M. & Nahlawi H. (2006). Water retention of nonwoven polyester geotextiles. *Polymer Testing*, 25, No. 8, 1038–1043.
- Bouazza A., Zornberg J., McCartney J. S. & Singh R. M. (2013). Unsaturated geotechnics applied to geoenvironmental engineering problems involving geosynthetics. *Engineering Geology*, 165, 143–153.
- Chen H. T., Hung W. Y., Chang C. C., Chen Y. J. & Lee C. J. (2007). Centrifuge modeling test of a geotextile-reinforced wall with a very wet clayey backfill. *Geotextiles and Geomembranes*, 25, No. 6, 346–359.
- Henry K. S., Stormont J. C. & Holte R. D. (2001). Geocomposite capillary barriers to reduce frost heave in soil. *Canadian Geotechnical Journal*, 38, No. 4, 678–694.

- Horpibulsuk S., Sukiripattanapong C., Niramitkoraburee A., Chinkulkijniwat A. & Tungsuthanon T. (2011). Performance of an earth wall stabilized with bearing reinforcements. *Geotextiles and Geomembranes*, 29, No. 5, 514–524.
- Iryo T. & Rowe R. K. (2003). On the hydraulic behavior of unsaturated nonwoven geotextiles. *Geotextiles and Geomembranes*, 21, No. 6, 381–404.
- Iryo T. & Rowe R. K. (2004). Numerical study of infiltration into a soil-geotextile column. *Geosynthetics International*, 11, No. 5, 377–389.
- Knight M. A. & Kotia S. M. (2001). Measurement of geotextile-water characteristic curves using a controlled outflow capillary pressure cell. *Geosynthetics International*, 8, No. 3, 271–282.
- Koerner R. M. (2005). *Designing with Geosynthetics*, 5th edn. Prentice Hall Publ Co, Englewood Cliffs, NJ, USA.
- Koerner R. M. & Soong T. Y. (2000). Design of drainage systems for segmental retaining walls. *Proceedings of the 18th ASCE/PennDOT Geotechnical Conference*, Hershey, PA, USA, November 1–3, vol. 1, pp. 1–38.
- Koerner R. M. & Soong T. Y. (2001). Geosynthetics reinforced segmental retaining walls. *Geotextiles and Geomembranes*, 19, No. 6, 359–386.
- Lafleur J., Lebeau M., Fauré Y. H., Savard Y. & Kehila Y. (2000). Influence of matrix suction on the drainage performance of polyester geotextiles. *Filters and Drainage in Geotechnical and Environmental Engineering*, Witkowski, W. and Mlynarek, J., Editors, Balkema, Rotterdam, the Netherlands, pp. 381–388.
- McKean J. & Inouye K. (2001). Field evaluation of the long-term performance of geocomposite sheet drains. *Geotextiles and Geomembranes*, 19, No. 4, 213–234.
- Morris C. E. (2000). Unsaturated flow in non-woven geotextiles. *GeoEng 2000: International Conference on Geotechnical and Geological Engineering, Melbourne, Australia*, Technomic, Lancaster, PA, USA, vol. 2, p. 322.
- Mualem Y. (1976). A new model for predicting the hydraulic conductivity of unsaturated porous stone media. *Water Resource Research*, 12, No. 3, 513–522.
- Nahawi H., Bouazza A. & Kodikara J. (2007). Characterisation of geotextiles water retention using a modified capillary pressure cell. *Geotextiles and Geomembranes*, 25, No. 3, 186–193.
- Potts D. M. & Zdravkovic L. (2001). *Finite Element Analysis in Geotechnical Engineering: Application*, Thomas Telford, London, UK.
- Ross B. (1990). The diversion capacity of capillary barriers. *Water Resources Research*, 26, No. 10, 2625–2629.
- Shibuya S., Kataguchi T. & Chae J. G. (2007). Failure of reinforced earth wall as attacked by typhoon No. 23 in 2004. *Soils and Foundations*, 46, No. 2, 153–160.
- Siemens G. & Bathurst R. J. (2010). Numerical parametric investigation of infiltration in one-dimensional sand-geotextile columns. *Geotextiles and Geomembranes*, 28, No. 5, 460–476.
- Stormont J. C. & Morris C. E. (2000). Characterization of unsaturated nonwoven geotextiles. In *Advances in Unsaturated Geotechnics*, Shackelford, C. D., Houston, S. L. and Chang, N. Y., Editors, ASCE, Reston, VA, USA, pp. 153–164.
- Stormont J. C., Henry K. S. & Evans T. M. (1997). Water retention functions of four nonwoven polypropylene geotextiles. *Geosynthetics International*, 4, No. 6, 661–672.
- van Genuchten M. T. (1980). A closed-form equation for predicting the hydraulic conductivity of unsaturated soil. *Soil Science Society of American Journal*, 44, No. 5, 615–628.
- Yoo C. A. & Jung H. Y. (2006). Case study of geosynthetic reinforced segmental retaining wall failure. *Journal of Geotechnical and Geoenvironmental Engineering, ASCE*, 132, No. 12, 1538–1550.
- Zornberg J. G., Bouazza A. & McCartney J. S. (2010). Geosynthetic capillary barriers: current state of knowledge. *Geosynthetics International*, 17, No. 5, 273–300.

The Editor welcomes discussion on all papers published in *Geosynthetics International*. Please email your contribution to discussion@geosynthetics-international.com

มหาวิทยาลัยเทคโนโลยีสุรนารี



GEOMATE



6719

Best Paper Award

to

*Duc Bui Van, Avirut Chinkulkijniwat, Suksun Horpibulsuk, Somjai Yubonchit,
Artit Udomchai, Irin Limrat and Tulasi Ram Bhattarai*

for the paper entitled:

**INFLUENCE OF NONWOVEN GEOTEXTILE ON THE HYDRAULIC
RESPONSE OF MECHANICAL STABILIZED EARTH WALL**

**The Sixth International Conference on Geotechnique, Construction
Materials and Environment, Bangkok, Thailand, November 14-16, 2016**

Prof. Suksun Horpibulsuk
Conference Chairman



Prof. Zakaria Hossain
Conference Director

มหาวิทยาลัยเทคโนโลยีสุรนารี

BIOGRAPHY

Mr. Duc Bui Van was born in Thanh Hoa province, Viet Nam on the 19th of May, 1982. He obtained his under-graduate degree and Master's degree in Underground construction, Mining and Special construction field from Hanoi University of Mining and Geology in 2005 and 2010, respectively. He is currently working as a lecturer at Department of Construction Techniques – Faculty of Civil Engineering – Hanoi University of Mining and Geology – Ha Noi, Viet Nam. In 2014, he has been awarded a SUT Ph.D scholarship for ASEAN students to study at School of Civil Engineering, Suranaree University of Technology, under supervision of Associate Professor Dr. Avirut Chinkunkijniwat. During his Ph.D. study (2014-2017), he has attended several international conferences in Civil Engineering field and received a best paper award in the international conference on his field study, GEOMATE 2017, Bangkok, Thailand. The author's current research interests include Reinforced Earth Techniques, Landslides, Application of geosynthetics, Underground construction techniques as well.